CYCLOSTRATIGRAPHY OF LATE CAMBRIAN CYCLIC CARBONATES: AN INTERBASINAL FIELD AND MODELLING STUDY, U.S.A.

by

David Allen Osleger

Dissertation submitted to the Faculty of the
Virginia Polytechnic Institute and State University
in partial fulfillment of the requirements for the degree of
DOCTOR OF PHILOSOPHY
in
Geology

APPROVED:

J.F. Read, Chairman

K. A. Eriksson

L. Glover, III

R. K. Bambach

N. L. Gilinsky

August, 1990

Blacksburg, Virginia

CYCLOSTRATIGRAPHY OF LATE CAMBRIAN CYCLIC CARBONATES: AN INTERBASINAL FIELD AND MODELLING STUDY, U.S.A.

by

David Allen Osleger

Committee Chairman: J.F. Read

Dept. of Geological Sciences

(ABSTRACT)

An interbasinal study of Late Cambrian cyclic carbonate successions in the Appalachian and Cordilleran passive margins, the Texas cratonic embayment and the southern Oklahoma aulacogen has provided controls on the simultaneous development of peritidal to subtidal meter-scale cycles and the larger scale depositional sequences on which they are superimposed. Fining-upward peritidal cycles grade seaward into coarsening-upward, shallow to deep subtidal cycles that form a continuum across the carbonate platforms and are genetically linked to one another by shared lithofacies. Eustacy appears to exert the dominant control on the simultaneous development of peritidal and subtidal cycles on different carbonate platforms. Based on the recognition of dominant periodicities on power spectra derived from time series of subtidal cycles, high frequency eustatic oscillations may be controlled by Milankovitch astronomical rhythms.

Interbasinal correlation of Late Cambrian depositional sequences was performed by graphic correlation and the time-equivalent intervals were correlated lithostratigraphically using isochronous biomere boundaries as time datums. *Fischer plots* of meter-scale cycles define changes in relative sea level

based on the amount of extra accommodation space produced by eustacy beyond that provided by subsidence. *Residual eustatic curves* derived from subsidence analysis are useful for correlating the longer-term Late Cambrian sea level events and changes in the rate of sea level rise and fall can be used to define shorter-term events. Combining the sea level curves defined by Fischer plots and subsidence analysis with paleobathymetric curves of Late Cambrian cyclic strata suggests that the curves may approximate the *form* of the eustatic sea level curve. A composite "eustatic" sea level curve for the Late Cambrian was created by qualitatively combining the sea level curves defined by the different techniques for each of the four localities.

"Eustatic" sea level curves defined by Fischer plots and subsidence analysis may be used to apply sequence stratigraphic concepts to one-dimensional outcrop sections. Combined with systematic changes in the stacking patterns of meter-scale cycles, they can be used to define the internal composition of systems tracts, sequence boundaries, and flooding surfaces of third-order depositional sequences.

One- and two-dimensional models of peritidal and subtidal cycle development indicate that peritidal cycle thickness is primarily controlled by accommodation space and deeper subtidal cycle thickness is primarily controlled by sedimentation rate. Whereas lithofacies within peritidal cycles alternate in response to fluctuations in sea level, subtidal cycle development may be related to fluctuations in fairweather and storm wave base that oscillate in harmony with sea level fluctuations.

ACKNOWLEDGEMENTS

I would like to thank Fred Read for his guidance throughout the duration of the research. Fred's idea-generating abilities and enthusiasm, as well as his talent for acquiring financial support, are greatly appreciated.

Field assistance and insight into the Cambrian was kindly provided by Jim Miller (Southwest Missouri State Univ.), Pete Palmer (Geological Society of America) and Lehi Hintze (Brigham Young Univ.). The text benefited from discussions with Gerard Bond (Lamont-Doherty) and Michelle Kominz (Univ. Texas at Austin) about subsidence analysis and periodicity in the stratigraphic record. They also provided the software for subsidence analysis. Spectral analysis was done on a VAX computer in the Geophysical Lab at Virginia Polytechnic Institute under the guidance of Dr. C. Coruh. Vincent Miranda refined the two-dimensional computer program.

Billy Newcomb and Steve van Aken provided able field assistance. Special thanks to my pals in the lab, Maya Elrick, Roger Barnaby, Vincent Miranda, and especially, Isabel Montanez.

My family has been incredibly patient, supportive and financially generous - I am forever grateful. Special appreciation is given to Isabel and Biff for being the best companions anyone could ask for.

Financial assistance was provided by NSF grants EAR 88-16664 and 87-07737 to J.F. Read; by a grant from the American Chemical Society (PRF grant 21282-AC2); by Texaco, Chevron, Marathon and Mobil; and by grants-in-aid from the Geological Society of America, Sigma Xi and the Appalachian Basin Industrial Associates.

TABLE OF CONTENTS

LIST OF TABLES

LIST OF ILLUSTRATIONS

LIST OF PLATES

CHAPTER 1

RELATION OF EUSTACY AND STACKING PATTERNS OF LATE CAMBRIAN METER-SCALE CARBONATE CYCLES, U.S.A.

ABSTRACT

An interbasinal study of Late Cambrian cyclic carbonate successions in the Appalachian and Cordilleran passive margins, the Texas cratonic embayment and the southern Oklahoma aulacogen has provided controls on the simultaneous development of peritidal to subtidal meter-scale cycles and the larger scale depositional sequences on which they are superimposed. Fining-upward peritidal cycles grade seaward into coarsening-upward, shallow to deep subtidal cycles that form a continuum across the carbonate platforms and are genetically linked to one another by shared lithofacies. In contrast to peritidal cycles, subtidal cycles are not capped by intertidal lithofacies nor do the subtidal cycles exhibit exposure features such as microkarsting or vadose dissolution/cementation.

Systematic changes in the stacking patterns of meter-scale cycles can be used in conjunction with Fischer plots to define long-term sea level cycles. On Fischer plots of peritidal cyclic successions, long-term relative sea level rises are characterized by thick, subtidal-dominated cycles with thin laminite caps. Long-term relative sea level falls are defined by stacks of thin, laminite-dominated cycles that show brecciated cycle caps and quartz sands toward the relative sea level lowstand. On Fischer plots of dominantly subtidal cyclic successions, long-term sea level rise is characterized by storm-dominated, open marine carbonate cycles or thick, deep ramp, shale-based cycles. Falling segments of the Fischer plot are characterized by thin, shallow subtidal cycles composed of restricted lithofacies. The relative thicknesses and compositions of the stacked meter-scale cycles are dependent on the amount of accommodation space generated by eustacy and subsidence. Cycle stacking

patterns provide the crucial link between the meter-scale cycles and the larger scale sequences and their component systems tracts.

Eustacy appears to exert the dominant control on the simultaneous development of peritidal and subtidal cycles on different carbonate platforms. Subtidal cycles that remain submerged throughout the duration of deposition provide clear evidence against autocyclic controls on meter-scale cycle development . However, processes intrinsic to the subtidal platform (sediment redistribution by storm and wave energy, hardground formation during non-depositional events and oceanographic conditions) do occur and should not be neglected as contributing to the internal composition of subtidal cycles. Based on the recognition of dominant periodicities in the cycles using histograms of cycle thickness and spectral analysis, high frequency eustatic oscillations may be controlled by Milankovitch astronomical rhythms.

One- and two-dimensional models of peritidal and subtidal cycle development indicate that peritidal cycle thickness is primarily controlled by accommodation space and deeper subtidal cycle thickness is primarily controlled by sedimentation rate. Whereas lithofacies within peritidal cycles alternate in response to fluctuations in sea level, subtidal cycle development may be related to fluctuations in fairweather and storm wave base that oscillate in harmony with sea level fluctuations.

INTRODUCTION

Superimposed scales of stratigraphic cyclicity have been increasingly recognized throughout the geologic record (Fischer, 1964; Read et al., 1986; Sarg, 1988; Koerschner and Read, 1989; Goldhammer et al., 1987; 1990) and appear to be related to the combined effects of several orders of relative sea level oscillations. Shallowing-upward, meter-scale carbonate cycles tend to be systematically arranged within larger-scale successions. Stacking patterns of the meter-scale cycles can be used to identify long-term relative sea level changes. Cycle stacking patterns provide the critical link between meter-scale cycles (parasequences) and the larger-scale sequences and their component systems tracts. An interbasinal study of Late Cambrian pericratonic cyclic carbonates was conducted by logging meter-scale cycles of time-equivalent cyclic successions in different tectonic settings to evaluate how the cycles differ and what factors may have controlled their origin. The recognition of time-equivalent successions composed of peritidal cycles, subtidal cycles and non-cyclic intervals suggest that the differing platform morphologies, subsidence histories and paleoenvironmental conditions of each locality had a unique response to relative sea level fluctuations through time.

The objectives of this paper are to: 1) define Late Cambrian peritidal to deep subtidal cycles and describe the environmental conditions under which upward-shallowing occurred; 2) illustrate characteristic stacking patterns of cycles that define rising and falling portions of sea level curves using Fischer plots; 3) evaluate the controlling mechanisms of meter-scale cycle formation in light of the simultaneous deposition of peritidal and subtidal cycles using

quantitative modelling to constrain the probable parameters of cycle development.

STRATIGRAPHIC AND TECTONIC SETTINGS

Tectonic Settings and Locations of Sections: Complete sections of Late Cambrian strata were measured and logged bed-for-bed in: 1) the House Range of west central Utah on the Cordilleran passive margin, 2) the Appalachian Mountains in Tennessee, Virginia and eastern Pennsylvania in the Appalachian passive margin, 3) the Llano uplift of central Texas on the southern craton, and 4) the Wichita Mountains of the southern Oklahoma aulacogen (Fig.1). Biostratigraphic control of the formations for each of the localities (Fig. 2) was obtained from published work (Palmer, 1954; 1965b; 1971; Robison, 1964; Derby, 1965; Rassetti, 1965; Longacre, 1970; Hintze, 1974; Hintze and Palmer, 1976; Barnes and Bell, 1977; Stitt, 1971; 1977; Hintze et al, 1980; Eby, 1981; Taylor and Miller, 1981; Stitt et al, 1981; Miller et al, 1982; Orndorff, 1988; Sundberg, 1990).

Field locations were chosen on the basis of: 1) quality of exposure and absence of structural complications, 2) availability of biostratigraphic data (especially biomere boundaries), and 3) platform location along the transition between shallow-water carbonates and deeper-water fine-grained siliciclastics where intertongueing relations define excursions in sea level. A total of 2400 meters of section were logged and numerous other sections previously described in the Appalachians (Markello, 1979; Koerschner, 1983) were field-checked. Hand samples of individual lithofacies were collected for slabbing

Figure 1: Location map of sections measured in the study. Late Cambrian base map modified from Lochman-Balk (1971) and Palmer (1974) to show the inner and outer detrital belts, the middle carbonate belt, the southern Oklahoma aulacogen and the Conasauga intrashelf basin.

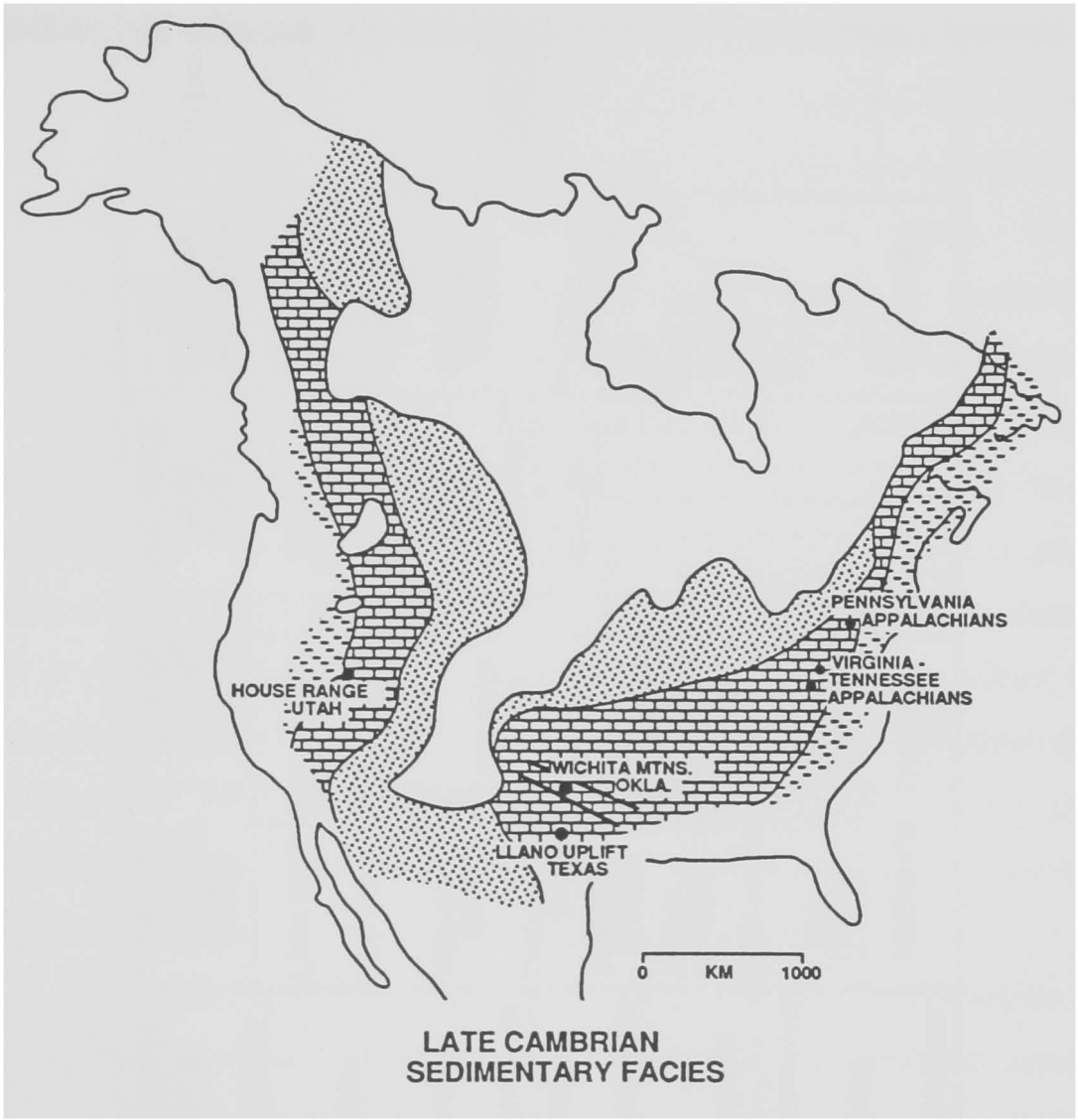

LATE CAMBRIAN
SEDIMENTARY FACIES

Figure 2: Biostratigraphic chart of Late Cambrian strata in this study. Note the three biomere boundaries in the Late Cambrian that separate the trilobite zones.

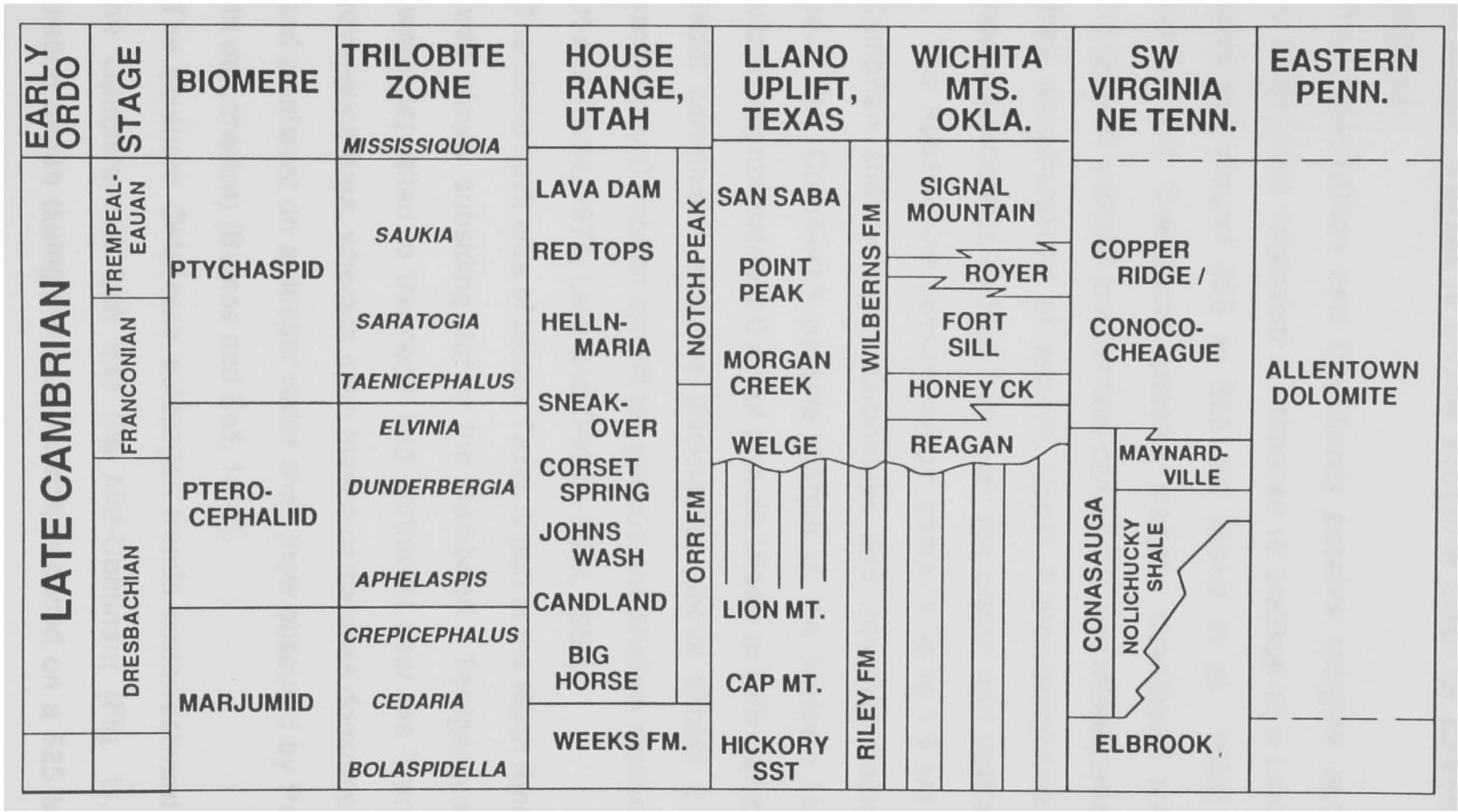
EARLY ORDO
LATE CAMBRIAN
STAGE
TREMPEAL-EAUAN
FRANCONIAN
DRESBACHIAN
BIOMERE
PTYCHASPID
PTERO-CEPHALIID
MARJUMIID
TRILOBITE ZONE
MISSISSIQUOIA
SAUKIA
SARATOGIA
TAENICEPHALUS
ELVINIA
DUNDERBERGIA
APHELASPIS
CREPICEPHALUS
CEDARIA
BOLASPIDELLA
HOUSE RANGE, UTAH
LAVA DAM
RED TOPS
HELLN-MARIA
SNEAK-OVER
CORSET SPRING
JOHNS WASH
CANDLAND
BIG HORSE
WEEKS FM.
NOTCH PEAK
ORR FM
LLANO UPLIFT, TEXAS
SAN SABA
POINT PEAK
MORGAN CREEK
WELGE
LION MT.
CAP MT.
HICKORY SST
WILBERNS FM
RILEY FM
WICHITA MTS. OKLA.
SIGNAL MOUNTAIN
ROYER
FORT SILL
HONEY CK
REAGAN
SW VIRGINIA NE TENN.
COPPER RIDGE /
CONOCO-CHEAGUE
MAYNARD-VILLE
CONASAUGA
NOLICHUCKY SHALE
ELBROOK
EASTERN PENN.
ALLENTOWN DOLOMITE

and thin section analysis to provide additional detail for paleoenvironmental interpretations.

The Appalachian and Cordilleran passive margins and the Texas cratonic embayment originated in response to breakup of a Late Proterozoic supercontinent around 625 to 555 Ma (Bond et al., 1984). Both the Appalachian and Cordilleran passive margins developed wedge-shaped prisms of post-rift subtidal and peritidal carbonates and interlayered siliciclastics over thick accumulations of syn-rift, Upper Proterozoic/Lower Cambrian, terrigenous siliciclastics derived from both the craton and uplifted rift blocks (Fig.3). The Appalachian passive margin contains up to 1.6 km of Middle to Late Cambrian shallow water carbonates and intrashelf basin shale and siltstone. The Cordilleran passive margin of the western United States accumulated approximately 2.0 km of post-rift Middle to Late Cambrian subtidal to peritidal carbonates and fine siliciclastics above almost 6 km of Late Proterozoic-Early Cambrian syn-rift terrigenous and shallow marine siliciclastics (Stewart and Poole, 1974; Levy and Christie-Blick, 1989).

The Llano uplift area of central Texas is part of the North American craton which was slowly subsiding during the Cambrian. Terrigenous siliciclastic facies were deposited to the north and northwest near the Transcontinental Arch provenance area, whereas open marine carbonates dominated toward the south and southeast on a deeper water shelf (now obscured by Pennsylvanian Ouachita deformation) (Barnes and Bell, 1977).

The southern Oklahoma aulacogen trends northwestward for 700 km from the Ouachita fold belt into the Mid-Continent (Fig. 1). Sediment accumulation began during the Late Cambrian based on a 525 Ma ± 25 m.y.

Figure 3: Late Cambrian platform morphologies of the Appalachian and Cordilleran passive margins, the Texas craton and the southern Oklahoma aulacogen. Formation and group names superimposed on lithologic symbols.

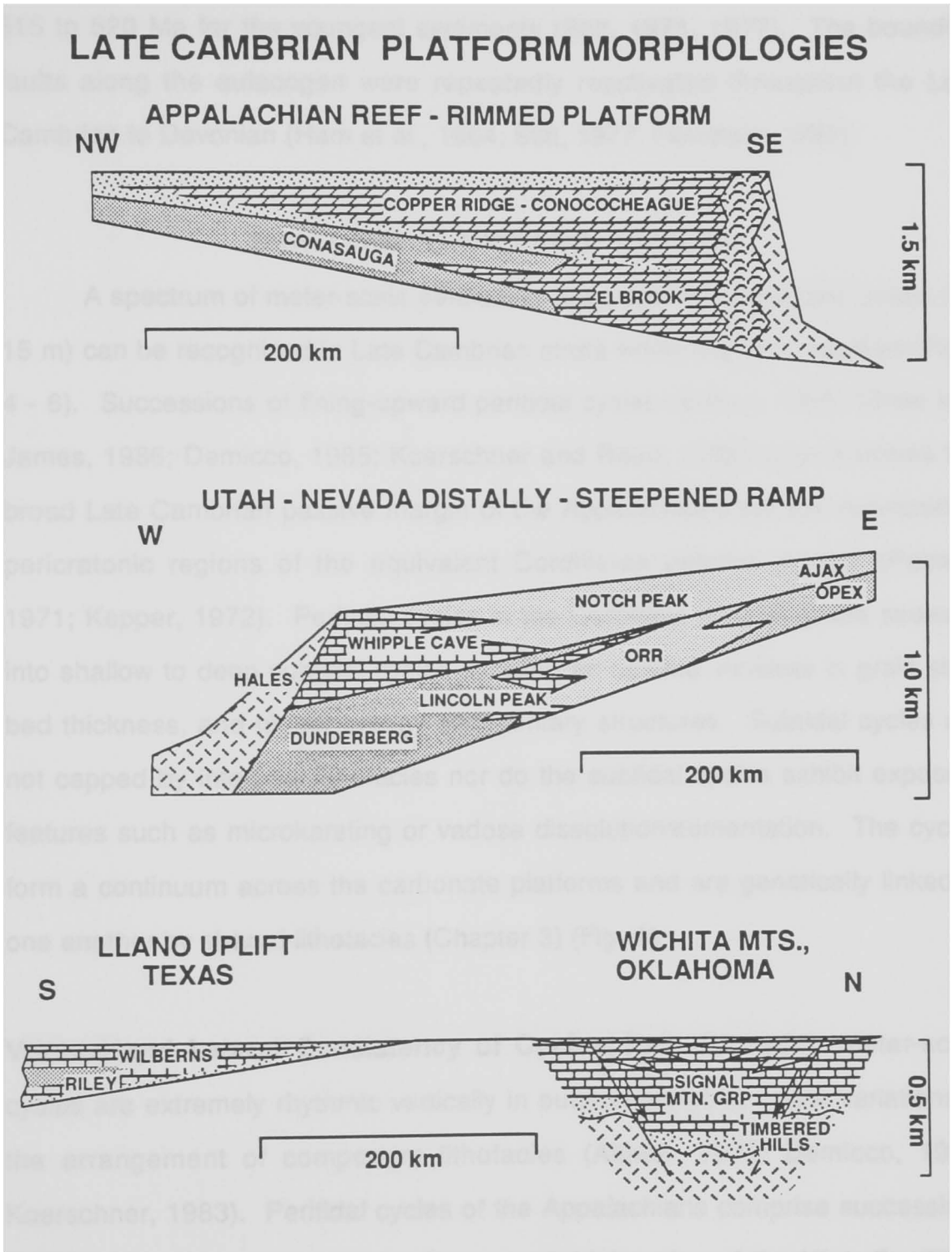
LATE CAMBRIAN PLATFORM MORPHOLOGIES
APPALACHIAN REEF - RIMMED PLATFORM
NW
SE
COPPER RIDGE - CONOCOCHEAGUE
CONASAUGA
ELBROOK
200 km
1.5 km
UTAH - NEVADA DISTALLY - STEEPENED RAMP
W
E
AJAX
OPEX
NOTCH PEAK
WHIPPLE CAVE
ORR
HALES
LINCOLN PEAK
DUNDERBERG
200 km
1.0 km
LLANO UPLIFT
TEXAS
WICHITA MTS.,
OKLAHOMA
S
N
WILBERNS
RILEY
SIGNAL
MTN. GRP
TIMBERED
HILLS
200 km
0.5 km

age for the youngest intrusives (Ham et al., 1964) and biostratigraphic ages of 515 to 520 Ma for the youngest sediments (Stitt, 1971, 1977). The bounding faults along the aulacogen were repeatedly reactivated throughout the Late Cambrian to Devonian (Ham et al., 1964; Stitt, 1977; Feinstein, 1981).

SHALLOWING-UPWARD CYCLES

A spectrum of meter-scale peritidal to deep subtidal carbonate cycles (1 - 15 m) can be recognized in Late Cambrian strata within the four localities (Figs. 4 - 6). Successions of fining-upward peritidal cycles (Wilson, 1952; Chow and James, 1986; Demicco, 1985; Koerschner and Read, 1989) extend across the broad Late Cambrian passive margin of the Appalachians but are restricted to pericratonic regions of the equivalent Cordilleran passive margin (Palmer, 1971; Kepper, 1972). Peritidal cycles in the Cordillera of Utah grade seaward into shallow to deep subtidal cycles showing an upward increase in grain size, bed thickness, and higher energy sedimentary structures. Subtidal cycles are not capped by intertidal lithofacies nor do the subtidal cycles exhibit exposure features such as microkarsting or vadose dissolution/cementation. The cycles form a continuum across the carbonate platforms and are genetically linked to one another by shared lithofacies (Chapter 3) (Fig. 4).

Vertical and Lateral Consistency of Cycles: Late Cambrian meter-scale cycles are extremely rhythmic vertically in outcrop with only minor variations in the arrangement of component lithofacies (Aitken, 1978; Demicco, 1981; Koerschner, 1983). Peritidal cycles of the Appalachians comprise successions of hundreds of stacked cycles. Deeper subtidal cycles of the Utah Cordillera

Figure 4: Arrangement of Late Cambrian peritidal to deep subtidal cycle types across a hypothetical platform. Note the location of fairweather and storm wave base and their relation to cycle types.

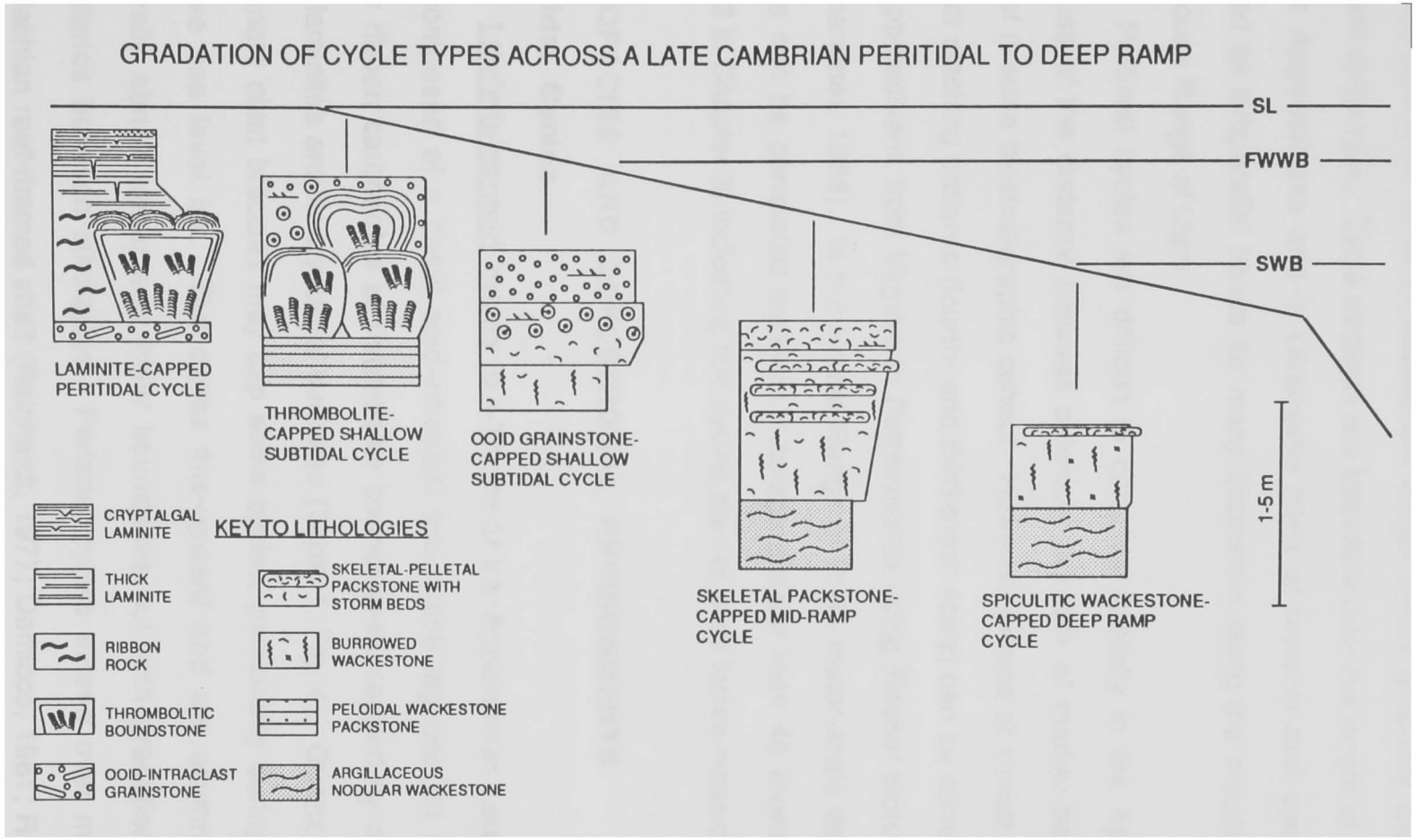
GRADATION OF CYCLE TYPES ACROSS A LATE CAMBRIAN PERITIDAL TO DEEP RAMP
SL
FWWB
SWB
LAMINITE-CAPPED PERITIDAL CYCLE
THROMBOLITE-CAPPED SHALLOW SUBTIDAL CYCLE
OOID GRAINSTONE-CAPPED SHALLOW SUBTIDAL CYCLE
SKELETAL PACKSTONE-CAPPED MID-RAMP CYCLE
SPICULITIC WACKESTONE-CAPPED DEEP RAMP CYCLE
1-5 m
KEY TO LITHOLOGIES
CRYPTALGAL LAMINITE
THICK LAMINITE
RIBBON ROCK
THROMBOLITIC BOUNDSTONE
OOID-INTRACLAST GRAINSTONE
SKELETAL-PELLETAL PACKSTONE WITH STORM BEDS
BURROWED WACKESTONE
PELOIDAL WACKESTONE PACKSTONE
ARGILLACEOUS NODULAR WACKESTONE

are repetitive over 15 to 40 successive cycles before gradually changing to a different cycle type. Cycle contacts are traceable over the length of the outcrop in the Appalachians and in Oklahoma (tens of meters) and cycles can be tracked as subparallel bands for many kilometers along the mountain flank in the House Range of Utah.

Peritidal cycles are difficult to correlate laterally in the Appalachians because of the distance between outcrops, the lack of marker beds and the lack of precise biostratigraphic control. However, groups of similar cycles with distinct stacking patterns (fourth- and third-order scale) can be correlated along the Appalachians from Virginia to Pennsylvania using Fischer plots (Read and Goldhammer, 1988). In the House Range of Utah, meter-scale deep subtidal cycles can be correlated between outcrops greater than 45 kilometers apart (Fig. 3 in Chapter 3) indicating that cycles are not local facies mosaics.

LITHOFACIES AND DEPOSITIONAL ENVIRONMENTS

Peritidal Cycles

Laminite-capped cycles (0.4-7.0 m) of the Appalachian Late Cambrian are composed of a basal ooid-intraclast grainstone lag deposit overlain by either ribbon carbonates or thrombolite boundstones capped by mudcracked thick laminites and/or cryptalgal laminites (Table 1; Fig. 4). Quartz arenites or carbonate clast breccias may cap some cycles, particularly during long-term relative sea level fall. The cycles fine-upward and are asymmetric, with generally abrupt upper and lower boundaries but with gradational internal boundaries between lithofacies. Peritidal cycles extend over much of the Appalachian reef-rimmed shelf (Reinhardt, 1977; Demicco, 1981; Read, 1985).

TABLE 1: PERITIDAL LITHOFACIES

Intraclast Breccia (5-20 cm)

Bedding Characteristics: Laterally discontinuous veneers of angular to elongate intraclasts in a calcrete matrix within mudcracked laminite lithofacies; often abundant quartz sand; intraclasts often poorly sorted with no preferred orientation or grading; irregular upper surface usually overlain by oolitic grainstone.

Internal Composition/Texture: Angular clasts composed of LLH stromatolites and cryptalgal laminites and have corroded edges and dolomitic rinds; quartz sand grains are moderately sorted, subrounded and frosted; vuggy voids common.

Cryptalgal Laminite (0.2-3.0 m)

Bedding Characteristics: Dolomite; mm-scale planar and crinkly laminations; mudcracks, deep prism cracks, tepees and silicified evaporite nodules common; thin flat pebble conglomerates and mud chip intraclast layers; occasional 1-3 grain thick quartz sand stringers; grades upward from ribbon rock or more commonly thick laminite; occasionally capped by irregular cherty breccias but more typically overlain by intraclastic transgressive lag of overlying cycle; some cycles are reversing with the cryptalgal laminite coarsening upward into less mudcracked thick laminite.

Internal Composition/Texture: Laminar couplets composed of basal silt-size peloidal packstones grading up into mudstone laminae; some low-angle cross-lamination and micro-scoured bases in peloidal silts; some laminoid fenestrae.

Thick Laminite (0.2-3.0 m)

Bedding Characteristics: Dolomite; cm-scale laminations of silt and mud couplets; laminations planar to wavy to discontinuous; common cross-laminated scour fills and current ripples; some short mudcracks and silicified evaporite nodules; commonly overlie ribbon rocks; usually grade up into cryptalgal laminite but sometimes wil cap incomplete cycles.

Internal Composition/Texture: Couplets consist of peloid-quartz silt packstone that grades up into dolomitic mudstone; some well-rounded quartz sand laminae 1 or 2 grains thick; some laminoid fenestrae.

Ribbon Carbonate (0.5-4.0 m)

Bedding Characteristics: Alternating irregular layers of peloidal limestone and dolomitic mud; discrete burrowing; some gutter scours with cross-laminated peloidal fill; shallow mudcracks become more abundant upward; common flat pebble conglomerate beds with internal scours, hardgrounds, and mud drapes; often flank and overlie thrombolite bioherms; fine upward into thick laminites.

Internal Composition/Texture: Peloidal packstones grade upward into argillaceous dolomite caps; peloidal laminae contain minor quartz silt and skeletal debris and show occasional scoured bases and low-angle cross-lamination; flat pebble beds composed of imbricate discoidal clasts of laminated peloidal packstone or dolomitic mudstone; matrix between clasts consists of sand-size intraclasts, trilobite and echinoderm debris, pellets and minor quartz silt.

Stromatolite Boundstone (0.5-2.5 m)

Bedding Characteristics: SH and LLH stromatolites typically encrust tops of thrombolite bioherms or basal grainstone lags; fingers often coalesce into fan-like forms or crenulated sheets; club shapes common toward the tops of bioherm complexes; commonly surrounded laterally by intraclast-peloidal packstones or ribbon rocks which onlap and smother the stromatolites.

Internal Composition/Texture: Alternating mm-scale laminae of dolomitic peloidal silts and muds; some irregular and laminoid fenestrae; some thin quartz silt laminae and coarser laminae of intraclasts.

Thrombolite Boundstone (0.5-2.5 m)

Bedding Characteristics: Globose to upward-widening flat-topped bioherms to coalescent biostromes; individual bioherms often stacked on top of one another (up to 12m thick) without intervening continuous bedded lithologies; digitate fingers (1-6 cm high x 1-2 cm wide) have erosional edges, are grouped in clusters and often overlie massive cores of thrombolites; lime sand interhead fill flank and locally onlap and blanket bioherms; bi-directional and high-angle cross-bedding, scours and multiple hardgrounds common in interhead fill; lime sands fine upward into ribbon carbonates; thrombolites typically nucleate on underlying intraclastic grainstone lag.

Internal Composition/Texture: Clotted micritic textures; commonly grain-rich reflecting the composition of the interhead fill; small intraclasts, skeletal debris, ooids and pellets are dominant components; fingers show traces of *Girvanella* , thin stringers of micrite and microspar cements; *Renalcis* recognized toward the base of many of the bioherms; common irregular fenestrae with geopetal fillings.

These cycles are recognized within the Elbrook, Copper Ridge, Conococheague and Allentown Formations of the Appalachians and they also occur in the Fort Sill, Royer and basal Signal Mountain Formations of the Wichita Mountains of Oklahoma (Fig. 2). Each cycle records rapid transgression followed by the progradation of tidal flats over a shallow subtidal sandy shelf with patchy thrombolitic bioherms (Koerschner and Read, 1989).

The basal ooid-intraclast sandy lag deposit of peritidal cycles migrated onto the underlying tidal flat cap from shallow offshore wave-agitated shoals during initial rapid transgression. Hardgrounds developed on the lag deposit as the transgressive rise of sea level outpaced sediment production. As the rate of relative sea level rise decreased, carbonate sedimentation was able to catch up. Thrombolites locally established themselves on marine-cemented grainstone lags and grew to sea level. Ribbon rocks began to accummulate adjacent to bioherms in shallow subtidal to lower intertidal conditions. The rippled peloidal silts/fine sands were laid down during storms with drapes of lime mud settling out during the waning stages (Demicco, 1983).

Progressive shallowing and progradation is reflected in the upward transition into increasingly mudcracked ribbon rocks, SH and LLH stromatolites and thick laminites. Centimeter-scale thick laminites are mechanically-deposited couplets of fine peloidal silts and mud drapes laid down on the intertidal flats by storm and tidal currents (Hardie and Ginsburg, 1977). This lithofacies often caps cycles or grades up into higher intertidal cryptalgal laminites. Lack of burrowing, abundant mudcracks, silicified evaporite nodules and windblown quartz sand within laminite lithofacies indicate hypersaline and semiarid conditions. Cratonically-derived quartz sands (Wilson, 1952;

Koerschner and Read, 1989) are found in some cycles as thin laminae within laminite beds, as discrete beds capping cycles or in the basal transgressive lag of overlying cycles. The sands were probably brought in during long-term falls in relative sea level and were incorporated into cycle caps during short-term regression or reworked by the succeeding marine transgression into the basal lag deposit of the succeeding cycle.

Some evidence of exposure, non-deposition and erosion is exhibited within peritidal cycles. Most laminite caps are flat-topped and erosional, suggesting deflation of the supratidal surface down to paleowater-tables. Fossil molds and crystal silts that geopetally fill leach voids in subtidal limestones indicate flushing by undersaturated meteoric waters (Koerschner and Read, 1989). Irregular veneers of carbonate clast breccia that fill solution-enhanced lows on exposed supratidal caps are thin regoliths that developed on the non-vegetated Late Cambrian exposed flats. These features provide evidence that relative sea level fell below the supratidal surface.

Shallow Subtidal Cycles

Shallow subtidal cycles are defined by the interpreted paleowater depth of the cycle cap and include thrombolite-capped, ooid grainstone-capped and skeletal packstone-capped cycles.

Thrombolite-capped cycles (1.5-12.0 m) of the Cordilleran Late Cambrian passive margin consist of a basal dark gray peloidal packstone overlain by stacked thrombolite-stromatolite bioherms and laterally equivalent light gray cross-bedded peloidal-oncolitic grainstone (Fig. 4). These cycles record progradation of peritidal biohermal patch reefs and associated high

energy grainstones over slightly deeper subtidal peloidal packstones of a restricted shelf. More than thirty of these cycles are recognized within the upper Hellnmaria Member of the Notch Peak Formation throughout the House Range of west central Utah. Similar cycles but at larger scales (>5 to 20 m) occur within the Wilberns Formation of central Texas.

Thrombolite-capped cycles were initiated by onlap of peloidal packstones/wackestones (Table 2) from the slightly deeper ramp onto thrombolite-stromatolite bioherms. Horizontal to low angle cross-lamination, lack of recognizable skeletal material, and dark gray bioturbated textures suggest restricted, quiet water (but not necessarily deep) deposition. With slowing of the rate of short-term relative sea level rise, thrombolitic bioherm complexes were able to establish themselves on hardgrounds or other stable substrates. The bioherms are laterally discontinuous suggesting development as isolated, shallow subtidal patch reefs on top of the basal peloidal veneer. Continued slow rates of relative sea level rise are indicated by the stacking of individual bioherms up to 12 m thick without intervening bedded lithofacies. Many of the thrombolitic bioherms have stromatolitic laminae outlining the outer surface of the mound and some stromatolitic biohermal layers are interbedded within the dominantly thrombolitic complex (Fig. 4). This implies either episodic shallowing to intertidal depths or perhaps variations in salinity (and associated grazing and boring epifauna) related to periodically restricted conditions on the platform (Aitken, 1967; Kennard and James, 1986).

Shallow subtidal conditions for the thrombolites are supported by the laterally equivalent light gray, crossbedded peloidal-oncolitic-oolitic-intraclastic grainstones which resemble modern, high energy, non-skeletal grainstones

TABLE 2: SHALLOW SUBTIDAL LITHOFACIES

Oold Grainstone (0.1-1.5 m)

Bedding Characteristics: Thin to medium bedded, common high angle crossbedding; occasional stacked hardgrounds; gradationaly overlie skeletal-oncolitic grainstones; abruptly overlain by burrowed wackestone/packstone lithofacies.

Internal Composition/Texture: 90-95% well-sorted ooids; common oolitic intraclasts and random subangular quartz sand grains; ooids are concentrically laminated and have echinoderm-trilobite-quartz silt nuclei; isopachous marine cement rims and fine to medium equant spar cements; some dolomitized ooids.

Peloidal Grainstone (1.0-4.0 m)

Bedding Characteristics: Thin to medium-bedded dolomite; light to medium gray cross-bedded grainstones; laterally equivalent to (and gradationally onlap) thrombolitic-stromatolitic bioherms; abruptly overlain by either thin-bedded, evenly-laminated dark gray peloidal dolomites or thrombolitic bioherms.

Internal Composition/Texture: Fine to medium crystalline dolomite; dominantly peloidal grainstones with variable numbers of large oncolites, ooids and intraclasts (all seen as ghosts); flat pebble conglomerates in lenses and scours; robust *Mathevia* and *Matherella* mollusk shells; some internal mm-scale gentle cross-lamination of peloids.

Skeletal-Oncolitic Grainstone (0.5-2.5 m)

Bedding Characteristics: Thin to medium bedded; megarippled, high angle crossbeds; commonly coarsen upward from skeletal packstone up to interbedded oncolitic and skeletal grainstones; random interbedded lenses of burrowed wackestone low in lithofacies and occasional interbedded short digitate stromatolite fingers high in lithofacies; gradationally overlies burrowed wackestone lithofacies and underlies oolitic grainstone lithofacies.

Internal Composition/Texture: Cm-size, well-rounded oncolites with large intraclast cores; some multigenerational oncolites; moderate sorting; random peloids and muddy intraclasts; micritic and abundant turbid marine cements. Skeletal packstone/grainstones composed of abundant trilobite and echinoderm debris and common pellets and rounded elongate muddy intraclasts; some alignment and imbrication of allochems; some crystal silt-filled geopetal voids and shelter porosity.

enveloping growing stromatolitic bioherms in tidal channels in the Bahamas (Dill et al., 1986). Irregularly laminated oncolites, coated peloids, and high-angle tabular crossbeds that alternate with horizontally bedded packstones in the Late Cambrian rocks reflect variable energy conditions created by the biohermal complexes that effectively baffled current energy except during storms. The lack of open marine fauna within the inter-bioherm grainstones may reflect either elevated salinities on the restricted platform or intermittent high wave or tidal energies on mobile sandy substrates that precluded the establishment of grazing organisms (Pratt and James, 1982). Only the robust mollusks *Mathevia* and *Matherella* are found associated with the bioherms, supporting the case for high energy conditions.

Ooid grainstone-capped cycles (0.5-4.2 m) of the Cordilleran passive margin consist of burrowed wackestone/packstone grading up into oncolite-skeletal packstone/grainstone capped by oolitic grainstone (Table 2; Fig. 4). The succession of lithofacies record progradation of oolitic shoals over deeper ramp lithofacies. They occur in the Big Horse Member, Orr Formation of the House Range of Utah (Lohmann, 1976).

Burrowed wackestone/packstones are subtidal facies deposited below fairweather wave base under normal marine conditions (Wilson and Jordan, 1983). Pervasive bioturbation, bioclastic debris and clusters of pellets suggest an active infauna. Laterally discontinuous skeletal packstone lenses with erosional bases and burrowed tops are rapidly deposited storm beds that escaped homogenization by burrowers. The abundant quartz silt was probably transported from the craton across the inner detrital belt (Palmer, 1971) and

onto the carbonate platform through a west-trending subtidal channel that debouched near the House Range (Lohmann, 1977).

With shoaling, skeletal sand sheets migrated across the burrowed wackestones and were reworked by storm and wave currents. Megarippled units suggest emplacement as sand waves and shallow bars. The upward transition from open marine skeletal packstones to oncolitic-peloidal grainstones indicates increasingly shallow, restricted conditions (Enos, 1983), perhaps peripheral to active ooid shoals (Hine, 1977).

The crossbedded oolitic grainstone cap resulted from progradation of ooid shoal complexes as migrating spillover lobes that formed in response to storm or tidal currents (Hine, 1977; Harris, 1979; Halley et al., 1983). Rounded oolitic intraclasts indicate early marine cementation and the lack of leached ooids or other vadose features suggests continual submergence.

Skeletal packstone-capped cycles (1.0-7.5 m) are composed of basal nodular argillaceous wackestone overlain by burrowed, storm-deposited wackestone/packstone coarsening upward into a skeletal packstone/grainstone cap. (Table 2; Fig. 4). They occur in the lower Big Horse Member (Orr Formation) of the House Range and in the Honey Creek and lower Fort Sill Formations of the Wichita Mountains of Oklahoma where they form thick successions composed of up to 25 cycles. These cycles in the House Range developed on the mid-ramp at intermediate water depths above storm wave base seaward of ooid grainstone-capped cycles. The succession of lithofacies record gradually increasing storm influence as the platform shallowed to skeletal shoal depths.

The basal nodular, argillaceous wackestone is a distal storm facies deposited on the middle ramp between burrowed wackestones and packstones and deeper water siliciclastic muds. The low angle cross-laminated micropeloidal and quartz silty layers within the nodular limestones were probably transported offshore from the shallow ramp during periodic storms. Nodules may have formed early by submarine lithification under weak bottom currents (Mullins et al., 1980) or may be the result of late pressure solution and compaction. Argillaceous muds fell out of suspension during waning storm activity. The two sediment types were mixed by the burrowing infauna.

As the depositional surface shallowed, the argillaceous content of the sediment decreased, grain size and skeletal content generally increased and the abundance of storm beds with hummocky cross-stratification increased. The storm-deposited units (5 - 20 cm) are laterally discontinuous, fine-upward and consist of: 1) sharp-based skeletal packstones with peloids and mud perched above shells and pendant bladed marine cements extending down into now-occluded shelter porosity, 2) hummocky cross-stratified peloidal packstones and 3) bioturbated calcisiltite caps. This allochthonous debris was transported as entrained sediment by storm-generated currents and then reworked by oscillatory shear currents (Kreisa, 1981). Upward within this lithofacies, skeletal material becomes more abundant and storm deposits appear amalgamated with numerous wavy beds of subtly graded skeletal debris. The cycle cap of crossbedded skeletal-intraclast grainstones manifests the development of storm-reworked skeletal sand sheets and migrating sand shoals. Common platy girvanellid crusts are imbricated and suggest that the grainstone cycle cap formed within the photic zone (Pfeil and Read, 1983).

Deep Ramp / Intrashelf Basin Cycles

Deep subtidal cycles are defined by the recognition of sub-fairweather wave base sedimentary structures within the lithofacies cap of the cycles and include spiculitic wackestone-capped cycles, carbonate-capped shaly cycles and flat pebble conglomerate-capped shaly cycles.

Spiculitic wackestone-capped cycles (0.7 - 3.1 m) are composed of basal nodular argillaceous mudstone overlain by a burrowed spiculitic wackestone with skeletal packstone lenses that become more abundant upward (Table 3; Fig. 4 & 5). These cycles occur in the Sneakover Member (Orr Formation) and in the basal Hellnmaria and Lava Dam Members (Notch Peak Formation) of Utah. Very similar deep ramp cycles have been described in the Upper Muschelkalk of the South-German Basin (Aigner, 1985) and the Catalan Basin of Spain (Calvet and Tucker, 1988). Spiculitic wackestone-capped cycles of the House Range developed on the deep ramp very near storm-wave base seaward of the skeletal grainstone-capped cycles. The abundant bioturbation and trilobite and echinoderm debris within storm beds attest to well-oxygenated, normal marine conditions.

Carbonate-capped shaly cycles (2.5-15.0 m) consist of a thick basal shale abruptly overlain by a coarsening-upward skeletal wackestone/packstone (Table 4; Fig. 6). These cycles occur in the Candland Shale, Corset Spring Shale and Steamboat Pass Members of the Orr Formation of Utah. They are associated with long-term rises in relative sea level that juxtapose deep outer ramp siliciclastic facies above shallow ramp carbonate facies.

TABLE 3: DEEP SUBTIDAL LITHOFACIES

Thin-bedded Peloidal Packstones (1.0-4.0 m)

Bedding Characteristics: Dolomitized, dark gray, thin to medium-bedded peloidal packstones; random cm-scale horizontally laminated horizons; abruptly overlie light gray cross-bedded peloidal facies and thrombolite bioherms; occasionally differentially compacted beneath biohermal mounds.

Internal Composition/Texture: Consist internally of dolomitized dark gray peloids and patchy micrite; evenly laminated; probable burrowing traces; lack any of the sedimentary features and grain types exhibited in the distinct cross-bedded peloidal grainstone lithofacies

Nodular Argillaceous Wackestone (1.0-8.0 m)

Bedding Characteristics: Discontinuous, nodular, wavy and thin-bedded; recessive weathering; argillaceous seams with concentrations of ferroan dolomite separate platy mudstone/wackestone; quartz silt lenses common; random very low-angle cross-laminated lenses and nodules; some mm-scale horizontal laminations; common horizontal burrows on tops of bedding planes.

Internal Composition/Texture: Variable intermixed textures from mudstone through packstone with wackestone dominant; micropeloids and quartz silt dominant along with finely comminuted skeletal debris including sponge spicules; patchy lime mud; occasional floating elongate trilobite fragments; peloids and quartz silt alternate in low angle mm-scale cross-laminations with divergent dip angles (hummocky cross-stratification?)

Burrowed Wackestone/Packstone (0.5-4.0 m)

Bedding Characteristic: Nodular to wavy thin beds of dolomitic, mottled limestone; thin quartz siltstone lenses abundant; occasional skeletal packstone lenses; pervasively bioturbated; gradational contact with overlying oncolitic-skeletal packstones; abrupt lower contact with ooid grainstones of underlying cycle.

Internal Composition/Texture: Silt-size finely comminuted grains dominant with floating, randomly oriented echinoderm-trilobite debris common; clusters of peloids; abundant subangular quartz silt to fine sand; discrete burrows commonly dolomitized (ferroan); medium equant dolomite/calcite void-filling cements.

Spiculitic Wackestone (0.7-2.5 m)

Bedding Characteristics: Ledge-forming, medium to thick-bedded; mottled medium to dark gray; black chert in discontinuous lenses and nodules; thoroughly bioturbated with ferroan dolomitized horizontal burrows; skeletal packstone lenses become more common toward top of lithofacies; gradual lower contact with underlying nodular mudstones and abrupt upper contact with overlying nodular mudstones.

Internal Composition/Texture: Alternating cm-scale mudstones/wackestones and subordinate lenses and wavy beds of skeletal packstones; wackestones are strongly burrow-homogenized; sponge spicules dominate with common trilobite and echinoderm debris; pellets associated with burrows; some admixed quartz silt; packstone lenses have erosive scoured bases and are composed of unbroken elongate skeletal debris and muddy intraclasts with occluded shelter porosity and perched peloidal muds; some grading is evident with lenses with mud drapes at the top; some gentle micro-cross-laminations of peloids with bidirectional orientations.

TABLE 4: SHALY DEEP RAMP / INTRASHELF BASIN LITHOFACIES

Flat Pebble Conglomerate (0.1-0.6 m)

Bedding Characteristics: Amalgamated irregular thin beds and lenses cap coarsening-upward cycles; scoured bases common into underlying peloidal grainstones and quartz siltstones; elongate clasts imbricated to edgewise to random orientations; mud drapes separate individual beds within amalgamated units; matrix includes skeletal debris and glauconite; abruptly overlain by shale (Nolichucky) or peloidal siltstone (Point Peak) lithofacies.

Internal Composition/Texture: Elongate rounded clasts typically composed of laminated peloidal grainstone and quartz siltstone of underlying lithofacies; clasts less commonly composed of skeletal packstone (Nolichucky) or micritic-spiculitic (Point Peak); many clasts have iron-stained rinds and are often bored; matrix between clasts consists of peloids and skeletal debris (abundant brachiopod-trilobite-echinoderm in Point Peak); quartz silt common; some occluded shelter porosity and perched peloidal muds.

Peloid Grainstone/Quartz Siltstone (0.4-2.0m)

Bedding Characteristics: Interlaminated calcareous siltstones and silty peloidal grainstones in thin irregular beds; internal parallel and hummocky cross-lamination; typically grades from quartz silty toward the base to dominantly peloidal grainstones at the top of the lithofacies; lower contact with shale lithofacies (Nolichucky Fm only) begins with very thin siltstone beds intercalated within the shale eventually becoming pure calcareous peloidal siltstone; this facies forms the base of the cycles in the Point Peak where they are platy bedded and less well-cemented but otherwise identical to the Nolichucky laminated peloidal quartz siltstones; *Cruziana* trace fossils; coarsens upward into amalgamated flat pebble conglomerates or, less commonly, skeletal-ooid packstones.

Internal Composition/Texture: Peloids and quartz silt are dominant grain types with subordinate finely-comminuted skeletal debris; some laminae show very fine normal grading; fine skeletal debris - dominantly echinoderms and trilobites.

Calcareous Shale (0.5-10.0 m)

Bedding Characteristics: Olive green to dark gray fissile shale; breaks into small chips upon separation suggesting bioturbation; random, very thin lime mudstone beds increase in frequency upward in the lithofacies; overlain by calcareous quartz siltstone lithofacies (Nolichucky) or thin nodular wackestone (Candland and Corset Springs); abruptly overlie flat pebble conglomerate / skeletal-ooid grainstone lithofacies or thrombolitic bioherms.

Internal Composition/Texture: Composed of clay-sized micas and associated clay minerals as well as calcareous micropeloids; occasionally fine trilobite and phosphatic brachiopod fragments.

Figure 5: Photograph of spiculitic wackestone-capped cycles of the deep ramp. Basal lithofacies is composed of argillaceous nodular wackestones and forms a recessive weathering pattern. Overlying ledge-forming cap consists of spiculitic wackestone with upward-increasing storm-deposited packstone lenses composed of open marine skeletal debris.

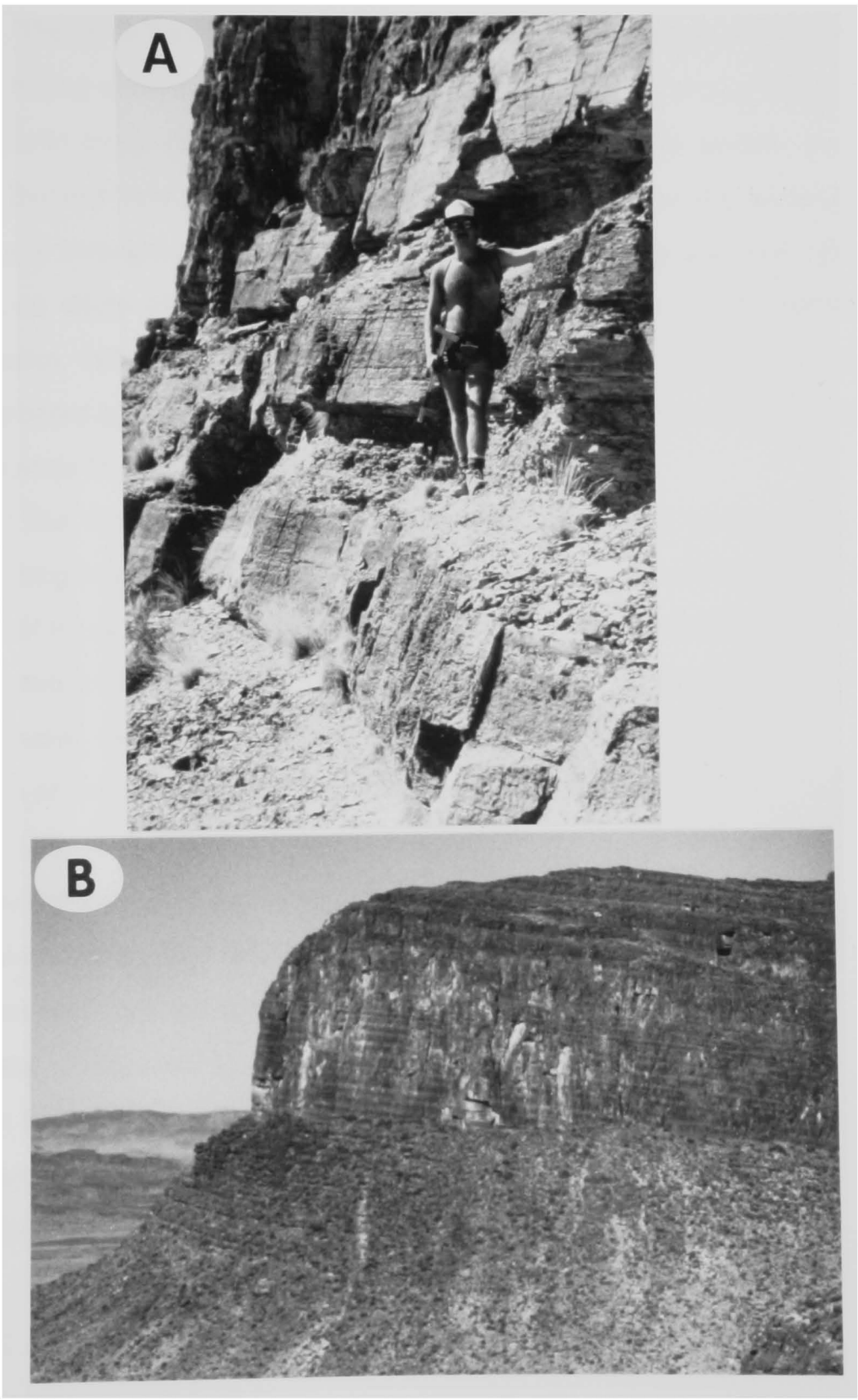
A
B

The thick basal shale units of these cycles formed below storm wave base during short periods of relative sea level rise that brought deep water siliciclastic clays up onto the carbonate platform. The fine clastics may have been derived from the craton.and were transported across the carbonate belt (perhaps through the House Range Embayment trough) and onto the deep ramp as dilute clouds or bottom-hugging nepheloid layers (Boardman and Neumann, 1984). Siliciclastic clays accumulated in a dysaerobic environment as indicated by the olive green to dark gray color, mildly bioturbated lamination, and sparse trilobite and phosphatic brachiopod fauna.

The thin carbonate caps of these shale-dominated cycles reflect rapid shallowing from shale to bioturbated wackestones up into skeletal packstones. A few of these cycles shallow up to large (1.5 x 1.5 m) thrombolitic bioherms that nucleated on flat pebble conglomerate storm beds. The abrupt transition in paleowater depths between the deep, quiet water shales (probable water depths of >40 to 60 m) and the shallow, clear water carbonates (probable water depths between 5 to 20 m) suggests that these cycles probably did not form by simple aggradation, which would provide a maximum of only 15 meters of shallowing, but rather experienced a relative sea level rise (shales) followed by relative sea level fall (carbonates). No evidence of subaerial exposure of the skeletal carbonates or the bioherms is recognized indicating that sea level never fell below the platform. With renewed relative short-term sea level rise, carbonate sedimentation ceased and the skeletal sands or bioherms were abruptly covered with sub-storm wave base shales.

Flat pebble conglomerate-capped shaly cycles, (0.8-5.5 m) consist of a basal calcareous green-brown shale grading upward into micro-hummocky

Figure 6: Late Cambrian shaly cycles of the Conasauga intrashelf basin of the Appalachians and of the Cordilleran deep ramp of Utah. Siliciclastic shales are abruptly overlain by "clear-water carbonates" with storm-deposited caps. Note the possible shallower position of storm wave base in the protected intrashelf basin.

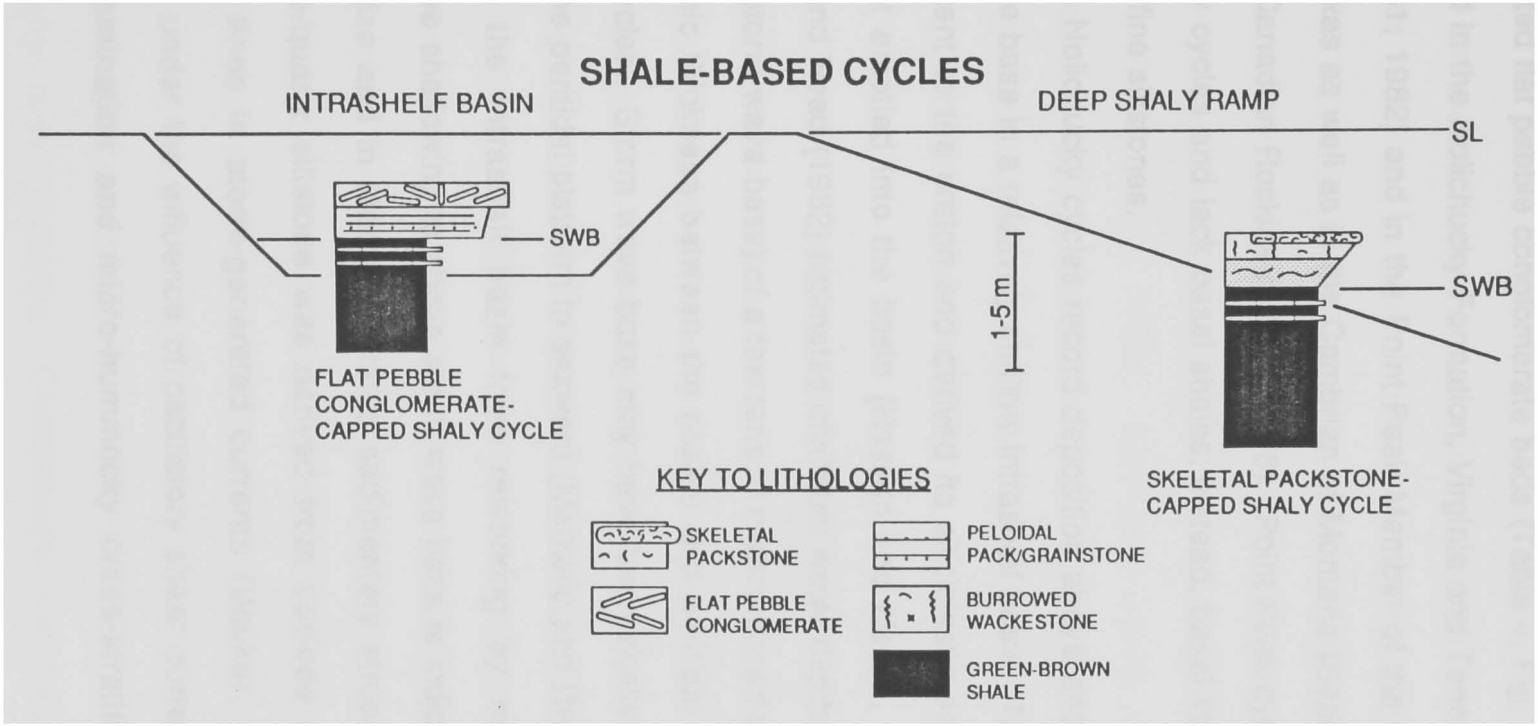
SHALE-BASED CYCLES
INTRASHELF BASIN
DEEP SHALY RAMP
SL
SWB
SWB
1-5 m
FLAT PEBBLE CONGLOMERATE-CAPPED SHALY CYCLE
SKELETAL PACKSTONE-CAPPED SHALY CYCLE
KEY TO LITHOLOGIES
SKELETAL PACKSTONE
PELOIDAL PACK/GRAINSTONE
FLAT PEBBLE CONGLOMERATE
BURROWED WACKESTONE
GREEN-BROWN SHALE

cross-laminated peloidal grainstones and quartz siltstones capped by amalgamated flat pebble conglomerate beds (Table 4; Fig. 6). They have been recognized in the Nolichucky Formation, Virginia and Tennessee (Markello and Read, 1981; 1982) and in the Point Peak Member of the Wilberns Formation, central Texas as well as in the Cambrian of Montana (Sepkoski, 1982) and the southern Canadian Rockies (Aitken, 1978). Point Peak cycles are thinner than Nolichucky cycles and lack basal shales; instead, basal lithofacies are parallel laminated fine siltstones.

The Nolichucky cycles record deposition above and below a fluctuating storm wave base in a relatively shallow intrashelf basin. The Conasauga basin was adjacent to the craton and derived its siliciclastic sediment from distant deltas that emptied into the basin (Hasson and Haase, 1988; Read, 1989). Markello and Read (1982) estimated minimum water depths for the shales (and therefore storm wave base) of a few tens of meters based on non-decompacted stratigraphic thickness between the shales and peritidal caps of shallowing-upward cycles. Storm wave base may have been shallow due to the barrier effect of the peritidal platform to seaward (Markello and Read, 1981; 1982) that protected the intrashelf basin from reworking by open ocean waves. Progressive shallowing to above storm wave base is indicated by an increase in grain size and in storm-generated sedimentary structures. The peloidal grainstone/quartz siltstone was derived from upslope and transported as entrained fines in storm-generated currents (Walker, 1984). They were deposited under the influence of oscillatory shear currents as indicated by parallel lamination and micro-hummocky cross-stratification. *Cruziana*

ichnofossils reflect increased oxygenation of the intrashelf basin as it shallowed.

The flat pebble conglomerate caps of the cycles were deposited above storm wave base during severe storms when the underlying semi-lithified peloidal grainstone was eroded and redeposited as tabular to lenticular beds of rounded, elongate clasts. Early marine cementation of the peloidal grainstone may have been facilitated by a lack of diverse burrowing infauna during the Late Cambrian (Sepkoski, 1982). Multi-generational clasts and thin mud drapes that separate conglomeratic beds within amalgamated units were formed by multiple storm deposition. Diverse fauna within the matrix between clasts reflects normal marine conditions.

SCALES OF CYCLICITY

Late Cambrian meter-scale cycles are grouped into shallowing-upward successions at the fourth-order scale (0.1 - 1.0 m.y.; 10's of meters) as well as at the third-order scale (1.0 - 10.0 m.y.; 10's to 100's of meters). For example, the Big Horse Member of the Orr Formation of the House Range (Fig. 7) comprises one long-term third-order shallowing-upward sequence (220 m thick; approximately 4 m.y. duration) composed of deep ramp cycles gradually shallowing up to oolite-capped shallow ramp cycles with large thrombolite bioherms. This long-term sequence has superimposed within it 11 fourth-order depositional cycles (average of 360 k.y.) that are characterized by gradual shallowing from deeper ramp lithofacies to shallow ramp lithofacies over stratigraphic thicknesses of 10's of meters followed by rapid transition back into thick, deeper ramp lithofacies. Characteristic meter-scale fifth-order cycles

Figure 7: Scales of cyclicity within the Big Horse Member of the Orr Formation of the House Range, Utah. Column on the left shows long-term third-order shallowing evident from the storm-influenced mid-ramp cycles with open marine faunas in the lower Big Horse that progressively give way to shallow subtidal cycles characterized by restricted lithofacies upward in the Big Horse Member. Dashes to the right of this column denote interpreted fourth-order cycles that are expanded in the columns on the right. Dashes to right of columns denote fifth-order cycles. Composition of the fourth-order cycles suggests rapid deepening in the basal cycle followed by progressively shallower conditions toward the upper cycles.

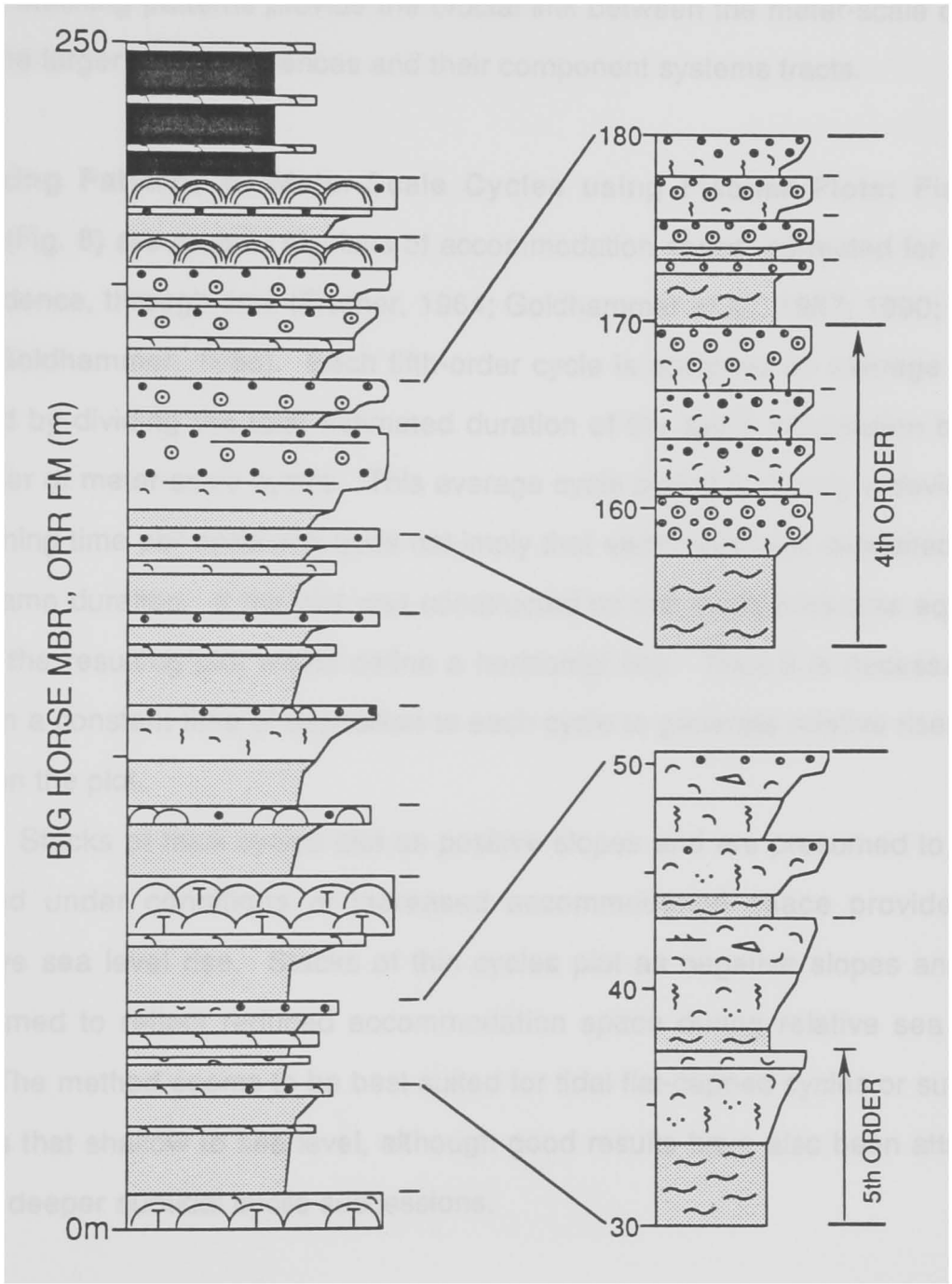
250
0m
BIG HORSE MBR., ORR FM (m)
180
170
160
4th ORDER
50
40
30
5th ORDER

systematically change upward within the third- and fourth-order sequences. Cycle stacking patterns provide the crucial link between the meter-scale cycles and the larger scale sequences and their component systems tracts.

Stacking Patterns of Meter-Scale Cycles using Fischer Plots: Fischer plots (Fig. 8) are graphic displays of accommodation space, corrected for linear subsidence, through time (Fischer, 1964; Goldhammer et al., 1987; 1990; Read and Goldhammer, 1988). Each fifth-order cycle is assigned an average cycle period by dividing the total estimated duration of the cyclic succession by the number of meter-scale cycles. This average cycle period is merely a device for assigning time per cycle and does not imply that each cycle was deposited over the same duration. If the plot was constructed so that cycle thickness equaled time, the resulting plot would define a horizontal line. Thus it is necessary to assign a constant time of deposition to each cycle to generate relative rises and falls on the plot.

Stacks of thick cycles plot as positive slopes and are presumed to have formed under conditions of increased accommodation space provided by relative sea level rise. Stacks of thin cycles plot as negative slopes and are presumed to reflect reduced accommodation space during relative sea level fall. The method seems to be best suited for tidal flat-capped cycles or subtidal cycles that shallow to sea level, although good results have also been attained using deeper subtidal cyclic successions.

Fischer Plots and Peritidal Successions: The relationship between cyclic peritidal carbonates of the Conococheague Formation of southwestern Virginia

Figure 8: Explanatory diagram of the Fischer plot technique. The horizontal scale of the plot represents time and the vertical scale is the cumulative cycle thickness in meters. For each cycle the amount of accommodation space provided by linear subsidence is plotted over the duration of the average cycle period. Cycle thickness is plotted vertically. The net difference defines the path of relative sea level through time.

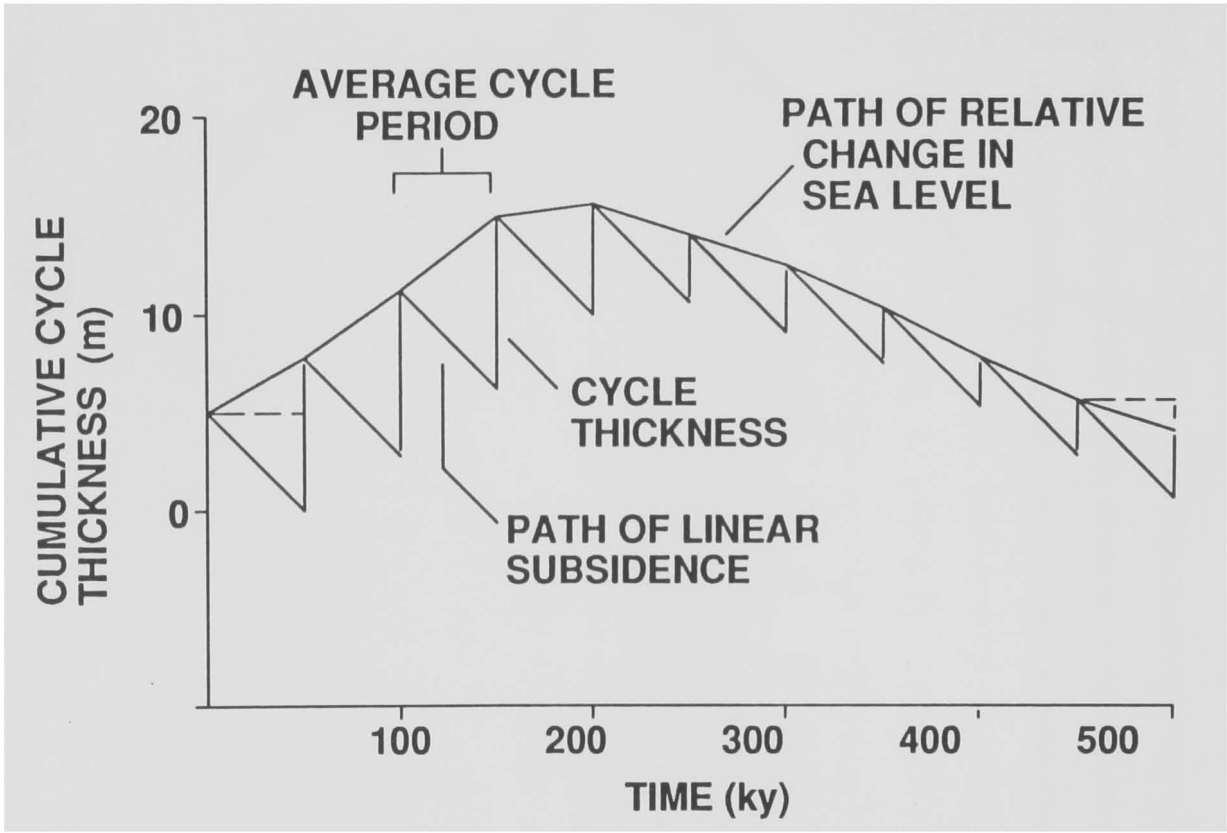
AVERAGE CYCLE PERIOD
PATH OF RELATIVE CHANGE IN SEA LEVEL
CUMULATIVE CYCLE THICKNESS (m)
20
10
0
CYCLE THICKNESS
PATH OF LINEAR SUBSIDENCE
100
200
300
400
500
TIME (ky)

Figure 9: Fischer plot of the Conococheague Formation constructed from the Wytheville, Virginia section (from data in Koerschner and Read, 1989). Cycles containing quartz sand are black. Stacking patterns of representative cycles are shown pulled out from their position on the Fischer plot. Note the difference in scales between the three columns of cycles and how the subtidal-dominated cycles are considerably thicker than the tidal flat-dominated cycles.

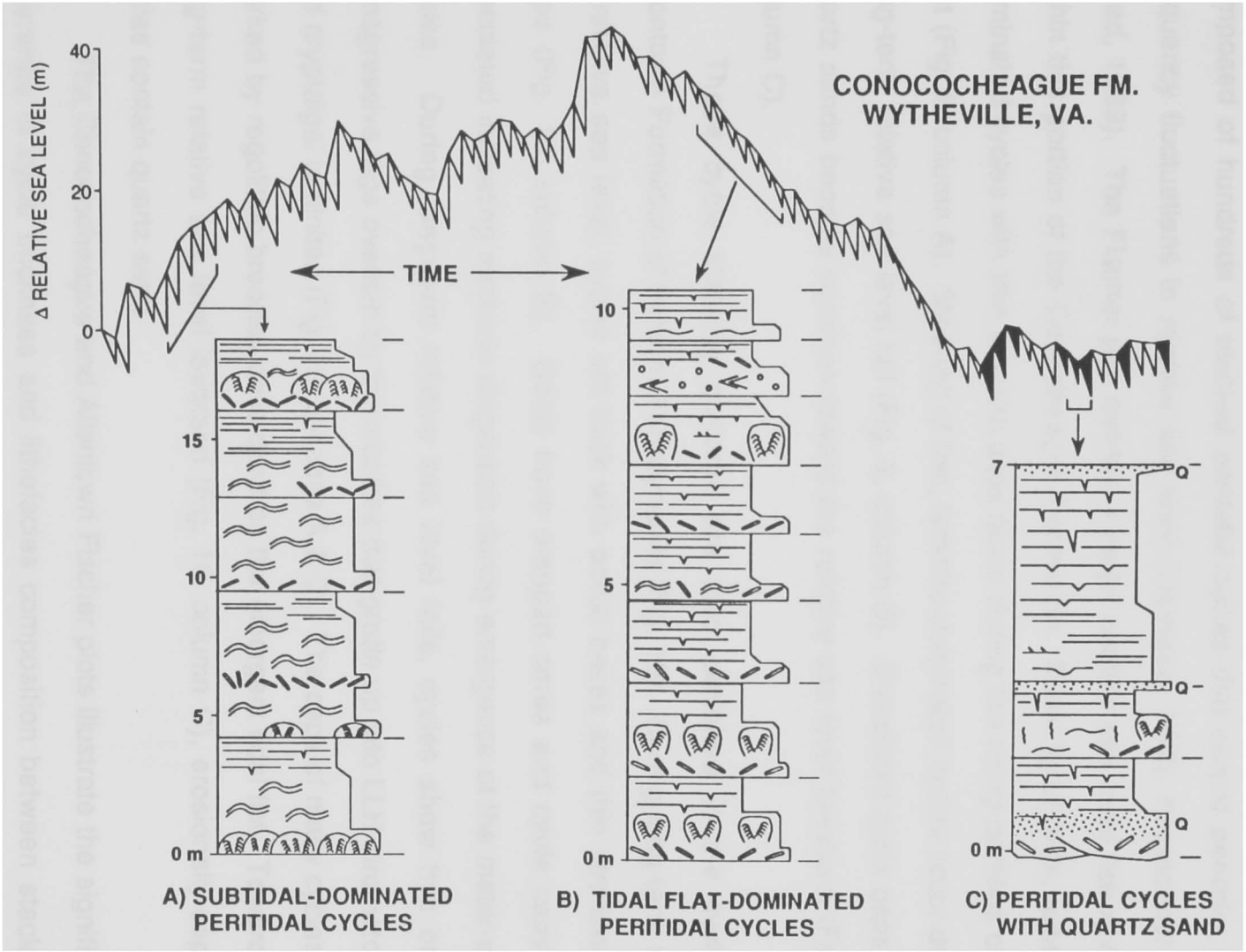
CONOCOCHEAGUE FM.
WYTHEVILLE, VA.
Δ RELATIVE SEA LEVEL (m)
40
20
0
TIME
15
10
5
0 m
10
5
0 m
7
Q
Q
Q
0 m
A) SUBTIDAL-DOMINATED PERITIDAL CYCLES
B) TIDAL FLAT-DOMINATED PERITIDAL CYCLES
C) PERITIDAL CYCLES WITH QUARTZ SAND

and long-term relative sea level cycles defined by its Fischer plot (Koerschner and Read, 1989) is shown in Figure 9. The Conococheague Formation is composed of hundreds of stacked peritidal cycles that record periodic, high frequency fluctuations in relative sea level (Demicco, 1985; Koerschner and Read, 1989). The Fischer plot defines a major relative sea level rise and fall within this portion of the Conocheague Formation. Stacking of thick, subtidal-dominated cycles with thin laminite caps occur during the rising portions of the plot (Fig. 9, column A). Stacking of thin, laminite-dominated cycles occur during long-term relative sea level fall (Fig. 9, column B). Brecciated cycle caps and quartz sands become common toward the relative sea level lowstand (Fig. 9, column C).

These cycle stacking patterns are also exhibited in the peritidal Allentown Formation of eastern Pennsylvania (Fig. 10). During long-term rises in relative sea level, cycles are thick with oolitic bases and thin stromatolitic caps (Fig. 10, column B). Ooids have dropped cores and cycle caps are brecciated indicating meteoric diagenesis during emergence of the meter-scale cycles. During long-term relative sea level falls, cycles show thin oolitic transgressive lags overlain by thrombolites that grade up into LLH stromatolites and cryptalgal laminites (Fig. 10, columns A & C). The caps of many cycles are marked by regolithic breccias developed on the emergent tidal flat. Toward the long-term relative sea level lowstand (Fig. 10, column C), erosionally-capped cycles contain quartz sand.

The Conococheague and Allentown Fischer plots illustrate the significant difference in cycle thickness and lithofacies composition between stacks of cycles on the rising and falling portions of the plots. Peritidal cycle thickness is

Figure 10: Fischer plot of the lower Allentown Formation constructed from the Easton, Pennsylvania section with cycle stacking patterns expanded from their position on the plot. Note the variation in scales between the three sections and the relative thickness of the component cycles. Oolitic grainstone bases of cycles on the rising portions of the Fischer plot are considerably thicker than those on the falling portions. Tidal flat caps are considerably thinner on cycles that formed during the relative sea level rise but dominate in the cycles that formed on the relative sea level fall.

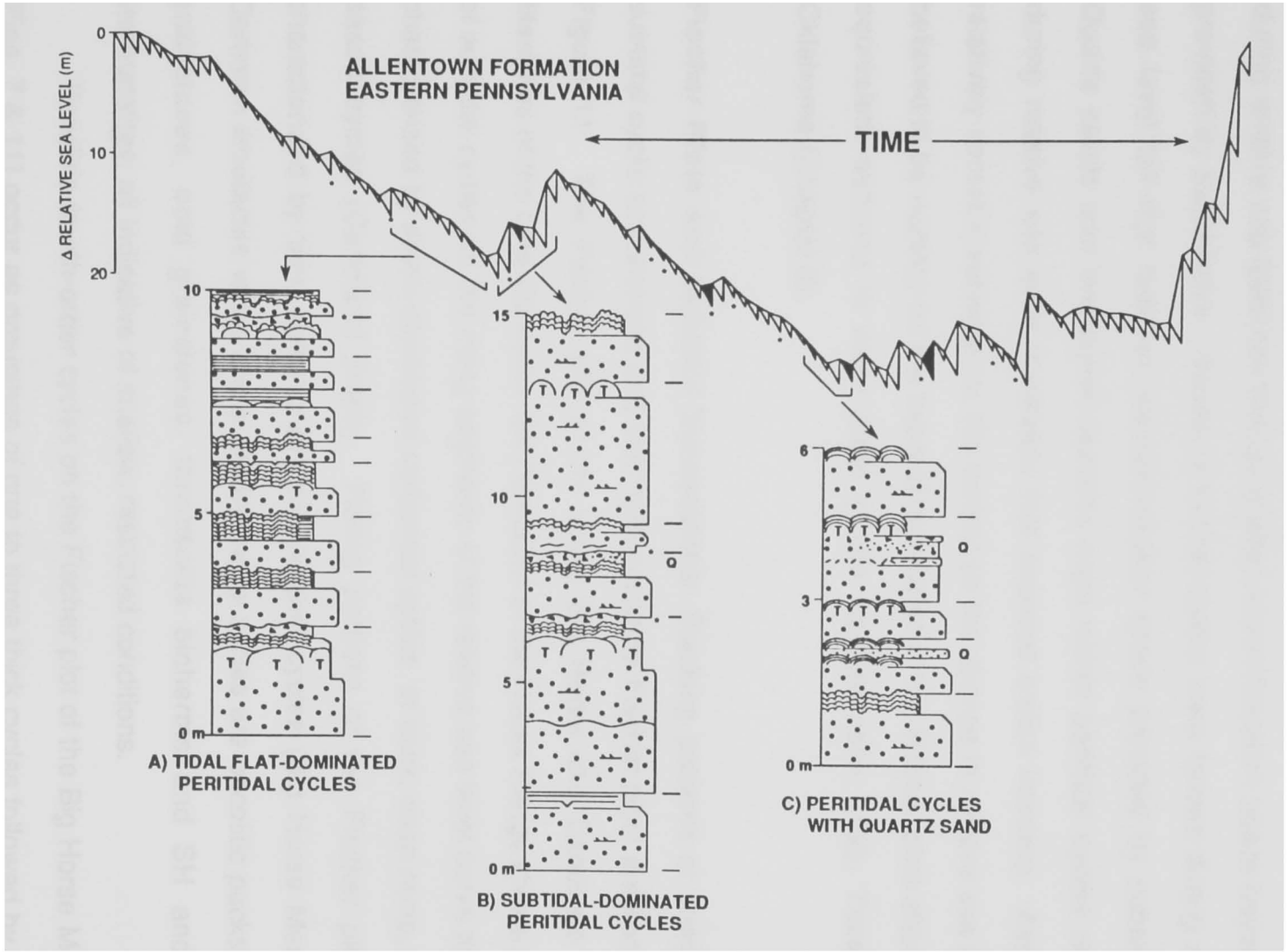
ALLENTOWN FORMATION
EASTERN PENNSYLVANIA
TIME
Δ RELATIVE SEA LEVEL (m)
0
10
20
10
5
0 m
A) TIDAL FLAT-DOMINATED
PERITIDAL CYCLES
15
10
5
0 m
Q
B) SUBTIDAL-DOMINATED
PERITIDAL CYCLES
6
3
0 m
Q
Q
C) PERITIDAL CYCLES
WITH QUARTZ SAND

controlled by the total amount of accommodation space provided by subsidence and eustacy. For these peritidal cycles, stacks of thicker cycles were formed during relative sea level rise that generated accommodation space beyond that provided by subsidence. Stacks of thinner cycles were formed during relative sea level fall that reduced accommodation space provided by subsidence. Quartz sands and brecciated laminite caps within peritidal cycles occured during relative sea level lowstands that exposed craton interiors. Assuming relatively constant subsidence, the control on the change in relative sea level is believed to be eustacy on the basis of correlation of the Fischer plots above with equivalent sections in other parts of the Appalachians, Utah, Texas and Oklahoma (Chapter 2).

Fischer Plots and Subtidal Successions: Stacking patterns of dominantly subtidal cyclic successions and their relationship to Fischer plots are shown on Figure 11. The Fischer plot of the upper Big Horse and Candland Shale Members of the Late Cambrian Orr Formation of the House Range shows stacks of subtidal cycles on the rising segments of the relative sea level curve that are characterized by storm-dominated carbonate cycles or thick, deep ramp, shale-based cycles (Candland Shale). Falling portions of the Fischer plot are characterized by thin, oolite grainstone-capped cycles (Big Horse Member). Common lithofacies within these shallow ramp cycles are oncolitic packstones-grainstones, ooid grainstones, thrombolite bioherms and SH and LLH stromatolites, all indicative of shallow, restricted conditions.

Possible fourth-order cycles on the Fischer plot of the Big Horse Member (Figs. 7 & 11) occur as groupings of one to three thick cycles followed by two to

Figure 11: Fischer plot of the upper Big Horse and Candland Shale Members of the Orr Formation, House Range, Utah. The scale is the same for all three stacks of cycles; note the thin shallow subtidal restricted cycles versus the substantially thicker deeper subtidal open marine carbonate and shaly cycles. Subtle bundling of fourth-order cycles (labelled) can also be discerned along the Fischer plot.

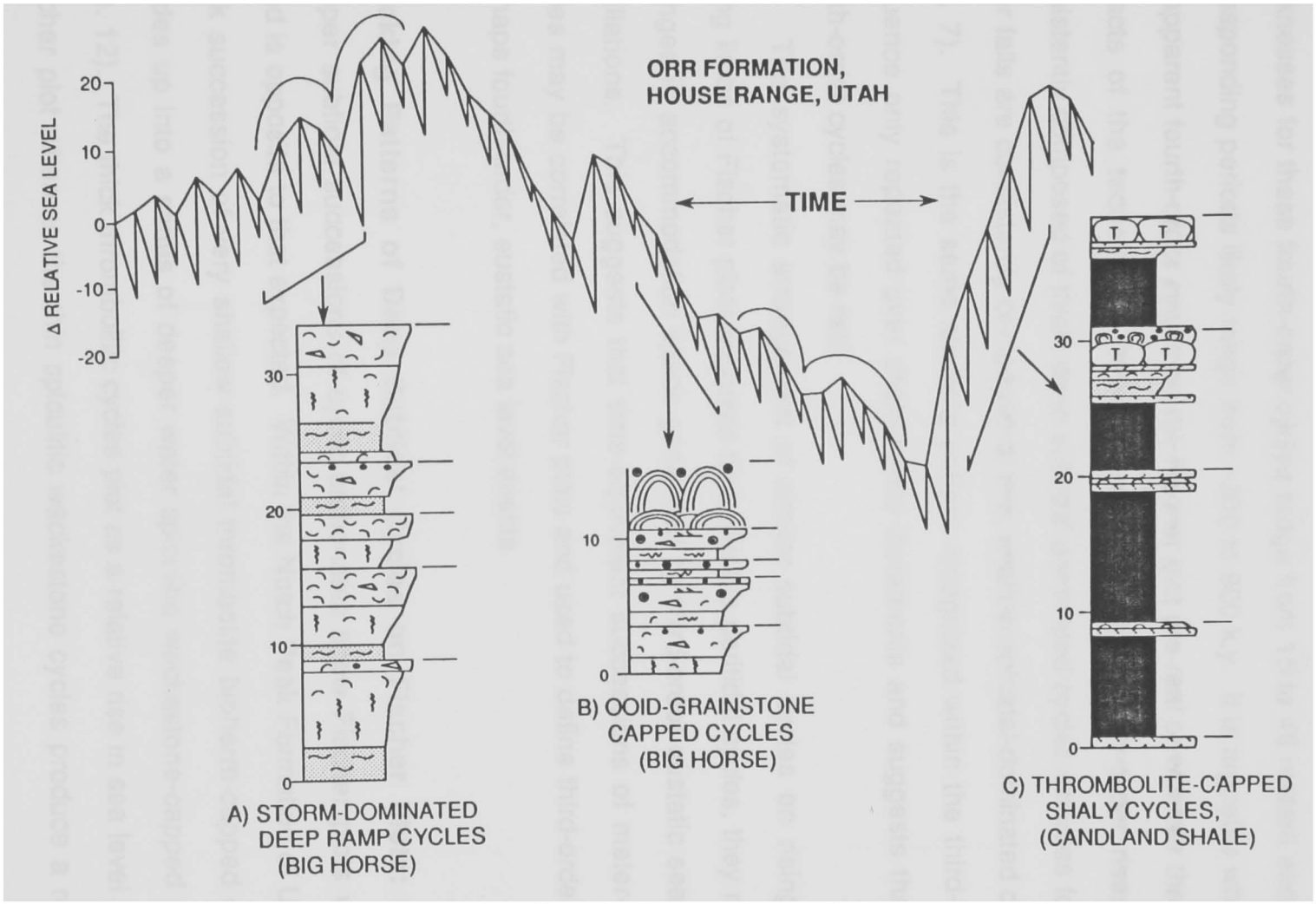
ORR FORMATION,
HOUSE RANGE, UTAH
TIME
Δ RELATIVE SEA LEVEL
20
10
0
-10
-20
30
20
10
0
A) STORM-DOMINATED
DEEP RAMP CYCLES
(BIG HORSE)
10
0
B) OOID-GRAINSTONE
CAPPED CYCLES
(BIG HORSE)
T
T
T
T
30
20
10
0
C) THROMBOLITE-CAPPED
SHALY CYCLES,
(CANDLAND SHALE)

seven thinner cycles that show no obvious internal bundling of fifth-order cycles. Thicknesses for these fourth-order cycles range from 15 to 45 meters and their corresponding periods likely range from ~300 to 900 k.y. It is arguable whether the apparent fourth-order cycles on the Fischer plot are real or whether they are artifacts of the technique. However, cycles on the fourth-order rises are consistently composed of thick, deep subtidal-dominated cycles whereas fourth-order falls are consistently composed of thin, shallow subtidal-dominated cycles (Fig. 7). This is the same stacking pattern recognized within the third-order sequence only repeated over shorter time increments and suggests that the fourth-order cycles may be real.

The systematic arrangement of similar subtidal cycles on rising and falling limbs of Fischer plots suggests that, like the peritidal cycles, they record changes in accommodation space generated by third-order eustatic sea level oscillations. This suggests that time-equivalent successions of meter-scale cycles may be correlated with Fischer plots and used to define third-order, and perhaps fourth-order, eustatic sea level events

Stacking Patterns of Deep Subtidal Cycles on Fischer Plots: Some deeper subtidal successions of cyclic carbonates show Fischer plots whose trend is opposite to that expected. Within the Notch Peak Formation of Utah, a thick succession of very shallow subtidal thrombolite bioherm-capped cycles grades up into a series of deeper water spiculitic wackestone-capped cycles (Fig. 12). The thick thrombolitic cycles plot as a relative rise in sea level on the Fischer plot whereas the thin spiculitic wackestone cycles produce a relative fall.

Figure 12: Vertically-oriented Fischer plot of the upper Notch Peak Formation, House Range, Utah. Dashes to right of column indicate cycle tops. Groups of like cycles are noted with arrows. Key horizons are connected to the Fischer plots by the dashed lines; they are not perfectly horizontal because the stratigraphic column is in thickness and the Fischer plot is in time. Relative water depth curve to the right is shown for comparison.

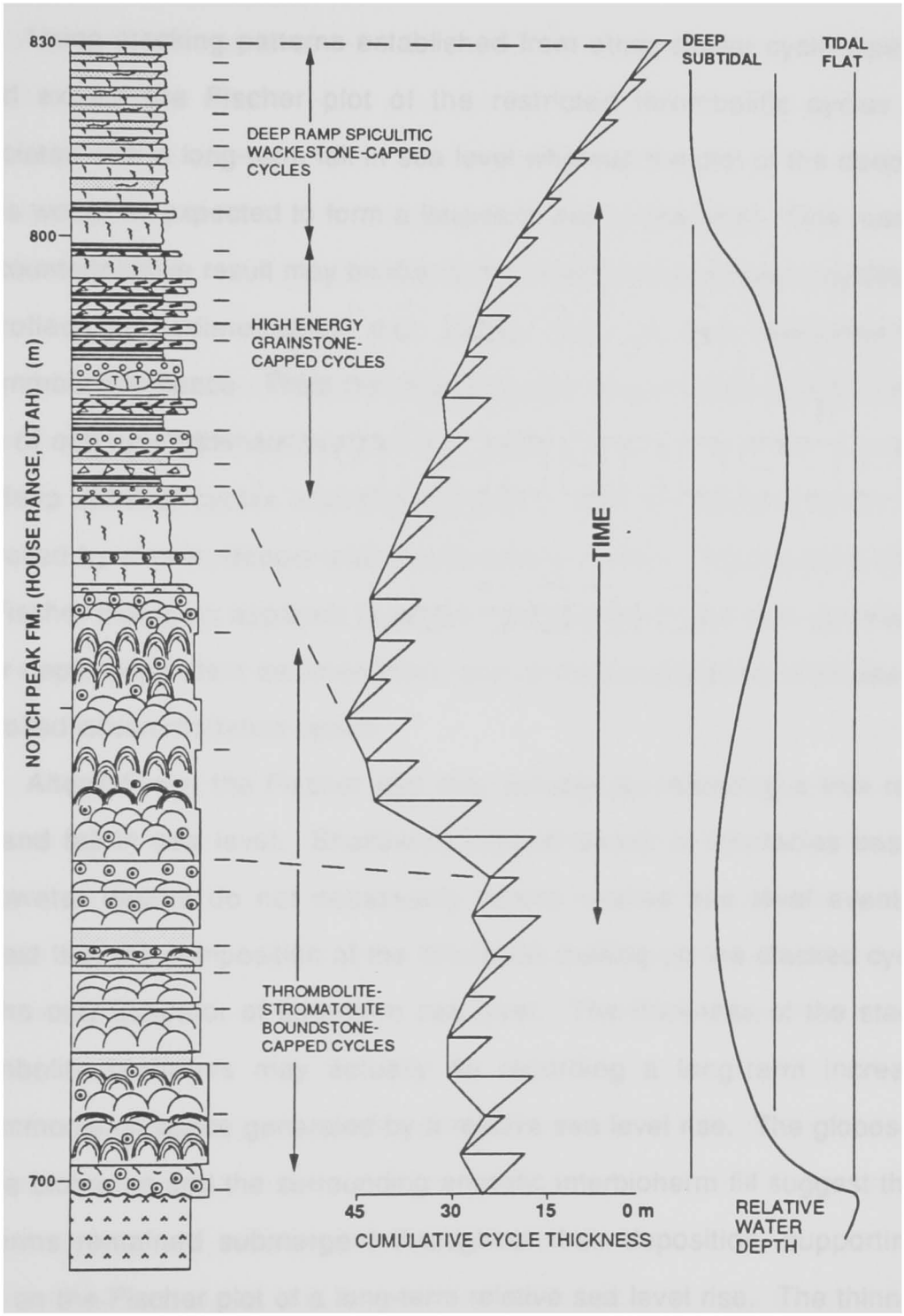
830
800
700
NOTCH PEAK FM., (HOUSE RANGE, UTAH) (m)
DEEP RAMP SPICULITIC WACKESTONE-CAPPED CYCLES
HIGH ENERGY GRAINSTONE-CAPPED CYCLES
THROMBOLITE-STROMATOLITE BOUNDSTONE-CAPPED CYCLES
TIME
DEEP SUBTIDAL
TIDAL FLAT
45
30
15
0 m
CUMULATIVE CYCLE THICKNESS
RELATIVE WATER DEPTH

Using stacking patterns established from other similar cycle types, one would expect the Fischer plot of the restricted thrombolitic cycles to be associated with a long-term fall in sea level whereas the plot of the deep water cycles would be expected to form a long-term rise in sea level. One reason for this counterintuitive result may be due to the relative thicknesses of cycles being controlled by sedimentation rate rather than by sea level-determined accommodation space. Thick thrombolitic cycles accumulated rapidly within the zone of optimal carbonate productivity, rapidly filling to sea level. In contrast, the deep subtidal cycles accumulated slowly; their thickness may be strictly controlled by slower, deeper-water sedimentation rates. The resulting trend on the Fischer plot is an apparent long-term rise and fall in sea level generated by water depth-dependent sedimentation rates of the cycles rather than sea level-controlled accommodation space.

Alternatively, the Fischer plot may actually be reflecting a true relative rise and fall in sea level. Shallowing-upward trends of lithofacies based on paleowater depths do not necessarily record relative sea level events and suggest that the composition of the lithofacies making up the stacked cycles is not the only indicator of long-term sea level. The thickness of the stacks of thrombolite bioherms may actually be recording a long-term increase in accommodation space generated by a relative sea level rise. The globose tops on the bioherms and the surrounding oncolitic interbioherm fill suggest that the bioherms remained submergent throughout their deposition, supporting the trend on the Fischer plot of a long-term relative sea level rise. The thinness of the argillaceous deeper water cycles may be a reflection of reduced

sedimentation rates caused by siliciclastic poisoning by clays brought in during long-term eustatic sea level fall. Time-equivalent cycles in the Appalachians contain abundant quartz sand derived from the craton during sea level lowstands. Fischer plots of these time-equivalent cyclic successions in both the Cordillera and the Appalachians can be correlated and show similar trends of long-term sea level rise and fall toward the end of the Late Cambrian (Chapter 2).

A third option for explaining the apparent rise and fall on the Fischer plot of the upper Notch Peak Formation produced by these cycles is the non-recognition of cycle tops. The thrombolitic cycles can be very thick because they commonly are composed of stacked thrombolite bioherms (3 to 5 levels over 12 meters) that become more stromatolitic upward. The possibility exists for internal cyclicity within these cycles but no unequivocal evidence for tidal flat deposition, subaerial exposure or vadose diagenesis can be recognized through the dolomitization. Without clear evidence for internal cyclicity within the stacked bioherms, cycle caps must be placed at the base of the overlying bedded peloidal packstones that manifest short-term drowning events and the initiation of a new cycle. Dividing the thick thrombolitic cycles up into more numerous thinner cycles would produce an entirely different form on the Fischer plot.

On the basis of correlations with Fischer plots of equivalent strata in the Appalachians, the trend on the Fischer plot of upper Notch Peak time may actually be reflecting a long-term sea level rise and fall. However, the role of sedimentation rate as well as the non-recognition of cycle boundaries may also contribute to trends on Fischer plots of subtidal cycles, distorting the relative sea

level history. This example from the upper Notch Peak Formation illustrates the caution that must be exercised when interpreting Fischer plots without looking at the internal composition of the cyclic succession.

MECHANISMS CONTROLLING CYCLE STRATIGRAPHY

Mechanisms proposed to explain the genesis of meter-scale carbonate cycles have focussed on tidal flat-capped cycles common throughout the rock record. The recognition of shallow to deep subtidal cycles that formed simultaneously with peritidal cycles requires some modification of the mechanisms proposed for the peritidal cycles. Three models have been suggested to explain the origin of shallowing-upward, meter-scale cycles: 1) autocyclicity, 2) episodic subsidence, and 3) high frequency oscillations in eustatic sea level. Each of the proposed mechanisms must explain the upward shallowing of individual cycles, the repetitive stacking of similar cycles throughout a vertical sequence, and the simultaneous development of tidal flat-capped cycles and subtidal cycles across a carbonate platform.

Autocyclicity: The autocyclic model (Ginsburg, 1971; Wilkinson, 1982; James, 1984) depends upon the periodic progradation of tidal flats over the subtidal carbonate factory to restrict the size of the carbonate source area, effectively shutting down carbonate production until tectonic subsidence provides water depths sufficient to resume production. Implicit in the model are the assumptions of static sea level over geologically long periods of time, complete shoaling to tidal levels and a lack of vadose diagenetic features within cycles. Weaknesses in this model (Grotzinger, 1986; Read, 1989) have focussed on the

inordinately long lag times (>20 k.y.) necessary for the creation of water depth sufficient to resume carbonate production. Perhaps the biggest drawback to autocyclic control is the simultaneous development of purely subtidal cycles that, by definition, have no progradational tidal flat cap that could relate to shrinking of the carbonate factory (Grotzinger, 1986). The inability of the autocyclic model to explain incomplete shallowing of subtidal cycles that develop seaward of peritidal cycles precludes it as a potential controlling process on Late Cambrian cycle development. Autocyclic mechanisms may only be viable as an explanation for stratigraphic "noise" *within* individual cycles and do not control the development of repetitive stacks of cycles or the synchronous development of peritidal and subtidal cycles thoughout the Late Cambrian platforms.

A variation on the autocyclic model has been proposed (Cloyd et al., 1990) that invokes the lateral migration of tidal channels to produce shallowing-upward, tidal flat-capped cycles. As with the progradational model, variations in sediment accumulation and redistribution may contribute to variability within peritidal cycles but cannot explain the origin of regional subtidal cycles. However, processes intrinsic to the subtidal platform (sediment redistribution by storm and wave energy, hardground formation during non-depositional events and oceanographic conditions) do occur and should not be neglected as contributing to the internal composition of subtidal cycles (Chapter 3).

Episodic Tectonism: Repeated pulses of downfaulting have been proposed (Hardie et al., 1986; Cisne, 1986) to generate the accommodation potential for sediment aggradation. If the stress limits between faulting episodes were

rhythmic based on some threshold value, then this model could conceivably explain the coexistence of peritidal and subtidal cycles. However, the lateral extent of such events would be extremely limited and could not explain the widespread nature of carbonate cycles across entire platforms (Demicco, 1985; Grotzinger, 1986; Hardie and Shinn, 1986). Additionally, modern examples of tectonic pulsing (Yeats, 1978; Ota et al., 1984; Bull and Cooper, 1986) are restricted to tectonically active settings such as Southern California and New Zealand, poor analogs for ancient mature passive margins such as existed during Late Cambrian time. Other tectonic mechanisms such as intraplate stress mechanisms (Cloetingh, 1986) are much too slow (0.01 - 0.1 m/ky) and non-periodic to produce high frequency meter-scale cycles.

Eustatic Sea Level Oscillations: High frequency oscillations in sea level, probably controlled by fluctuations in glacial ice volume, provide the simplest explanation for the origin of meter-scale peritidal and subtidal cycles (Fischer, 1964; Matthews, 1984; Goodwin and Anderson, 1985; Goldhammer et al., 1987; Koerschner and Read, 1989; numerous others). Considering the evidence for eustatic control on third-order sequence development (Chapter 2; Vail et al., 1977; Haq et al., 1987; Ross and Ross, 1988), it seems likely that higher frequency sea level fluctuations were superimposed on the longer-term sea level events and, by association, were also eustatic in origin. Superimposed orders of eustatic sea level oscillations provide the best explanation for the upward shallowing of individual cycles, stacking patterns within cyclic successions, and the simultaneous development of peritidal cycles and subtidal cycles across a carbonate platform.

Milankovitch-Controlled Glacio-Eustacy: Although it seems clear that sea level had to have fluctuated eustatically to generate individual meter-scale cycles as well as stacked cyclic successions, the forcing mechanism behind high frequency sea level oscillations is far from certain. It has been proven that Plio-Pleistocene sea levels fluctuated in response to variations in global ice volume as a function of changes in solar insolation forced by Milankovitch astronomical rhythms (Hays et al., 1976; Berger, 1977; Berger et al., 1984). By association of having extensive continental glaciation and periods that cluster around the long eccentricity cycle, the Permo-Carboniferous cyclothems have been suggested to have been controlled by Milankovitch orbital modulation (Wanless and Shepard, 1936; Heckel, 1986). However, proving Milankovitch control on stratigraphic cyclicity in ancient rock sequences deposited during times of more equable climates and no major glaciations has been elusive. Olsen (1986) and Anderson (1986) used varve-calibrated sedimentation rates to show Milankovitch periodicities for rocks of Triassic and Permian age, respectively. Goldhammer and others (1987) used a 5:1 recurrence ratio of meter-scale cycles within megacycles, representing the precession signal modulated by the short eccentricity signal, to prove Milankovitch control of Triassic cycles. However, other attempts at showing a Milankovitch influence on ancient cyclic sequences have depended upon the average periodicities of cycles that roughly coincide with one of the Milankovitch periods of 19 - 23 k.y., 41 k.y., 95 - 123 k.y. or 413 k.y. As cautioned by Hardie and Shinn (1986), Algeo and Wilkinson (1986) and Klein (1990), calculations of average cycle

period are meaningless in terms of identifying a controlling mechanism on cycle formation.

An objective way of determining cycle periods is by spectral analysis of cyclic successions where dominant periodicities can be extracted and ratios between the periods can be used to establish Milankovitch control (Schwarzacher, 1975; Schwarzacher and Fischer, 1982; Arthur et al., 1984; Herbert and Fischer 1986; Kominz and Bond, 1989). An inherent weakness of the method, when used for ancient rocks with poor age control, is the difficulty of calibrating peaks on the spectral plot using long-term accumulation rates that are dependent upon the radiometric time scale with its large margins of error. In addition, the assumption of constant sediment accumulation throughout the duration of the cyclic sequence precludes the use of peritidal cycles, where much of the cycle period is taken up by non-deposition (Read et al., 1986; Goldhammer et al., 1987; 1990). However, stacks of deep subtidal cycles provide a good data set for time series analysis since accumulation is probably relatively constant.

Peritidal and Subtidal Cycle Durations: A rough estimate of the range of cycle periods can be made from the histograms of cycle thickness per cycle type (Fig. 13). Although no systematic trend between average cycle period and cycle position on the platform is recognized, periods estimated from cycle thickness range from roughly 40 to almost 150 k.y. (Table 5) Taking a conservative margin of error into account, about 50%, this range of periods may extend from about 20 to 225 k.y., the normal range expected for meter-scale cycles (Algeo and Wilkinson, 1986).

Figure 13: Histograms of the frequency of cycle thickness per cycle type. All thicknesses are non-decompacted except for the intrashelf basin and deep ramp shaly cycles which were decompacted by 50%. Histograms A through D are from the Orr Formation, House Range, Utah and E is from the Nolichucky Formation, Duffield, Virginia. A) Oolitic grainstone-capped shallow subtidal cycles. B) Skeletal packstone-capped mid-ramp cycles. C) Spiculitic wackestone-capped deep ramp cycles. D) Skeletal packstone-capped shaly cycles deep ramp cycles. E) Flat pebble conglomerate-capped shaly intrashelf basin cycles.

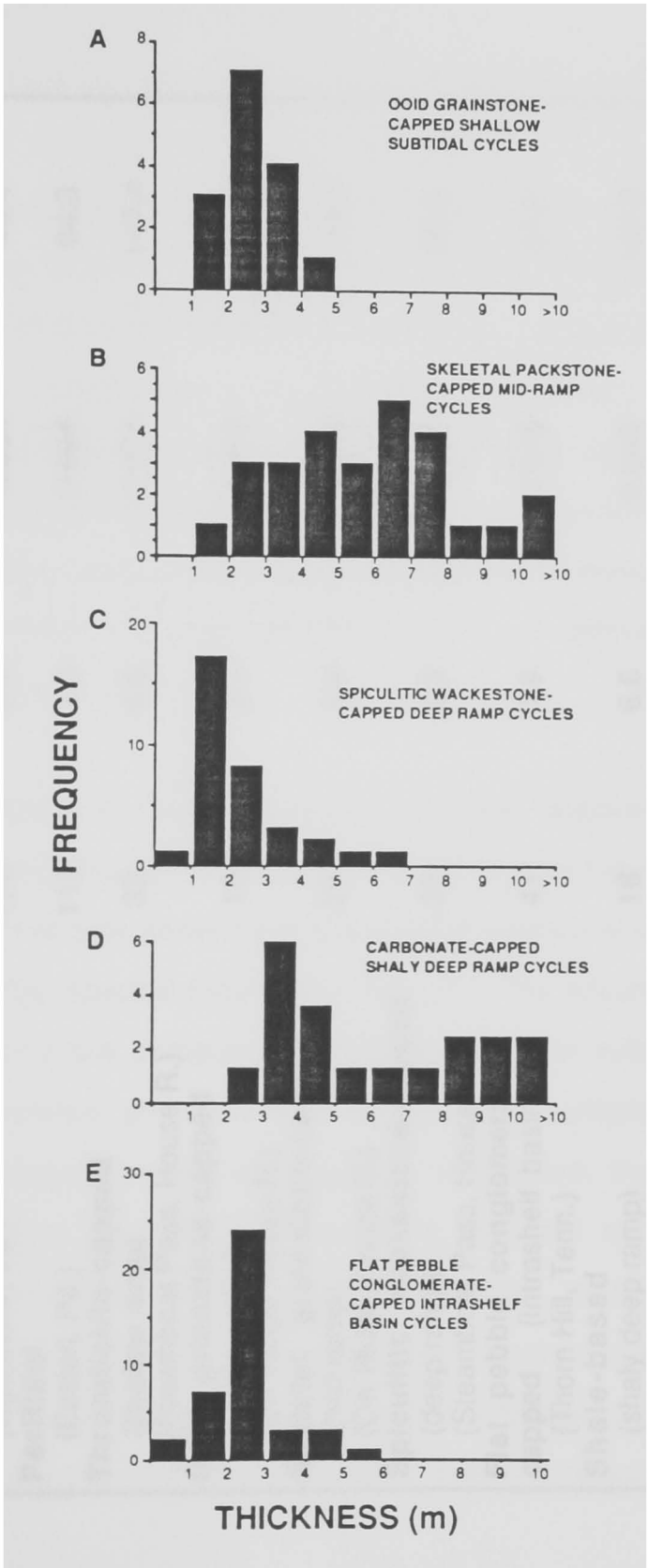
A
OOID GRAINSTONE-
CAPPED SHALLOW
SUBTIDAL CYCLES
B
SKELETAL PACKSTONE-
CAPPED MID-RAMP
CYCLES
C
SPICULITIC WACKESTONE-
CAPPED DEEP RAMP CYCLES
FREQUENCY
D
CARBONATE-CAPPED
SHALY DEEP RAMP CYCLES
E
FLAT PEBBLE
CONGLOMERATE-
CAPPED INTRASHELF
BASIN CYCLES
THICKNESS (m)

TABLE 5

Cycle Type	Number of Cycles	Average Cycle Thk (m)	Subsidence Rate (m/ky)	Average Cycle Period (ky)
Peritidal (Wytheville, Va.)	129	2.4	0.054	44.4
Peritidal (Easton, Pa.)	113	1.8	0.028	64.3
Thrombolite-capped (shallow ramp) (Steamboat Pass, House R.)	32	5.6	0.038	147.4
Ooid grainstone-capped (shallow ramp) (Orr Ridge, House R.)	15	2.9	0.048	60.4
Skeletal grainstone-capped (mid-ramp) (Orr Ridge, House R.)	27	5.8	0.048	120.8
Spiculitic wackestone-capped (deep ramp) (Steamboat Pass, House R.)	33	2.3	0.038	60.5
Flat pebble conglomerate-capped (intrashelf basin) (Thorn Hill, Tenn.)	41	1.6	0.026	61.5
Shale-based (shaly deep ramp) (Orr Ridge, House R.)	18	6.6	0.048	137.5

* Subsidence rates and cycle thicknesses non-decompacted.
* ±50% margin of error on the subsidence rate and average cycle period estimates.

Any estimate of cycle duration based on cycle thickness has broad margins of error. First, calculations of long-term accumulation rate (Table 5) are dependent upon absolute age dates of rocks that have wide error bars (± 30 m.y. for the Late Cambrian using the DNAG scale; Palmer, 1983). Another major source of error is the effect of compaction on estimations of time based upon thickness. Additionally, using stratigraphic thickness to estimate cycle period assumes constant sedimentation rate throughout the duration of a cyclic succession (Algeo and Wilkinson, 1986; Read and Goldhammer, 1988). This problem is probably more acute in cyclic successions of mixed cycle types that formed within different depositional environments with different sedimentation rates.

Spectral Analysis of Late Cambrian Cycles: Stacked deep subtidal cycles from the Nolichucky Formation of the Tennessee-Virginia Appalachians were converted into time series then subjected to spectral analysis using MESE (Maximum Entropy Spectral Estimation) (Fig. 14). The advantages of the data sets are that they are composed of stacks of similar subtidal cycle types dominated by shales; problems with variable sedimentation rates or long periods of non-deposition are minimalized. In addition, they comprise long sections of greater than 20 cycles each, a sufficient number for reliable determination of dominant periodicities (Schwarzacher, 1975).

Spectral analysis was done on time series constructed from two locations in Virginia and Tennessee. The time series were created using relative water depth ranks of component lithofacies (Olsen, 1986). Periods of the peaks on

Figure 14: Time series and representative power spectra from two locations of the Nolichucky Formation in Virginia and Tennessee. The Virginia section was divided into lower and upper intervals and analyzed separately.

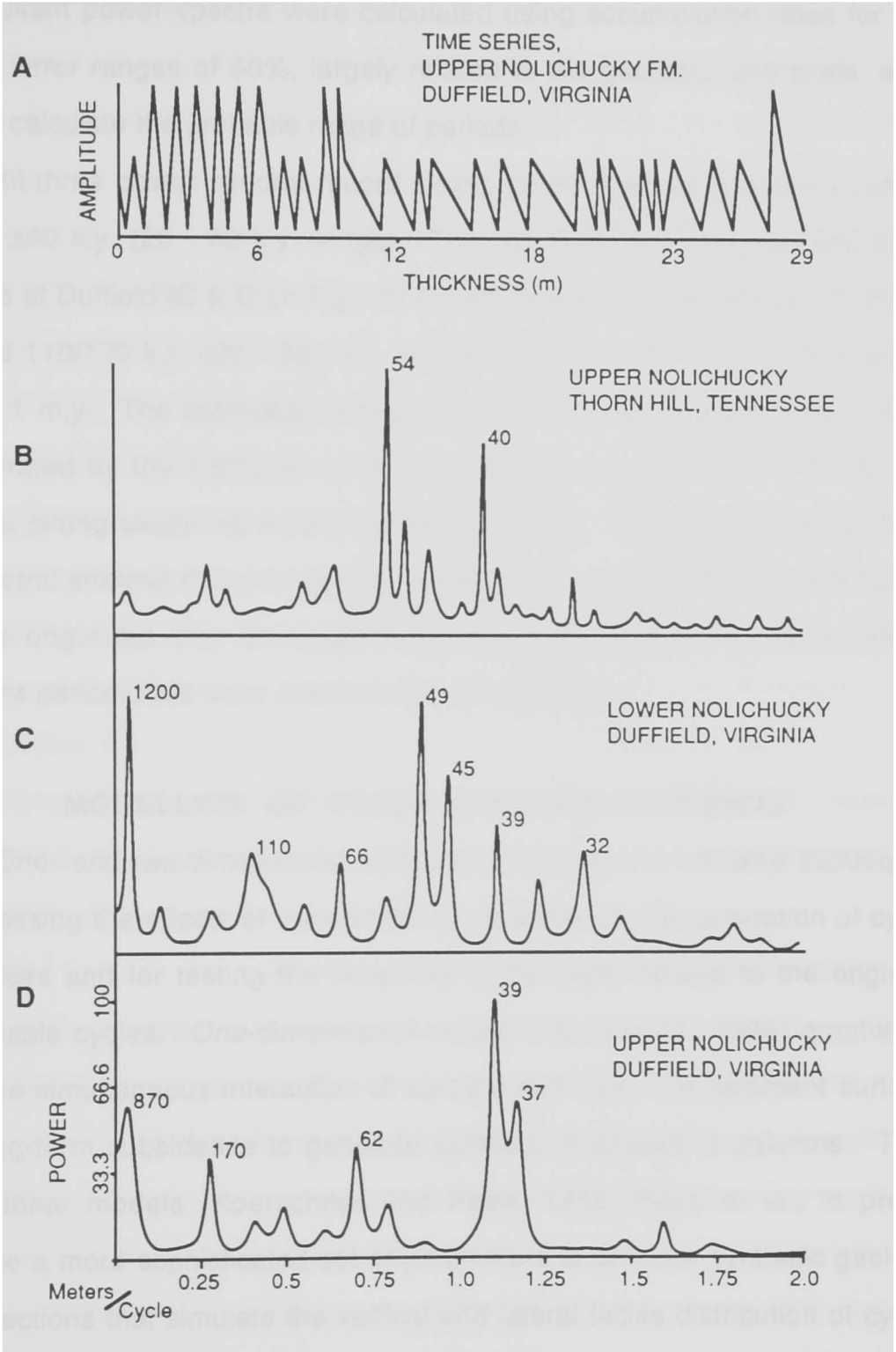
A
TIME SERIES,
UPPER NOLICHUCKY FM.
DUFFIELD, VIRGINIA
AMPLITUDE
0
6
12
18
23
29
THICKNESS (m)
B
54
40
UPPER NOLICHUCKY
THORN HILL, TENNESSEE
C
1200
49
45
39
110
66
32
LOWER NOLICHUCKY
DUFFIELD, VIRGINIA
D
100
66.6
33.3
POWER
870
170
62
39
37
UPPER NOLICHUCKY
DUFFIELD, VIRGINIA
0.25
0.5
0.75
1.0
1.25
1.5
1.75
2.0
Meters/Cycle

the resultant power spectra were calculated using accumulation rates for that locality; error ranges of 50%, largely related to the geologic time scale, were used to calculate the probable range of periods.

All three power spectra record strong peaks near calculated periods of around ±40 k.y. (20 - 60 k.y. range). The two plots for the upper and lower intervals at Duffield (C & D on Fig. 14) record subordinate periods around 62/66 k.y. and 110/170 k.y. (30 - 300 k.y. range) as well as a low frequency signal around 1 m.y. The estimated periods derived from the spectral analysis are corroborated by the histogram of cycle thickness (histogram E, Fig. 13) that shows a strong clustering around mid-range values. The periods derived from the spectral analysis of these subtidal cycles do not prove a Milankovitch control on their origin but they do suggest that sea level fluctuations controlled by dominant periodicities were influencing their deposition.

MODELLING OF CYCLE STACKING PATTERNS

One- and two-dimensional computer modelling are valuable techniques for assessing the effects of the controlling variables on the generation of cyclic sequences and for testing the feasibility of concepts related to the origin of meter-scale cycles. *One*-dimensional models (Read et al., 1986) graphically track the simultaneous interaction of eustatic sea level, the sediment surface, and long-term subsidence to generate synthetic stratigraphic columns. *Two*-dimensional models (Koerschner and Read, 1989; Read et al., in press) integrate a more sophisticated set of parameters to produce synthetic geologic cross-sections that simulate the vertical and lateral facies distribution of cycles and the internal geometry of longer-term depositional sequences. Both models

can be used to compliment each other by showing the simpler concepts with the one-dimensional modelling and then reproducing a more detailed, more realistic simulation of actual stratigraphic data using the two-dimensional modelling.

The *one*-dimensional models (Read et al., 1986) incorporate linear long-term subsidence, simplified sea level curves composed of high frequency in-phase oscillations superimposed on a longer-term rise/fall, water depth-dependent sedimentation rates of lithofacies and lag time after flooding to produce synthetic stratigraphic columns (Figs. 15 & 16). The *two*-dimensional models (Read et al., in press) (Fig. 17) incorporate many of the same variables as the one-dimensional models but with significant refinements. Antecedant topography and platform slope is digitized before the program runs and is constrained by modern analogs of carbonate platform morphologies. The model divides the platform into 200 localities whose increment width varies with the pre-determined length of the platform. Tectonic subsidence is separated into regional and rotational components and isostatic subsidence is calculated for each time slice to account for sediment and water loading.

The form of the eustatic sea level curve can be generated by any combination of high frequency, asymmetric or symmetric sine waves superimposed on a long-term sine wave or digitized curve. The input values for the sea level curve allow for any combination of cycle periods and amplitudes that interfere to produce a complex sea level signal. Water depths of lithofacies and their respective sedimentation rates are constrained by modern analogs and vertical stratigraphic relations. Lag times are used in the model to simulate nondeposition following flooding of a previously emergent carbonate platform.

Figure 15: Explanatory diagram of the 1-D modeling. The sea level curve is composed of in-phase, symmetrical 20 and 40 k.y. periods and asymmetrical 100 k.y. periods superimposed on a long-term sea level rise/fall. Any combination of amplitudes of sea level cycles can be input and define the vertical axis. Sloping lines to lower right represent linear subsidence of deposited sediments through time. The lines sloping to the upper right represent the aggrading sediment surface and changes in slope reflect differing sedimentation rates of water depth-dependent lithofacies. The period of non-deposition following drowning is a pre-determined lag time.

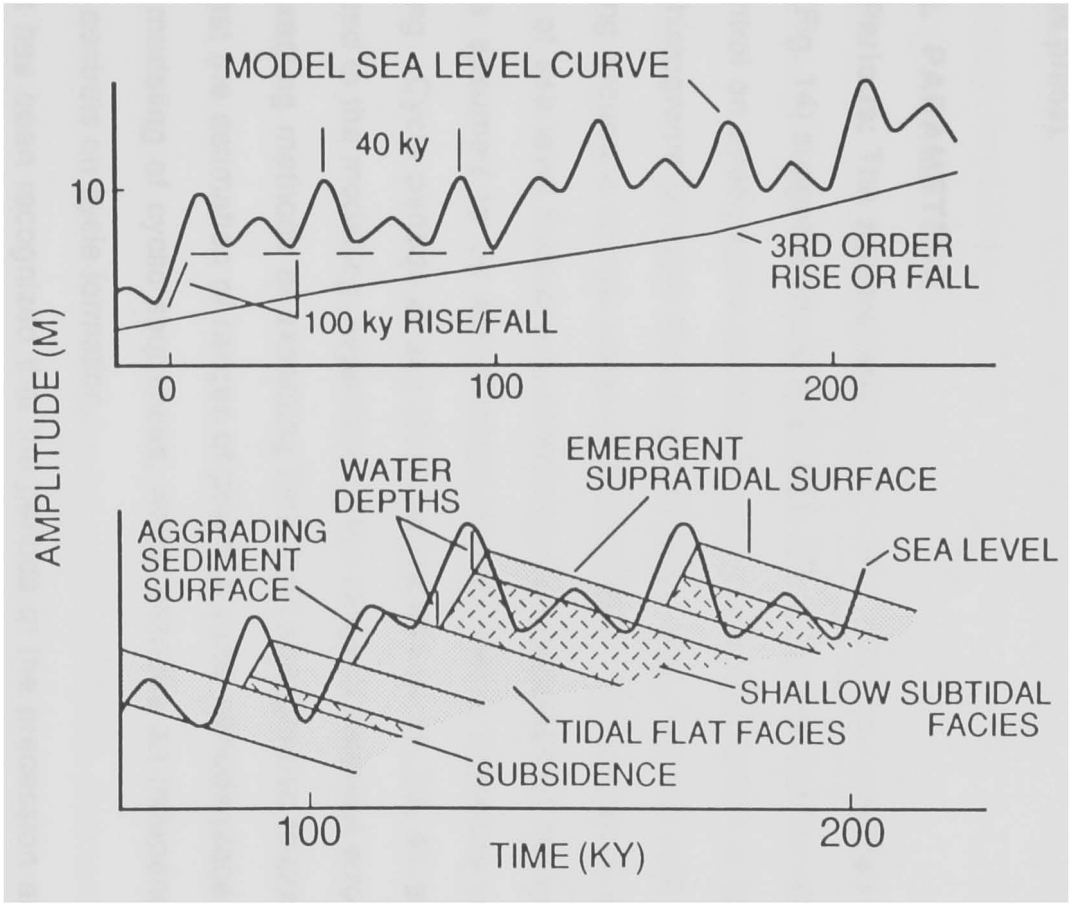
MODEL SEA LEVEL CURVE
40 ky
10
3RD ORDER
RISE OR FALL
100 ky RISE/FALL
0
100
200
AMPLITUDE (M)
EMERGENT
SUPRATIDAL SURFACE
WATER
DEPTHS
AGGRADING
SEDIMENT
SURFACE
SEA LEVEL
SHALLOW SUBTIDAL
FACIES
TIDAL FLAT FACIES
SUBSIDENCE
100
200
TIME (KY)

The interaction of sea level, subsidence and sedimentation occurs on an elastic beam that flexes in response to differential loading of sediment and water. The program executes the calculations in user-specified (usually 100 to 1000 years) time slices. Additional details about the sequence of steps per time slice, as well as the specifics of parameter determination, can be found in Read and others (in press).

MODEL PARAMETERS

Cycle Periods: The spectral analysis of Late Cambrian intrashelf basin shaly cycles (Fig. 14) suggests strong mid-range values of periodicities (40 k.y. ±50%). The control on stratigraphic cyclicity by dominant periodicities is strengthened by the histograms of cycle thickness per cycle type (Fig. 13) that show good clustering around a narrow range of thicknesses. The evidence of dominant periods of sea level fluctuations controlling the deposition of the various cycle types is assumed to be Milankovitch-related and is therefore used in the modelling. Cycle periods of sea level fluctuations of 19, 23, 41 and 100 k.y. were used in the modelling, regardless of the range of potential error. In lieu of more exacting methods of extracting time from stratigraphic thickness, at the very least the estimation of ranges of potential cycle periods place constraints on the modeling of cyclic sequences, which provides an independent test of various controls on cycle formation.

It has been recognized that the periods of the precession and obliquity signals have changed through geologic time due to changing earth - moon relationships whereas the long and short eccentricity cycles probably have remained constant through time since they are based on interplanetary

gravitational forces (Walker and Zahnle, 1986; Berger et al., 1989). The ranges of variance (the 21 k.y. precession signal may have approached 17 k.y. and the 41 k.y. obliquity signal may have approached 28 k.y.) are insignificant when compared to the large errors associated with absolute age dates for rocks. Additionally, individual Milankovitch periods are "quasi-periodic" in that they are composed of a broad range of periodicities that interfere to produce a complex signal through time (Berger, 1977). Therefore, the cycle periods will seldom be in-phase and should vary between cycles within a cyclic succession. However, for similar cycle types generated under relatively constant subtidal conditions, a dominant range of periodicities should become apparent.

Amplitudes of Relative Sea Level Oscillations: Amplitudes of relative sea level fluctuations that generated the Late Cambrian meter-scale cycles must account for the simultaneous development of peritidal cycles as well as deep ramp shaly cycles that formed on different parts of the Late Cambrian platforms. For *peritidal* cycles where the uppermost datum is known to be tide level, the average cycle thickness may be a minimum approximation of the total amount of accommodation space created by the combined effects of subsidence and sea level (Grotzinger, 1986; Goldhammer et al., 1987; Koerschner and Read, 1989).

Stratigraphic thickness of *subtidal* cycles cannot be used to approximate the amplitudes of relative sea level oscillations because no datum such as intertidal facies are available. Furthermore, none of the subtidal cycles exhibits evidence of exposure except near major unconformities, suggesting that the cycles were submergent throughout the duration of their cycle period. Perhaps

the only way to estimate the amplitudes of the high frequency relative sea level oscillations that generated subtidal cycles is to use the difference in water depths between estimated storm-deposited and fairweather-reworked lithofacies. The best evidence for paleo-water depth is provided by lithofacies that mark the base of wave reworking by storm-generated currents and the base of constant sediment winnowing under fairweather conditions. Storm wave base may be defined geologically by the first appearance of storm-deposited, hummocky cross-stratified carbonate packstones and grainstones with interbedded wackestones above suspension-settled carbonate mudstones and siliciclastic shales. Fairweather wave base is defined geologically by the base of winnowed carbonate sands above storm-influenced sandy muds. Estimates of fairweather- and storm wave base are speculative and must be based on oceanographically-defined modern analogs.

Fairweather wave base has been estimated at 10 to 20 meters on the Yucatan shelf (Logan et al., 1969), less than 10 meters on the northwest Australian inner shelf (Dix,1989) and, based on the depth of the Great Pearl Bank, at 8 to 20 meters in the Persian Gulf (Purser and Evans, 1973). *Storm wave base* in semi-enclosed ocean basins that may have fronted the Appalachian (Thomas, 1977) and Cordilleran passive margins (Stewart and Suczek, 1977), may have been approximately 60 meters based upon the Yucatan platform where Logan and others (1969) documented a wave base of 60 meters controlled by *prevailing* winds.

Potential amplitudes of short-term sea level oscillations can be estimated using the ranges between fairweather- and storm wave base. Estimating the maximum range to be about 50 meters (60 m storm wave base minus 10 m

fairweather wave base) and the minimum range to be about 10 meters (30 m storm wave base minus 20 m fairweather wave base), a reasonable mid-range might be about 30 meters. Several reasons exist for even this mid-range value of about 30 meters to be too high. One constraint on the total amplitude of the high frequency sea level oscillations is provided by the composition of Appalachian peritidal cycles. The duration of exposure of peritidal cycles has been estimated to be up to 85% of the cycle period (Read et al., 1986) but the depth of the vadose zone is dependent on the amplitude, and therefore the rate of fall, of the sea level fluctuation. Rapid sea level falls would preclude the development of thick tidal flat caps (Koerschner and Read, 1989) and result in dominantly subtidal, disconformity-capped cycles similar to the Plio-Pleistocene of the Bahama platform (Beach and Ginsburg, 1980) and the Quaternary of south Florida (Perkins, 1977), suggesting that sea level amplitudes could not have been too high. Sea level fall rates had to have been reasonably slow to allow for the accumulation of tidal flat caps that average between 1 to 2 meters in thickness. Koerschner and Read (1989) suggested total amplitudes of 10 meters for the high frequency sea level oscillations that formed Late Cambrian peritidal cycles of the Appalachians. However, this value is too low to simultaneously generate subtidal cycles where the range between storm and fairweather wave base is probably greater than 10 meters. Perhaps the best estimate for the amplitudes of the high frequency relative sea level oscillations that formed both the peritidal and equivalent subtidal cycles is around 20 ±5 m. The key is to use the computer modeling to find the right combination of sea level fall rate and sedimentation rates that allow for deposition of tidal flat facies

and periodic exposure of the peritidal platform but also maintain submergence of the subtidal platform and allow the generation of subtidal cycles.

Another factor that supports the low to moderate estimates of 20 ±5 m amplitudes is the warm overall climate of the Late Cambrian. If these high frequency sea level fluctuations are glacio-eustatically controlled, then the high sea levels, low latitude continents and lack of continental glaciation during the Late Cambrian suggest that overall amplitudes may have been low in comparison to times of widespread continental glaciation (e.g., Pennsylvanian, Plio-Pleistocene) and their attendant high (>100 m) amplitude sea level oscillations.

MODELLING RESULTS

One-Dimensional Modelling: The 1-D models show how peritidal (Fig. 16A) and subtidal (Fig. 16B) synthetic cycles develop under conditions of oscillating sea level, linear subsidence and carbonate sedimentation rates. The sea level curve for both runs is composed of in-phase 20, 40 and 100 k.y periods with amplitudes of 4, 7 and 8 meters, respectively, superimposed on a 0.02 m/k.y. long-term rise. After tidal flat caps of cycles are resubmerged, a 3 k.y. lag in deposition occurs to permit drowning; this is necessary to generate asymmetric synthetic cycles similar to actual cycles. Only the subsidence rates and the starting water depths vary between the two runs.

Synthetic Peritidal Cycles: The synthetic peritidal cycles are shown in Figure 16A. Starting the run within the shallow subtidal zone of optimal carbonate productivity (<10 m) allows for the rapid aggradation of lithofacies

Figure 16A: 1-D model of peritidal cycles with same initial starting parameters as those for the synthetic subtidal cycles of Figure 16B except for a 0.04 m/ky linear subsidence rate and a starting water depth of zero. To the right is a stratigraphic column of synthetic peritidal cycles.

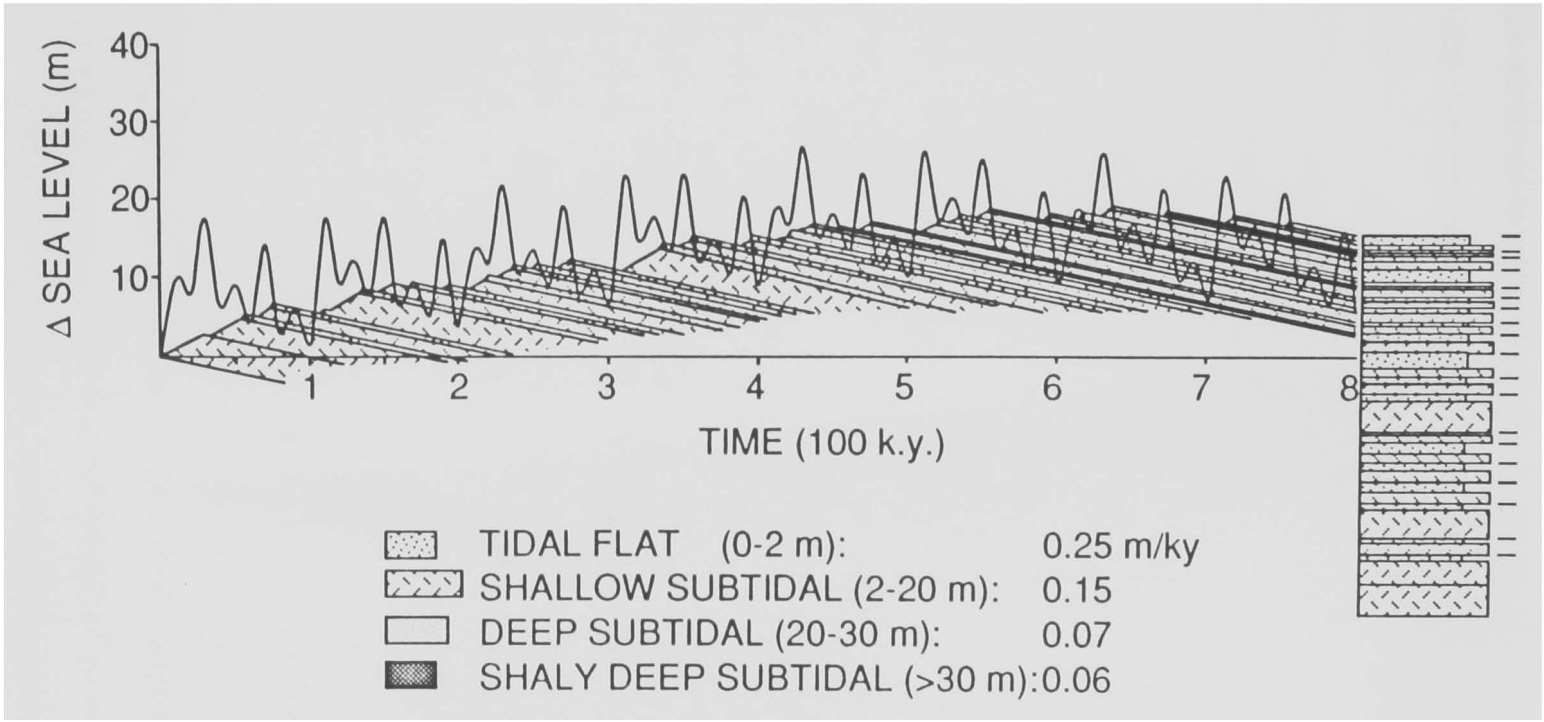
Δ SEA LEVEL (m)
40
30
20
10
1
2
3
4
5
6
7
8
TIME (100 k.y.)
TIDAL FLAT (0-2 m): 0.25 m/ky
SHALLOW SUBTIDAL (2-20 m): 0.15
DEEP SUBTIDAL (20-30 m): 0.07
SHALY DEEP SUBTIDAL (>30 m): 0.06

Figure 16B: 1-D model of subtidal cycles with a 0.05 m/ky subsidence rate and an 18 meter starting water depth. To the right is a stratigraphic column of synthetic subtidal cycles.

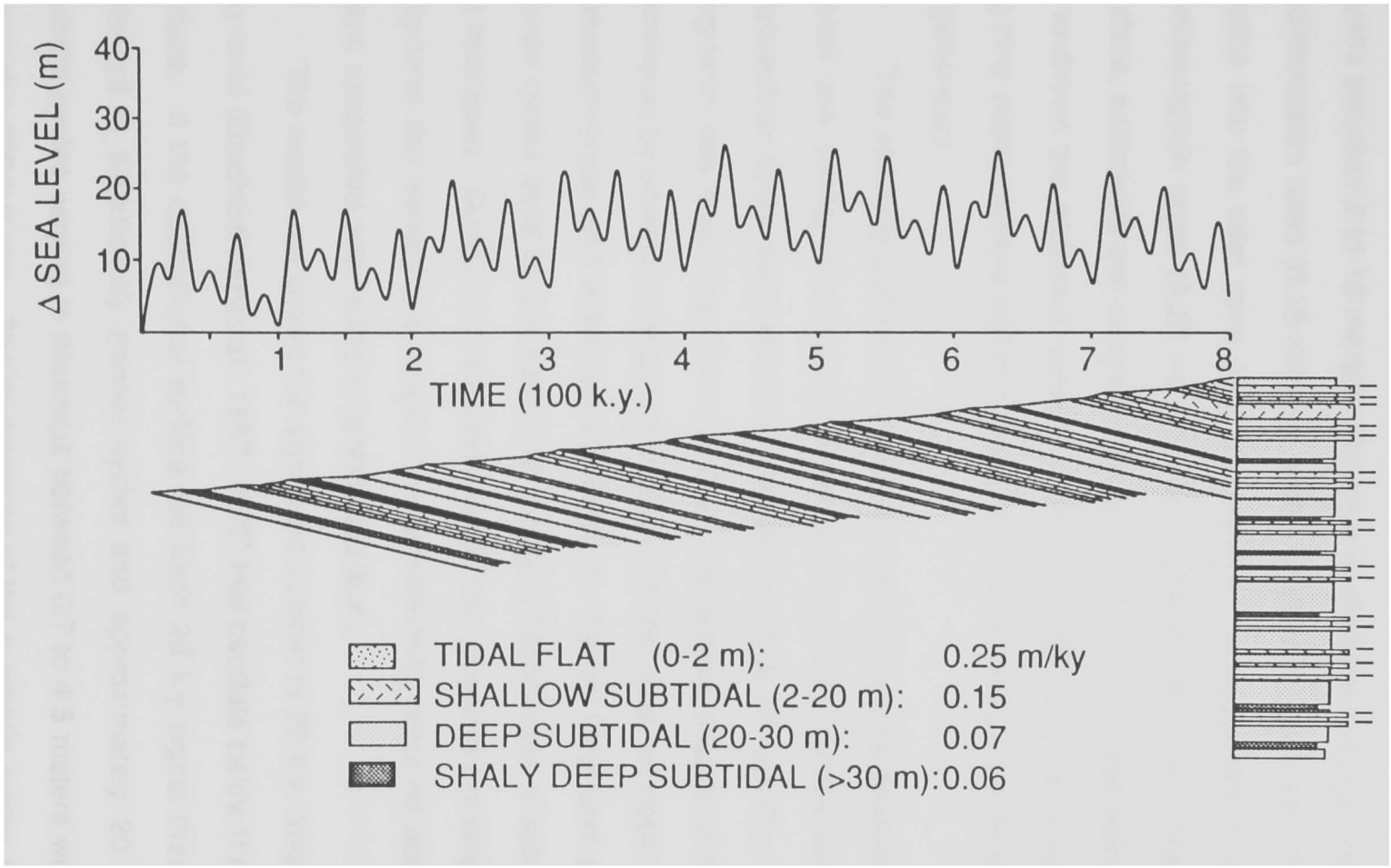
Δ SEA LEVEL (m)
40
30
20
10
1
2
3
4
5
6
7
8
TIME (100 k.y.)
TIDAL FLAT (0-2 m): 0.25 m/ky
SHALLOW SUBTIDAL (2-20 m): 0.15
DEEP SUBTIDAL (20-30 m): 0.07
SHALY DEEP SUBTIDAL (>30 m): 0.06

into peritidal water depths. When short-term pulses of sea level generate water depths between 2 to 10 meters, sediment is deposited at input shallow subtidal sedimentation rates (0.15 m/k.y.). When short-term sea level fall brings water depths into the tidal zone (0-2 m), sediment is deposited at input tidal flat sedimentation rates (0.25 m/k.y.). If sea level falls below the depositional surface, sediments are exposed until a later sea level pulse rises high enough to re-drown the sediment surface. Following submergence, a specified 3 k.y. lag time passes before sedimentation can resume and a new depositional cycle is generated.

The stacking patterns of synthetic peritidal cycles produced in the 1-D model are similar to stacking patterns of peritidal cycles seen in typical Appalachian cyclic successions (compare Figs. 9 & 10 with Fig. 16A). During long-term sea level rise, the 1-D model generates stacks of thicker cycles dominated by shallow subtidal lithofacies with thin tidal flat caps, similar to the Conococheague and Allentown Formations. During long-term sea level fall, thinner cycles develop and consist of subequal thicknesses of subtidal and tidal flat lithofacies. Durations of exposure at the tops of cycles are longer during the long-term fall versus the long-term rise reflecting reduced accommodation space associated with falling long-term sea level.

The model run shows the significant number of 20 k.y. "missed beats" of sea level (Goldhammer et al., 1987; 1990) that oscillate below the depositional surface. If the depositional surface felt each 20 k.y signal then it would be reflected in significantly thinner cycles and approximately 20 k.y. periods. Peritidal cycles varying in thickness between 0.7 to 4.5 meters were deposited during the 800 k.y. run. The thicknesses of the synthetic cycles and the gross

lithologies are roughly correlatable with cycle thicknesses and lithologies of typical Late Cambrian peritidal cycles of the Appalachians (Table 5) (Koerschner and Read, 1989).

Synthetic Subtidal Cycles: Beginning the run (Fig. 16B) at initial water depths of 18 meters allows for the depositional surface to remain submerged throughout the duration of the run and, given the low sedimentation rates at these depths, aggrade at a rate similar to the long-term sea level rise. To maintain submergence, sedimentation rates used in the modeling must be lower than most rates measured for Holocene subtidal depositional environments (typically 0.1 to 1.0 m/k.y.). If slightly higher rates are used in the modeling, the sediment surface rapidly aggrades into the zone of optimal carbonate productivity (<10 m) and remains there, producing stacks of peritidal cycles. Sedimentation rates have to be suppressed to values approximating long-term accumulation rates (0.01 to 0.1 m/k.y.) in order to produce stacks of subtidal cycles. Processes intrinsic to the platform such as storm- and wave reworking and sediment redistribution, reduced productivity in turbid waters, and depositional lags in sedimentation during rapidly rising sea level may have acted to inhibit aggradation into the zone of optimal carbonate production (Chapter 3).

As sea level rises and falls above the sediment surface throughout the duration of the model run, storm wave base fluctuates in unison 30 meters below. When the sediment surface is below 30 meters (estimated storm wave base), near-storm wave base sediments are deposited at 0.05 m/k.y., simulating deposition of nodular, argillaceous wackestones. With falling sea level, the

sediment surface rises above storm wave base and storm-influenced sediment is deposited. If sea level falls far enough so that the sediment surface rises above 20 meter water depths, sediment is deposited representing lithofacies such as skeletal packstone storm beds at the tops of cycles. During the most rapid rate of long-term sea level rise (between 250 and 450 k.y.), the thickest subtidal cycles are produced. As the long-term stillstand is reached and sea level begins to fall, thinner overall cycles are produced with thicker shallow subtidal caps.

The stacks of synthetic cycles produced by the model generally reproduce cycle stacking patterns observed in Late Cambrian subtidal successions of the Utah Cordillera. Subtidal cycles produced during the long-term sea level rise are dominated by slightly deeper subtidal lithofacies. During the long-term stillstand and subsequent fall, cycles develop thicker shallow subtidal caps reflecting the progressively shallower water depths associated with reduced accommodation space during falling sea level. However, in contrast to the stacks of peritidal cycles whose thickness is controlled by the amount of accommodation space determined by fluctuating sea level, subtidal cycle thickness appears to be controlled by reduced deeper subtidal sedimentation rates and long-term sea level rise and fall. Alternations of lithofacies within deeper subtidal cycles are produced in response to a fluctuating storm wave base whereas alternations of lithofacies in peritidal cycles are produced in response to a fluctuating sea level. Similarly, shallow subtidal cycles composed of lithofacies that reflect alternations of wave reworked and storm-dominated lithofacies may reflect fluctuations of fairweather wave base.

The synthetic subtidal cycles range in thickness from 1 to 4 meters and are composed of alternating lithofacies with estimated water depths ranging from ±30 meters to ±10 meters. These cycles grossly simulate "typical" spiculitic wackestone-capped subtidal cycles of the Utah Cordillera in that they remain submergent throughout their depositional history and have similar ranges of thicknesses. However, the synthetic cycles are more symmetric than the actual cycles seen in the field. This occurs due to the lack of a deep water lag time after renewed drowning that would allow the sediment surface to subside into deeper water depths before resuming sedimentation. Evidence of a lag in sedimentation near cycle contacts in the field is supplied by hardgrounds in the coarse-grained limestones and the abundant argillaceous content in the basal lithofacies that may have inhibited carbonate accumulation. Asymmetry could also be simulated by using an asymmetric sea level signal consisting of a rapid relative sea level rise and subsequent gradual fall.

Even though these 1-D models are simplified and do not reproduce accurate simulations of cyclic successions due to the simplified sea level curve and lack of isostatic adjustment for sediment and water loading, they provide a good introduction to the more sophisticated 2-D modelling. They help to constrain some of the basic parameters of cycle formation such as likely sedimentation rates and sea level amplitudes. The amplitudes of the high frequency sea level oscillations (18 m total) and the range of sedimentation rates (0.25 to 0.05 m/k.y.) appear to grossly simulate typical Late Cambrian peritidal and subtidal cycles and were used in the 2-D modeling.

Two-Dimensional Modelling: The 2-D model (Fig. 17) uses essentially the same parameters as in the 1-D modelling above but with certain refinements. Periods of sea level oscillations were input as 19, 23, 41 and 100 k.y. periods and allowed to interfere to produce a complex sea level curve. The same amplitudes of sea level used in the 1-D models were input in the 2-D run but act on variable initial water depths on the antecedent depositional topography. The apparent abrupt break in slope around 550 kilometers on Figure 17 is an artifact of the vertical exaggeration and translates to 0.2 m/km or a fraction of a degree. The slope was created to compare the peritidal portion of this hypothetical platform with the simultaneously developing subtidal portion of the platform. The synthetic cross-section and the columns of synthetic cycles expanded from the plot allow for a visual comparison of the different characteristics of the various cycle types that form synchronously across a carbonate platform.

On the ***inner peritidal platform*** (Fig. 17, column A), thin peritidal cycles are generated that reflect numerous "missed beats" of sea level. Cycles are composed of thin subtidal bases with thicker tidal flat facies and significant disconformable caps reflecting long episodes of exposure on the slowly subsiding inner platform (0.020 m/k.y.). Thickness of these cycles is controlled by the amount of accommodation space made available by the high frequency sea level oscillations coupled with the low subsidence rates of the inner platform and long periods of emergence. During long-term sea level rise, only the occasional pulse of sea level rose high enough to drown the inner platform and allow for sediment accumulation. During the short-term falls superimposed on the long-term rise, the inner platform was exposed for as long as 80 to 100 k.y, forming the disconformable caps to the cycles. During long-term sea level

Figure 17A: 2-D model of a peritidal to subtidal transition across a hypothetical platform. Amplitudes of the sea level oscillations and the water depth-dependent sedimentation rates are the same as in the 1-D models but the periods have been input as 19, 23, 41 and 100 k.y. and allowed to interfere to produce the complex sea level curve in the inset. Initial depositional slopes on the peritidal platform are < 0.01 m/km and are ~0.04 m/km on the subtidal platorm. Rotational subsidence at the outer edge of the platform is 0.015 m/k.y. Duration of the run is 800 k.y.

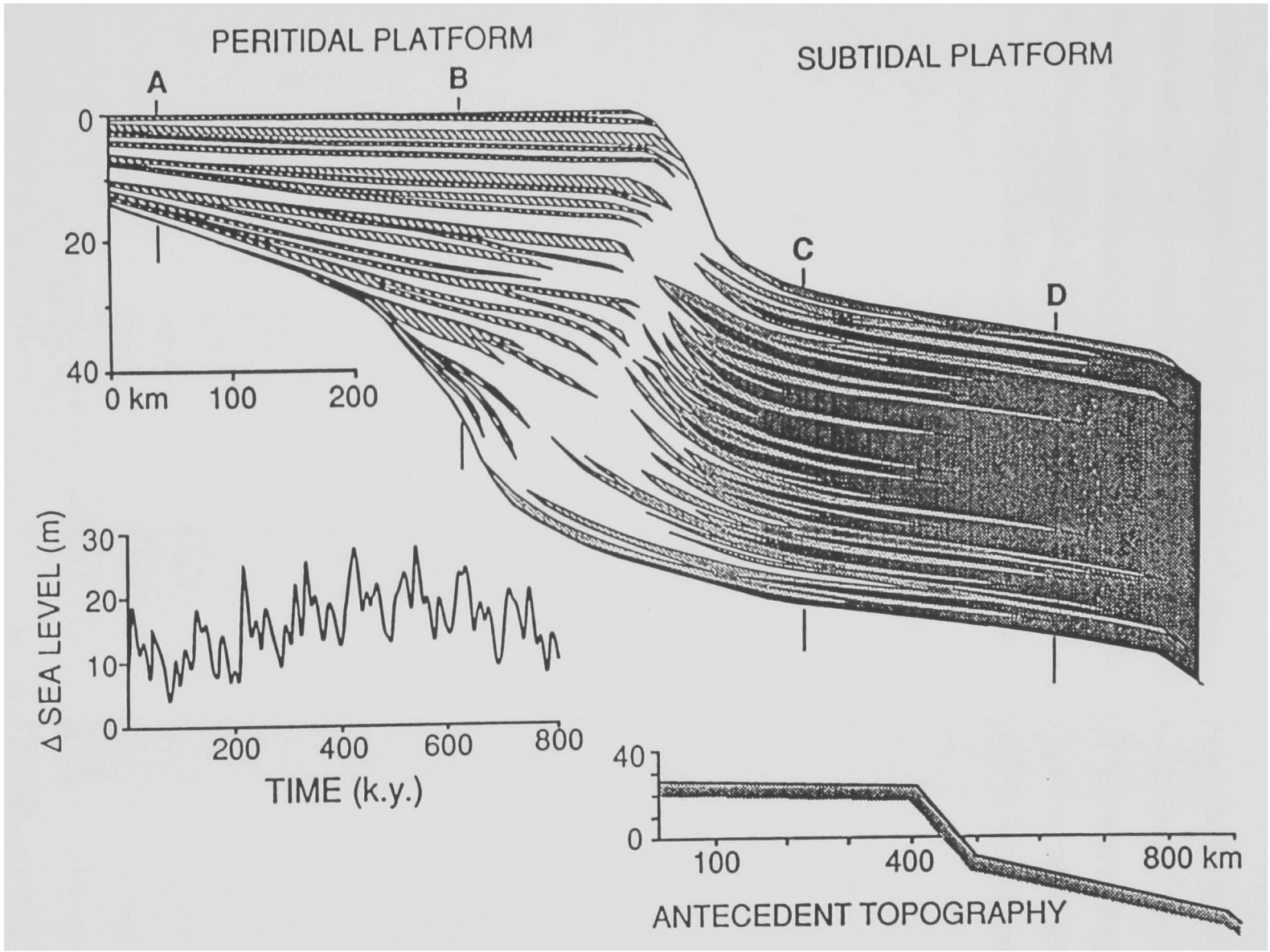
PERITIDAL PLATFORM
SUBTIDAL PLATFORM
A
B
C
D
0
20
40
0 km
100
200
Δ SEA LEVEL (m)
30
20
10
0
200
400
600
800
TIME (k.y.)
40
0
100
400
800 km
ANTECEDENT TOPOGRAPHY

Figure 17B: Columns of stacked synthetic cycles generated in the 2-D model of 17A. Column A is from the inner peritidal platform; column B is from the outer peritidal platform; column C is from the inner subtidal platform; column D is from the outer subtidal platform. Actual stacked cycles of Late Cambrian cyclic successions are aligned below the synthetic cycles for comparison.

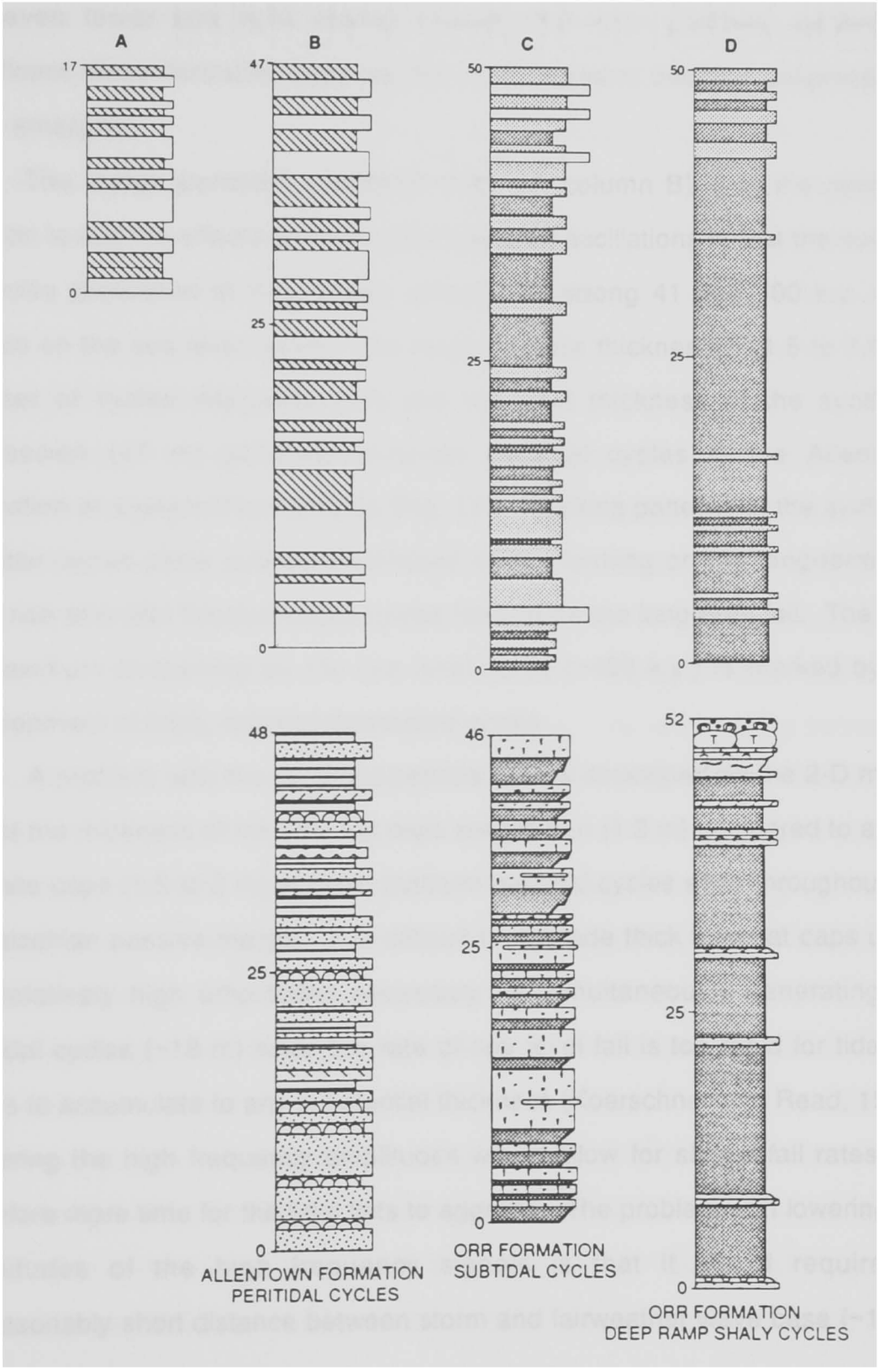
A
B
C
D
17
0
47
25
0
50
25
0
50
25
0
48
25
0
46
25
0
52
25
0
ALLENTOWN FORMATION
PERITIDAL CYCLES
ORR FORMATION
SUBTIDAL CYCLES
ORR FORMATION
DEEP RAMP SHALY CYCLES

fall, even fewer sea level events flooded the inner platform, generating significant disconformable caps as the inner platform became progressively more emergent.

The ***outer peritidal platform*** (Fig. 17, column B) is in the optimum location to feel the effects of most major sea level oscillations in that the number of cycles generated at this locality reflects the strong 41 and 100 k.y. input signals on the sea level curve. The range of cycle thicknesses (1.5 to 7.0 m), number of cycles deposited (17) and the total thickness of the synthetic succession (47 m) generally simulate peritidal cycles in the Allentown Formation of eastern Pennsylvania (Fig. 17). Stacking patterns of the synthetic peritidal cycles show subtidal-dominated cycles forming on the long-term sea level rise and tidal flat-dominated cycles forming on the long-term fall. The time of maximum deepening on the sea level curve (~400 k.y.) is marked by the development of thick, subtidal-dominated cycles.

A problem with the synthetic peritidal cycles developed on the 2-D model is that the thickness of the tidal flat caps are too thin (1.2 m) compared to actual laminite caps (1.5 to 2 m) of outer platform peritidal cycles seen throughout the Appalachian passive margin. It is difficult to aggrade thick tidal flat caps using the relatively high amplitudes necessary for simultaneously generating the subtidal cycles (~18 m) since the rate of sea level fall is too rapid for tidal flat facies to accumulate to any substantial thickness (Koerschner and Read, 1989). Lowering the high frequency amplitudes would allow for slower fall rates and therefore more time for the tidal flats to aggrade. The problem with lowering the amplitudes of the high frequency signals is that it would require an unreasonably short distance between storm and fairweather wave base (~10 m)

to generate the subtidal cycles. Factors not recognizable in the rocks may have been interacting to influence depositional environments. Storm wave base may have shallowed toward the inner platform by frictional dissipation along the depositional slope, narrowing the distance between fairweather- and storm wave base. This may have had the effect of simultaneously creating deep subtidal cycles toward the outer platform that appear to reflect high amplitudes of sea level fluctuations and shallow subtidal and peritidal cycles toward the inner platform that appear to reflect lower amplitudes of sea level fluctuations.

A related problem is the extensive development of disconformable caps on most of the peritidal cycles on the model. It has been argued that relatively few vadose diagenetic caps have been observed in peritidal cycles of the Appalachians and that autocyclic mechanisms provide an attractive alternative explanation for their absence (Hardie and Shinn, 1986). In Late Cambrian cycles of the Appalachians, the only evidence for sea level falling below the platform is provided by brecciated regoliths filling solution-enhanced depressions along the upper surface of some tidal flat caps and some subtidal lithofacies that exhibit leached aragonitic fossils locally containing crystal silt (Koerschner and Read, 1989; Read, 1989). However, other features of subaerial exposure and vadose diagenesis may have been removed by post-depositional processes or have been masked by dolomitization of tidal flat caps.

The absence of evaporites (other than isolated silicified nodules), the relative scarcity of dissolution breccias and the lack of much erosional relief along the top of laminite caps may indicate their partial removal during the formation of a deflation surface atop the exposed flat. Supratidal evaporites may have been dissolved during the occasional rains that occurred in the semi-

arid climate. Lack of land plants would have not favored caliche development and the prevailing desiccating conditions might have inhibited cementation, making erosional removal of supratidal sediment by eolian action a tenable mechanism for forming the planar surface at the tops of many laminite caps.

The ***subtidal platform*** (Fig. 17, column C) shows good development of subtidal cycles that are composed of thin, very deep subtidal bases (>30 m water depths) shallowing up into thicker subtidal caps deposited in intermediate water depth ranges (20 - 30 m). Nineteen subtidal cycles were developed during the 800 k.y. run (42 k.y./cycle) reflecting the higher amplitudes of the 41 and 100 k.y. signals on the input sea level curve and the relatively suppressed 19 and 23 k.y. signals. The range of cycle thicknesses (1.4 to 5.0 m), number of cycles deposited (19) and the total thickness of the synthetic succession (50 m) generally simulate subtidal cycles in the Sneakover Member of the Orr Formation of the House Range (Fig. 17).

Stacking patterns of the synthetic subtidal cycles show thick cycles toward the base reflecting the increased accommodation space generated during initial long-term sea level rise. These cycles grade up into two thick cycles dominated by the deepest subtidal lithofacies and are associated with maximum flooding by high frequency pulses of sea level superimposed on the highest rates of long-term sea level rise. A few of the uppermost synthetic cycles show shallow subtidal lithofacies capping the cycles, reflecting progradation during long-term falling sea level. The thickness of these subtidal cycles appears to be a function of the slower sedimentation rates of the deep subtidal platform. This is in contrast to the synchronously developed peritidal cycles (Fig. 17, column B) whose disconformable cycle caps suggest that their

thickness is controlled by accommodation space made available by oscillating sea level coupled with subsidence.

The ***outer deep subtidal platform*** (Fig. 17, column D) is composed of subtidal cycles that are substantially thicker than those to landward. The cycles are dominated by the deepest water lithofacies overlain by very thin tongues of slightly shallower water facies. As sea level oscillated above the platform, storm wave base (>30 m in the model) oscillated in phase but only fell below the sediment surface during major sea level lows, allowing for the deposition of storm-influenced lithofacies (20-30 m). Fewer cycles are developed and the thickness of the cycles (up to 17 m) reflect the significant number of higher frequency sea level beats evident in the sea level curve that were "missed" on the deep ramp. The synthetic cycles generated on the outer subtidal ramp generally simulate deep water cycles of the Candland Shale Member of the Orr Formation of the House Range where thick sub-storm wave base shales are periodically capped by storm-deposited carbonates (Fig. 17). Cycle thickness on the deep outer ramp appears to be a function of sediment accumulation at relatively constant rates below storm wave base, episodically interupted by sea level falls that force storm wave base below the sediment surface, depositing storm-influenced cycle caps.

The synthetic cross-section generated by 2-D modelling illustrates how peritidal and subtidal cycles may simultaneously be generated by the same input sea level signal. The peritidal portion of the hypothetical platform may be a good representation of the Appalachian flat-topped, aggraded platform whereas the subtidal portion of the hypothetical platform may reflect the generalized conditions across the Cordilleran distally steepened ramp.

Disconformably-capped peritidal cycles are generated as a function of accommodation space provided by the high frequency sea level oscillations superimposed on long-term sea level rise and fall in conjunction with slow rates of subsidence. Conformably-capped subtidal cycles that remain submergent throughout their depositional history are generated as a function of slower, deeper water sedimentation rates in conjunction with slightly higher rates of subsidence. Successions of subtidal cycles may occur as a response to fluctuating storm- or fairweather wave base that oscillate in phase with sea level.

DISCUSSION

Origin of Non-Cyclic Intervals: Certain intervals of the Late Cambrian of the Llano uplift of central Texas are characterized by non-cyclic successions of stacked carbonate grainstone beds with little variation in composition over 10 to 50 meters. These intervals are composed of amalgamated, wavy beds of well-sorted, coarse-grained, oolitic, skeletal, intraclastic packstones and grainstones with some intermixed quartz sand grains. They show common uni- and bi-directional crossbedding along with numerous stacked hardgrounds. These carbonate sands suggest deposition in high energy, open marine, shallow subtidal to possibly intertidal environments. Some interbedded thrombolitic bioherms with elongate orientations and coarse skeletal sands filling interbioherm channels also support high tidal or wave current energies. Rapid lateral facies changes of the grainstones reflect deposition in a complex mosaic of migrating barrier bars, tidal inlets and sandy beaches (King and Chafetz, 1975). The lack of cryptalgal laminites or terrigenous clays suggests that low

energy environments were absent on this part of the central Texas cratonic embayment, although they may have been present toward the Transcontinental Arch to the northwest.

The non-cyclic carbonate sands were deposited simultaneously with peritidal and subtidal meter-scale cycles on the Appalachian and Cordilleran passive margins and in the southern Oklahoma aulacogen 400 kilometers to the north. This rules out static sea level as an explanation for the apparent non-cyclicity on the Texas craton since sea level had to have been fluctuating to generate meter-scale cycles at the other Late Cambrian localities. The high elevations and low subsidence rates on the Texas craton probably permitted only the highest amplitude sea level oscillations to extend up onto the platform. Accommodation space for sediment accumulation was provided by long-term rises in sea level and by the occasional short-term sea level pulse. If sediment was accumulating during short-term sea level rises, the effects of the subsequent rapid sea level fall should be evident as vadose diagenetic features (similar to diagenetic caps of Goldhammer et al., 1987). However, rather than exhibiting evidence of periodic exposure, the coarse-grained carbonate sands show abundant evidence of marine cementation. Turbid, inclusion-rich syntaxial cements surrounding echinoderm grains, bladed pendant cements extending down into shelter voids of storm beds and abundant rip-up intraclasts and hardgrounds all indicate sea floor cementation. The only evidence of vadose dissolution is provided by leached gastropod shells and even this may be a burial event.

A possible explanation for the apparent contradiction is that the grainstones actually may been deposited in deeper water than previously

interpreted. They may have responded to fluctuating sea levels by sediment reworking and redistribution rather than aggradation up to sea level. The cratonic embayment near central Texas may have been a relatively deep, open marine shelf exposed to large swells generated in the deeper ocean. A modern analog may be the northwest Australian inner shelf where Dix (1989) has documented accumulation of skeletal sand sheets in less than 10 meters of water that are kept submergent by constant sediment reworking by tidal currents and a strong storm-generated wave regime.

The abundant crossbedding and coarse textures within the amalgamated grainstones suggest mobile substrates that may have inhibited the establishment of carbonate producers and suppressed aggradation into shallower subtidal water depths. The rapid lateral shifts in facies and the common stacked hardgrounds also support the possibility of sediment cementation and redistribution under high current energies. The constant turbulent conditions may have precluded the deposition of lower energy lithofacies that would have permited easier recognition of cyclicity within these intervals. Meter-scale cyclicity may exist within these amalgamated grainstones but may be cryptic due to insufficient differentiation of lithofacies that would enable the definition of depositional cycles.

A lack of identifiable meter-scale cycles also characterizes the Signal Mountain Formation in the Wichita Mountains of Oklahoma. Cryptalgal laminites at the base of the Signal Mountain culminate a long-term shallowing-upward sequence recognized within cyclic strata of the underlying rocks. With long-term upward deepening in the Signal Mountain, the meter-scale cycles are succeeded by randomly arranged muddy skeletal wackestones and packstones

of an open marine platform. However, even in the absence of fifth-order cyclicity, several longer-term, coarsening- and shallowing-upward successions can be identified over 15 to 30 meter intervals (third- and fourth-order scale).

Meter-scale cyclicity developed in time-equivalent strata of the Appalachian and Cordilleran passive margins suggests that cycle development in the Late Cambrian portion of the Signal Mountain Formation may have been masked by local tectonism associated with episodic movement along boundary faults of the southern Oklahoma aulacogen. Subsidence analysis of the Wichita Mountains section shows rapid sediment accumulation a few million years before the end of the Late Cambrian (Chapter 2). Feinstein (1981) has documented the same pulse of subsidence during an 8 m.y. period coincident with deposition of the Signal Mountain Formation which he ascribed to reactivation of locked boundary faults separating the aulacogen from the adjacent cratonic platform. Episodic movement along these faults may have supplied extra accommodation space beyond that provided by eustacy, masking the recognition of meter-scale cycles. However, some of the longer-term, third-order cycles can be correlated with equivalent strata in the Utah, Texas and Appalachian sections suggesting a eustatic control on their development.

Glacio-Eustacy During the "Non-Glacial" Late Cambrian: The connection between Milankovitch orbital variations, the shrinkage and growth of continental ice sheets and eustacy has been well-documented (Hays et al., 1976; Fischer, 1986; Berger et al., 1984). However, a direct link between changes in solar insolation related to Milankovitch astronomical rhythms and

changes in sea level and sedimentation during globally warm periods of Earth history has yet to be found (Barron et al., 1985). To account for the 10 to 20 meter sea level oscillations proposed to simultaneously generate Late Cambrian peritidal and subtidal cycles, a sink for the storage of moderate volumes of seawater needs to be identified.

Paleogeographic reconstructions for the Late Cambrian place most continental land masses between 60°N and S latitudes (Scotese and McKerrow, 1990). Only Baltica and the southern margin of Gondwana extend into higher southern latitudes where climates may have been significantly cooler than the generally warm global climate. Ziegler and others (1981) have suggested that the paleogeographic configuration of the continents during the Cambrian facilitated a latitudinal zonation of prevailing winds and ocean currents within the high latitudes that may have reduced the absorbtion of solar radiation, enhancing the possibility of cooler Cambrian climates than previously believed. Additionally, climate modelling of presumably warm periods of Earth history suggest that the interiors of mid- to high latitude continents may have had subfreezing temperatures and that no global climate is truly "equable" (Sloan and Barron, 1990). Even though no major large-scale continental glaciers existed during the Late Cambrian, alpine glaciers may have been present in ancestral mountain belts of continental interiors of major land masses. Diamictites and striated cobbles have been reported in lower Tremadocian strata of Argentina and Bolivia (Erdtmann and Miller, 1981) which were located in a part of Gondwana believed to have experienced cool climates during the Late Cambrian-Early Ordovician (Scotese and McKerrow, 1990). Perhaps the most tenable explanation for the connection between Milankovitch-

controlled solar insolation and the low to moderate amplitude sea level fluctuations that produced the stratigraphic cyclicity is alpine glaciation.

SUMMARY AND CONCLUSIONS

1) A spectrum of peritidal to deep subtidal cycle types can be recognized in Late Cambrian carbonate platform sequences of the Appalachian and Cordilleran passive margins, the Texas craton and the southern Oklahoma aulacogen. Cycle types, defined on the basis of the capping lithofacies, extend from shallow to deep as follows: a) peritidal, laminite-capped cycles, b) shallow subtidal, thrombolite bioherm-capped cycles, c) shallow subtidal, ooid grainstone-capped cycles, d) intermediate subtidal, skeletal packstone-capped cycles, e) deep subtidal, spiculitic wackestone-capped cycles, f) intrashelf basin, flat pebble conglomerate-capped shaly cycles, and g) deep ramp, carbonate-capped shaly cycles.

2) Asymmetric meter-scale Late Cambrian cycles record abrupt deepening of relative sea level followed by gradual upward shallowing over periods of 20 to 200 k.y. Subtidal cycles that remain submerged throughout their deposition provide evidence against autocyclic controls on meter-scale cycle development. The simultaneous development of peritidal and subtidal cycles on different carbonate platforms supports a eustatic control on the origin of the meter-scale cyclicity. High frequency eustatic oscillations may be controlled by Milankovitch astronomical rhythms based on spectral analysis that show strong clustering of periods around a narrow range of values. Alpine glaciation may have supplied a reservoir large enough to control the relatively low volumes of ocean water

required for the 10 to 20 meter sea level oscillations necessary for the simultaneous generation of peritidal and subtidal cycles.

3) Within cyclic successions of Late Cambrian strata (and presumably for other ancient cyclic successions as well), systematic stacking patterns of meter-scale cycles may be used in conjunction with Fischer plots to predict third-order, and perhaps fourth-order, eustatic sea level events. The Fischer plot technique is based upon changes in accommodation space and seems to be best suited for *peritidal* cycles whose thicknesses are largely controlled by sea level. However, stacking patterns of *subtidal* carbonates and their resultant Fischer plots need to be further tested since they can give inconsistent trends of apparent rise and fall of relative sea level as a function of sedimentation rate rather than accommodation space.

4) One- and two-dimensional computer modelling provide constraints on the parameters that control the development of cyclic successions. Stacking patterns of synthetic meter-scale cycles can be compared to actual cyclic successions to assess the possible combination of sea level amplitudes and periods that may have generated the long-term depositional sequence. The synthetic stratigraphic columns and cross-sections do not provide unique solutions but help to clarify the interacting effects of eustacy, subsidence and sedimentation.

Two-dimensional models of peritidal to subtidal transitions across a hypothetical platform indicate that peritidal cycle thickness is primarily controlled by accommodation space and deeper subtidal cycle thickness is

primarily controlled by sedimentation rate. Subtidal cycle development may be related to fluctuations in fairweather and storm wave base that oscillate in harmony with sea level fluctuations. Stratigraphic variability not predicted by the modelling both *within* carbonate cycles and *laterally* across carbonate platforms may be influenced by factors not recognized in the rocks such as depositional topography and oceanographic dynamics.

5) Simultaneous development of peritidal to subtidal meter-scale cycles is probably a more common phenomenon on many carbonate platforms than previously believed. Subtidal cycles are equal in importance to peritidal cycles as fundamental components of cyclic carbonate platforms. They provide critical information about the relative roles of eustacy, subsidence and sedimentation beyond that provided by peritidal cycles alone.

Interbasinal comparisons of time-equivalent cyclic successions of strata may provide insight into global mechanisms that may have controlled cycle deposition that otherwise may be missed within single depositional basins.

CHAPTER 2

COMPARATIVE ANALYSIS OF METHODS USED TO DEFINE EUSTACY IN OUTCROP: LATE CAMBRIAN INTERBASINAL SEQUENCE DEVELOPMENT

ABSTRACT

Interbasinal correlation of Late Cambrian cyclic carbonates from the Appalachian and Cordilleran passive margins, the Texas craton and the southern Oklahoma aulacogen allows definition of six major third-order depositional sequences that may be eustatic in origin. Graphic correlation of biostratigraphically-constrained strata was used to establish equivalency of stratigraphic cycles (tens to hundreds of meters thick) between the individual sections. The time-equivalent intervals determined from graphic correlation were correlated lithostratigraphically using isochronous biomere boundaries as time datums. Even though the individual sections are composed of different cycle types and component lithofacies that reflect the various environmental settings of the localities, the overall shallowing-upward character of the sequences is evident. The sequences were named on the basis of their relative time ranges according to the trilobite biostratigraphy and are: 1) late *Cedaria*, 2) mid-*Crepicephalus*, 3) late *Crepicephalus*, 4) *Aphelaspis* to earliest *Elvinia*, 5) *Elvinia* to early *Saukia*, and 6) *Saukia* to the Cambrian-Ordovician boundary.

Interbasinal correlation of third-order sequences permits an evaluation of quantitative techniques for determining eustatic sea level history. *Fischer plots* of meter-scale cycles define changes in relative sea level based on the amount of extra accommodation space produced by eustacy beyond that provided by subsidence. Correlated Fischer plots of cyclic successions from different localities support a eustatic control on Late Cambrian sequence development. *Residual eustatic curves* derived from subsidence analysis are useful for correlating the longer-term Late Cambrian sea level events and changes in the rate of sea level rise and fall can be used to define shorter-term events.

Combining the sea level curves defined by Fischer plots and subsidence analysis with paleobathymetric curves of Late Cambrian cyclic strata suggests that the curves may approximate the *form* of the eustatic sea level curve. A composite "eustatic" sea level curve for the Late Cambrian was created by qualitatively combining the sea level curves defined by the different techniques for each of the four localities.

"Eustatic" sea level curves defined by Fischer plots and subsidence analysis may be used to apply sequence stratigraphic concepts to outcrop sections. Combined with systematic changes in the stacking patterns of meter-scale cycles, they can be used to define the internal composition of systems tracts, sequence boundaries, and flooding surfaces of third-order depositional sequences. However, relatively conformable sequence boundaries and maximum flooding surfaces are difficult to document in outcrop sections since they are complicated by repeated high frequency sea level oscillations that generated meter-scale cycles. Consequently, systems tract boundaries commonly are transitional zones of stacked cycles that may include parts of the underlying and overlying systems tracts.

INTRODUCTION

Numerous workers have shown through interbasinal correlation that many stratigraphic sequences are synchronous and genetically related. Sloss (1963) and Vail et al. (1977) recognized synchroneity at the second-order scale (10-100 m.y.) and subsequently, correlations at the third-order scale (1-10 m.y.) have been proposed throughout the Phanerozoic (Vail et al., 1977; Hallam, 1984; Hancock and Kaufmann, 1979; Cisne et al., 1984; House, 1985; Johnson et al, 1985; Haq et al, 1987; Ross and Ross, 1988; Johnson et al., 1989). However, the degree of synchroneity and the recognition of specific depositional sequences in some basins but not in others are major problems in establishing a eustatic versus tectonic control on sequence development (Hallam, 1984; 1988; Miall, 1984). A detailed, interbasinal study of Late Cambrian pericratonic carbonates was performed to evaluate the degree of resolution and correlatability of meter-scale cycles and larger scale sequences to determine whether the sequences likely reflect global eustatic events or relative sea level fluctuations intrinsic to individual basins responding to local or regional tectonism.

Well-exposed and biostratigraphically-constrained Late Cambrian sections within the Appalachian and Cordilleran passive margins, the Texas cratonic embayment, and the southern Oklahoma aulacogen were used to evaluate synchroneity of long- and short-term sequence development. The differing subsidence histories, lithofacies, and paleoenvironmental conditions of each locale provide differing insights into how each platform responded to relative sea level fluctuations through time. This study integrates detailed lithostratigraphic analysis of Late Cambrian pericratonic sections with good

biostratigraphic control to develop a refined chronostratigraphic correlation between geographically and tectonically distinct settings. The results of this study suggest a dominant eustatic control on major sequence development with subordinate local tectonic input contributing to variability between locations.

STRUCTURAL AND STRATIGRAPHIC SETTING

Location and Tectonic Setting of Sections: Complete sections of Late Cambrian strata were measured and logged bed-for-bed in the House Range of west central Utah, the Appalachian Mountains in Tennessee, Virginia and eastern Pennsylvania, the Llano uplift of central Texas, and the Wichita Mountains of Oklahoma (Figs.18 & 19). These localities represent Late Cambrian tectonic settings in the Cordilleran and Appalachian passive margins, the Texas cratonic embayment and the southern Oklahoma aulacogen. Field locations were chosen on the basis of: 1) quality of exposure and absence of structural complications; 2) availability of biostratigraphic data (especially biomere boundaries); and 3) platform location along the transition between shallow-water carbonates and deeper-water fine-grained siliciclastics where intertongueing relations define excursions in sea level. A total of 2200 meters of section were logged and numerous other sections previously described in the Appalachians (Markello, 1979; Koerschner, 1983) were field-checked. Hand samples of individual lithofacies were collected for slabbing and thin section analysis to provide additional detail for paleoenvironmental interpretations.

The Appalachian and Cordilleran passive margins and the Texas cratonic embayment originated in response to breakup of a Late Proterozoic

Figure 18: Location map of sections measured in the study. Late Cambrian base map modified from Lochman-Balk (1971) and Palmer (1974) to show the inner and outer detrital belts, the middle carbonate belt and the southern Oklahoma aulacogen.

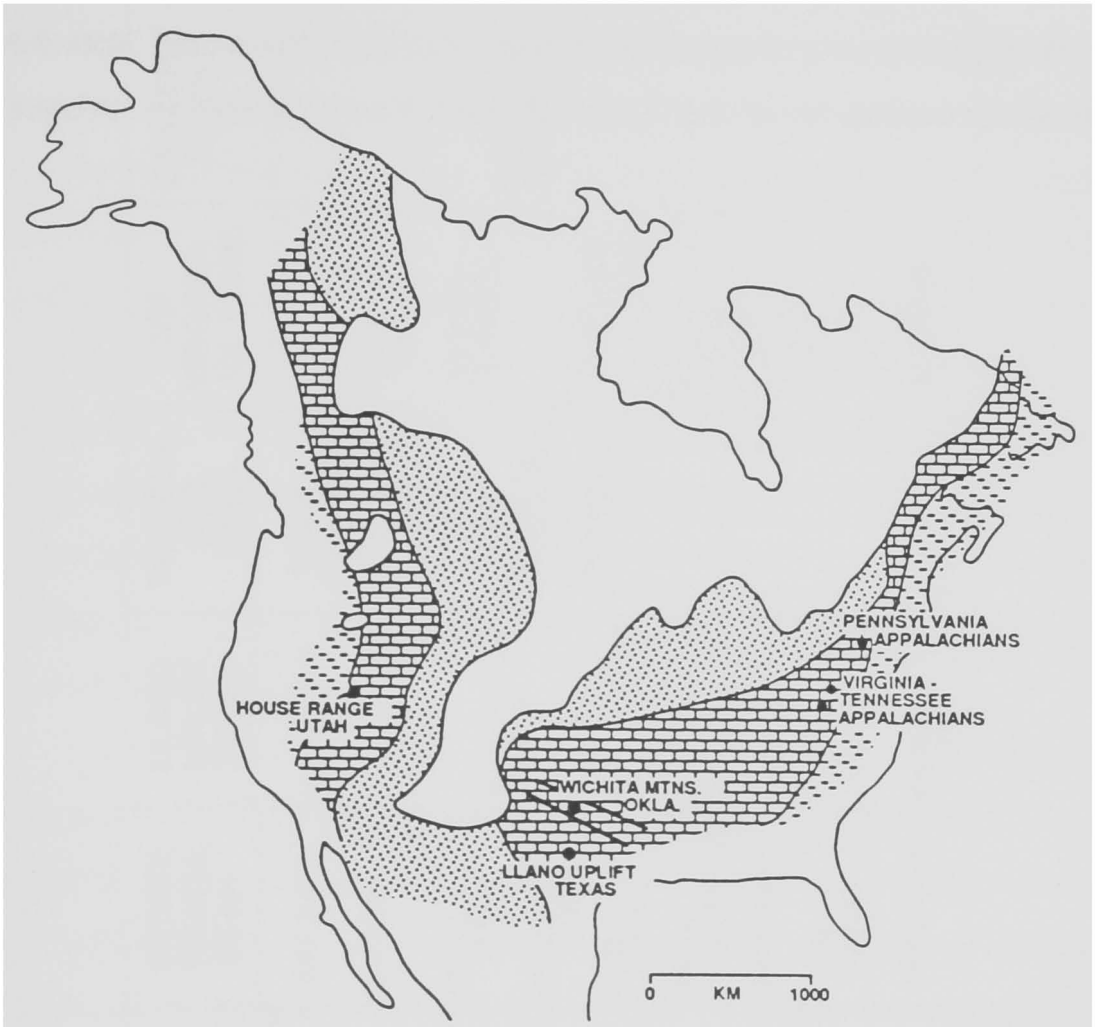

LATE CAMBRIAN
SEDIMENTARY FACIES

Figure 19: Biostratigraphic chart of Late Cambrian strata in this study. Note the three biomere boundaries in the Late Cambrian that separate the trilobite zones.

EARLY ORDO
LATE CAMBRIAN
STAGE
TREMPEAL-EAUAN
FRANCONIAN
DRESBACHIAN
BIOMERE
PTYCHASPID
MARJUMIID
PTERO-CEPHALIID
TRILOBITE ZONE
MISSISSIQUOIA
SAUKIA
SARATOGIA
TAENICEPHALUS
ELVINIA
DUNDERBERGIA
APHELASPIS
CREPICEPHALUS
CEDARIA
BOLASPIDELLA
HOUSE RANGE, UTAH
LAVA DAM
RED TOPS
HELLN-MARIA
SNEAK-OVER
CORSET SPRING
JOHNS WASH
CANDLAND
BIG HORSE
WEEKS FM.
NOTCH PEAK
ORR FM
LLANO UPLIFT, TEXAS
SAN SABA
POINT PEAK
MORGAN CREEK
WELGE
LION MT.
CAP MT.
HICKORY SST
WILBERNS FM
RILEY FM
WICHITA MTS. OKLA.
SIGNAL MOUNTAIN
ROYER
FORT SILL
HONEY CK
REAGAN
SW VIRGINIA NE TENN.
COPPER RIDGE /
CONOCO-CHEAGUE
CONASAUGA
MAYNARD-VILLE
NOLICHUCKY SHALE
ELBROOK
EASTERN PENN.
ALLENTOWN DOLOMITE

supercontinent around 625 to 555 Ma (Bond et al., 1984; Stewart and Suczek, 1977). Both the Appalachian and Cordilleran passive margins developed wedge-shaped prisms of post-rift subtidal and peritidal carbonates and interlayered siliciclastics (Fig. 20) over thick accumulations of syn-rift, Upper Proterozoic/Lower Cambrian, terrigenous siliciclastics derived from both the craton and uplifted rift blocks. The Appalachian passive margin contains up to 1.6 km of Middle to Late Cambrian shallow water carbonates and intrashelf basin shale and siltstone. Passive margin sedimentation was influenced by depocenters in Tennessee and Pennsylvania and arches in central Virginia and New Jersey (Palmer, 1971; Read, 1989). The passive margin was deformed during the early Middle Ordovician with the development of a foreland basin by Taconic thrust loading.

The Cordilleran passive margin of the Great Basin accumulated approximately 2 km of post-rift Middle and Late Cambrian subtidal to peritidal carbonates and fine siliciclastics above almost 6 km of Late Proterozoic-Early Cambrian syn-rift terrigenous and shallow marine siliciclastics (Stewart and Poole, 1974; Levy and Christie-Blick, 1989). Sedimentation patterns on the platform were affected by the east-west trending Uinta-Tooele arch of northern Utah, which separated the Great Basin platform into two depocenters: the Ibex basin of western Utah - eastern Nevada and the Tristate basin of northwestern Utah, northeastern Nevada and southern Idaho (Stewart and Poole, 1974). Thermally-controlled subsidence continued into Late Devonian time when a change to foreland basin conditions occurred in response to Antler thrust loading (Stewart and Suczek, 1977; Bond et al., 1989).

Figure 20: Late Cambrian platform morphologies of the Appalachian and Cordilleran passive margins, the Texas craton and the southern Oklahoma aulacogen. Formation and group names superimposed on lithologic symbols.

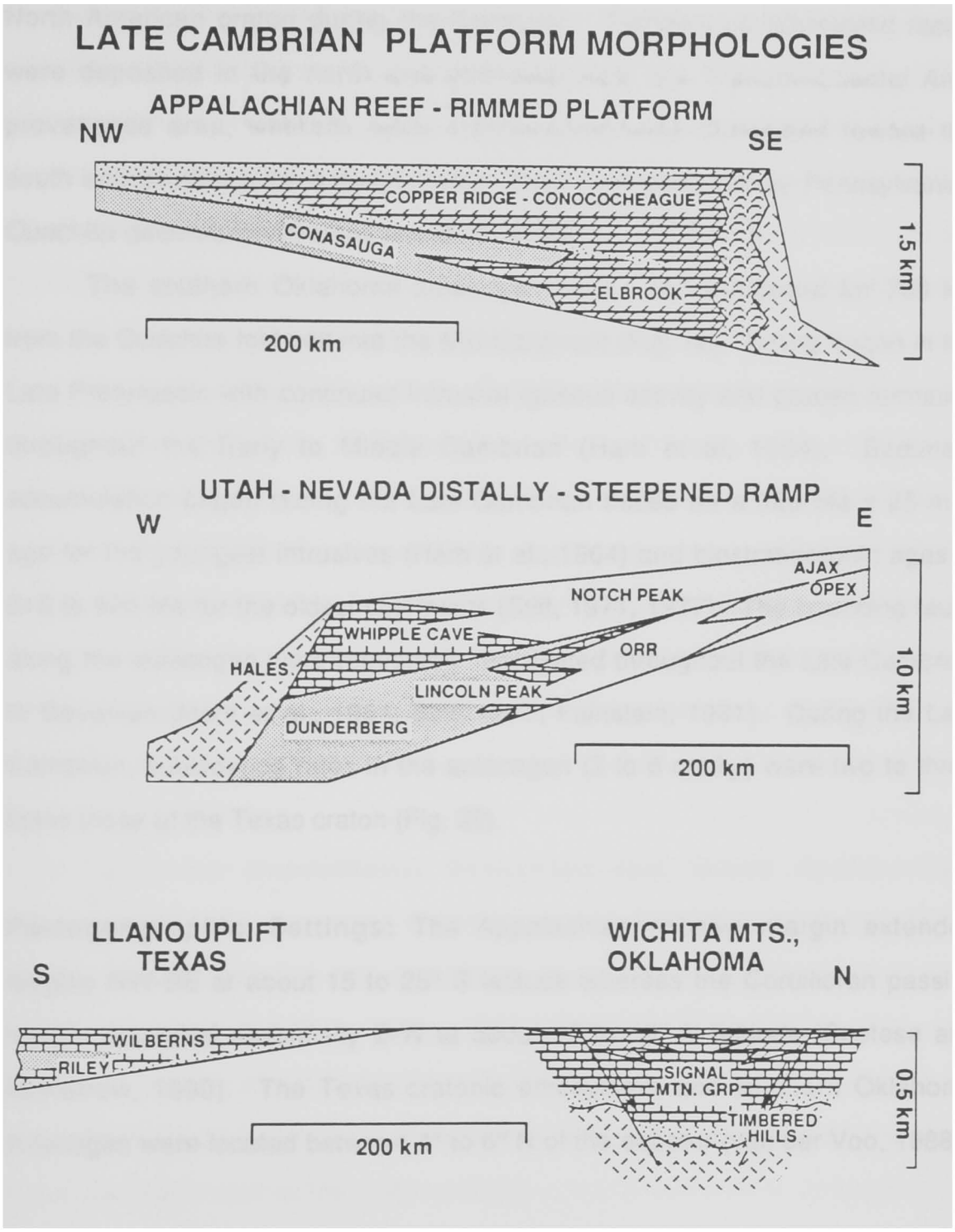
LATE CAMBRIAN PLATFORM MORPHOLOGIES
APPALACHIAN REEF - RIMMED PLATFORM
NW
SE
COPPER RIDGE - CONOCOCHEAGUE
CONASAUGA
ELBROOK
200 km
1.5 km
UTAH - NEVADA DISTALLY - STEEPENED RAMP
W
E
AJAX
OPEX
NOTCH PEAK
WHIPPLE CAVE
ORR
HALES
LINCOLN PEAK
DUNDERBERG
200 km
1.0 km
LLANO UPLIFT
TEXAS
WICHITA MTS.,
OKLAHOMA
S
N
WILBERNS
RILEY
SIGNAL
MTN. GRP
TIMBERED
HILLS
200 km
0.5 km

The Llano uplift area of central Texas was part of the slowly subsiding North American craton during the Cambrian. Terrigenous siliciclastic facies were deposited in the north and northwest near the Transcontinental Arch provenance area, whereas open marine carbonates dominated toward the south and southeast on a deeper water shelf, now obscured by Pennsylvanian Ouachita deformation (Barnes and Bell, 1977).

The southern Oklahoma aulacogen trends northwestward for 700 km from the Ouachita fold belt into the Mid-Continent (Fig. 18). Rifting began in the Late Proterozoic with continued intrusive igneous activity and graben formation throughout the Early to Middle Cambrian (Ham et al, 1964). Sediment accumulation began during the Late Cambrian based on a 525 Ma ± 25 m.y. age for the youngest intrusives (Ham et al., 1964) and biostratigraphic ages of 515 to 520 Ma for the oldest sediments (Stitt, 1971, 1977). The bounding faults along the aulacogen were repeatedly reactivated throughout the Late Cambrian to Devonian (Ham et al., 1964; Stitt, 1977; Feinstein, 1981). During the Late Cambrian, subsidence rates in the aulacogen (3 to 6 cm/ky) were two to three times those of the Texas craton (Fig. 20).

Paleogeographic Settings: The Appalachian passive margin extended roughly NW-SE at about 15 to 25° S latitude whereas the Cordilleran passive margin extended essentially E-W at about 10 to 15° N latitude (Scotese and McKerrow, 1990). The Texas cratonic embayment and southern Oklahoma aulacogen were located between 4° to 6° N of the equator (van der Voo, 1988).

Biostratigraphy and Absolute Ages: Biostratigraphic control for Late Cambrian strata consists of 10 major trilobite zones, a few subzones and conodont zonation toward the later stages of the period (Fig. 19). This relative time control is enhanced by the occurrence of three biomere boundaries, narrow intervals of abrupt changes in trilobite faunas (Palmer, 1965; 1984). Generally agreed to be isochronous time markers, biomere boundaries provide excellent datums for chronostratigraphic correlation. Relative age assignments were determined from published biostratigraphic data (Palmer, 1954; 1965; 1971; Robison, 1964; Derby, 1965; Rassetti, 1965; Longacre, 1970; Hintze, 1974; Hintze and Palmer, 1976; Barnes and Bell, 1977; Stitt, 1971; 1977; Hintze et al, 1980; Eby, 1981; Taylor and Miller, 1981; Stitt et al, 1981; Miller et al, 1982; Orndorff, 1988; Sundberg, 1990). Upper and lower age limits of 525 Ma to 505 Ma were used for the Late Cambrian based on the DNAG time scale (Palmer, 1983). Dividing the 20 m.y. of Late Cambrian time by the ten trilobite zones equates to an average of ±2 million years per zone, relatively good resolution for the Early Paleozoic.

Late Cambrian Depositional Sequences and Grand Cycles: Two major second-order sequences separated by a cratonwide unconformity at the Dresbachian-Franconian boundary have long been recognized within Late Cambrian strata (Lochman-Balk, 1971; Palmer, 1971; 1981b) (Fig. 19). Subaerial erosion associated with unconformity development has removed the *Dunderbergia* and part of the *Aphelaspis* zones from localities on the North American craton and on the craton margin.

Shorter-term (1-10 m.y. duration) depositional sequences, including grand cycles of the southern Canadian Rockies, have also been defined in the Late Cambrian (Aitken, 1978; 1981; King and Chafetz, 1975; Stitt, 1977; Palmer, 1981a; Chow and James, 1987; James et al., 1989; Koerschner and Read, 1989; Read, 1989). Grand cycles, consisting of a lower shaly half-cycle and an upper carbonate half-cycle spanning two or more trilobite zones over 90 to 720 meters (Aitken, 1981), appear to be synonymous with large-scale third-order sequences of Vail and others (1977).

Attempts at interbasinal correlation of Late Cambrian grand cycles (Aitken, 1981; Chow and James, 1987) have focused on the isochroneity of grand cycle boundaries as datums for correlation with limited success. Other attempts at interbasinal correlation of Late Cambrian sequences (Palmer, 1981a) have been hampered by a lack of bio- and lithostratigraphic resolution. However, Aitken (1981) and Bond and others (1989) used detailed lithostratigraphic correlation of biostratigraphically well-constrained sections of Late Cambrian strata to recognize numerous third-order shallowing-upward sequences both within grand cycles and within dominantly carbonate successions elsewhere on the continent. In the following section, the degree of time equivalence of Late Cambrian depositional sequences and the relative sea level fluctuations that generated them are examined.

DEFINITION OF LATE CAMBRIAN SEA LEVEL CURVES

Graphic correlation of biostratigraphically well-constrained strata was used to establish equivalency between stratigraphic cycles (tens to hundreds of meters thick) between the individual sections. Third-order sequences and the

sea level cycles that generated them can be defined qualitatively and semi-quantitatively by the following techniques.

1) Paleobathymetric curves distinguish deepening-upward and shallowing-upward successions of genetically-related stratigraphic intervals.

2) Fischer plots of meter-scale cycles define changes in relative sea level based on the amount of extra accommodation space produced by eustacy beyond that provided by subsidence.

3) Subsidence analysis is useful in determining the net eustatic component of total subsidence after the effects of tectonic subsidence, sediment loading, compaction and water depths of lithofacies have been removed from the observed cumulative subsidence curve.

All of these techniques can be combined and crosschecked to evaluate the degree of synchroneity between equivalent sections in the various locations and to establish a composite Late Cambrian sea level curve.

GRAPHIC CORRELATION

Graphic correlation (Shaw, 1964; Miller, 1977; Edwards, 1984) was used in this study to determine whether the sequences are recognized interbasinally and to establish the relative degree of synchroneity. The Utah section was chosen as the standard reference section due to its good biostratigraphic control, its completeness of section with no visible major erosional unconformities and its excellent exposure. It also has the advantage of having three biomere boundaries each defined to within less than one meter which provide excellent isochronous datums useful for establishing a reliable line of correlation.

Only the first occurrence of each faunal zone is plotted (Fig. 22); this has been justified by Kauffman (1988) who considered the first appearance of a fossil to be "near-isochronous", whereas last appearances are notably diachronous. Trilobite zones define most of the control points with conodont zonation incorporated throughout the Trempealeauan stage. The line of correlation was determined from least squares regression and implies a constant ratio between the average accumulation rates of the two sections (Miller, 1977). The effects of differential compaction on the slope of the line of correlation were not investigated, but Nemec (1988) recognized, in a series of experiments between compacted and decompacted sections, that the slopes remained essentially the same regardless of the heterogeneity of the sections being compared.

A significant problem that was encountered was tying together biostratigraphically well-constrained sections in Utah, Texas and Oklahoma with poorly fossiliferous sections of the Appalachians. Biostratigraphic control is reasonable in the Conasauga Basin shaly sections but is poor within the peritidal Elbrook, Copper Ridge, Conococheague and Allentown sections due to the restricted environments under which they were deposited. Correlation was accomplished by using relative subsidence rates of the sections to establish a slope of the line of correlation. The line of correlation was anchored to a common biostratigraphic pick between the two sections (e.g., the Cambrian - Ordovician boundary) and the first occurrences of the trilobite zones from the fossiliferous section were located along the line of correlation.

Depositional sequences were defined on the basis of deepening- and shallowing-upward trends and were considered to be essentially coeval if their

points of intersection fell within reasonable proximity to the line of correlation. One example of how depositional sequences were correlated between sections in Utah and Texas is shown in Figure 22 (see Fig. 21 for a key to symbols and Appendix I for the other graphic correlation plots). These sections span the entire Late Cambrian interval and show the correlations of the tops of six shallowing-upward sequences. The flat line offsetting the two segments of the line of correlation corresponds to a major unconformity that separates Dresbachian from Franconian strata in central Texas. The equivalent interval in Utah is a well-defined shallowing-upward sequence in the Johns Wash Member of the Orr Formation (Rees et al., 1976). This unconformity appears to represent about 1.5 m.y. of erosion and/or non-deposition by estimating time from the 180 meters or so of section in the continually subsiding Utah locality.

Tops of other major shallowing-upward depositional sequences occur near the end of *Cedaria* time and the end of *Crepicephalus* time as well as throughout the *Elvinia* to *Saukia* trilobite zones. A major depositional sequence contact can also be recognized in the two sections near the Cambrian - Ordovician boundary.

Superimposed smaller-scale depositional sequences, recognized within the six events correlated on the plot in Figure 22, can also be correlated between sections. To refine the resolution of sequence correlation, the slopes of the line of correlation were used for shorter stratigraphic intervals where more lithologic detail could be integrated into the method. The projected time-equivalent intervals determined from the graphic correlation were correlated lithostratigraphically using isochronous biomere boundaries as time datums.

Figure 21: Key to depositional lithofacies for subsequent figures.

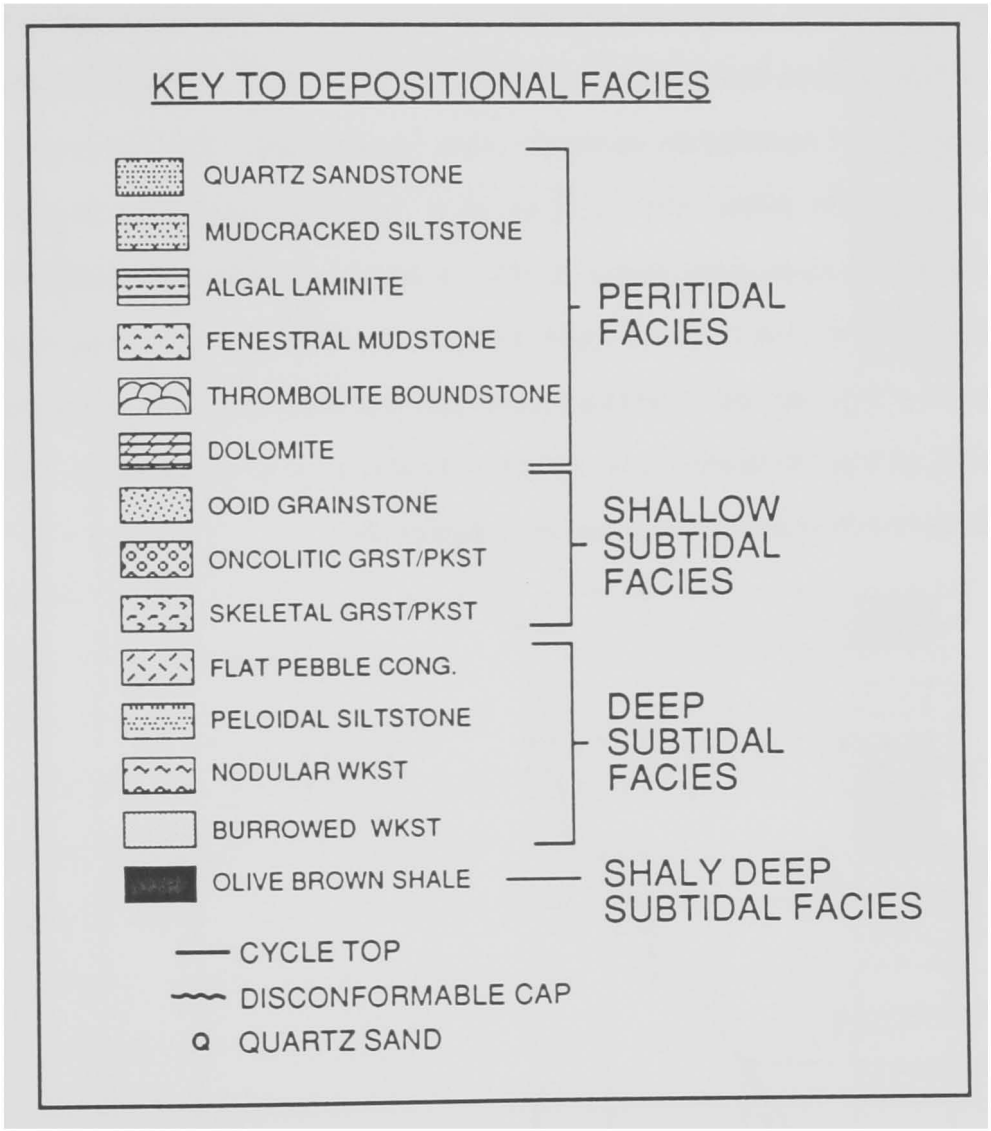
KEY TO DEPOSITIONAL FACIES
QUARTZ SANDSTONE
MUDCRACKED SILTSTONE
ALGAL LAMINITE
FENESTRAL MUDSTONE
THROMBOLITE BOUNDSTONE
DOLOMITE
PERITIDAL FACIES
OOID GRAINSTONE
ONCOLITIC GRST/PKST
SKELETAL GRST/PKST
SHALLOW SUBTIDAL FACIES
FLAT PEBBLE CONG.
PELOIDAL SILTSTONE
NODULAR WKST
BURROWED WKST
DEEP SUBTIDAL FACIES
OLIVE BROWN SHALE
SHALY DEEP SUBTIDAL FACIES
CYCLE TOP
DISCONFORMABLE CAP
Q QUARTZ SAND

Figure 22: Graphic correlation plot of the Utah (horizontal) and Texas (vertical) sections. Black dots are the first occurrences of trilobite and conodont zones and were used to establish the line of correlation between the sections. Biomere boundaries have a cross through the black dot. Trilobite zones noted along the line of correlation between zone boundaries. The flat trend on the line of correlation marks the location of a major unconformity in the Texas section and its equivalent strata in the continuously subsiding Utah section. Vertical and horizontal tie lines mark the tops of major transgressive-regressive successions that can be correlated between the two sections. Note the good alignment of the correlated sequences with the line of correlation. All other graphic correlation plots can be found in Appendix I.

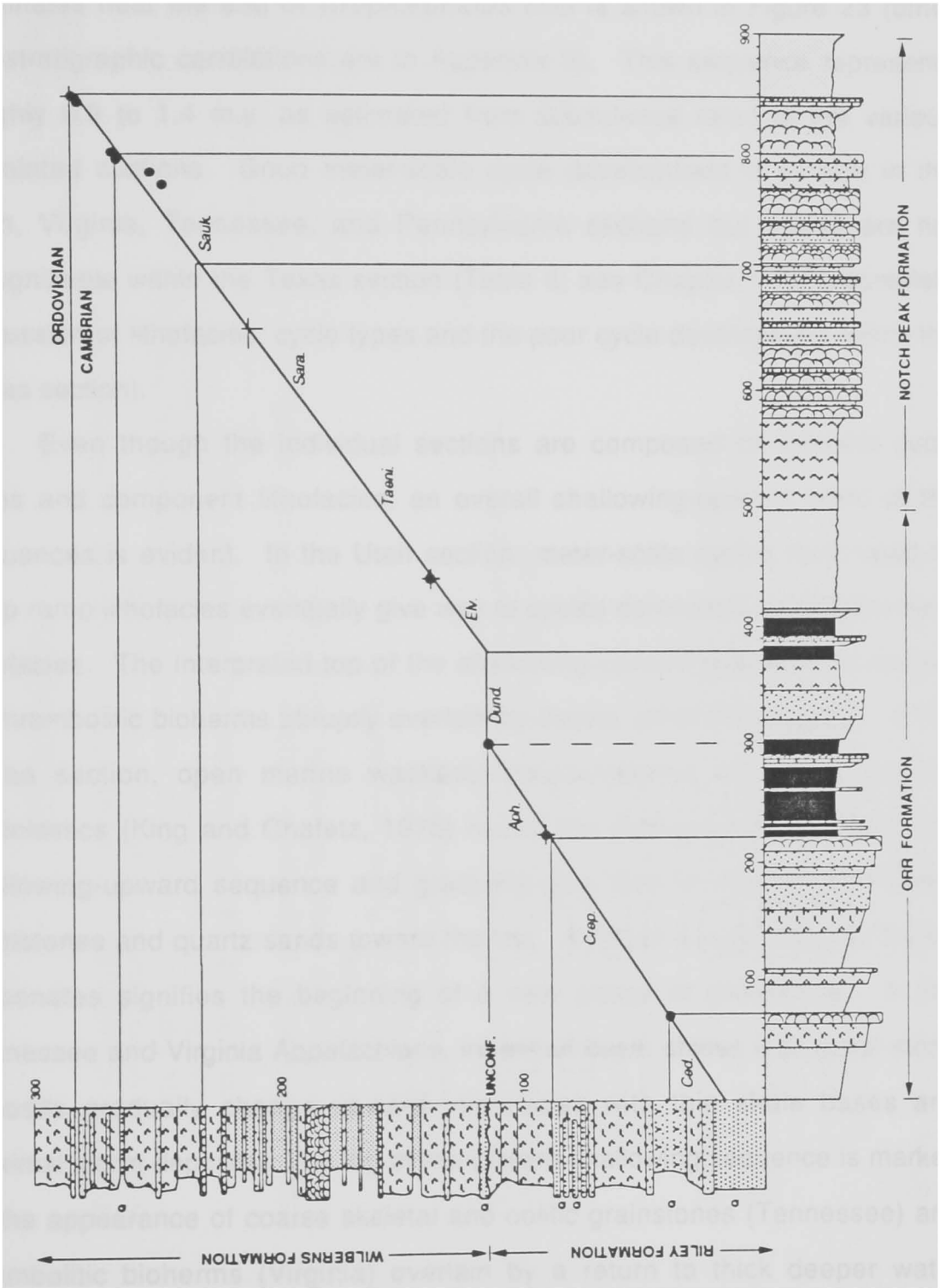
ORDOVICIAN
CAMBRIAN
Sauk
Sara.
Taeni.
Ev.
Dund.
Ash
Crep
Ced
UNCONF.
300
200
100
900
800
700
600
500
400
300
200
100
NOTCH PEAK FORMATION
ORR FORMATION
WILBERNS FORMATION
RILEY FORMATION

An example of a smaller-scale shallowing-upward sequence that terminates near the end of *Crepicephalus* time is shown in Figure 23 (other lithostratigraphic correlations are in Appendix II). This sequence represents roughly 0.9 to 1.4 m.y. as estimated from subsidence rates of the various correlated sections. Good meter-scale cycle development is evident in the Utah, Virginia, Tennessee, and Pennsylvania sections but cycles are not recognizable within the Texas section (Table 6; see Chapter 1 for a complete discussion of lithofacies, cycle types and the poor cycle development within the Texas section).

Even though the individual sections are composed of different cycle types and component lithofacies, an overall shallowing-upward trend of the sequences is evident. In the Utah section, meter-scale cycles dominated by deep ramp lithofacies eventually give way to cycles dominated by shallow ramp lithofacies. The interpreted top of the shallowing-upward sequence is marked by thrombolitic bioherms abruptly overlain by deeper ramp shaly cycles. In the Texas section, open marine wackestones/packstones overlying tidal flat siliciclastics (King and Chafetz, 1975) record the transgressive phase of the shallowing-upward sequence and gradually give way to coarse, well-sorted grainstones and quartz sands toward the top. A return to open marine muddy carbonates signifies the beginning of a new phase of deepening. In the Tennessee and Virginia Appalachians, intrashelf basin shales with distal storm deposits gradually change upward into cycles with thin shale bases and proximal storm deposits. The top of the upward-shallowing sequence is marked by the appearance of coarse skeletal and oolitic grainstones (Tennessee) and thrombolitic bioherms (Virginia) overlain by a return to thick deeper water

TABLE 6

LITHOFACIES	ESTIMATED WATER DEPTHS
Peritidal Lithofacies: Lithologies showing evidence of periodic intertidal exposure or accumulation just below low tide levels.	
- Quartz Sandstone; Cryptalgal Laminite; Fenestral Mudstone; Intraclast Breccia; Mudcracked Siltstones; Thick Laminite; Ribbon Carbonate; Thrombolite-Stromatolite Boundstone; Grainstone Lags	0-2 m
Shallow Subtidal Lithofacies: High energy carbonate sands deposited generally above fairweather wave base.	
- Ooid Grainstone Skeletal-Oncolitic Packstone/Grainstone Globose Thrombolite Bioherms Peloidal Grainstones/Packstone	0-15 m
Deep Subtidal Lithofacies: Storm-influenced muddy sands deposited between fairweather- and storm wave base.	
- Burrowed Wackestone/Packstone Spiculitic Wackestone Nodular Argillaceous Wackestone Micropeloidal Wackestone/Packstone	10-25 m
Intrashelf Basin Lithofacies: Storm-deposited carbonate gravels to fine sands and sub-storm wave base laminated shales deposited within a protected basin.	10-40 m
- Flat Pebble Conglomerate Peloidal Grainstones/Quartz Siltstones Calcareous Shale	
Shaly Deep Ramp: Sub-storm wave base laminated shales with thin mudstone interbeds.	> 30-40 m

Figure 23: Lithostratigraphic chart of correlated sequence at the end of *Crepicephalus* time between Utah, Texas, Tennessee, Virginia and Pennsylvania as determined from graphic correlation. The upper datum is a biomere boundary that is picked to an individual surface in Utah and Texas and a 10 meter zone in Tennessee and Virginia. The boundary is not recognized in Pennsylvania but the section was tied in to the others on the basis of known *Crepicephalus* faunas. Lower correlation line is the top of an earlier shallowing-upward sequence determined from graphic correlation. Short dashes to left of columns are individual meter-scale cycle tops. Field measured thicknesses in meters.

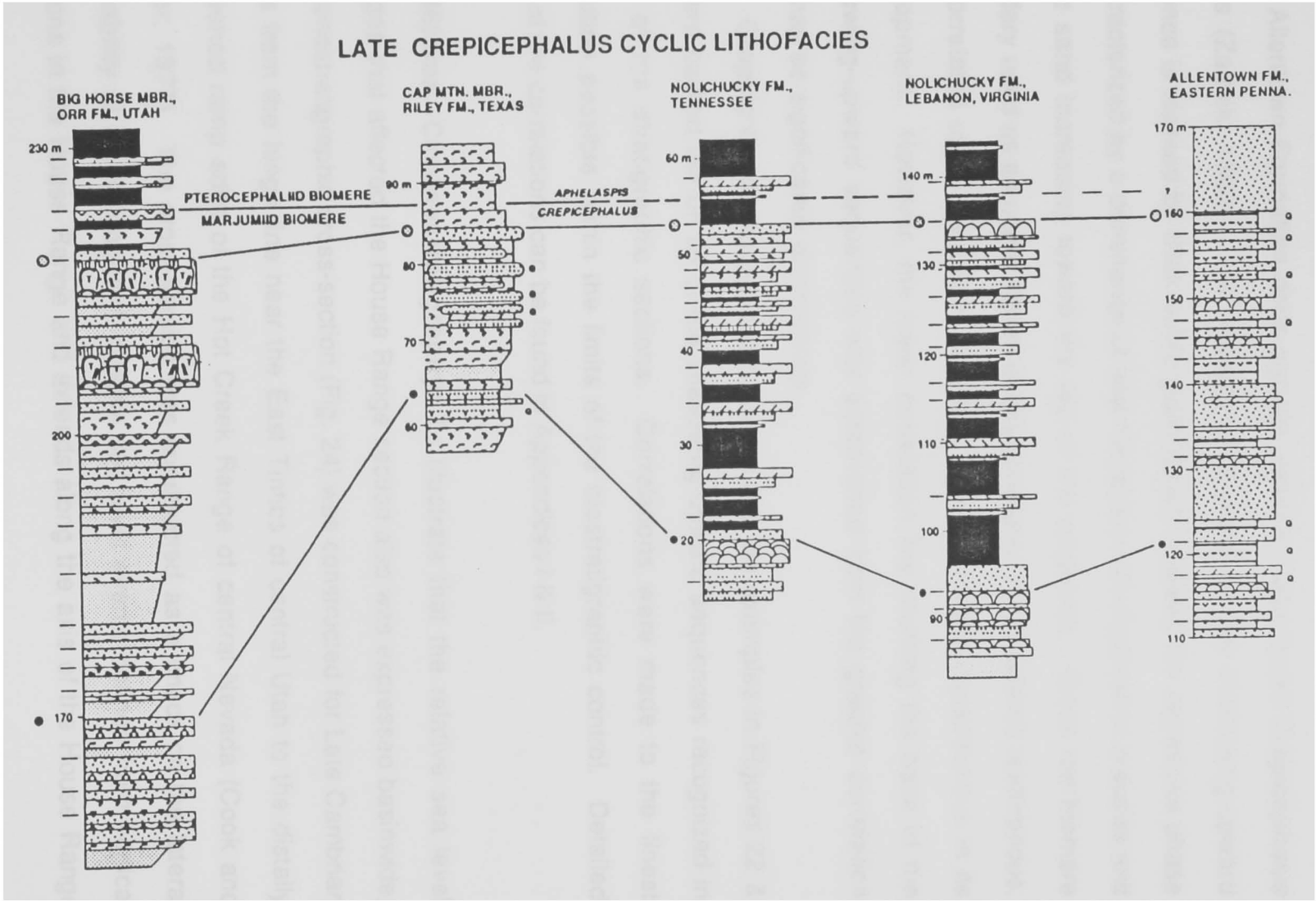
LATE CREPICEPHALUS CYCLIC LITHOFACIES
BIG HORSE MBR., ORR FM., UTAH
CAP MTN. MBR., RILEY FM., TEXAS
NOLICHUCKY FM., TENNESSEE
NOLICHUCKY FM., LEBANON, VIRGINIA
ALLENTOWN FM., EASTERN PENNA.
PTEROCEPHALID BIOMERE
MARJUMIID BIOMERE
APHELASPIS
CREPICEPHALUS
230 m
200
170
90 m
80
70
60
60 m
50
40
30
20
140 m
130
120
110
100
90
170 m
160
150
140
130
120
110

shales. Biostratigraphic control in the Pennsylvania section is lacking but the lower Allentown Formation does contain isolated *Cedaria* and *Crepicephalus* faunas (Zadnik, 1960). The transgressive phase of the shallowing-upward sequence is marked by thick oolitic grainstones whereas the regressive phase is characterized by a dominance of tidal flat facies with desiccation breccias and quartz sand increasing toward the top of the sequence. Since the biomere boundary used as an upper datum in this correlation is considered isochronous, the correlated upper sequence boundary may be roughly synchronous in its development. However, the lower correlation line marking the base of the shallowing-upward sequences was established from the graphic correlation and may be significantly diachronous.

Graphic/lithostratigraphic correlations like the examples in Figures 22 & 23 were carried out on all of the shallowing-upward sequences recognized in each of the stratigraphic sections. Correlations were made to the finest resolution possible within the limits of the biostratigraphic control. Detailed plots of the correlations can be found in Appendices I & II.

Cordilleran Chronostratigraphy: To illustrate that the relative sea level changes that affected the House Range section also was expressed basinwide, a chronostratigraphic cross-section (Fig. 24) was constructed for Late Cambrian strata from the hinge line near the East Tintics of central Utah to the distally steepened ramp edge of the Hot Creek Range of central Nevada (Cook and Taylor, 1977). The cross-section was constructed as a check on the lateral traceability of major long-term relative sea level events defined from vertical sections in the House Range and extends along the axis of the House Range

Figure 24: Chronostratigraphic chart for Late Cambrian strata of Utah - Nevada. Trend of cross-section is down the axis of the House Range Embayment from the hinge line in central Utah to the distally-steepened ramp edge in central Nevada. Distances between ranges were estimated using the palinspastic base map of Levy and Christie-Blick (1989). Data for the plot was derived from detailed logs of the House Range section, field checks of published sections, isopach trends, paleogeographic maps and pinch-out directions.

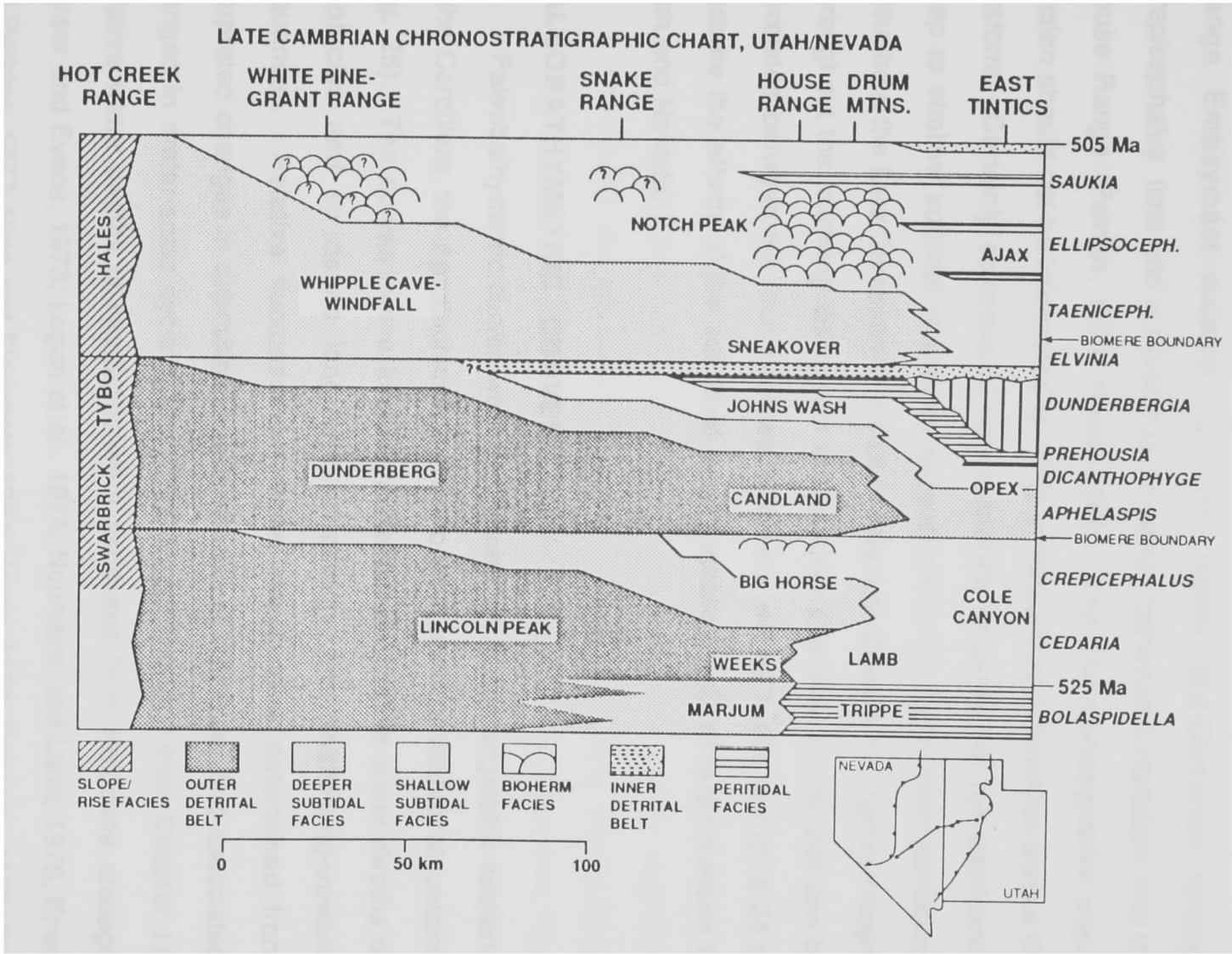
LATE CAMBRIAN CHRONOSTRATIGRAPHIC CHART, UTAH/NEVADA
HOT CREEK RANGE
WHITE PINE-GRANT RANGE
SNAKE RANGE
HOUSE RANGE
DRUM MTNS.
EAST TINTICS
505 Ma
SAUKIA
NOTCH PEAK
AJAX
ELLIPSOCEPH.
HALES
WHIPPLE CAVE-WINDFALL
TAENICEPH.
BIOMERE BOUNDARY
SNEAKOVER
ELVINIA
TYBO
JOHNS WASH
DUNDERBERGIA
PREHOUSIA
DUNDERBERG
OPEX
DICANTHOPHYGE
CANDLAND
APHELASPIS
SWARBRICK
BIOMERE BOUNDARY
BIG HORSE
CREPICEPHALUS
COLE CANYON
LINCOLN PEAK
CEDARIA
WEEKS
LAMB
525 Ma
MARJUM
TRIPPE
BOLASPIDELLA
SLOPE/ RISE FACIES
OUTER DETRITAL BELT
DEEPER SUBTIDAL FACIES
SHALLOW SUBTIDAL FACIES
BIOHERM FACIES
INNER DETRITAL BELT
PERITIDAL FACIES
0
50 km
100
NEVADA
UTAH

embayment, avoiding all peritidal areas along the southern flank. The House Range Embayment existed from the middle Mid-Cambrian through *Crepicephalus* time and is marked by an abrupt bathymetric transition near the House Range (Palmer, 1971; Rees, 1986). The chronostratigraphic cross-section should not be interpreted to imply continuous sedimentation across the platform. Certainly episodes of non-deposition occurred but the dominantly deep to shallow subtidal lithofacies suggest generally submergent conditions throughout the Late Cambrian of the Utah - Nevada Cordilleran passive margin. Throughout the following discussion of the major sea level events that can be correlated between the four localities, reference will be made to Figure 24 to illustrate the effects of the sea level events across the Cordilleran platform in Utah and Nevada.

PALEOBATHYMETRIC CURVES

Paleobathymetric curves were constructed for four stratigraphic sections in the Cordillera, the Appalachians, the Llano uplift and the Wichita Mountains (Fig. 25). The curves define long-term changes in relative water depths of lithofacies and so define long-term deepening- and shallowing-upward sequences. Relative fluctuations in water depth were determined from interpreted changes in depositional environments of lithofacies and associated changes in meter-scale cycle types (Table 6, summarized from Chapter 1). Relative water depths of lithofacies were estimated from Holocene analogs (Purser and Evans, 1973; Logan et al., 1974; Neumann and Land, 1975; Enos and Perkins, 1977; Hine and Steinmetz, 1984; Harris, 1979; Demicco, 1983; Dill et al., 1986), stratigraphic distance of lithofacies below tidal flat caps of peritidal

cycles (Grotzinger, 1986; Koerschner and Read, 1989), and by the relative ordering of facies successions in cycles. Two scales of long-term cyclicity are evident on Fig. 25. The third-order shallowing-upward curves were drawn on the basis of the dominant water depth range represented by stacks of meter-scale cycles that make up the depositional sequences. The two longer-term events separated by the cratonwide unconformity at the Dresbachian - Franconian (*Dunderbergia/Elvinia*) boundary (roughly 9 and 11 m.y., respectively) are noted by the thick horizontal to wavy line crossing the diagram.

Interbasinal Third-Order Shallowing-Upward Events

Dresbachian stage (*Cedaria - Dunderbergia*): Four distinct transgressive-regressive sequences can be recognized within the long-term event that spans the Dresbachian stage (Fig. 25). Using stratigraphic thicknesses and accumulation rates to estimate durations of these events, they range from about 1.5 to 3.0 m.y. (±50%) in duration.

Late *Cedaria*: The earliest correlatable shallowing-upward event occurs toward the end of the *Cedaria* biozone and is recognized in the Utah, Appalachian and Texas sections (Fig. 25). In Utah, upward shallowing of deep ramp lithofacies in the basal Big Horse Member of the Orr Formation culminates in a thick interval of stacked thrombolite bioherms that occur near the *Cedaria - Crepicephalus* contact (Eby, 1981). In the Conasauga intrashelf basin strata of the Virginia-Tennessee Appalachians, upward shallowing toward the end of *Cedaria* time (Sundburg, 1990) is suggested by an upward transition from deep intrashelf basin shales into quartzose peloidal packstones and flat pebble

Figure 25: Plots of relative interpreted paleo-water depths of lithofacies for stratigraphic sections in the House Range of Utah, the Virginia-Tennessee Appalachians, Threadgill Creek in the Llano uplift of central Texas and Kindeblade Ranch, Wichita Mountains, Oklahoma. Lithofacies on the diagrams are generalized with the shaded rectangles identifying tidal flat-dominated lithofacies (TF) from shallow subtidal- (SS), deep subtidal- (DS) and shaly deep subtidal-dominated lithofacies (SH). The sections have been expanded for ease of correlation; notice the difference in thickness between each of the sections. The Cambrian-Ordovician boundary establishes the upper datum. Trilobite zonation noted to the right of each relative water depth curve. The two long-term shallowing-upward events of the Late Cambrian are separated by the heavy dark horizontal line crossing the middle of the diagram (wavy near unconformities). Other major shallowing-upward events are correlated by thin horizontal tie lines. The Appalachian column is a composite of three sections from the Conasauga intrashelf basin and the peritidal platform.

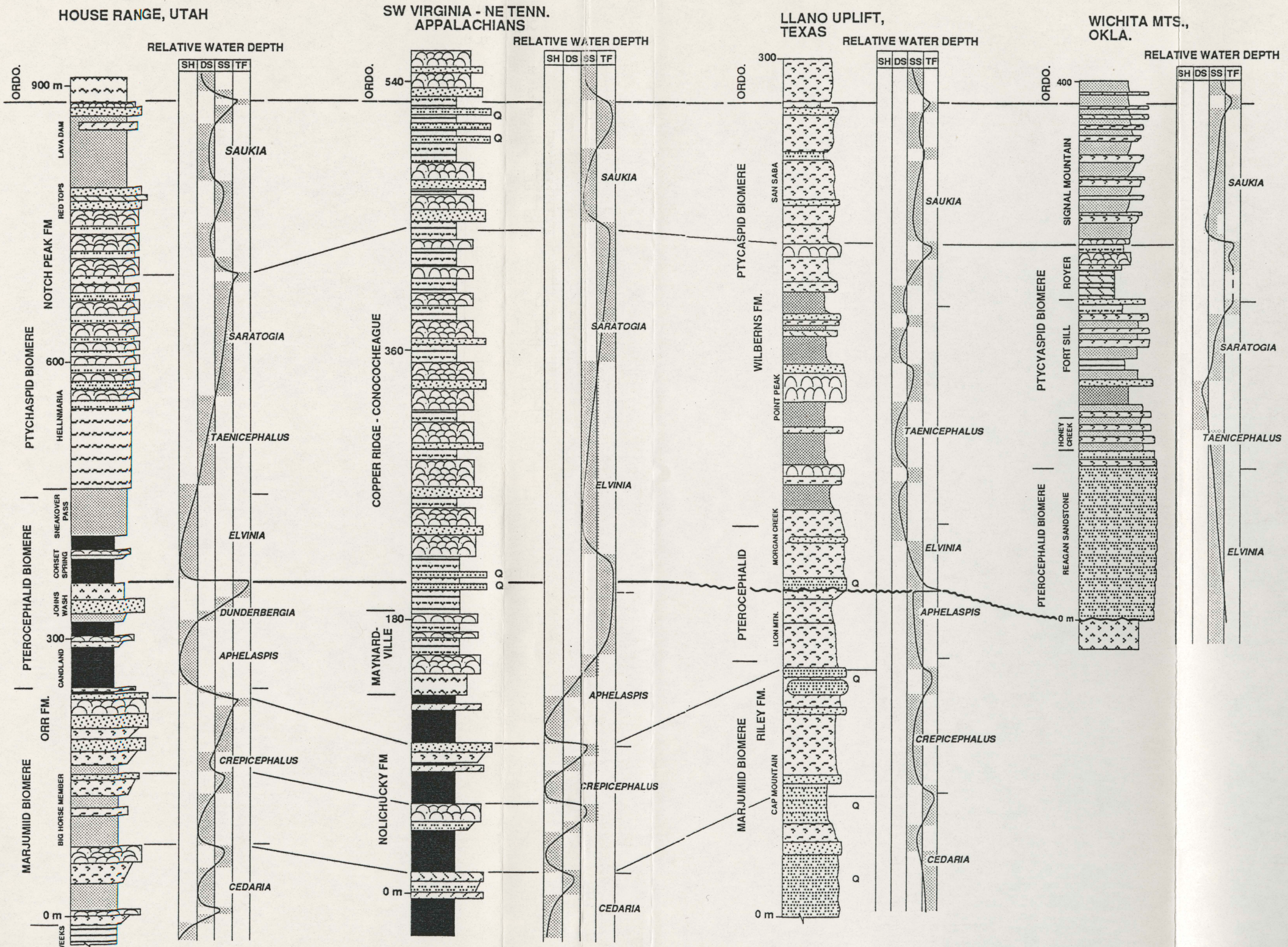
HOUSE RANGE, UTAH
SW VIRGINIA - NE TENN. APPALACHIANS
LLANO UPLIFT, TEXAS
WICHITA MTS., OKLA.
RELATIVE WATER DEPTH
SH DS SS TF
ORDO.
900 m
600
300
0 m
540
360
180
0 m
300
0 m
400
0 m
PTYCHASPID BIOMERE
NOTCH PEAK FM
LAVA DAM
RED TOPS
HELLNMARIA
PTEROCEPHALID BIOMERE
SNEAKOVER PASS
CORSET SPRING
JOHNS WASH
CANDLAND
ORR FM.
MARJUMID BIOMERE
BIG HORSE MEMBER
WEEKS
COPPER RIDGE - CONOCOCHEAGUE
MAYNARD-VILLE
NOLICHUCKY FM
WILBERNS FM.
SAN SABA
POINT PEAK
PTYCASPID BIOMERE
MORGAN CREEK
LION MTN.
PTEROCEPHALID
RILEY FM.
CAP MOUNTAIN
MARJUMID BIOMERE
PTYCYASPID BIOMERE
SIGNAL MOUNTAIN
ROYER
FORT SILL
HONEY CREEK
REAGAN SANDSTONE
PTEROCEPHALID BIOMERE
Q
SAUKIA
SARATOGIA
TAENICEPHALUS
ELVINIA
DUNDERBERGIA
APHELASPIS
CREPICEPHALUS
CEDARIA

conglomerates of the lower limestone member of the Nolichucky Formation. Shallowing in the Texas section occurs within flaser-bedded quartz siltstones of the Cap Mountain Member of the Riley Formation previously interpreted as tidal flat facies (King and Chafetz, 1975) and correlated with a disconformity in the Mid-continent by Palmer (1954). These shallowing-upward sequences in all three localities are abruptly overlain by deeper water cycles that mark the initial transgression of the overlying event.

Mid-*Crepicephalus*: Deepening followed by distinct shallowing occurs in the Big Horse Member of Utah within a transition from open marine, deep ramp cycles into shallow ramp oolitic-oncolitic cycles that indicate increasingly restricted conditions. Graphic correlation suggests that this same event in the Appalachians is represented by intrashelf basin shales that grade up into interbedded oolitic grainstones and thrombolitic bioherms of the middle limestone member of the Nolichucky Formation. This event is not recognized within the Texas section due to the monotonously stacked skeletal packstones and grainstones that comprise the upper Cap Mountain Member.

Late *Crepicephalus*: This upward-deepening followed by upward-shallowing event is comprised of two smaller-scale events (not shown on Fig. 25), the upper one of which is shown on the lithostratigraphic correlation diagram (Fig. 23). In Utah, upward shallowing culminates in a transition from shallow subtidal oolitic grainstone-capped cycles into large thrombolitic bioherms capped by club-shaped stromatolites (Lohmann, 1976). A transgressive oolitic grainstone blankets the bioherms and is immediately

overlain by deep ramp shaly cycles of the Candland Shale Member. This shallowing event is evident on the chronostratigraphic diagram (Fig. 24) by seaward progradation of shallow subtidal facies that mark the termination of the House Range embayment at the end of *Crepicephalus* time (Rees, 1986).

Graphic correlation with Appalachian sections of the Nolichucky Formation suggests that this event is manifested by upward shallowing from distal to proximal storm deposits capped by amalgamated flat pebble conglomerate storm beds, oolitic grainstones and thrombolitic bioherms (Fig. 23). In peritidal sections of the Appalachians such as the Allentown Formation of eastern Pennsylvania, this event may be represented by upward transitions from subtidal-dominated peritidal cycles into tidal flat-dominated cycles with brecciated regolithic caps and quartz sands reworked into laminite facies (Fig. 23).

A major influx of quartz sands interbedded with coarse skeletal grainstones occurs near the end of *Crepicephalus* time in the Cap Mountain Member of Texas suggesting proximity of a siliciclastic shoreline associated with regressive conditions. However, the superimposed smaller-scale shallowing within this interval recognized in the other localities is not evident within the homogeneous skeletal grainstones of the Cap Mountain Member.

Aphelaspis* to earliest *Elvinia: Abrupt deepening during early *Aphelaspis* time is evident in Utah by deep ramp shaly cycles of the Candland Shale Member. These grade upward into burrowed wackestones/packstones of the Johns Wash Member that ultimately shallow up into oolitic grainstones and fenestral mudstones (Rees et al., 1976) of earliest *Elvinia* age (Hintze and

Palmer, 1976). The chronostratigraphy of the Utah-Nevada passive margin (Fig. 24) shows this event as major onlapping of outer detrital belt shales onto the platform followed by subsequent offlap of shallow subtidal and peritidal lithofacies, and development of an unconformity near the Cordilleran hinge line (East Tintic region).

Aphelaspis time in the Conasauga basin of the Appalachians is marked by widespread expansion of upper Nolichucky shales onto the surrounding peritidal platform. These deep intrashelf basin shales grade up into deep ramp ribbon rocks and overlying cryptalgal laminites of the Maynardville Formation. The Dresbachian/Franconian unconformity on the craton is represented in the Tennessee - Virginia Appalachians as a very thin interval in the basal Copper Ridge Formation (earliest *Elvinia*; Palmer, 1971, pers. comm.) characterized by an influx of quartz sand, thin, tidal flat-dominated peritidal cycles, an absence of *Dunderbergia* faunas and subtle erosional truncation to some cycle tops (Appendix II). However, the biostratigraphic control in the Appalachians is insufficient to estimate a duration of exposure, and unequivocal evidence for a major exposure surface is lacking.

In the Texas cratonic section, the long-term lowstand at the Dresbachian-Franconian boundary is manifested as an unconformity (Lochman-Balk, 1971; Palmer, 1981a) that has cut out the *Dunderbergia* and part of the underlying *Aphelaspis* trilobite zones. The initial deepening during early *Aphelaspis* time is not recognized within stacked skeletal grainstones of the Lion Mountain Member but may have been removed by erosion associated with unconformity development. Graphic correlation with the constantly subsiding House Range section suggests that subaerial erosion persisted for about 1.5 m.y.

Franconian-Trempealeauan Stages (*Elvinia - Saukia*): The long-term event that spans the Franconian-Trempealeauan stages culminates in a major lowstand near the Cambrian-Ordovician boundary. Two third-order transgressive-regressive sequences can be recognized within the long-term event. The shallowing event that separates these two third-order sequences is subtle in some localities where no major differences in relative water depth of lithofacies occur, but is clearly evident in other sections. From stratigraphic thicknesses and accumulation rates in each of the sections, the older event is estimated to span approximately 7 m.y. and the younger event about 4 m.y. (±50%).

***Elvinia* to early *Saukia*:** In Utah, the transgressive base of the long-term Franconian-Trempealeauan second-order event is represented by shaly cycles of the inner detrital belt Corset Spring Member. These shales grade up into argillaceous carbonates of the Sneakover Pass Member "subtidal blanket" of Brady and Rowell (1976) which they recognized to extend across the entire Cordilleran passive margin during middle-late *Elvinia* time (Fig. 24). This drowning event shallows within the basal Hellnmaria Member of the Notch Peak Formation before grading into shallow subtidal/peritidal carbonates with extensive stromatolite-thrombolite bioherm development within the upper Hellnmaria Member. This shallowing is recognized on the chronostratigraphic cross-section (Fig. 24) as a widespread expansion of aggraded, shallow subtidal lithofacies (Hales, Whipple Cave and Windfall Formations) with no direct evidence of detrital siliciclastics recognized anywhere on the platform.

The top of this transgressive-regressive sequence in the House Range is marked by dolomitized fenestral mudstones featuring scalloped erosion surfaces overlain by coarse oncolitic lag deposits. By graphic correlation with the Texas section, this shallowing occurs during earliest *Saukia* time (Appendix I). Deepening above the fenestral mudstones is indicated by thick stacks of globose thrombolitic bioherms.

The predominance of peritidal lithofacies in the Copper Ridge-Conococheague Formations of the Appalachians make the qualitative recognition of long-term transgressive-regressive sequences difficult but systematic changes in stacking patterns of peritidal cycles appear to define long-term fluctuations in relative sea level (Chapter 1). Relative deepening above the basal sands of the Copper Ridge-Conococheague is subtle and may be recognized by the appearance of stacks of thick cycles dominated by thrombolitic bioherms. Upward shallowing is suggested by a change in cycle stacking pattern to thin, tidal flat-dominated cycles. Graphic correlation with the top of this depositional sequence in the other sections where it is better defined suggests that relative shallowing is terminated by the abrupt appearance of thick, slightly deeper water, thrombolitic peritidal cycles.

In Texas, the basal unconformity is overlain by transgressive marine sandstones (Welge Member of the Wilberns Formation) and open marine skeletal packstones and grainstones (Morgan Creek Member). Maximum deepening occurs within cyclic fine siltstones and flat pebble conglomerates of the Point Peak Member. Relative water depths progressively shoal into crossbedded skeletal grainstones (San Saba Member) and graphic correlation with the Utah section suggests that maximum shallowing in early *Saukia* time

corresponds to stromatolitic bioherms that exhibit elongate orientations with intervening troughs filled with coarse tidal-deposited skeletal-pelletal grainstones. This entire transgressive-regressive interval is punctuated by episodic shallowing to stacked thrombolitic bioherms over intervals of 10 to 20 meters (fourth-order scale). These intervals cannot be correlated with equivalent strata in the Cordilleran and Appalachian sections.

In the Wichita Mountains of Oklahoma, initial drowning of the southern Oklahoma aulacogen (Fig. 25) began in *Elvinia* time (Stitt, 1971, 1977) with the deposition of the Reagan Sandstone over the rhyolitic basement. Deepening is indicated by cyclic deposition of the open marine skeletal limestones of the Honey Creek and lower Fort Sill Formations. Major shallowing occurs during early *Saukia* time when open marine lithofacies below give way to highly restricted tidal flat facies within the Royer and lower Signal Mountain Formations (cryptalgal laminites and stacked thrombolite bioherms). Coarsely-crystalline dolomite within the Royer contains remnants of fenestral mudstone and oncolitic packstone and probably represents a tongue of peritidal facies that prograded out into the center of the aulacogen from the cratonic margins (Stitt, 1971; 1977). Cryptalgal laminites in the lower Signal Mountain Formation are overlain by open marine wackestones/packstones featuring stacked hardgrounds and glauconite that signal a return to transgressive conditions.

***Saukia* to Cambrian-Ordovician Boundary:** The beginning of the *Saukia* event in the Utah section is marked by subtle deepening into thick stacks of thrombolitic bioherms above the fenestral facies of the previous event. After a brief shoaling into shallow subtidal coarse grainstones and thrombolitic

bioherms (Red Tops Member) a return to deeper subtidal conditions is suggested by the argillaceous wackestone cycles of the Lava Dam Member. However, water depths of this lithofacies may not have been very deep because equivalent age thrombolite bioherms exist in other sections in the House Range and nearby Wah Wah Mountains.

The third-order shallowing evident throughout *Saukia* time culminates at the Cambrian-Ordovician boundary and has been recognized in many sections worldwide (Lange Ranch Eustatic Event of Miller, 1984). Abrupt shallowing from the Lava Dam argillaceous wackestones is manifested by the abrupt appearance of oncolitic packstones and club-shaped stromatolites that are overlain by earliest Ordovician mudstones/wackestones of the upper Lava Dam Member and House Limestone. This lowstand at the end of the Cambrian is recognizable cratonward by a major influx of quartz sand (Wilson, 1952; Palmer, 1971) and is exhibited toward the Cordilleran hinge line in the East Tintic Range by 2 to 6 meters of quartzite (Opahanga Formation; Fig. 24) that are reworked along the Cambrian-Ordovician boundary (Palmer, 1971).

The sea level lowstand at the end of the Cambrian in the Copper Ridge-Conococheague Formations of the Appalachians is marked by thin tidal flat-dominated cycles that contain abundant quartz sand derived from the craton (Wilson, 1952; Palmer, 1971; Orndorff, 1988). In the Tennessee section, the Cambrian-Ordovician boundary is marked by quartz-filled tidal channels cut into laminite facies (Walker, 1985).

In the upper San Saba Member of Texas, coarse skeletal grainstones and interbedded thin dolomitic silty units grade into wave-rippled oolitic grainstones and fenestral mudstones at the Cambrian-Ordovician boundary.

Craton-derived quartz sands are recognized near the end of the Cambrian in Texas toward their northwest provenance (Barnes and Bell, 1977).

Saukia time in Oklahoma is characterized by abrupt deepening into peloidal-skeletal wackestones and packstones of the Signal Mountain Formation followed by gradual shallowing to nonfossiliferous mudstones, peloidal grainstones and flat pebble conglomerates deposited under restricted peritidal conditions at the end of Cambrian time (Taylor, 1984). Four coarsening-upward, short-term third-order cycles are recognized within the lower Signal Mountain Formation but correlation with equivalent intervals in the other localities are equivocal.

The Cambrian-Ordovician boundary appears to have been marked by a faunal crisis among both trilobites and conodonts (top of the Ptychaspid Biomere) (Stitt, 1977; Miller et al., 1982; Miller, 1984). In the Virginia Appalachians, Orndorff (1988) showed that two conodont subzones may be missing or are represented by only 2 meters of strata along the boundary. Taylor (1984) documented a missing trilobite subzone along the boundary in the Texas cratonic section whereas it spanned a 5 meter interval in the Oklahoma section suggesting a significant hiatus in more cratonward sections.

FISCHER PLOTS

Fischer plots (Fig. 26A) are graphic displays of accommodation space, corrected for linear subsidence, through time (Fischer, 1964; Goldhammer et al., 1987; 1990; Read and Goldhammer, 1988; Read, 1989). Each fifth-order, meter-scale cycle is assigned an average cycle period by dividing the total estimated duration of the cyclic succession by the number of meter-scale cycles.

Figure 26A: Explanatory diagram of the Fischer plot technique. Vertical line on each triangle represents the thickness of an individual meter-scale cycle. Sloping line to lower right is the path of linear subsidence. Cycle is assigned an average cycle period over which it is allowed to subside. Line connecting the tops of cycles represents the path of relative sea level through time.

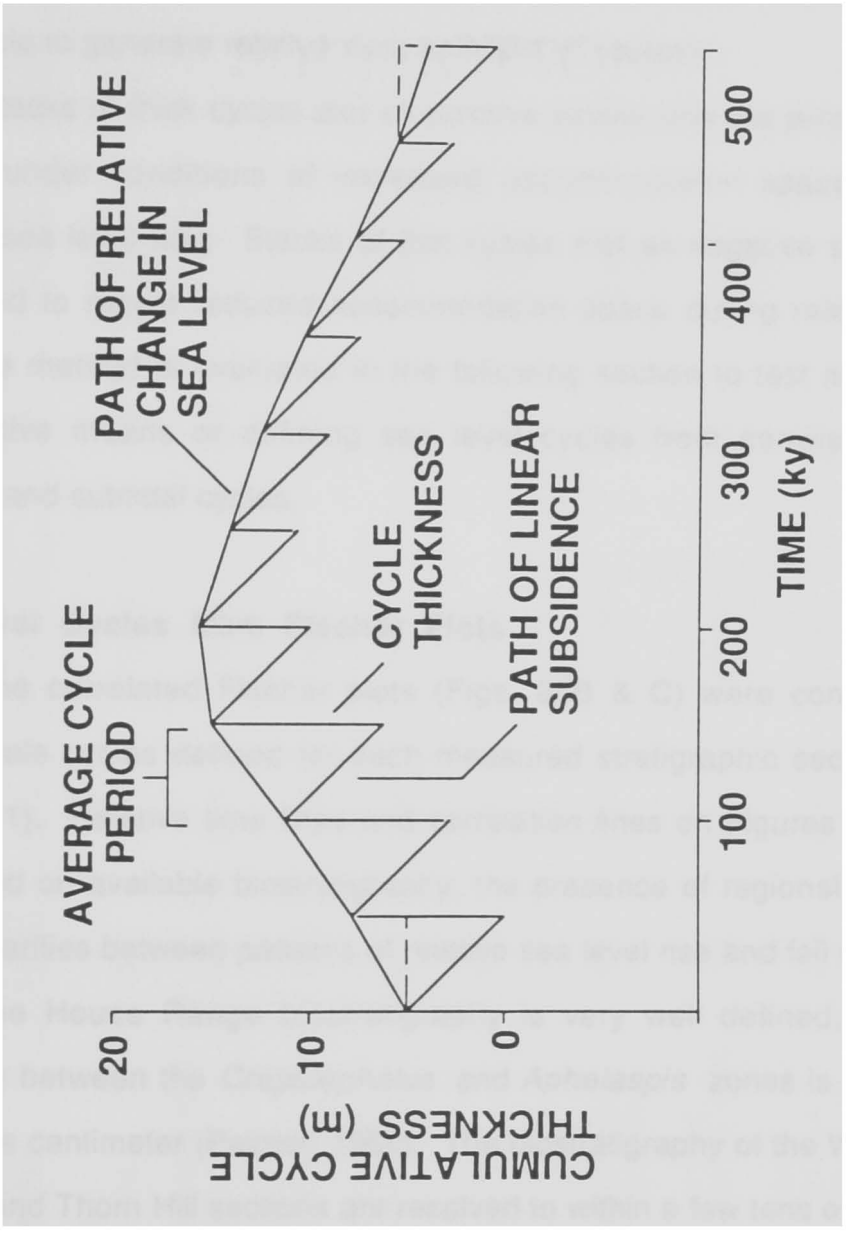
AVERAGE CYCLE PERIOD
PATH OF RELATIVE CHANGE IN SEA LEVEL
CYCLE THICKNESS
PATH OF LINEAR SUBSIDENCE
CUMULATIVE CYCLE THICKNESS (m)
20
10
0
100
200
300
400
500
TIME (ky)

The average cycle period is merely a device for assigning time per cycle and does not imply that each cycle had the same duration. If the plot was constructed so that cycle thickness equaled time, the resulting plot would define a horizontal line. Thus it is necessary to assign a constant time of deposition to each cycle to generate relative rises and falls on the plot.

Stacks of thick cycles plot as positive slopes and are presumed to have formed under conditions of increased accommodation space provided by relative sea level rise. Stacks of thin cycles plot as negative slopes and are presumed to reflect reduced accommodation space during relative sea level fall. The method is evaluated in the following section to test its validity as a quantitative means of defining sea level cycles from correlated stacks of peritidal and subtidal cycles.

Sea Level Cycles from Fischer Plots

The correlated Fischer plots (Figs. 26B & C) were constructed from meter-scale cycles defined for each measured stratigraphic section (Table 7; Chapter 1). Relative time lines and correlation lines on Figures 26B and 26C are based on available biostratigraphy, the presence of regional quartz sands and similarities between patterns of relative sea level rise and fall on the curves.

The House Range biostratigraphy is very well defined; the biomere boundary between the *Crepicephalus* and *Aphelaspis* zones is determined to within one centimeter (Palmer, 1984). The biostratigraphy of the Wright Branch, Duffield and Thorn Hill sections are resolved to within a few tens of meters. The biostratigraphy of the Allentown Formation is poorly defined but the lower part is considered to be Dresbachian in age as determined from sections elswhere

TABLE 7

Formation (locality)	Late Cambrian thk (m)	Total Time (my)	Undecompacted Subsidence Rate (m/ky) (±50%)	Measured Section Thk (m)	Number of cycles Thk (m)	Average Cycle Thk (m)	Average Cycle Period (ky) (±50%)
ALLENTOWN (Easton,Pa.)	560	20.0	0.028	198	113(±8) 198	1.8	64.3
(Carpentersville, N.J.)	560	20.0	0.028	407	109 (±9) 407	3.7	133
ELBROOK (Wytheville, Va.)	525	15.0	0.035	525	270(±25) 525	1.95	54
CONOCOCHEAGUE (Wytheville, Va.)	600	15.0	0.054	394	247(±20) 394	2.4	44.5
NOLICHUCKY-COPPER RIDGE (Thorn Hill)	524	20.0	0.026	160	41(±5) 66	1.6	61.5
ORR-NOTCH PEAK (Orr Ridge, House Range, Utah)	960	20.0	0.048	460	87 (±8) 400	4.6	96
(Steamboat Pass, S. House Range, Utah)	760	20.0	0.038	470	102(±9) 356	3.5	92
RILEY-WILBERNS (Threadgill Creek, Llano uplift, Tx.)	438	20.0	0.022	302			
TIMBERED HILLS-SIGNAL MT. GROUPS (Kindblade Ranch, Wichita Mts., Okla.)	383	9.0	0.043	292	39(±5) 92	2.4	55

(Wilson, 1952; Zadnik, 1960; Palmer, 1971). The curves are plotted along relative time axes but the total time equates to 20 m.y. as estimated from the DNAG time scale (Palmer, 1983).

Calculations of average cycle period and total subsidence rate for each section are shown in Table 7. Shale-based cycles of the Conasauga basin sections (Nolichucky Fm.) were decompacted before plotting (although non-decompacted Fischer plots show the same relative sea level rises and falls but of a lower magnitude). All other sections are limestones and dolomites with minor quartz sandstones and were not decompacted before plotting. The few minor covered intervals were plotted as straight lines and are shown as gaps within the plots.

Several sea level events can be correlated between widely-separated localities using the Fischer plots. The plot for Dresbachian time (Fig. 26B) illustrates generally falling sea level toward the end of *Cedaria* time in both peritidal and subtidal cyclic successions. This gradually falling trend on the Fischer plots correspond to the late *Cedaria* regression recognized on the paleobathymetric curves. A superimposed shorter-term event is also evident during *Cedaria* time within the Allentown, Elbrook and Nolichucky Formations.

A well-defined rise in relative sea level at the beginning of *Crepicephalus* time followed by a relative sea level fall toward the *Crepicephalus /Aphelaspis* biomere boundary is evident on the subtidal cyclic sections of the Nolichucky in Virginia and Tennessee and of the Big Horse Member in Utah. The long-term *Crepicephalus* event is not evident within the peritidal Allentown and Elbrook localities although covered intervals in the Elbrook may mask the event.

Figure 26B: Correlation of Fischer plots for Dresbachian time. Trilobite zonation along the horizontal axis and cumulative thickness in meters, corrected for linear subsidence, along the vertical axis. Upper two Fischer plots (and the latest portion of the Tennessee Fischer plot) are from peritidal cyclic sections whereas the lower three Fischer plots are from shallow to deep subtidal cyclic sections. Quartz sands denoted by black-filled triangles. Covered intervals have been left blank. Vertical dashed lines mark possible correlations of sea level events. Vertical wavy lines indicate the position of the Dresbachian-Franconian unconformity recognized from graphic correlation with other sections.

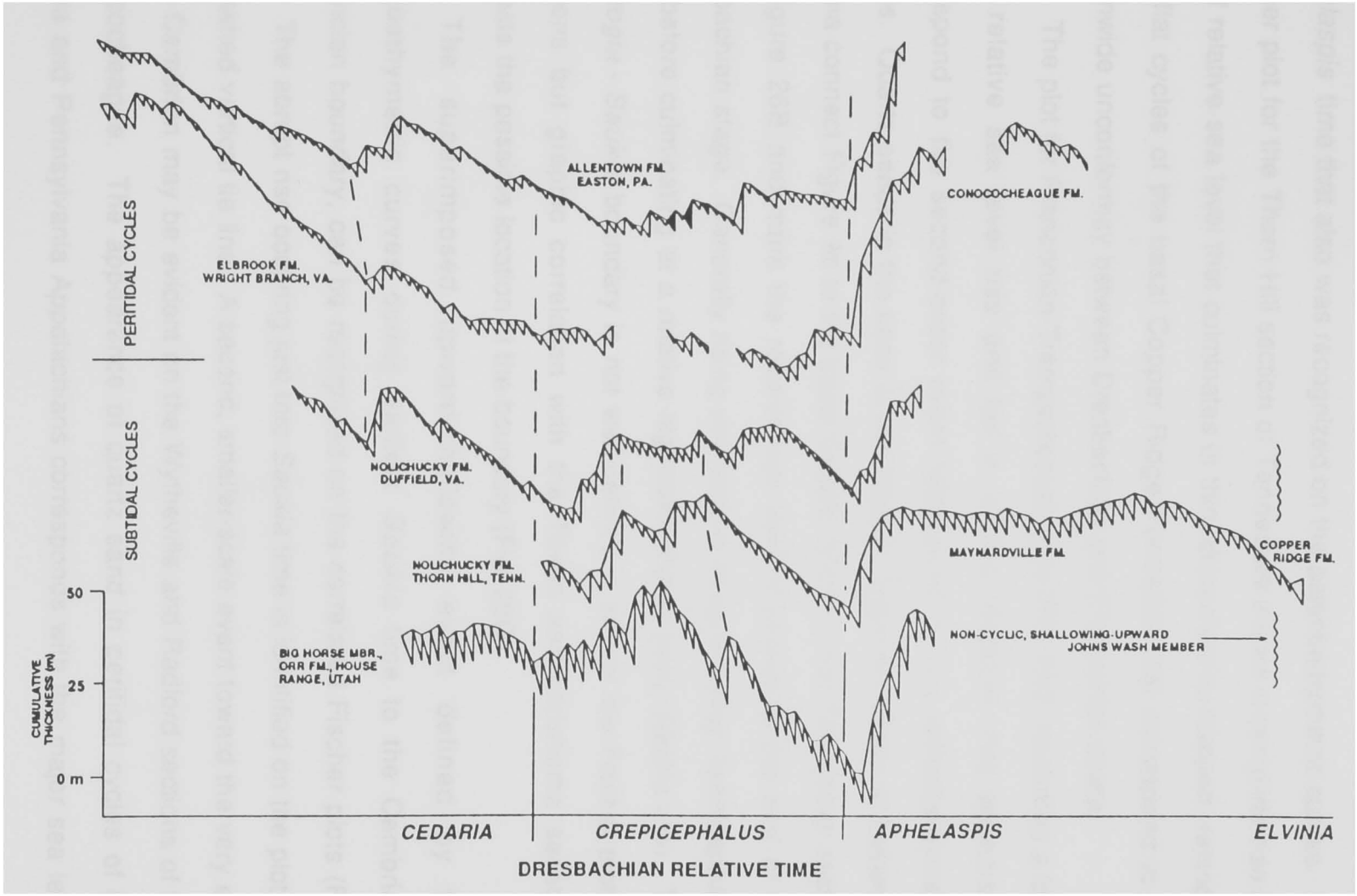
PERITIDAL CYCLES
SUBTIDAL CYCLES
ALLENTOWN FM.
EASTON, PA.
CONOCOCHEAGUE FM.
ELBROOK FM.
WRIGHT BRANCH, VA.
NOLICHUCKY FM.
DUFFIELD, VA.
NOLICHUCKY FM.
THORN HILL, TENN.
MAYNARDVILLE FM.
COPPER RIDGE FM.
BIG HORSE MBR., ORR FM., HOUSE RANGE, UTAH
NON-CYCLIC, SHALLOWING-UPWARD JOHNS WASH MEMBER
CUMULATIVE THICKNESS (m)
50
25
0 m
CEDARIA
CREPICEPHALUS
APHELASPIS
ELVINIA
DRESBACHIAN RELATIVE TIME

All five localities show the rapid sea level rise at the beginning of *Aphelaspis* time that also was recognized on the paleobathymetric curves. The Fischer plot for the Thorn Hill section of Tennessee shows a complete rise and fall of relative sea level that culminates in thin, disconformity-capped, restricted tidal flat cycles of the basal Copper Ridge Formation that correspond to the cratonwide unconformity between Dresbachian and Franconian strata.

The plot for Franconian-Trempealeauan time (Fig. 26C) illustrates a long-term relative sea level rise and fall in all five sections that appears to correspond to the second-order event recognized on the paleobathymetric curves. Quartz sands in the base of the Copper Ridge Formation at Lebanon, Virginia connect Figure 9c to the basal Copper Ridge in the Tennessee section on Figure 26B and mark the relative sea level lowstand at the end of the Dresbachian stage. Generally rising sea level is evident during *Taenicephalus* time before culminating at a relative highstand during early *Saukia* time. The *Saratogia* - *Saukia* boundary is not well-defined in any of the Fischer-plotted locations but graphic correlation with the Texas and Oklahoma sections suggests the possible location of the boundary (Fig. 26C).

The superimposed upward-shallowing event defined by the paleobathymetric curves during earliest *Saukia* time to the Cambrian-Ordovician boundary, can be recognized on the correlated Fischer plots (Fig. 26C). The abrupt rise occuring just into *Saukia* time is identified on the plot by the dashed vertical tie line. A second, smaller-scale event toward the very end of the Cambrian may be evident on the Wytheville and Radford sections of the Conococheague. The appearance of quartz sand in peritidal cycles of the Virginia and Pennsylvania Appalachians corresponds with the major sea level

Figure 26C: Correlated Fischer plots for Franconian-Trempealeauan time. Note position of Cambrian-Ordovician boundary and the appearance of quartz sandy cycles during the sea level lowstand at the end of the Late Cambrian. Plots from the Appalachian sections are peritidal whereas the Utah section is composed of shallow to deep subtidal cycles.

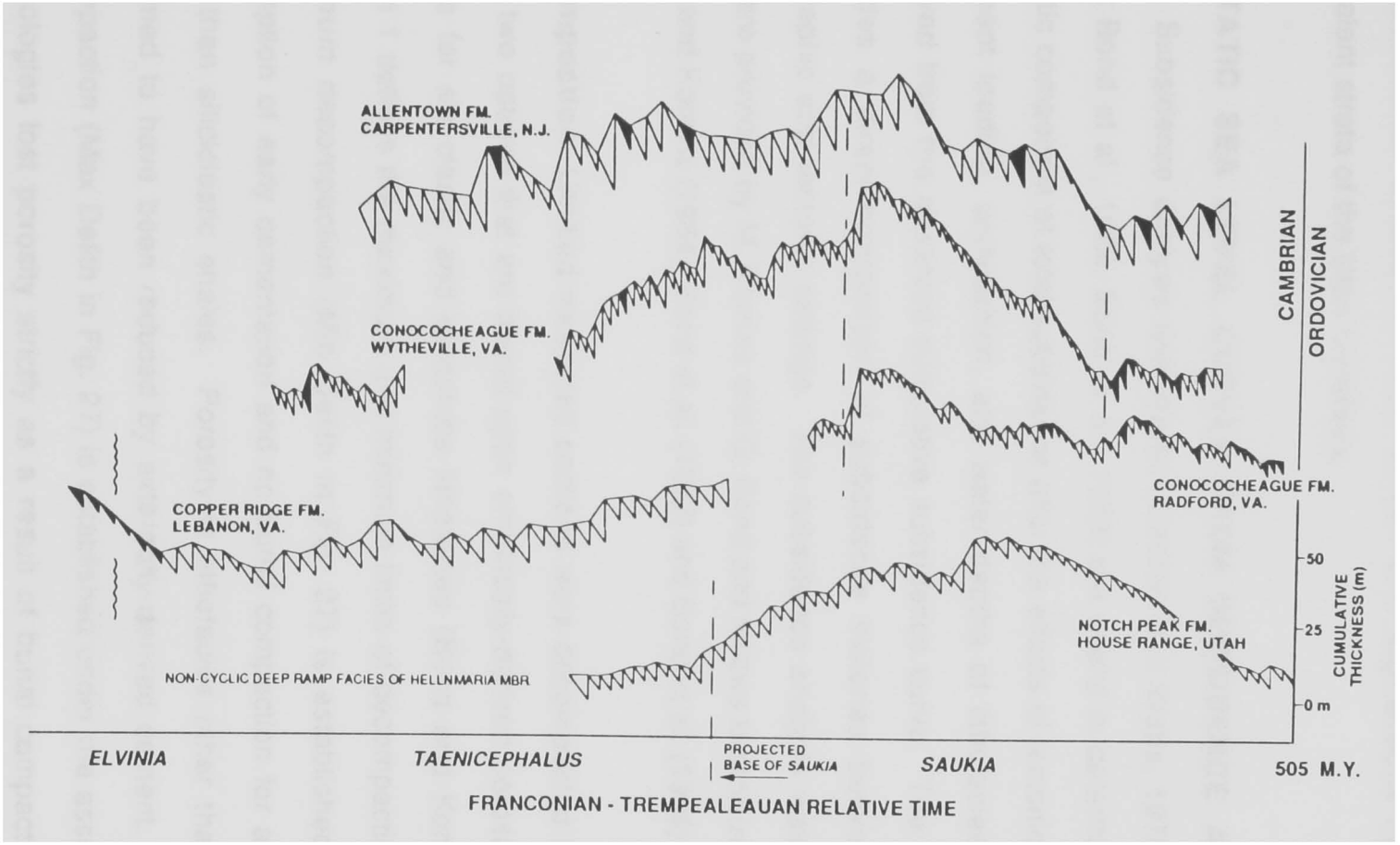
ALLENTOWN FM.
CARPENTERSVILLE, N.J.
CONOCOCHEAGUE FM.
WYTHEVILLE, VA.
CONOCOCHEAGUE FM.
RADFORD, VA.
COPPER RIDGE FM.
LEBANON, VA.
NOTCH PEAK FM.
HOUSE RANGE, UTAH
NON-CYCLIC DEEP RAMP FACIES OF HELLNMARIA MBR
CAMBRIAN
ORDOVICIAN
50
25
0 m
CUMULATIVE THICKNESS (m)
ELVINIA
TAENICEPHALUS
PROJECTED BASE OF SAUKIA
SAUKIA
505 M.Y.
FRANCONIAN - TREMPEALEAUAN RELATIVE TIME

lowstand near the Cambrian-Ordovician boundary. This event may also explain the appearance of shallow water shales and argillaceous carbonates in equivalent strata of the Utah Cordillera.

EUSTATIC SEA LEVEL CURVES FROM SUBSIDENCE ANALYSIS

Subsidence analysis techniques (Steckler and Watts, 1978; van Hinte, 1978; Bond et al., 1988, Bond et al., 1989) are useful in determining the net eustatic component of total subsidence after the effects of tectonic subsidence, sediment loading, compaction, and water depths of lithofacies have been removed from the observed cumulative subsidence curve. The method also provides a direct comparison of subsidence histories between different geographic and tectonic settings. The subsidence analysis was done using software provided by M. Kominz and G. Bond and follows techniques outlined in Bond and Kominz (1984), Bond et al. (1988) and Bond et al. (1989).

Decompaction: Lithified measured sections were decompacted by computer using two options that are based upon empirically-derived porosity vs. depth curves for six clastic and carbonate lithofacies (Bond and Kominz, 1984). Option 1 defines the maximum and minimum limits of decompaction (Fig. 27). *Minimum* decompaction (Min Delith in Fig. 27) is established under the assumption of early cementation and no burial compaction for all lithologies other than siliciclastic shales. Porosity in lithofacies other than shales is presumed to have been reduced by externally-derived cement. *Maximum* decompaction (Max Delith in Fig. 27) is established under the assumption that all lithologies lost porosity strictly as a result of burial compaction. Actual

Figure 27: Diagram illustrating the basic elements of subsidence analysis. Observed sediment thickness is delithified according to Option 1 to establish the probable range of delithified thicknesses (Min and Max Delith). Max Diff refers to delithification of observed sediment thicknesses using Option 2 that emphasizes the differential compaction of fine versus coarse sediments. R1 Min, R1 Max and R1 Max Diff are the backstripped residual curves of the delithified subsidence curves. The Best Fit curve represents the exponential decrease in driving subsidence and is subtracted from the R1 Max Diff curve to derive the amount of subsidence likely due to eustacy (the residual eustatic curves of subsequent plots).


EC
MC
LC
EO
MO
LO
550
530
510
490
470
450
DEPTH (km)
1
2
3
4
5
R1 MIN
R1 MAX DIFF
BEST FIT
R1 MAX
OBSERVED SEDIMENT THICKNESS
MIN DELITH
MAX DIFF
MAX DELITH
HOUSE RANGE

delithified thicknesses probably lie within the range of thicknesses defined by this first option.

Option 2 (Max. Diff. in Fig. 27) emphasizes maximum decompaction of fine-grained lithofacies (shales and muddy carbonates) but assumes that coarser-grained lithofacies decompact minimally. Shales and micritic carbonates are assumed to have been lithified by purely mechanical compaction during progressive burial and are delithified using the maximum values of the porosity vs. depth curves. This assumption is corroborated by abundant evidence of compaction during burial such as stylolites, nodular bedded mudstones surrounded by argillaceous seams, fluid escape structures, contorted sandstone dikes within shales, and sutured grains. Terrigenous sandstones and carbonate sands are assumed to have undergone minimal burial compaction as a result of early lithification by externally-derived cements and are delithified using the minimum values of the porosity vs. depth curves. These lithofacies commonly exhibit open packing and abundant marine cements suggesting rapid cementation within the depositional environment..

Comparison of Delithified Subsidence Curves: The delithification procedure added about 10 to 25% to the observed thicknesses of the sections from the House Range, southwestern Virginia, Texas and Oklahoma and about 20 to 50% to the observed thicknesses of the shale-rich Conasauga basin. Delithified subsidence curves defined by mid-point values between minimum and maximum estimates for all five regions are plotted in Figure 28 and illustrate the differences in tectonic setting between the localities. The

Figure 28: Comparative subsidence curves for the Utah, Virginia, Tennessee, Texas and Oklahoma localities. Late Cambrian subsidence rates (in parentheses) were calculated from the mid-point values between minimum and maximum delithification estimates.

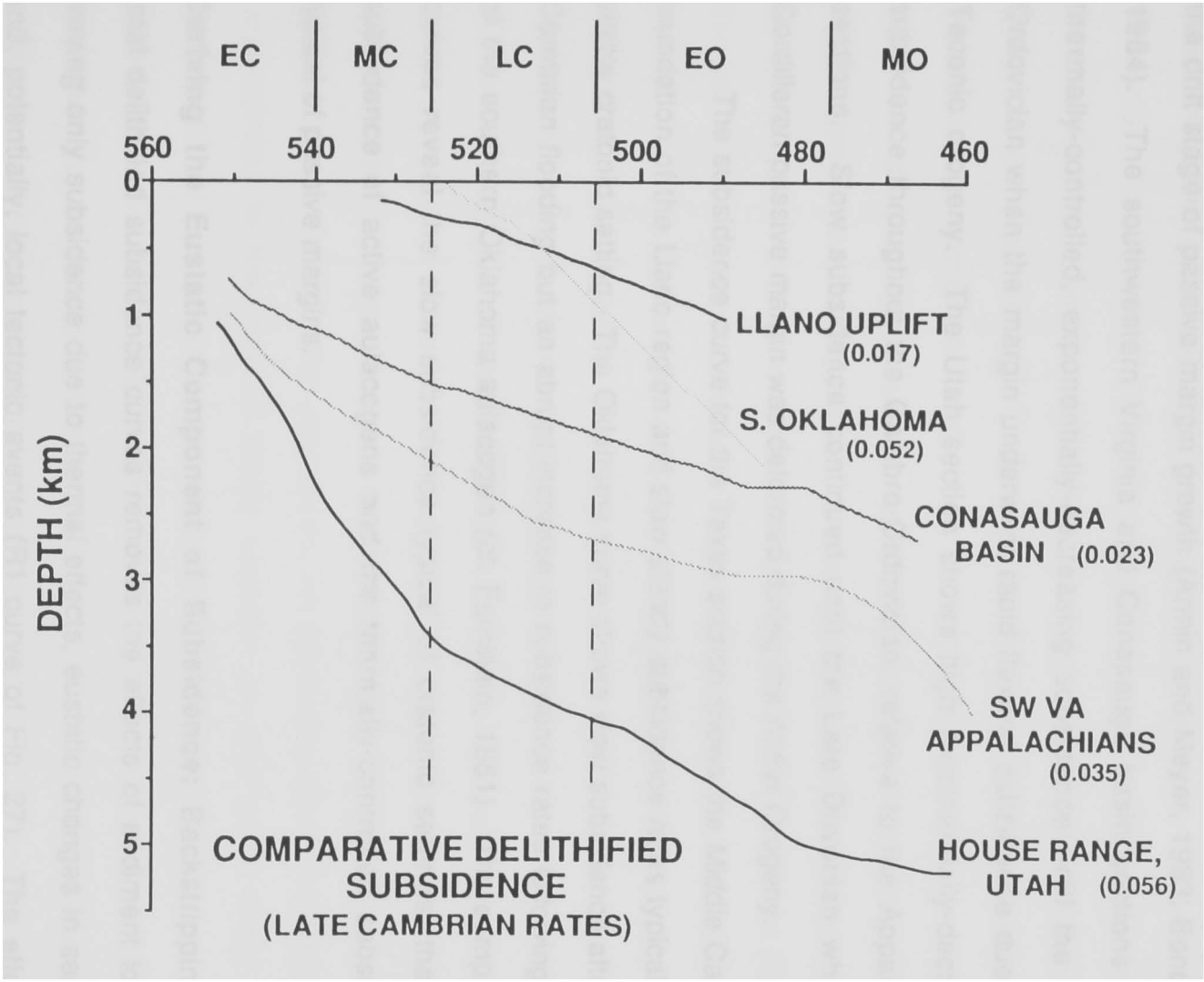
EC
MC
LC
EO
MO
560
540
520
500
480
460
0
1
2
3
4
5
DEPTH (km)
LLANO UPLIFT
(0.017)
S. OKLAHOMA
(0.052)
CONASAUGA
BASIN (0.023)
SW VA
APPALACHIANS
(0.035)
HOUSE RANGE,
UTAH (0.056)
COMPARATIVE DELITHIFIED
SUBSIDENCE
(LATE CAMBRIAN RATES)

calculated delithified subsidence rates for just the Late Cambrian are shown on Figure 28 in parentheses and in Table 8 for comparison.

The Appalachian and Cordilleran curves begin around 550 Ma, within the drift stage of passive margin growth (Armin and Meyer, 1983; Bond et al., 1984). The southwestern Virginia and Conasauga basin sections exhibit thermally-controlled, exponentially-decreasing subsidence until the Middle Ordovician when the margin underwent rapid flexural subsidence due to the Taconic orogeny. The Utah section shows high exponentially-decreasing subsidence throughout the Cambro-Ordovician, relative to the Appalachian sections. Slow subsidence continued until the Late Devonian when the Cordilleran passive margin was deformed during the Antler Orogeny.

The subsidence curve for the Texas section shows the Middle Cambrian inundation of the Llano region and slow steady subsidence rates typical of the stable cratonic setting. The Oklahoma curve shows slow subsidence after Late Cambrian flooding but an abrupt increase in subsidence rates following rifting of the southern Oklahoma aulacogen (cf. Feinstein, 1981). The comparative curves reveal the slow subsidence typical of cratonic settings, the rapid subsidence of active aulacogens and the thermally-controlled subsidence typical of passive margins.

Deriving the Eustatic Component of Subsidence: Backstripping the total delithified subsidence curves removes the effects of sediment loading, leaving only subsidence due to thermal effects, eustatic changes in sea level and, potentially, local tectonic events (R1 curve of Fig. 27). The effects of changes in water depth have been ignored for the long-term (Cambro-

Ordovician) analysis since most of the carbonate and siliciclastic lithofacies were probably deposited in less than a few tens of meters of water. Additionally, even the deeper water shaly lithofacies exhibit relatively rapid shallowing-upward trends that are capped by shallow water carbonate lithofacies. The net effect of the water depth changes on the long-term analysis is relatively small, compared to the overall form of the backstripped subsidence curve. Water depth changes become much more important when modeling the Late Cambrian sections in detail.

To calculate the eustatic (and local tectonic) component of the backstripped curve, a best-fit model cooling curve was subtracted from the backstripped curve to remove the component of driving subsidence (Fig. 27). Except for the southern Oklahoma aulacogen, all of the backstripped curves closely resemble the form of exponentially-decreasing thermal cooling curves suggesting thermal control of driving subsidence, a safe assumption for the Appalachian and Cordilleran passive margins (Bond et al., 1988). All of the post-rift cooling curves were calculated using the one-layer instantaneous stretching model of McKenzie (1978) and procedures outlined in Angevine and others (1988). Potential errors in the technique include absolute age determinations, delithification procedures, the blanketing effect of sediment and uncertainties in the thermal decay constant as well as in other model parameters for constructing the exponential cooling curves (Bond et al., 1988, 1989). Bond and others (1988, 1989) concluded that all of the above problems may affect the *magnitude* of the backstripped curve and residual eustatic curve, but the *form* of the curves remains essentially intact.

TABLE 8

	Late Cambrian Decompacted Subsidence Rate (±0.006)	Late Cambrian Tectonic Subsidence Rate (±0.004)	Second Order Sea Level Rise Rate (540 Ma to peak)	Second Order Sea Level Fall Rate (peak to 478 Ma)	Third Order Late Cambrian Sea Level Fall Rate (513-505 Ma)
HOUSE RANGE	0.056	0.020	0.0130	0.0061	0.0065
CONASAUGA	0.023	0.008	0.0055	0.0024	0.0045
SW VIRGINIA	0.035	0.010	0.0117	0.0039	0.0025
LLANO UPLIFT	0.017	0.010			0.0015
S. OKLAHOMA	0.052	0.029			0.0094

* All values in m/ky
* Decompacted subsidence rate calculated using LC Delith(MaxDiff) values divided by 20 m.y.
    * Error calculated by the difference between max and min range around the maxdiff values and assuming a 20 m.y. duration for the LC.
* Tectonic subsidence calculated using best-fit exponential (Y) to the R1 Maxdiff backstripped curve.
    * Error calculated using the range with Y Tobserved value.
* Sea level rise/fall rates calculated from the R2 delith magnitudes and their relative ages.

Comparative Long-Term Eustacy: After delithifying, backstripping and removing the component of driving subsidence, the net subsidence due to eustacy (and perhaps local tectonism) remains. The eustatic component of total subsidence from the beginning of the drift stage during the early Middle Cambrian through the Early Ordovician for the House Range, Conasauga basin, and southwestern Virginia Appalachians is shown on Figure 29. Magnitudes of sea level fluctuations are not absolute due to the various assumptions implicit in the method and is noted on the vertical axis of the plot. Generally rising sea level characterizes the Middle and early Late Cambrian, a sea level highstand occurs during the early to middle Late Cambrian, and generally falling sea levels mark the latest Late Cambrian through Early Ordovician. The eustatic curves generated for the three sections correspond well with similar curves defined from different locations by Bond et al. (1988) for the southern Canadian Rockies, the Great Basin, and the south-central Appalachians. The superimposed curves, together with the Bond et al. (1988) curves, essentially define the Sauk second-order "supersequence" and suggests a eustatic control on its development. Using the magnitudes of the curves and reasonable estimates of error, approximate long-term sea level rise and fall rates for the Sauk "supersequence" were calculated to be between 0.01 (±0.005) m/ky and 0.004 (±0.002) m/ky, respectively (Table 8).

Comparative Late Cambrian Eustatic Curves: Superimposed shorter-term (third-order) departures in sea level are evident on the long-term second-order curves of Fig. 29. To better distinguish these third-order events, detailed measured sections of meter-scale cycles in the Late Cambrian strata were

Figure 29: Long-term residual eustatic curves determined from stratigraphic sections in the House Range (Utah), Conasauga intrashelf basin (Tennessee) and the peritidal platform in the Virginia Appalachians. Note the correspondence between long-term second-order eustatic rise and fall among the three locations. Magnitudes of the eustatic change are not absolute.

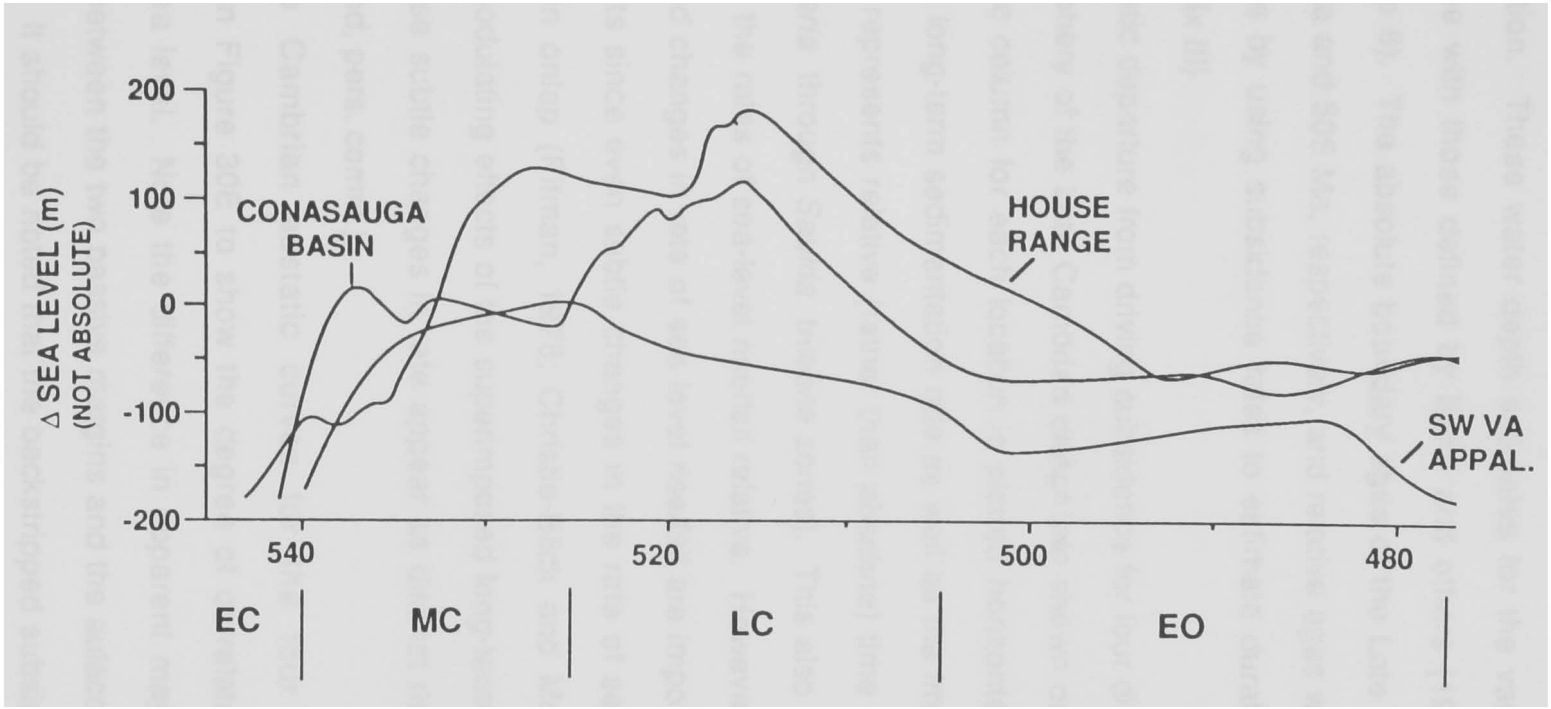
200
100
0
-100
-200
Δ SEA LEVEL (m)
(NOT ABSOLUTE)
CONASAUGA
BASIN
HOUSE
RANGE
SW VA
APPAL.
540
520
500
480
EC
MC
LC
EO

delithified and backstripped with estimated water depth changes incorporated into the calculation. These water depth estimates for the various lithofacies essentially agree with those defined by Bond and others (1988) with minor variations (Table 6). The absolute boundary ages of the Late Cambrian were picked at 525 Ma and 505 Ma, respectively, and relative ages were established within this range by using subsidence rates to estimate durations of trilobite zones. (Appendix III)

The eustatic departure from driving subsidence for four different locations around the periphery of the Late Cambrian craton are shown on Figure 30A-E. The stratigraphic column for each location is plotted horizontally and, due to variations in the long-term sedimentation rate as well as the imprecision of the biostratigraphy, represents relative (rather than absolute) time during the Late Cambrian (*Cedaria* through *Saukia* trilobite zones). This also makes both the magnitudes and the rates of sea-level rise/fall relative. However, only the form of the curves and changes in rate of sea level rise/fall are important in defining third-order events since even subtle changes in the rate of sea level fall can produce shifts in onlap (Pitman, 1978; Christie-Blick and Mountain, 1989). Removing the modulating effects of the superimposed long-term eustatic signal would make these subtle changes in rate appear as distinct rises and falls of sea level (G. Bond, pers. comm.).

The Late Cambrian eustatic curves for the four localities are superimposed on Figure 30E to show the degree of correlatability of major departures in sea level. Note the difference in apparent magnitudes of the eustatic curves between the two passive margins and the aulacogen versus the cratonic section. It should be noted that the backstripped subsidence curve for

Figure 30A-B: Comparative Late Cambrian residual eustatic curves for the House Range, Utah and the Virginia-Tennessee Appalachian sections as determined from subsidence analysis. The stratigraphic column for each locality is oriented horizontally with Late Cambrian relative time marked by trilobite zones. Solid vertical lines connecting troughs on the curve mark tops of major shallowing-upward events evident on the stratigraphic columns. Dashed vertical lines denote smaller-scale events and are located at changes in the rate of sea level rise or fall.

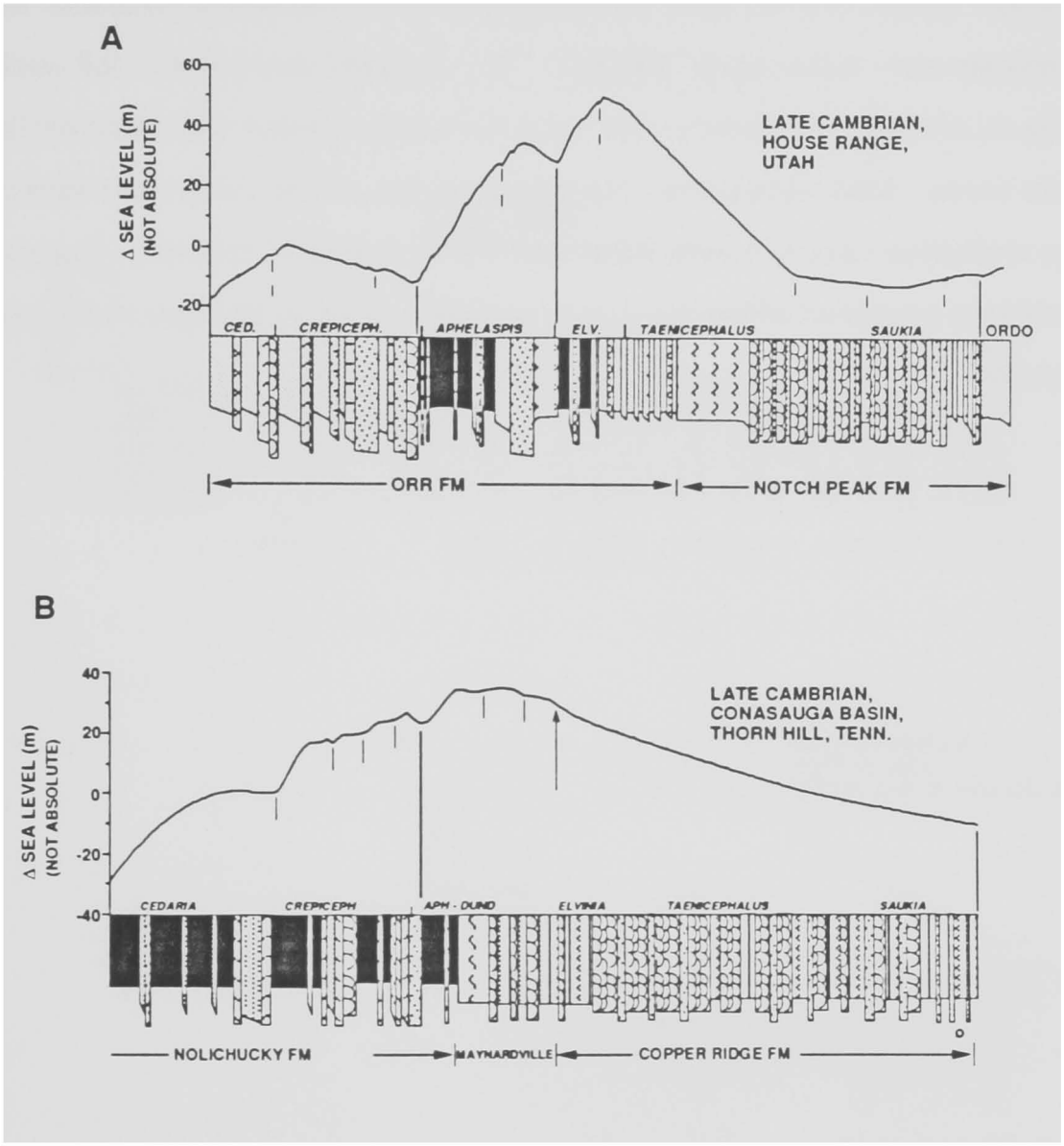
A
Δ SEA LEVEL (m)
(NOT ABSOLUTE)
60
40
20
0
-20
LATE CAMBRIAN,
HOUSE RANGE,
UTAH
CED.
CREPICEPH.
APHELASPIS
ELV.
TAENICEPHALUS
SAUKIA
ORDO
ORR FM
NOTCH PEAK FM
B
Δ SEA LEVEL (m)
(NOT ABSOLUTE)
40
20
0
-20
-40
LATE CAMBRIAN,
CONASAUGA BASIN,
THORN HILL, TENN.
CEDARIA
CREPICEPH
APH - DUND
ELVINIA
TAENICEPHALUS
SAUKIA
NOLICHUCKY FM
MAYNARDVILLE
COPPER RIDGE FM

Figure 30C-D: Comparative Late Cambrian residual eustatic curves for the Threadgill Creek, Texas and Kindeblade Ranch, Oklahoma sections as determined from subsidence analysis. The stratigraphic column for each locality is oriented horizontally with Late Cambrian relative time marked by trilobite zones. Solid vertical lines connecting troughs on the curve mark tops of major shallowing-upward events evident on the stratigraphic columns. Dashed vertical lines denote smaller-scale events and are located at changes in the rate of sea level rise or fall.

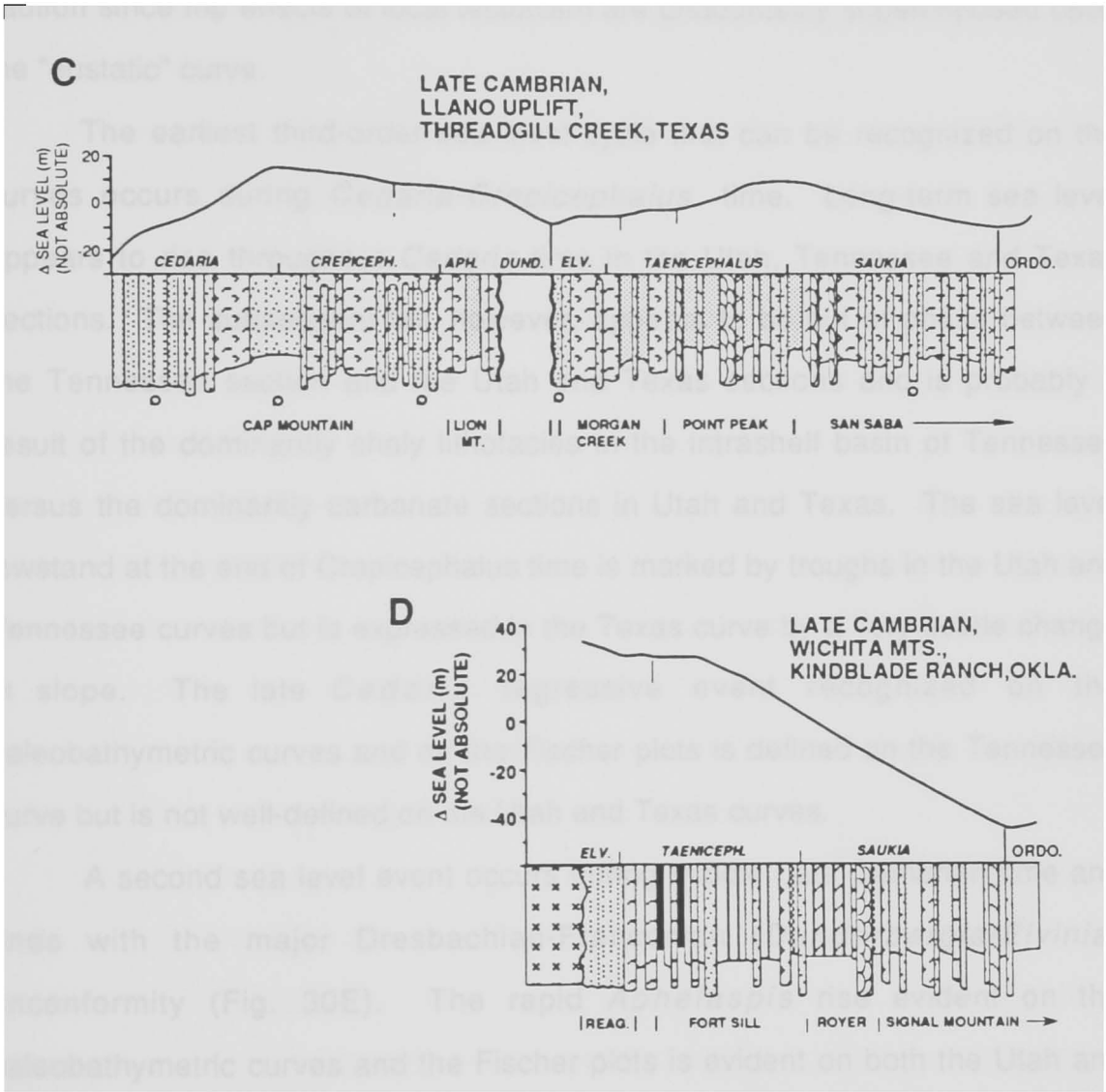
C
LATE CAMBRIAN,
LLANO UPLIFT,
THREADGILL CREEK, TEXAS
Δ SEA LEVEL (m)
(NOT ABSOLUTE)
20
0
-20
CEDARIA
CREPICEPH.
APH.
DUND.
ELV.
TAENICEPHALUS
SAUKIA
ORDO.
CAP MOUNTAIN
LION MT.
MORGAN CREEK
POINT PEAK
SAN SABA
D
LATE CAMBRIAN,
WICHITA MTS.,
KINDBLADE RANCH,OKLA.
Δ SEA LEVEL (m)
(NOT ABSOLUTE)
40
20
0
-20
-40
ELV.
TAENICEPH.
SAUKIA
ORDO.
REAG.
FORT SILL
ROYER
SIGNAL MOUNTAIN

the Wichita Mountains region of Oklahoma does not approximate theoretical cooling curves generated for passive margins but rather reflects the rapid subsidence characteristic of aulacogenic settings (see Fig. 28). A residual "eustatic" curve was calculated however (Fig. 30D), but must be interpreted with caution since the effects of local tectonism are undoubtedly superimposed upon the "eustatic" curve.

The earliest third-order sea level cycle that can be recognized on the curves occurs during *Cedaria-Crepicephalus* time. Long-term sea level appears to rise throughout *Cedaria* time in the Utah, Tennessee and Texas sections. The subsequent fall, however, appears to be out of phase between the Tennessee section and the Utah and Texas sections and is probably a result of the dominantly shaly lithofacies in the intrashelf basin of Tennessee versus the dominantly carbonate sections in Utah and Texas. The sea level lowstand at the end of Crepicephalus time is marked by troughs in the Utah and Tennessee curves but is expressed in the Texas curve by a very subtle change in slope. The late *Cedaria* regressive event recognized on the paleobathymetric curves and on the Fischer plots is defined on the Tennessee curve but is not well-defined on the Utah and Texas curves.

A second sea level event occurs during middle Late Cambrian time and ends with the major Dresbachian-Franconian (*Dunderbergia/Elvinia*) unconformity (Fig. 30E). The rapid *Aphelaspis* rise evident on the paleobathymetric curves and the Fischer plots is evident on both the Utah and Tennessee curves but the opposite trend is seen on the Texas curve. The lowstand at the unconformity is well-defined in the Texas and Utah sections but only a very subtle change in the rate of fall is evident in the Tennessee curve

Figure 30E: Comparative Late Cambrian residual eustatic curves for all four localities overlain for ease of comparison.

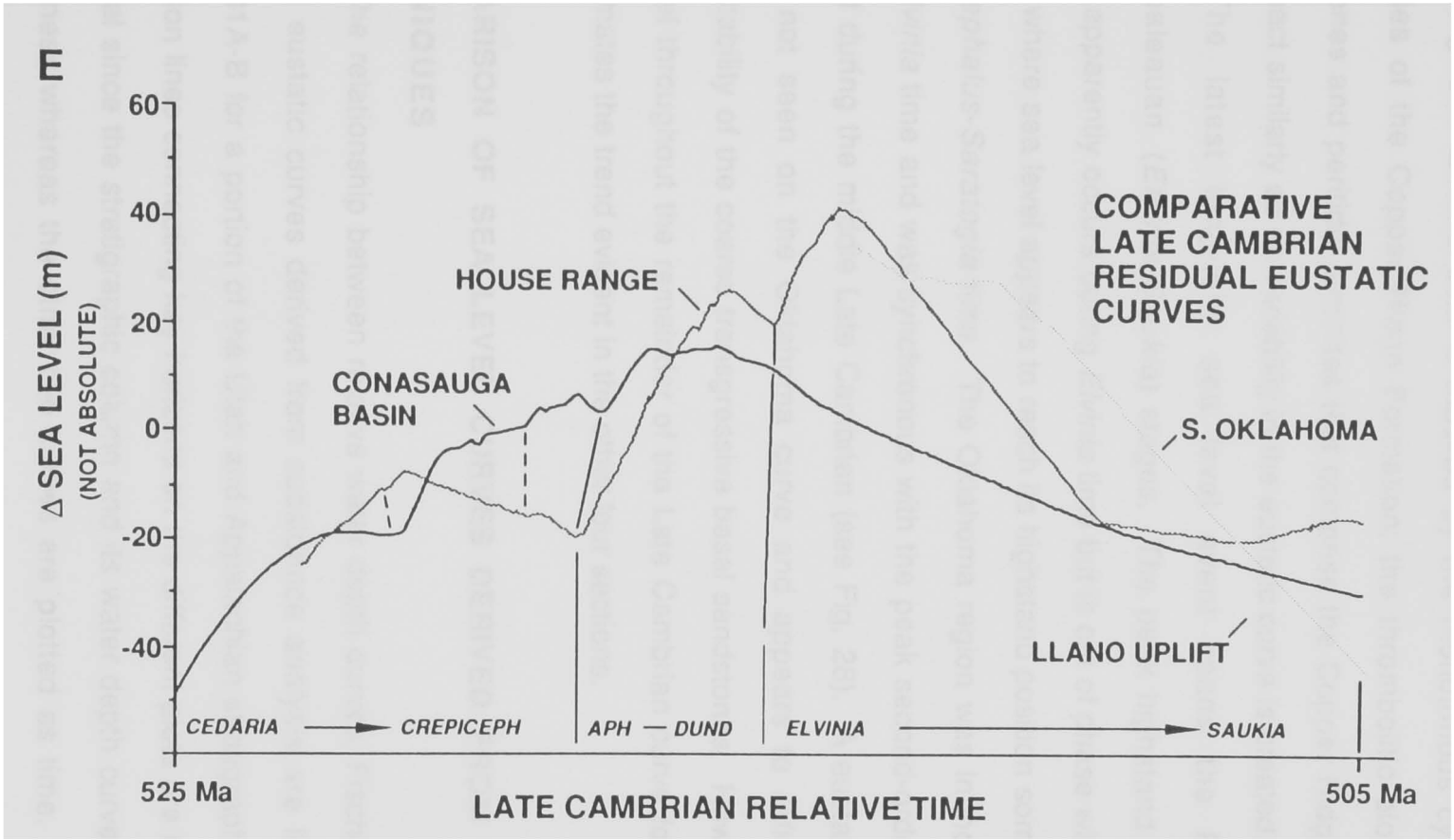
E
60
40
20
0
-20
-40
Δ SEA LEVEL (m)
(NOT ABSOLUTE)
HOUSE RANGE
CONASAUGA
BASIN
COMPARATIVE
LATE CAMBRIAN
RESIDUAL EUSTATIC
CURVES
S. OKLAHOMA
LLANO UPLIFT
CEDARIA
CREPICEPH
APH — DUND
ELVINIA
SAUKIA
525 Ma
505 Ma
LATE CAMBRIAN RELATIVE TIME

near the base of the Copper Ridge dolomites (arrow on plot). Any subsequent rise during later *Elvinia* time is masked by the monotonous cyclic peritidal lithofacies of the Copper Ridge Formation; the thrombolitic bioherms, ooid grainstones and peritidal laminites that comprise the Copper Ridge all tend to decompact similarly so no variability in the eustatic curve is created.

The latest long-term sea level event spans the Franconian-Trempealeauan (*Elvinia-Saukia*) stages. The peak highstand in the Utah section apparently occurs during *Elvinia* time but is out of phase with the Texas section where sea level appears to reach its highstand position sometime within *Taenicephalus-Saratogia* time. The Oklahoma region was inundated during early *Elvinia* time and was synchronous with the peak second-order highstand attained during the middle Late Cambrian (see Fig. 28). A eustatic sea level rise is not seen on the Oklahoma curve and appears to reflect the low compactability of the coarse transgressive basal sandstones. However, falling sea level throughout the remainder of the Late Cambrian curve for Oklahoma approximates the trend evident in the other four sections.

COMPARISON OF SEA LEVEL CURVES DERIVED FROM VARIOUS TECHNIQUES

The relationship between relative water depth curves, Fischer plots and residual eustatic curves derived from subsidence analysis are illustrated in Figure 31A-B for a portion of the Utah and Appalachian stratigraphic columns. Correlation lines connecting key horizons on the different plots are not perfectly horizontal since the stratigraphic column and its water depth curve are plotted as thickness whereas the other two curves are plotted as time. Solid lines

Figure 31A: Direct comparison of the techniques used to derive sea level curves for the Big Horse, Candland Shale and Johns Wash Members of the Orr Formation, House Range, Utah. Stratigraphic column on the left has a vertical axis in meters as does the adjacent, interpreted relative water depth curve based on lithofacies. The Fischer plot curve and the residual eustatic curve from subsidence analysis are plotted as relative time. The residual eustatic curve is decompacted relative to the other curves. Sequence stratigraphic interpretation is included for direct comparison with each of the curves.

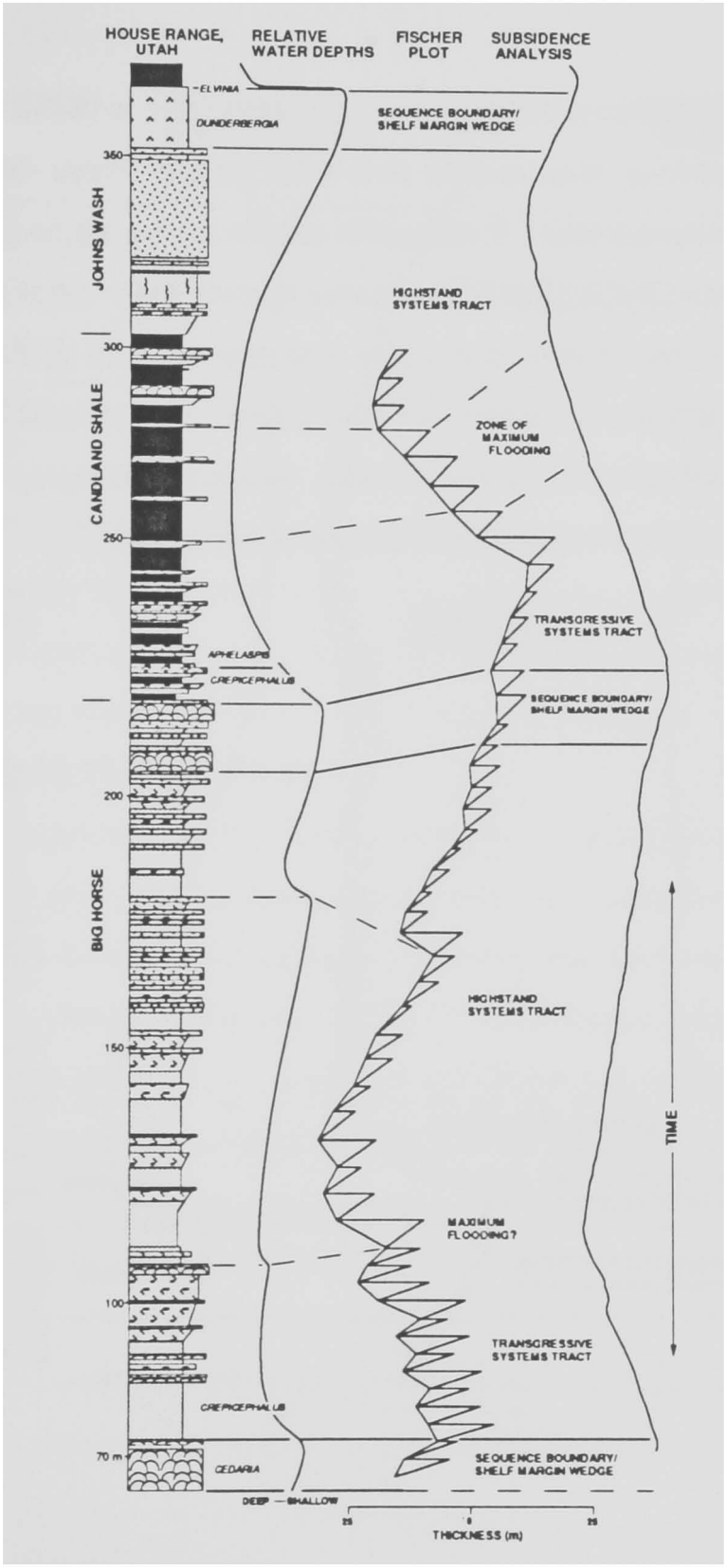
HOUSE RANGE, UTAH
RELATIVE WATER DEPTHS
FISCHER PLOT
SUBSIDENCE ANALYSIS
ELVIRA
DUNDERBERGIA
SEQUENCE BOUNDARY/ SHELF MARGIN WEDGE
360
JOHNS WASH
HIGHSTAND SYSTEMS TRACT
300
CANDLAND SHALE
ZONE OF MAXIMUM FLOODING
250
TRANSGRESSIVE SYSTEMS TRACT
APHELASPIS
CREPICEPHALUS
SEQUENCE BOUNDARY/ SHELF MARGIN WEDGE
200
BIG HORSE
HIGHSTAND SYSTEMS TRACT
150
TIME
MAXIMUM FLOODING?
100
TRANSGRESSIVE SYSTEMS TRACT
CREPICEPHALUS
70 m
CEDARIA
SEQUENCE BOUNDARY/ SHELF MARGIN WEDGE
DEEP — SHALLOW
25
0
25
THICKNESS (m)

Figure 31B: Direct comparison of the techniques used to derive sea level curves for the Nolichucky, Maynardville and lower Copper Ridge Formations in the Tennessee Appalachians. Stratigraphic column on the left has a vertical axis in meters as does the adjacent, interpreted relative water depth curve based on lithofacies. The Fischer plot curve and the residual eustatic curve from subsidence analysis are plotted as relative time. The residual eustatic curve is decompacted relative to the other curves. Sequence stratigraphic interpretation is included for direct comparison with each of the curves.

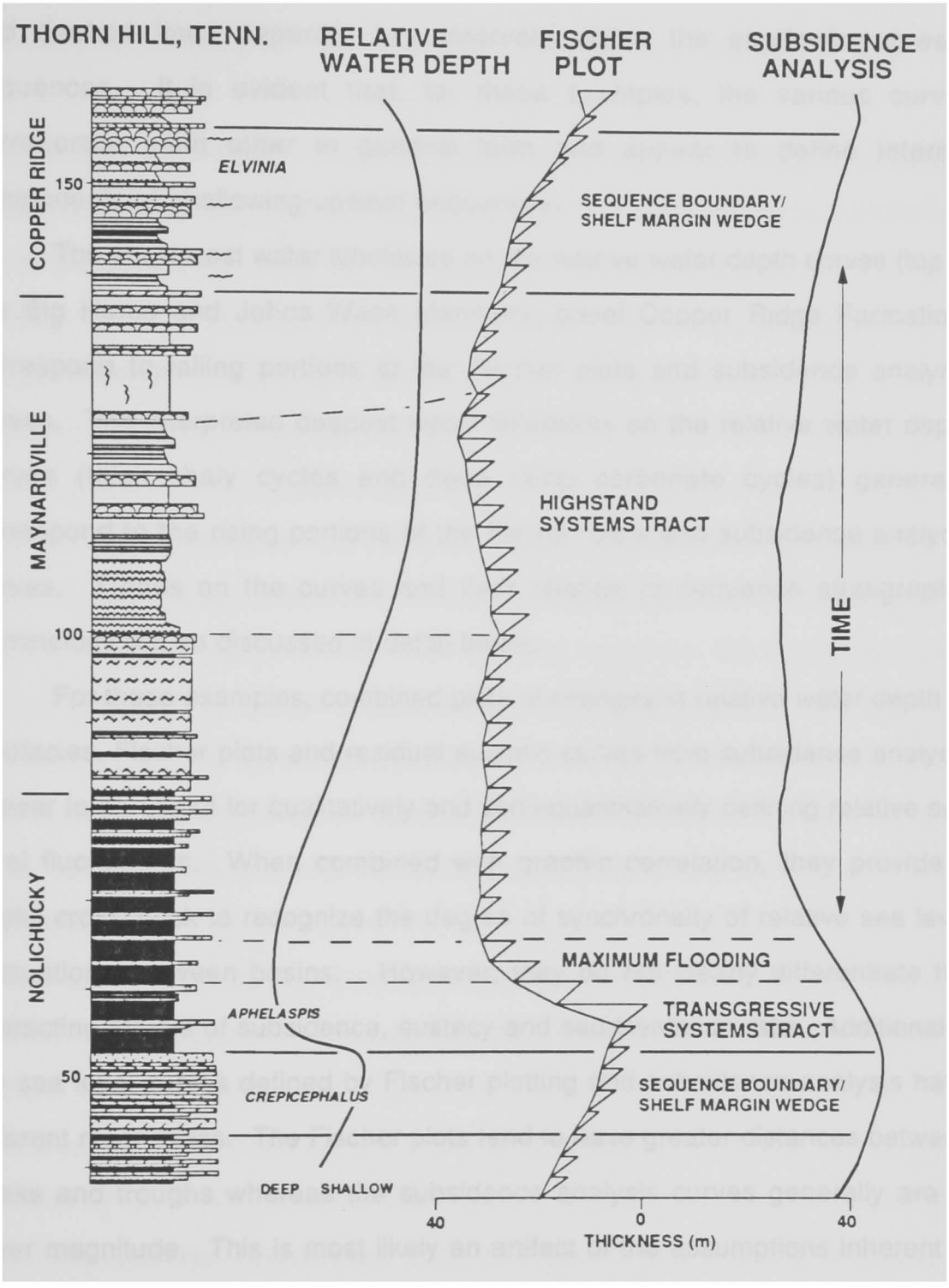
THORN HILL, TENN.
RELATIVE WATER DEPTH
FISCHER PLOT
SUBSIDENCE ANALYSIS
COPPER RIDGE
MAYNARDVILLE
NOLICHUCKY
150
100
50
ELVINIA
APHELASPIS
CREPICEPHALUS
DEEP
SHALLOW
SEQUENCE BOUNDARY/ SHELF MARGIN WEDGE
HIGHSTAND SYSTEMS TRACT
MAXIMUM FLOODING
TRANSGRESSIVE SYSTEMS TRACT
SEQUENCE BOUNDARY/ SHELF MARGIN WEDGE
TIME
40
0
40
THICKNESS (m)

denote major boundary zones between upward-shallowing cyclic successions and dashed lines separate key intervals within the shallowing-upward sequences. It is evident that, for these examples, the various curves corroborate each other in general form and appear to define internal components of shallowing-upward sequences.

The shallowest water lithofacies on the relative water depth curves (top of the Big Horse and Johns Wash Members; basal Copper Ridge Formation) correspond to falling portions of the Fischer plots and subsidence analysis curves. The interpreted deepest water lithofacies on the relative water depth curves (thick shaly cycles and deep ramp carbonate cycles) generally correspond to the rising portions of the Fischer plots and subsidence analysis curves. Trends on the curves and their relation to sequence stratigraphic terminology will be discussed in detail below.

For these examples, combined plots of changes in relative water depth of lithofacies, Fischer plots and residual eustatic curves from subsidence analysis appear to be useful for qualitatively and semi-quantitatively defining relative sea level fluctuations. When combined with graphic correlation, they provide a useful crosscheck to recognize the degree of synchroneity of relative sea level fluctuations between basins. However, they do not clearly differentiate the interacting effects of subsidence, eustacy and sedimentation rate. Additionally, the sea level curves defined by Fischer plotting and subsidence analysis have different magnitudes. The Fischer plots tend to have greater distances between peaks and troughs whereas the subsidence analysis curves generally are of lower magnitude. This is most likely an artifact of the assumptions inherent in

each technique and suggests that each of the various methods have limitations that need to be established before interpreting their combined trends.

Limitations of Fischer Plots: In the Fischer plots, individual meter-scale cycles are plotted using an average cycle period although it is realized that they do not represent the same duration of deposition but likely form within a 20 to 200 k.y. range (Read and Goldhammer, 1988). This variability of cycle period suggests that absolute magnitudes and rates derived from the Fischer plots are inherently inaccurate since changing cycle period will have the effect of skewing the peaks and troughs and also modifying their magnitudes. Additionally, the method may produce trends opposite to those predicted by stacking patterns of cycle types when plotting cycles composed of deep water lithofacies where sedimentation rate appears to control the thickness of the cycles (Chapter 1). Fischer plots seem to be best-suited for peritidal and shallow subtidal cycles whose thickness is accommodation space-dependent. The stacking patterns of cycles (cycle thickness and component facies) can then be compared to the Fischer plots to verify the trends of relative rises and falls of sea level.

Another drawback of the Fischer plots is the inability of the technique to plot non-cyclic sections. Plots could not be generated in the Texas cratonic section where random or poor cycle development precludes their use. They also could not be used for the shallowing-upward, non-cyclic Johns Wash Member (Fig. 31A). Despite the inherent inconsistencies, the reasonable correlation between Fischer plots (Fig. 26) suggests that they may be useful for recognizing eustatic events even though their magnitudes may not be accurate,

and the peaks may be slightly shifted relative to each other (Read and Goldhammer, 1988; Koerschner and Read, 1989).

Limitations of Subsidence Analysis: Assumptions inherent in subsidence analysis (time scales, decompaction, choice of model parameters, two-dimensional effects) indicate that the magnitudes and rates of the residual eustatic curve are not absolute. Error analysis by Bond and others (1988; 1989) showed that the various potential errors affect the magnitude and rates of the backstripped and eustatic curves but their form remained essentially unchanged. They suggested that to prove a eustatic connection between equivalent intervals of Early Paleozoic rocks the *number* of events should be used rather than absolute amounts in change of sea level.

The eustatic curves derived from subsidence analysis of the Late Cambrian sections provide clues to interbasinal correlatability of second-order and long-term third-order sea level changes but are far from conclusive in illustrating a eustatic control on shorter-term third-order sequence development. Smaller-scale depositional sequences are not well-defined, except as deviations in the rate of sea level rise or fall, and certain critical boundaries between major shallowing-upward sequences are not evident on each of the plots (Fig. 30). However, modest changes in the rate of sea level rise and fall (dashed vertical lines) suggest short-term events that can be identified and correlated with other locations by graphic correlation.

Problems of resolution also arise in sections that have relatively homogeneous lithologies that show no major difference in degree of compaction. An example is the peritidal carbonates of the Maynardville to

Copper Ridge transition in the Appalachians that do not define the major sea level lowstand at the Dresbachian-Franconian boundary that is recognized on the Utah and Texas residual eustatic curves as well as on the basis of field evidence, graphic correlation with localities where the unconformity is known to exist and on certain Fischer plots. This transitional interval is marked by uniformly peritidal lithofacies that all show evidence of dominantly syndepositional compaction. Their signature on the Appalachian residual eustatic curve is that of generally falling sea level across this important contact between major eustatic events (Fig. 30B). The relatively consistent skeletal grainstones of the San Saba Member of the Texas section (Fig. 30C) provide another example. The curves that best define eustatic events are those that have distinct differences in relative grain size and therefore decompact differently.

Another problem is the relative timing of presumably equivalent sea level events. They are frequently out of phase on the plot of the superimposed eustatic curves (Fig. 30E). This may be a consequence of the limited biostratigraphic control or it may be a true response of a eustatic event on different platforms. For example, the relative timing of the highstand during the Franconian-Trempealeauan occurs at distinctly different times in the Utah and Texas sections. This may simply reflect diachroneity of the peak highstand conditions related to the slow driving subsidence and elevated cratonic position of the central Texas locality or it could be an artifact of the subsidence analysis technique since the graphic correlation suggests roughly synchronous peak highstand conditions between the two locations.

Finally, there is really no way to separate out local tectonic pulses superimposed on the residual eustatic curves. The Oklahoma region was experiencing rapid subsidence during the end of the Late Cambrian (Fig. 28) associated with the development of the southern Oklahoma aulocogen. The residual eustatic curve for Oklahoma appears to have a significantly higher rate of fall than the Conasauga or Llano sections suggesting increased accommodation space that was generated by fault movement along the flanks of the aulacogen. However, the synchroneity with falling long-term sea levels in the other regions may imply an overall eustatic control superseding the local tectonic component In summary, eustatic curves derived from subsidence analysis of Late Cambrian strata are most valuable when combined with the other techniques to derive a composite Late Cambrian sea level curve.

Composite Late Cambrian Sea Level Curve: Acknowledging the limitations of the different techniques used to determine sea level history, the various sea level curves for each section were qualitatively combined and a composite "eustatic" sea level curve was derived for the Late Cambrian (Fig. 32). Magnitudes of sea level fluctuations and rates of sea level rise and fall on the curves are strictly relative. Only depositional sequences recognized by a combination of techniques and correlatable with the other three localities are included on the composite curve. Non-correlatable events or fourth-order events only correlatable between two localities are considered regional in origin and are not included. The long-term second-order event, on which all of the other curves are superimposed, was defined from residual eustatic curves

Figure 32: Chronostratigraphic comparison of the "eustatic" sea level curves defined for the Utah Cordillera, the Virginia-Tennessee Appalachians, the Texas craton and the southern Oklahoma aulacogen. Composite Late Cambrian "eustatic" sea level curve was derived by qualitatively combining the different curves from the various locations.

LATE CAMBRIAN
ORDO.
STAGE
TREMPEALEAUAN
FRANCONIAN
DRESBACHIAN
BIOMERE
PTYCHASPID
PTEROCEPHALID
MARJUMIID
TRILOBITE ZONE
MISSISSQUOIA
SAUKIA
SARATOGIA
TAENICEPH-ALUS
ELVINIA
DUNDERBERGIA
APHELASPIS
CREPICEPH-ALUS
CEDARIA
HOUSE RANGE UTAH
SW VIRGINIA NE TENN. APPALACHIANS
LLANO UPLIFT TEXAS
WICHITA MTS. OKLA.
LATE CAMBRIAN COMPOSITE SEA LEVEL CURVE

generated from the subsidence analysis of the entire Cambrian-Ordovician (Fig. 29).

Determining the magnitude of a "eustatic" sea level curve from individual stratigraphic sections is not really possible given the complicated interactions of subsidence, sedimentation and eustacy (Burton et al., 1987; Kendall and Lerche, 1988). This is illustrated by the differences in calculated magnitudes of sea level oscillations by direct comparison of the Fischer plots and the residual eustatic curves derived from subsidence analysis (Fig. 31). Magnitudes determined from Fischer plots tend to be substantially larger than those on the residual eustatic curves. This trend may be related to the Fischer plots not being corrected for isostatic response to sediment and water loading (i.e., backstripped). However, any of a number of the various assumptions implicit in each method could be the source of differences in apparent magnitude of equivalent sea level events. Since the relative effects of these factors cannot be separated to make the curves come into better agreement, the composite curve must be considered "eustatic" only in the sense of the curves being correlatable between widely separated localities and not in the sense of any measurable change in elevation from a stationary datum.

The composite "eustatic" curve for the Late Cambrian is intended to be used as a template for the correlation of Late Cambrian depositional sequences recognized elsewhere. The curve was generated without the preconceived bias associated with the shale/carbonate alternations of the grand cycles of the southern Canadian Rockies. Grand cycles would provide an ideal test for the validity of the "eustatic" curve defined by Late Cambrian sections around the pericratonic platform of the United States.

SEA LEVEL CURVES AND DEFINITION OF SYSTEMS TRACTS AND SEQUENCE BOUNDARIES IN OUTCROP

In this section, the systematic changes in stacking patterns of meter-scale cycle types and their component lithofacies (Chapter 1) are examined to determine if they can be used to define different systems tracts that make up the Late Cambrian sequences. This is done by comparing the stacking patterns with their relative position on "eustatic" sea level curves for specific Late Cambrian sequences (Figs. 31). For this discussion, sequences are defined as "a relatively conformable succession of genetically related strata bounded by unconformities and their correlative conformities" (Mitchum, 1977).

Compared to the traditional methods of defining sequences and their component systems tracts by geometric relations of reflection contacts on seismic sections, distinct problems are encountered when translating sequence stratigraphic concepts to the outcrop. Seismic stratigraphy depends on tracing regional reflections that approximate time lines across a platform to basin transition (Vail et al., 1977). Individual sections are subject to the limitations of the biostratigraphic control that is necessary to accurately correlate updip and downdip between sections. Graphic correlation using isochronous biomere boundaries as datums has been used in this study to compensate for this problem of imprecise time control. Additionally, Fischer plots of numerous sections along a platform (and between platforms as in Figure 26B-C) may aid in correlation and also help to define systems tracts.

Sequence Boundaries: The majority of sequence boundaries within Late Cambrian strata are Type 2 (Van Wagoner et al., 1987). That is, they are not major unconformity surfaces with long-term subaerial exposure (Type 1) but rather are expressed as transitional zones of maximum regressive lithofacies and intermittent exposure features generated by high frequency sea level fluctuations. They are the "correlative conformities" equivalent to the more extensive erosional unconformities on the craton and reflect third-order sea level fall rates that are less than subsidence rates on the pericratonic platform. The only true Type 1 sequence boundary in Late Cambrian strata occurs in the Texas section where the unconformity separating Dresbachian from Franconian strata has been recognized biostratigraphically by the absence of the *Dunderbergia* trilobite zone and by correlation with cratonic sections of the Mid-continent (Lochman-Balk, 1971; Barnes and Bell, 1977).

Type 2 sequence boundaries are difficult to define in vertical outcrop sections since they are complicated by the repeated pulses of high frequency sea level oscillations that generated the meter-scale cycles. Instead of a single recognizable horizon, cyclic sections merely may show a transitional zone of stacked cycles with features indicating emergence of the zone relative to underlying and overlying beds. Sequence boundary zones may include parts of the upper highstand systems tract or the shelf margin wedge and will be discussed within their respective sections below. Sequence boundary zones appear to correspond with falling segments of Fischer plots and residual eustatic curves from subsidence analysis (Fig. 31).

In peritidal sections, thin tidal flat-dominated cycles containing brecciated regoliths and quartz sand units appear to characterize sequence boundaries

(Koerschner and Read, 1989). The sea level lowstand during earliest *Elvinia* time within the disconformably-capped peritidal cycles of the basal Copper Ridge Formation (Fig. 31B) is represented by falling segments of the Fischer plot and residual eustatic curve. This same sea level lowstand in the Johns Wash fenestral mudstones of the House Range section (Fig. 31A) also plots along the sea level fall near the trough on the residual eustatic curve.

In the peritidal Allentown Formation of eastern Pennsylvania, angular desiccation breccias often overlie laminite caps and fill vertical dissolution pipes that extend down into the caps. These features are usually stacked within successive cycles and are not just isolated, randomly exposed cycle tops. Examples of quartz sands and brecciated regoliths associated with sequence boundary zones can be seen in peritidal Fischer plots (Fig. 26B & 26C) and appear to correspond to falling segments and troughs on the plots.

Influxes of quartz sand brought in from the craton during rapid falls in sea level are important criteria for recognizing sequence boundaries in the Late Cambrian Texas cratonic embayment. For example, the Cap Mountain siltstone marks the top of the late *Cedaria* sea level event and corresponds to a depositional hiatus on the craton (Palmer, 1954).

In shallow to deep subtidal carbonate successions, sequence boundary zones are defined by the transition from the shallowest water cycles into overlying deeper water cycles. The late *Cedaria* event in the lower Big Horse Member of the House Range is marked by stacked thrombolitic bioherms overlain by deep subtidal cycles characterized by thick argillaceous nodular wackestone bases (bottom of Fig. 31A). The upper sequence boundary zone of the *Elvinia* through early *Saukia* event in the House Range (Fig. 25) is

composed of stromatolitic bioherms shallowing up into fenestral mudstones featuring stacks of scalloped erosion surfaces. The microkarstic surfaces provide evidence of episodic subaerial erosion developed during times of maximum decreases in accommodation space generated by high frequency sea level falls superimposed on long-term falling sea level. This transitional zone is overlain by thick cycles of globose thrombolite bioherms that record the subsequent sea level rise.

On the outer deep ramp, sequence boundaries can be recognized by the abrupt appearance of stacked, deep water *shaly* cycles above thin peritidal or very shallow subtidal carbonate cycles at the top of a shallowing-upward sequence. The sequence boundary zone at the end of *Crepicephalus* time in the Utah section (top of Big Horse Member in Fig. 31A) is represented by relatively thin cycles composed of restricted lithofacies (oolitic/oncolitic grainstones and thrombolite/stromatolite bioherms) overlain by deeper water shaly cycles (Candland Shale Member). The basal thin shaly cycles are characterized by numerous stacked hardgrounds within carbonate caps and manifest incipient drowning. The zone plots toward the bottom of the sea level fall on the Fischer plot and the residual eustatic curve.

In intrashelf basin sections of the Appalachians, the late *Crepicephalus* sequence boundary zone (Fig. 31B) corresponds to cycles composed of thin shales capped by proximal storm deposits and ooid grainstones. These cycles are abruptly overlain by thick shales capped by distal storm deposits. The stacking patterns of these cycles generate a relative sea level fall followed by a relative sea level rise with the interpreted sequence boundary zone located toward the trough on the Fischer plot.

Shelf Margin Wedge: Since the majority of Late Cambrian sequence boundaries are Type 2, only shelf margin wedges are included in this discussion and lowstand systems tracts are not considered. Shelf margin wedges are the first systems tract above Type 2 sequence boundaries and are characterized by slightly progradational to aggradational facies developed during the later phases of a eustatic sea level fall (Van Wagoner et al., 1987). They are very difficult to recognize in outcrop without several downdip sections that extend out onto the platform slope. With individual sections, it is difficult to determine whether the shoal water facies near a sequence boundary represents the platformwide upper highstand systems tract or the shelf margin wedge with no updip facies equivalents. A differentiation between the older sequence boundary and the younger shelf margin wedge is typically beyond the resolution of biostratigraphy. For most Late Cambrian sequences determined from geographically-separated vertical outcrops, the interpreted sequence boundary zone may represent either the upper highstand systems tract or the shelf margin wedge. Therefore, sequence boundary zones interpreted from the tops of shallowing-upward sequences and their position on sea level curves defined by Fischer plots and residual subsidence analysis curves (Fig. 31) are defined as Sequence Boundaries/Shelf Margin Wedges.

Transgressive Systems Tract: The transgressive systems tract is expressed across platforms by a retrogradational geometry that develops during a rapid eustatic rise in sea level (Van Wagoner et al., 1987). In outcrop sections, the transgressive systems tract is characterized by an upward-

deepening of relative water depths of lithofacies as well as successions of thick cycles that reflect the increased accommodation space generated by rapidly rising sea level. They may be recognized as relative long-term rises on Fischer plots and on residual eustatic curves.

In vertical outcrop of peritidal sequences, the transgressive systems tract may be a subtle feature recognized by the appearance of thick cycles dominated by subtidal lithofacies (oolitic grainstones, thrombolitic bioherms and shaly ribbon rocks) with thin tidal flat caps overlying thin, tidal flat-dominated cycles. This systems tract can be defined within the Allentown and Conococheague Formations by stacks of thick oolitic grainstones with thin stromatolitic caps directly above thin laminite-capped cycles (Figs. 10 & 11 in Chapter 1). The abrupt rise during early *Aphalaspis* time on the Fischer plot for Dresbachian time for all of the peritidal sections (Fig. 26B) is a good example and reflects the increase in accommodation space provided by rising sea level.

In vertical sections of deep ramp, open marine sequences, deepening-upward trends of the transgressive systems tract can be recognized by the appearance of deep water shaly cycles or argillaceous carbonate cycles overlying the uppermost facies of shallowing-upward sequences. Examples from the Utah section can be seen as rising segments of the sea level curves defined by Fischer plots and subsidence analysis (Fig. 31A). Other evidence for recognizing the transgressive systems tract within deeper water carbonates can be seen within the lower Signal Mountain Formation of Oklahoma. Immediately overlying stacked thrombolitic bioherms and cryptalgal laminites of the sequence boundary zone at the end of the *Elvinia* to early *Saukia* event, burrowed spiculitic wackestones featuring glauconite and numerous

hardgrounds indicate stalled sedimentation during rapidly rising sea level and represent the transgressive systems tract of the overlying *Saukia* sequence.

Additional evidence for slow deposition associated with rapid sea level rise rates is exhibited in intrashelf basin facies of the Appalachians at the top of the mid-*Crepicephalus* sea level event. In the Lebanon, Virginia section, thin, peritidal thrombolitic cycles representing maximum regressive conditions within the sequence boundary zone are overlain by a transgressive oolitic grainstone (6 m thick) in turn overlain by deeper water shaly cycles. The upper half meter of the ooid shoals exhibit stacked hardgrounds and glauconite and have a reworked megarippled upper surface with a mud drape, suggesting a depositional hiatus before complete drowning by the overlying shaly cycles.

Transgressive systems tracts in the Texas cratonic section are characterized by thick subtidal cycles composed of open marine skeletal carbonates (lower Cap Mountain Member, Riley Formation) and deeper water siliciclastic siltstones (Point Peak Member, Wilberns Formation) (Fig. 25). As opposed to the Appalachian and Cordilleran passive margins where meter-scale cycle development is relatively continuous throughout the section, the Texas section exhibits cyclicity only within the transgressive systems tract and lower highstand systems tract. Thus, the cycles that characterize the transgressive systems tract in these regions are thick relative to the poorly-developed "condensed cycles" that distinguish the upper highstand systems tract of the Texas cratonic section.

Maximum flooding surface: The surface that defines the change from retrogradational to aggradational stacks of cycles and separates the

transgressive systems tract from the highstand systems tract (Van Wagoner et al., 1987) is difficult to recognize in outcrop sections. It is defined seismically by the marine-flooding surface onto which progradational fronts of the overlying highstand systems tracts downlap. Since downlap surfaces and their equivalent deeper water condensed sections evident on seismic sections are difficult if not impossible to unequivocally identify in the field, the maximum flooding surface is probably best defined as a transitional zone separating thick cycles reflecting a deepening-upward trend from thinner cycles exhibiting a slight shallowing-upward trend. The definition of the maximum flooding surface is also complicated by the multiple, high frequency fluctuations in sea level that generate the meter-scale cycles. For example, stacks of thick cycles composed of basal deeper water lithofacies that grade up into shallow subtidal caps may represent periodic pulses of flooding followed by gradual shallowing. Actually defining anything more than a transitional zone separating long-term deepening-upward trends from long-term shallowing-upward trends may be the best that can be done when applying sequence stratigraphic concepts to cyclic field sections. A potential method to estimate the position of the maximum flooding surface is to define the thickest cycles developed just before the apex of the sea level highstand on Fischer plots.

Within peritidal sections, the location of the maximum flooding surface is arbitrarily determined because no great differences in cycle types and component lithofacies exist. Perhaps the best location may be estimated at the change from thick to thinner cycles just before the crest of sea level highstands on Fischer plots.

Within shaly deep ramp sections, the maximum flooding surface may coincide with one to three thick cycles that mark the break between rapid sea level rise and the slower rise rates (and more carbonate-rich cycles) of the sea level highstand. Thick cycles characterized by siliciclastic shales with thin carbonate storm-deposited caps represent the deepest water interval in the Candland Shale of the Utah section (Fig. 31A) and correspond to the uppermost part of the sea level rise on its Fischer plot. It also corresponds to the rising portion of the residual eustatic curve although it appears to be lower on the rise than on the Fischer plot.

In intrashelf basin sections, the maximum flooding surface may be recognized in thick shaly cycles such as those in the upper Nolichucky Shale of the Appalachians (Fig. 31B). The trend is similar to that exhibited for shaly deep ramp sections; the thickest shaly cycles tend to plot along the uppermost portions of the sea level rise defined by Fischer plots and residual eustatic curves.

Highstand Systems Tract: The highstand systems tract is composed of aggradational cycles overlain by progradational cycles that extend across the platform (Van Wagoner et al., 1987). It forms during the late eustatic rise and throughout the highstand and early eustatic fall (Vail, 1987; Haq et al., 1987). The highstand systems tract may be distinguished in vertical field sections as stacks of open marine subtidal cycles shallowing up into stacks of progressively more restricted cycles, reflecting progradation under conditions of reduced accommodation space during falling sea level.

On Fischer plots of peritidal sections, the highstand systems tract plots as either a stillstand or as generally falling sea level defined by intervals of progressively thinner cycles that become more tidal flat-dominated upward. These trends are shown on the Fischer plot and residual eustatic curve for the Maynardville to lower Copper Ridge transition (Fig. 31B). Peritidal cycles within the upper highstand systems tract may show abundant evidence of diagenetic modification such as brecciation, leaching of aragonitic components of subtidal lithofacies, and dolomitization (Koerschner and Read, 1989). Distinguishing the upper portions of the highstand systems tract from the sequence boundary zone (and even from the overlying shelf margin wedge for outer platform settings) is probably arbitrary in outcrop sections.

In deep ramp cycles of the Utah section, the highstand systems tract may be recognized by a progressive upward shallowing from storm-dominated, open marine carbonate cycles into thin, restricted oolitic grainstone-capped cycles (upper Big Horse Member, Fig. 31A). The signature of this trend on the Fischer plots and residual eustatic curves is of stillstand conditions followed by generally long-term falling sea level.

Summary of Sequence Stratigraphy Applied to Outcrop Sections: The major problems associated with defining systems tracts and sequence boundaries in vertical sections are:

1) Updip and downdip correlations of outcrop sections across a platform are subject to the limitations of the biostratigraphic control, in contrast to seismic stratigraphy where reflectors manifest time lines.

2) Boundaries between systems tracts are complicated by meter-scale cycles that were generated by repeated pulses of high frequency sea level oscillations. Many systems tract boundaries may best be defined as transitional zones rather than single recognizable horizons. For example, type 2 sequence boundaries may include parts of the upper highstand systems tract or the shelf margin wedge, depending on position on the platform.

3) Shelf margin wedges may be difficult to recognize without several downdip sections that extend out onto the platform slope.

4) Transitions between systems tracts may be subtle in shallow to deep subtidal successions where major shallowing or deepening events may not be manifested by distinct lithofacies (e.g., exposure features, condensed sections, etc.) but rather may show gradual changes in cycle stacking patterns. Similarly, dominantly peritidal sections may not show major differentiation of lithofacies that represent distinct shallowing or deepening events.

Despite these problems, certain benefits can be gained by applying sequence stratigraphic concepts to the outcrop. Because systems tracts and sequence boundaries are defined by their position on a theoretical eustatic sea level curve (Van Wagoner et al., 1987), it appears possible that Fischer plots and residual eustatic curves may approximate the *form* of a eustatic signal. The good correspondence between relative water depths of lithofacies, their interpretation as components of sequences, and their expression on Fischer plots and residual eustatic curves, supports the use of the techniques to define third-order eustatic sea level events. Additionally, the correlation of Fischer plots and residual eustatic curves of cyclic successions between different basins helps to verify third-order eustatic sea level cycles.

The recognition of high frequency cycles in outcrop provides important details about the internal architecture of larger-scale sequences and their component systems tracts that otherwise may be missed seismically. Systematic changes in stacking patterns of meter-scale cycle types and their component lithofacies characterize the different systems tracts that make up sequences (Chapter 1). However, it must be emphasized that systems tracts and sequence boundaries defined in outcrop are often subjectively assigned to transitional zones between gradually changing lithofacies and cycle types.

DISCUSSION

Synchroneity of Sequences: A number of factors contribute to the relative timing of the initiation and termination of sequences in different depositional basins. First, the degree of synchroneity of events is difficult to determine due to the inherent errors in biostratigraphy. Biomere boundaries are considered isochronous (Palmer, 1984) making correlation based on biomere boundaries the only true measure of the relative degree of synchroneity between sections. Correlated intervals *between* biomere boundaries can be considered chronostratigraphic equivalents whereas sequences defined *within* a biomere and correlated interbasinally may be diachronous since the zonal boundaries are subject to the origin, dispersal and extinction of the trilobite populations.

Another major limitation to determining whether correlated sequences are synchronous or not is the difference in sedimentologic response between individual platforms to rising or falling relative sea level. It has long been recognized that the initiation of transgressive-regressive sequences on a platform are dependent upon the relative rate of sea level rise/fall versus the

subsidence rate, assuming that sedimentation rates remains constant (Pitman, 1978; Parkinson and Summerhayes, 1985). If the individual sections of the various depositional basins being correlated were subsiding at different rates, then their sedimentologic response to changes in the rate of sea level rise or fall will differ. Additional reasons for apparent diachroneity between correlated sequences were suggested by Pitman and Golovchenko (1988) which relate to differences in platform morphology as well as differential subsidence rates between basins. They maintained that differences in depositional slope and platform width affect the lateral migration of facies; steep and narrow platforms will show a different timing of depositional events than broad, flat platforms.

All of the different factors for diachroneity between "equivalent" sequences - limits of biostratigraphy, differential subsidence rates between basins and different platform morphologies - imply that sequences correlated between basins are probably never exactly synchronous. Broad ranges of "synchroneity" of up to one-fourth the duration of the long-term event (Angevine et al., 1988) may be expected between correlated sequences. Perhaps a better approach than trying to establish a synchronous development of sequences between basins is to simply define the absolute number of events that can be interbasinally correlated within a given time interval (Bond et al., 1988; 1989).

Eustatic vs. Tectonic Control of Third-Order Sequences: Second-order cycles (equivalent to Sloss's "sequences" (1963) and Vail and others "supercycles" (1977)) are generally agreed to have been caused by volume changes in global mid-oceanic spreading ridge systems (Pitman, 1978; Kominz, 1984). However, the relative roles of tectonism versus eustacy as dominant

controlling mechanisms on third-order sequence development have yet to be fully agreed upon since an unequivocal cause for their origin has not been identified. Numerous 1-10 m.y. sea level events have been correlated throughout the Phanerozoic as being roughly synchronous within the limits of the bio- and magnetostratigraphy and this is presumed to be evidence for eustatic control of sequence development (Vail et al., 1977; Hallam, 1984; Vail et al, 1984; Haq et al., 1987). However, proponents of eustatic control of third-order sequences are forced to resort to some combination of variations in spreading rates and glacio-eustacy, especially during times of major continental glaciations, to explain the controlling mechanisms of third-order eustacy.

Proponents of tectonic control suggest that sub-crustal thermal activity (Sloss and Speed, 1974), or major periods of plate tectonic reorganization (Bally, 1980) explain synchronous sequence development and consider eustacy to be a subordinate response. Others, (Parkinson and Summerhayes, 1985; Heidlauf et al., 1986; Cloetingh, 1986; ; Watso and Klein, 1989), while not denying possible global sea level fluctuations, suggest that local and regional tectonism cannot be neglected as potential controls on certain stratigraphic sequences. Cloetingh (1986) has proposed intraplate stress mechanisms that generate regional stress adjustments at passive margins to explain recognized deviations from global sea level curves but it seems unlikely that this mechanism would exert the overall control on widely separated basins.

Since the Late Cambrian was a time of dominantly low latitude continents and open polar oceans (Scotese and McKerrow, 1990), changes in polar ice volume are not a viable controlling factor behind third-order sea level fluctuations. Alpine glaciation and perhaps polar pack ice may have supplied a

reservoir large enough to store the necessary volumes of ocean water to control the shorter third-order events but more likely were a subsidiary factor to some as yet unrecognized control.

SUMMARY AND CONCLUSIONS

1) Interbasinal correlation of Late Cambrian cyclic carbonates in the Appalachian and Cordilleran passive margins, the Texas cratonic embayment and the southern Oklahoma aulacogen suggests that third-order depositional sequences are eustatic in origin. Graphic correlation of biostratigraphically-constrained strata was used to establish equivalency between shallowing-upward successions (tens to hundreds of meters thick) between individual sections. Six major third-order depositional sequences can be correlated interbasinally. Numerous smaller-scale stratigraphic cycles also were recognized but correlations were less conclusive. Depositional sequences were named on the basis of their relative time ranges according to the trilobite biostratigraphy and are: 1) late *Cedaria*, 2) mid-*Crepicephalus*, 3) late *Crepicephalus*, 4) *Aphelaspis* to earliest *Elvinia*, 5) *Elvinia* to early *Saukia*, and 6) *Saukia* to the Cambrian-Ordovician boundary.

2) Interbasinal correlation of depositional sequences allows for an evaluation of various methods of determining eustatic sea level history. Fischer plots define the path of relative sea level based on the amount of extra accommodation space produced by eustacy beyond that provided by subsidence. Interbasinal correlation of Fischer plots for Late Cambrian cyclic successions adds support for a eustatic control on their development. They also show how stacking

patterns of meter-scale cycles relate to longer-term sea level events. Residual eustatic curves derived from subsidence analysis also were used for interbasinal correlation because they are corrected for isostatic and tectonic subsidence. The residual eustatic curves for Late Cambrian relative time support a eustatic control on the long-term sea level events but the method is less sensitive for correlating smaller-scale (< 2 m.y.) sequences.

3) Direct comparison of both the Fischer plots and time-equivalent residual eustatic curves with paleobathymetric curves of Late Cambrian cyclic strata point out the limitations to the techniques but also suggest that the semi-quatitative sea level curves may approximate the *form* of the eustatic sea level curve. By qualitatively combining the correlated sea level curves for each of the four localities, a composite "eustatic" sea level curve for the Late Cambrian was generated. The composite curve is considered "eustatic" on the basis of the interbasinal correlatability of depositional sequences. It is not possible to define absolute magnitudes of sea level departures without a known datum.

4) The application of sequence stratigraphic concepts to outcrop sections of depositional sequences is done by comparing the stacking patterns of meter-scale cycles with their relative position on "eustatic" sea level curves for specific Late Cambrian sequences to define sequence boundaries, systems tracts and flooding surfaces. Type 2 sequence boundaries are difficult to define in vertical outcrop sections since they are complicated by repeated pulses of high frequency sea level oscillations that generated meter-scale cycles. Instead of a single recognizable horizon, cyclic sections may merely show a transitional

zone of stacked cycles with features indicating emergence of the zone relative to underlying and overlying beds. Maximum flooding events also may best be recognized by a transitional zone of stacks of thick cycles reflecting a deepening-upward trend from stacks of thinner cycles exhibiting a slight shallowing-upward trend. The meter-scale cycles observed in outcrop provide important information about the internal composition of third-order sequences and component systems tracts.

CHAPTER 3

SUBTIDAL CYCLES: IMPLICATIONS FOR ALLOCYCLIC VS. AUTOCYCLIC CONTROLS

ABSTRACT

Thick successions of repetitive meter-scale subtidal cycles require suppressed sedimentation rates to maintain submergence below peritidal depths. Intrinsic processes such as storm and wave reworking and redistribution, reduced productivity within turbid waters, and lags in sedimentation during rapidly rising sea level may act to inhibit aggradation into the zone of optimal carbonate production. These processes may be a function of energy regime that in turn may relate to platform morphology. The ultimate control on stacked subtidal cycles appears to be eustacy with internal variability being controlled by subordinate sedimentary processes.

INTRODUCTION

Meter-scale cycles composed of purely subtidal carbonate lithofacies have increasingly been recognized throughout the geologic record (Lohmann, 1976; Markello and Read, 1982; Harwood and Moore, 1984; Aigner, 1985; Bova and Read, 1987; Calvet and Tucker, 1988; Yose and Heller, 1989). Subtidal cycles are distinct from classic tidal flat-capped peritidal cycles, the basic genetic unit of many carbonate platforms (Wilson, 1975; James, 1984), in that they do not shoal to tidal levels but remain submergent. Given the relatively rapid sedimentation rates of many modern shallow carbonate environments, subtidal cycles should, upon aggradation into the zone of maximum carbonate productivity, rapidly shallow up into the tidal zone. However, subtidal cycles remain within shallow to deep subtidal water depths suggesting that other factors must be operating to preclude complete shoaling. This paper proposes mechanisms by which shallowing-upward trends terminate within subtidal

depths and assesses the implications of subtidal cycles with regard to allocyclic versus autocyclic controls.

SUBTIDAL CYCLE CHARACTERISTICS: LATE CAMBRIAN EXAMPLES

A spectrum of shallow to deep subtidal cycles in the Late Cambrian of the House Range of west central Utah (Fig. 33) have many of the characteristics of subtidal cycles recognized elsewhere in the geologic record. As opposed to the fining-upward, thinning-upward trend that characterizes peritidal cycles (James, 1984; Demicco, 1985; Hardie and Shinn, 1986; Koerschner and Read, 1989), subtidal cycles are distinguished by an upward increase in grain size, bed thickness, crossbedding and other high energy sedimentary structures. Cycles are not capped by intertidal lithofacies nor do any of the subtidal cycles exhibit exposure features such as microkarsting or vadose dissolution/cementation. These cycles all fall within the range of average periods (20 - 400 ky) and thicknesses (0.4 - 12.0 m) expected for shallowing-upward, meter-scale cycles (Algeo and Wilkinson, 1989). Shallow to deep subtidal cycles form a continuum across carbonate platforms and are genetically linked to one another by shared lithofacies (Fig. 33).

Shallow subtidal cycles (0.7-5.2 m) of the Cordilleran Late Cambrian passive margin consist of a lower burrowed skeletal wackestone grading up into an oncolite-skeletal packstone/grainstone (characterized by numerous stacked hardgrounds) capped by a clean oolitic grainstone (Fig. 33). No evidence of intertidal exposure is recognized although the cross-bedded oolitic caps likely reached up into less than 2 meters of water (Hine, 1977; Harris,

Fig. 33: Shallow to deep ramp cycles of the House Range, Utah. Dashes off to the right denote cycle boundaries. Numbers off to the left are field-measured thicknesses in meters.

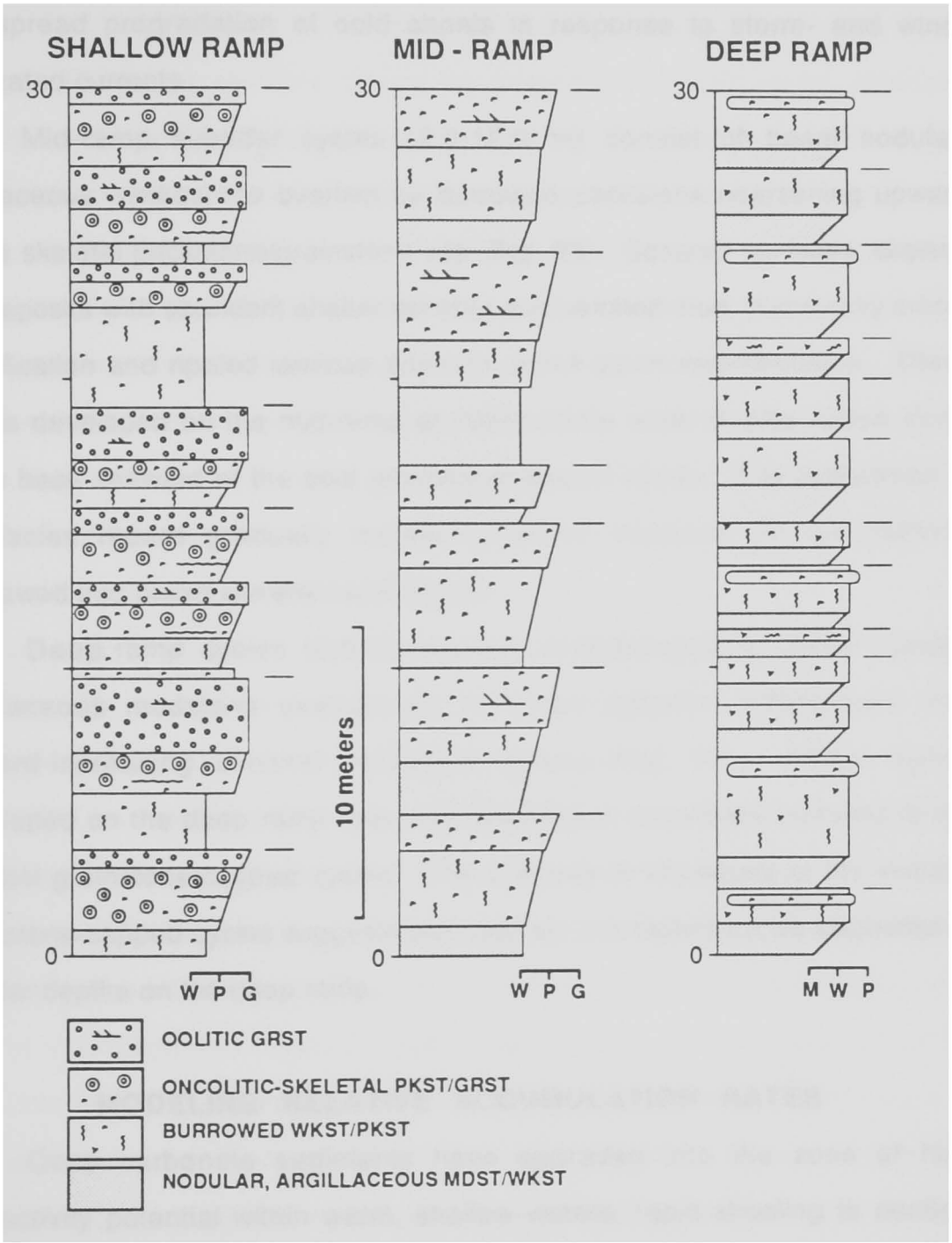
SHALLOW RAMP
MID - RAMP
DEEP RAMP
30
0
10 meters
W P G
W P G
M W P
OOLITIC GRST
ONCOLITIC-SKELETAL PKST/GRST
BURROWED WKST/PKST
NODULAR, ARGILLACEOUS MDST/WKST

1979; Halley et al., 1983). These cycles formed on the shallow ramp by migration of skeletal sand sheets across the burrowed wackestones followed by widespread progradation of ooid shoals in response to storm- and wind-generated currents.

Mid-ramp subtidal cycles (2.0-12.0 m) consist of basal nodular, argillaceous wackestone overlain by burrowed packstone coarsening upward into a skeletal packstone/grainstone cap (Fig. 33). Scoured surfaces, skeletal lag deposits with abundant shelter porosity and perched mud, hummocky cross-stratification and rippled laminae attest to active storm sedimentation. These cycles developed on the mid-ramp at intermediate water depths above storm wave base seaward of the ooid grainstone-capped cycles. The succession of lithofacies record gradually increasing storm influence as the platform shallowed into broad skeletal sand sheets.

Deep ramp cycles (0.6-3.1 m) are characterized by basal nodular argillaceous mudstone overlain by burrowed spiculitic wackestone with upward-increasing skeletal packstone lenses (Fig. 33). These cycles developed on the deep ramp near maximum storm wave-base seaward of the skeletal grainstone-capped cycles. The similarity in lithofacies to the skeletal grainstone-capped cycles suggests that they are incomplete cycles deposited at greater depths on the deep ramp.

MODELING RELATIVE ACCUMULATION RATES

Once carbonate sediments have aggraded into the zone of high productivity potential within warm, shallow waters, rapid shoaling to peritidal depths should occur within a geologically short period of time. The simplest

explanation for why subtidal cycles do not rapidly aggrade to sea level is that they are a product of reduced deeper water sedimentation rates. This concept can be illustrated with one-dimensional computer modeling (Read et al., 1986; Read, 1989) that graphically shows the interaction of subsidence, sediment accumulation and fluctuating sea level over time (Fig. 34). Figure 34A shows the major components of the modeling (details can be found in Read et al., 1986). All parameters in figures34B and 34C have been held equal except for sedimentation rates of the water depth-dependent lithofacies. The first run (Fig. 34B) uses sedimentation rates roughly approximating measured high rates from modern carbonate environments (Logan et al., 1974; Neumann and Land, 1975; Enos, 1977; Shinn et al., 1982; Bosence, 1989). Beginning in 20 meter water depths, the sediment surface remains submerged for about 150 ky producing two purely subtidal cycles. When the aggrading sediment surface reaches above 10 meter water depths however, the rapid shallow subtidal sedimentation rates become active and force the platform to abruptly shallow to peritidal depths producing a stack of tidal flat-capped cycles.

The second run (34C) uses sedimentation rates that roughly approximate net long-term accumulation rates for passive margins (0.01 - 0.1 m/ky). The aggrading sediment surface remains submergent throughout the entire 500 ky run producing a stack of purely subtidal cycles similar to those recognized in outcrop (compare with Figure 33 deep ramp cycles). To keep subtidal cycles from completely shallowing to sea level, some mechanism (or combination of mechanisms) had to have acted within the subtidal zone to suppress sedimentation rates relative to the high rates of modern shallow water settings (<20 m). Changing other parameters in the model such as short-term sea level

Fig. 34: 1-D models of interacting subsidence, fluctuating sea level and sedimentation. 34A) Explanatory diagram of model components. 34B) Model of rapidly aggrading stacked peritidal cycles generated using Holocene shallow-water (<20 m) sedimentation rates. Water depth ranks: tidal flat = 0-2 m; shallow subtidal = 2-10 m; deep subtidal = 10-20 m; very deep subtidal = >20 m. Simplified sea level curve consists of in-phase 20, 40, and 100 ky sine waves superimposed upon a 5 m/500 ky sea level rise.

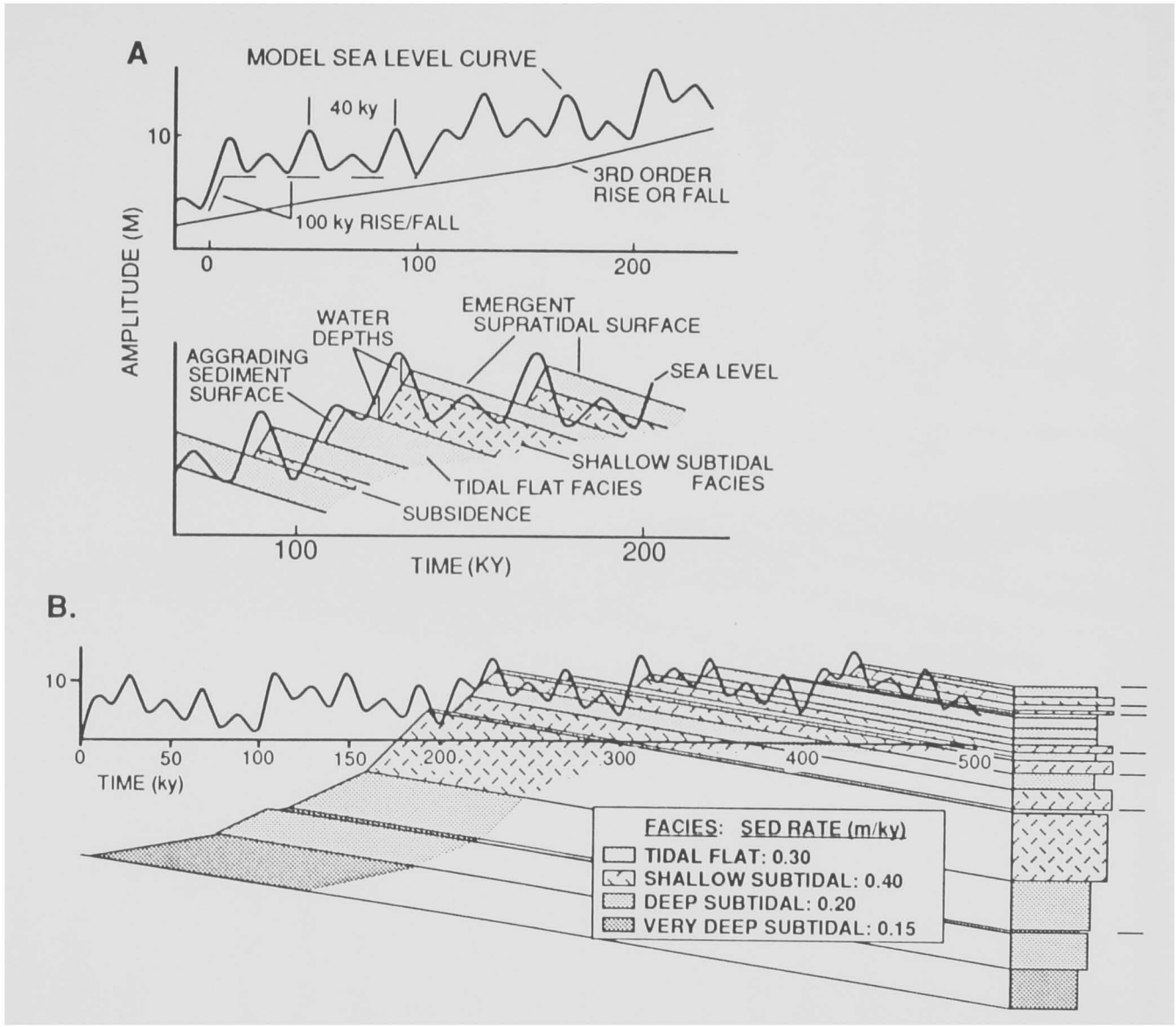
A
MODEL SEA LEVEL CURVE
40 ky
10
3RD ORDER
RISE OR FALL
100 ky RISE/FALL
AMPLITUDE (M)
0
100
200
WATER
DEPTHS
EMERGENT
SUPRATIDAL SURFACE
AGGRADING
SEDIMENT
SURFACE
SEA LEVEL
SHALLOW SUBTIDAL
FACIES
TIDAL FLAT FACIES
SUBSIDENCE
100
200
TIME (KY)
B.
10
0
50
100
150
200
300
400
500
TIME (ky)
FACIES: SED RATE (m/ky)
TIDAL FLAT: 0.30
SHALLOW SUBTIDAL: 0.40
DEEP SUBTIDAL: 0.20
VERY DEEP SUBTIDAL: 0.15

Figure 34C: Model of stacked subtidal cycles generated using the same water depth ranks as 34B but with sedimentation rates that roughly approximate long-term accumulation rates. Note the similarities to the deep subtidal cycles of Fig. 33.

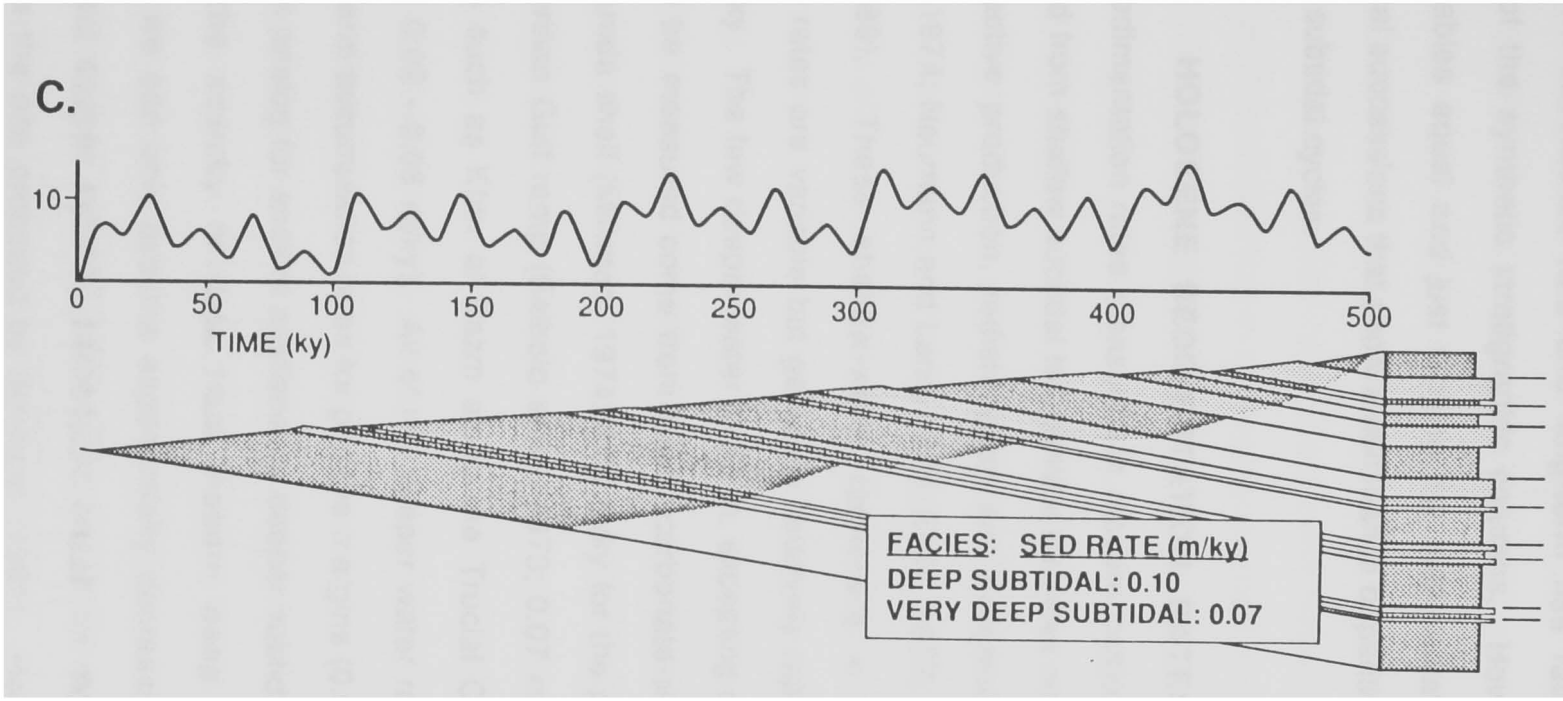
C.
10
0
50
100
150
200
250
300
400
500
TIME (ky)
FACIES: SED RATE (m/ky)
DEEP SUBTIDAL: 0.10
VERY DEEP SUBTIDAL: 0.07

amplitude, total subsidence rate and long-term rise rate will change the appearance of the synthetic stratigraphic columns. However, holding the changed variables equal and just varying the sedimentation rates will still produce vertical successions that show a dominance of peritidal cycles versus a dominance of subtidal cycles.

HOLOCENE SEDIMENTATION RATES

Most sedimentation rates measured in modern carbonate environments are determined from shallow subtidal to intertidal localities well within the photic zone where active production, redistribution and accumulation is occurring (Logan et al., 1974; Neumann and Land, 1975; Enos, 1977; Shinn et al., 1982; Bosence, 1989). These shallow-water (generally < 20m), short-term sedimentation rates are variable but generally relatively rapid and range from 0.1 to 10.0 m/ky. The few deeper water (> 20 m, excepting periplatform areas) rates that can be measured come from mixed carbonate-siliciclastic systems such as the Sunda shelf (Milliman, 1974; 0.08 m/ky for the post-Miocene) and the deeper Persian Gulf ramp (Seibold et al., 1973; 0.07 m/ky) or from deep water lagoons such as Khor al Bazm along the Trucial Coast (Purser and Seibold, 1973; 0.02 - 0.06 m/ky). All of the deeper water rates fall within the range of long-term accumulation rates for passive margins (0.01 - 0.1 m/ky) and may provide an analog for ancient argillaceous deeper subtidal lithofacies.

Given the scarcity of data from modern deep shelf carbonate environments, we can only assume exponentially decreasing sedimentation rates for ancient deeper subtidal carbonates based on relative productivity curves such as the one proposed by Schlager (1981). However, short-term

sedimentation rates reflect the residual of production after redistribution of sediment occurs and may not necessarily decrease exponentially with depth. The characteristic wedge-shape of individual depositional units, partially reflecting slope and the higher subsidence rates of the outer platform, requires that accumulation rates increase toward the outer ramp. This thickening is accounted for by: 1) redistribution of sediment produced on the shallow subtidal ramp out onto the more rapidly subsiding deeper ramp, and 2) intermittent deposition within the peritidal zone versus more continuous deposition in deeper subtidal environments. To maintain deposition within the subtidal zone without shallowing to peritidal depths, sedimentation rates active over the average duration of a typical shallowing-upward cycle (20-200 ky) must approach accumulation rates characteristic of longer periods of time (Sadler, 1981).

MECHANISMS FOR CONTINUED SUBMERGENCE

Time could be lost within subtidal cycles, thereby reducing net sedimentation rates, as a result of four processes.

Suppression of carbonate accumulation by wave sweeping: Net sedimentation rates could be suppressed by reworking and redistribution of sediment once accumulation has shallowed up to an energy barrier such as normal fairweather or storm wave base. On the mid-ramp, storm-dominated cycles may have aggraded into the zone of active storm current winnowing where their accumulation slowed down due to submarine erosion of sediment and subsequent redistribution out into lower energy, deeper subtidal

environments. Numerous actualistic models exist. Aigner (1985) has documented siliciclastic sediment transport from shallow to deep water within German Bay (North Sea) by offshore flowing "gradient" currents that develop in response to barometrically-induced coastal set-up. Sandy sediments are stirred up into suspension and carried offshore as dilute bottom-hugging density currents. The extensive blanket of coral-algal sands of the Great Pearl Bank of the Persian Gulf lie within water depths of 8 to 20 meters suggesting little aggradation above fairweather wave base (about 20 m; Purser and Seibold, 1973). Sediments are either carried out into the deeper Gulf where muddy sands predominate in water depths of 20 to 40 meters or are swept back toward the lagoon where they build up as steep accretion slopes (Purser and Evans, 1973). Also in the deeper Persian Gulf, Seibold and others (1973) have recognized a "widespread, vertically restricted zone of maximum sedimentation of echinoid and ophiuran skeletons that can also be related to the base of wave action". Along the northwest Australian inner shelf a thin (< 50 cm) semi-continuous sand sheet marks the upward termination of carbonate accumulation caused by constant sediment reworking by tidal currents and a strong storm-generated wave regime (Dix, 1989). Similarly, ancient storm-influenced subtidal cycles may have been unable to build above the zone of active wave sweeping due to the high energy conditions suppressing aggradation into the zone of optimal carbonate productivity.

Lack of low energy nucleation sites for tidal flats: The clean ooid grainstone caps of shallow ramp subtidal cycles probably aggraded to low tide under agitated conditions. However, energy levels may have been high

enough to preclude the nucleation of tidal flats, thereby maintaining shallow subtidal conditions. The shoal would have expanded laterally, filling in lows and forming an extensive sand sheet.

Turbidity: Carbonate productivity could be suppressed (but not necessarily shut down) by constant influx of fine siliciclastics that reduce the depth of light penetration as suggested by Schlager (1981) to explain the drowning of carbonate platforms. An actualistic model can be found in the Belize southern shelf lagoon where Purdy and others (1975) made a qualitative estimate of light penetration of 3-5 meters as opposed to effective photic depths of 30-40 meters for the Belize outer reef tract and >100 meters for the open ocean. Reduced biogenic productivity of filter feeders in concert with diminished light penetration and photosynthetic activity may interact to suppress sedimentation rates on the deep ramp where significant amounts of time could be represented by argillaceous limestones. The thinness of deep ramp cycles in the House Range (Fig. 33) versus thicker shallow and mid-ramp cycles may reflect reduced sedimentation rates due to turbidity.

Non-deposition during hardground formation: Hardgrounds are a common feature near the top of many subtidal cycles (Dravis, 1979; Moore, 1989) and may represent significant amounts of time. An actualistic analog is the grapestone facies of the Great Bahama Bank (4 - 10 m water depths) where very slow deposition and marine cementation of peloids and ooids is occuring as a result of active wave energy redistributing carbonate muds off the leeward flank of the platform (Winland and Matthews, 1974). Similar slow sedimentation

may be reflected in Late Cambrian shallow subtidal lithofacies by stacked hardgrounds within high energy oncolitic-skeletal grainstones.

CYCLE TYPE AND PLATFORM MORPHOLOGY

Subtidal cycles seem to be more common on carbonate ramps than on flat-topped rimmed shelves. They have been recognized on ramps in the U.S. Cordilleran Late Cambrian (Lohmann, 1976; Cook and Taylor, 1977); Mid- to Late Cambrian of Virginia-Tennessee (Markello and Read, 1982); Early Ordovician of the Appalachians (Bova and Read, 1987; Montanez, 1989); Early Mississippian of Wyoming-Montana (Elrick and Read, 1989); Pennsylvanian of southeastern California (Yose and Heller, 1989); Triassic of South Germany (Aigner, 1985; Calvet and Tucker, 1988); and the Jurassic Smackover Formation (Harwood and Moore, 1984).

Peritidal cycles may be more common on flat-topped, rimmed shelves such as the Lower Proterozoic Rocknest platform, Northwest Territories, Canada (Grotzinger, 1986); Cambrian Appalachian platform from Newfoundland to Tennessee (Demicco, 1985; Chow and James, 1987; Koerschner and Read, 1989); Cambrian of the southern Canadian Rockies (Aitken, 1978); Devonian of the Canning basin, western Australia (Read, 1973); and the Permian Capitan platform (Jacka et al., 1969).

The connection between platform morphology and cycle type may be related to energy regime. Open, deeply submerged ramps would be subject to higher energy conditions since they are vulnerable to strong wave and current activity generated in response to swells originating in the open ocean (Logan et al., 1969). Normal storm-related swells would travel unimpeded onto the ramp

with little loss of energy until they impinged on the ramp bottom (20-200 m for 5-12 second waves; Friedman and Sanders, 1978) when they would begin to lose energy by frictional dissipation. In this way, fines generated on the shallow ramp would be winnowed and redeposited along narrow tidal flats adjacent to the shoreline or carried out to the deeper ramp where they would settle out of suspension. The higher energies would preclude the nucleation and progradation of tidal flats and thereby maintain subtidal conditions across the ramp.

In contrast, flat-topped, reef-rimmed shelves would be dominated by low energy conditions because swells generated in the open oceans would rapidly lose energy during contact with the protective reefal rim. Fine-grained sediments would accumulate within restricted shallow subtidal lagoons where they could be fed onto rapidly prograding tidal flats. The platform would maintain a fully aggraded, low energy, flat-topped profile enhancing the development of widespread peritidal lithofacies.

SUBTIDAL CYCLES: AUTOCYCLIC VS. ALLOCYCLIC CONTROLS

Mechanisms proposed for meter-scale carbonate cycle generation include the tidal flat-controlled autocyclic model (Ginsburg, 1971) , variations in sedimentation-redistribution (Spencer and Demicco, 1989; Cloyd et al, 1990), episodic tectonism (Cisne, 1986), and eustatic oscillations of sea level (Goldhammer et al., 1987; Koerschner and Read, 1989). Essential to the autocyclic model is the progradation of tidal flats over the subtidal carbonate factory, terminating sediment generation until sufficient water depths can be attained by subsidence to resume carbonate production. By definition, shallow

subtidal cycles lack a tidal flat cap that might have inhibited productivity during its progradation. Therefore, the autocyclic model involving tidal flats has to be discarded as a plausible mechanism of subtidal cycle development although a variant involving wave-base may still apply.

Variations in sedimentation-redistribution certainly occur within subtidal carbonate platforms. Hardgrounds that formed during non- depositional events and the sheetlike geometry of carbonate sands produced by storm- and wave-reworking and redistribution attest to these processes. However, the variability of shifting loci of carbonate sedimentation and deposition cannot explain the persistent vertical and lateral rhythmicity and predictability of stacked subtidal cycles. In the House Range, cycle contacts can be traced as subparallel bands for many kilometers along the mountain flank. Deep subtidal cycles of the Sneakover Pass Member of the Orr Formation can be correlated from outcrops greater than 45 kilometers apart (Fig. 35). Also, the cycles are vertically predictable. Stacked subtidal cycles in the House Range show essentially the same repetition of lithofacies in 16 shallow subtidal and 34 deep subtidal successive cycles (Fig. 33). Processes intrinsic to the platform contribute to variability *within* cycles but are subordinate to a more dominant control on cycle formation such as eustatic sea level fluctuations.

Figure 36 illustrates the probability of an oscillating sea level as the primary control on development of subtidal cycles and the improbability of episodic tectonism as a potential control. The shallow subtidal cycles of the House Range (average 4 meter thickness) require deposition of a clean oolitic grainstone cap in water depths of 0 to 10 meters (Hine, 1977; Harris, 1979; Halley et al., 1983). To account for the abrupt change in lithofacies between the

Fig. 35: Correlation of deep subtidal cycles within the Sneakover Pass Member, Orr Formation, across 45 km within the House Range. Correlation based upon Notch Peak - Orr formational boundary and projected biomere boundary from Orr Ridge to Steamboat Pass.

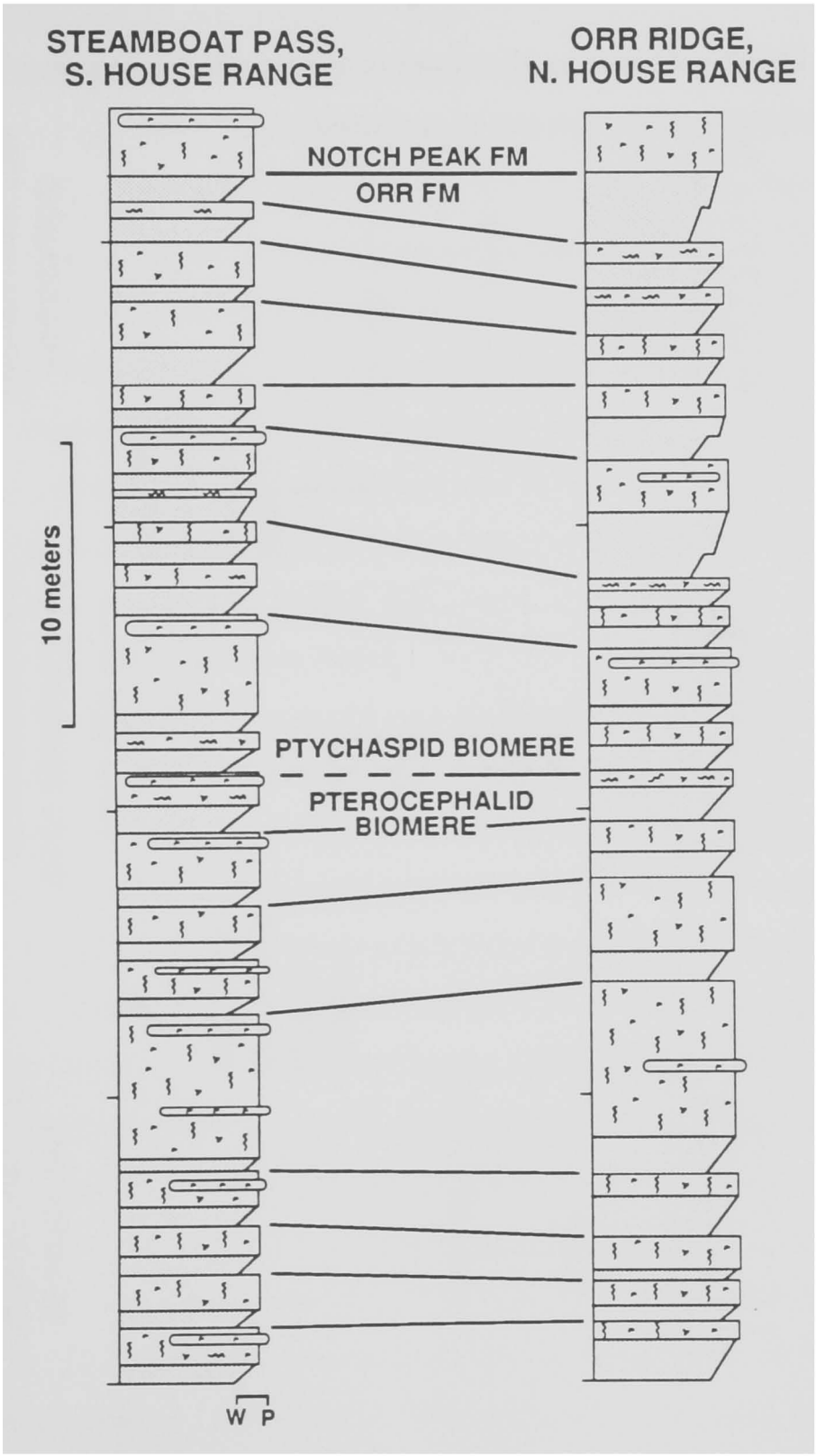
STEAMBOAT PASS,
S. HOUSE RANGE
ORR RIDGE,
N. HOUSE RANGE
NOTCH PEAK FM
ORR FM
10 meters
PTYCHASPID BIOMERE
PTEROCEPHALID
BIOMERE
W P

Fig. 36: Diagram illustrating the necessity of an oscillating sea level to generate typical subtidal cycles. See text for explanation.

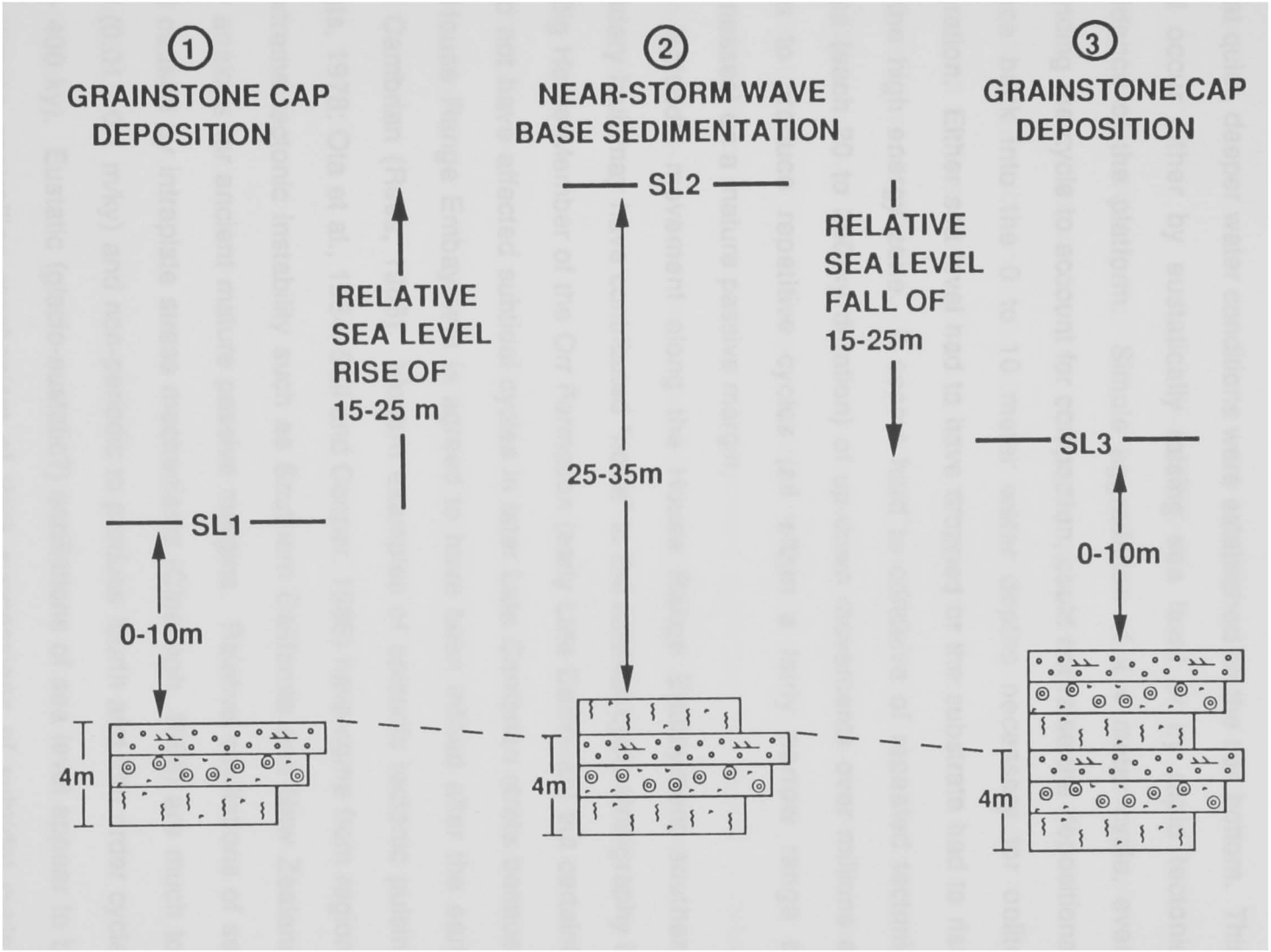
1
GRAINSTONE CAP DEPOSITION
2
NEAR-STORM WAVE BASE SEDIMENTATION
3
GRAINSTONE CAP DEPOSITION
SL1
SL2
SL3
RELATIVE SEA LEVEL RISE OF 15-25 m
RELATIVE SEA LEVEL FALL OF 15-25m
0-10m
25-35m
0-10m
4m
4m
4m

grainstone cap and the open-marine, burrowed wackestone base of the overlying cycle, relative sea level had to have risen, perhaps 15 to 25 meters, so that quiet, deeper water conditions were established on the sea bottom. This could occur either by eustatically raising sea level or by rapid tectonic subsidence of the platform. Simple aggradation of a 4 meter cycle, even expanding the cycle to account for compaction, could not raise the depositional surface back into the 0 to 10 meter water depths necessary for oolite generation. Either sea level had to have dropped or the substrate had to rise into the high energy zone. It seems hard to conceive of repeated tectonic pulses (each 20 to 200 ky duration) of up-down movements over millions of years to produce repetitive cycles (all within a fairly narrow range of thicknesses) on a mature passive margin.

Episodic movement along the House Range Embayment southern boundary fault may have contributed "noise" to the subtidal cycle stratigraphy in the Big Horse Member of the Orr Formation (early Late Cambrian) but certainly could not have affected subtidal cycles in later Late Cambrian strata because the House Range Embayment is agreed to have been infilled after the early Late Cambrian (Rees, 1986). Modern examples of episodic tectonic pulsing (Yeats, 1978; Ota et al., 1984; Bull and Cooper, 1986) have come from regions of extreme tectonic instability such as Southern California and New Zealand, poor analogs for ancient mature passive margins. Relative oscillations of sea level caused by intraplate stress mechanisms (Cloetingh, 1986) are much too slow (0.01 - 0.1 m/ky) and non-periodic to produce fourth and fifth order cycles (20 - 400 ky). Eustatic (glacio-eustatic?) oscillations of sea level appear to be the ultimate controlling mechanism of thick successions of subtidal cycles,

especially where they are developed on cratonic interiors and passive continental margins.

CONCLUSIONS

1. Repetitive successions of carbonate cycles composed of purely subtidal lithofacies are a common component of many carbonate ramps.

2. To maintain submergence, subtidal lithofacies had to have experienced suppressed sedimentation rates relative to rapidly-shoaling peritidal cycles.

3. Intrinsic processes such as storm- and wave-reworking and redistribution near fairweather or storm wave-base may act to maintain submergence below the zone of optimal carbonate productivity.

4. Subtidal cycles appear to be the dominant cycle type on ramps whereas peritidal cycles appear to dominate flat-topped rimmed shelves. The relationship between cycle type and platform morphology may be a function of energy regime.

5. Subtidal cycles on passive margins appear to be a product of eustacy acting in concert with subordinate sedimentary processes.

REFERENCES

Aigner, T. A., 1985, Storm depositional systems: Dynamic stratigraphy in modern and ancient shallow-marine sequences, Berlin, Springer-Verlag, 174 pp.

Aitken, J. D., 1967, Classification and environmental significance of cryptalgal limestones and dolomites, with illustrations from the Cambrian and Ordovician of southwestern Alberta: Journal of Sedimentary Petrology, v.37, p.1163-1178.

Aitken, J. D., 1981, Generalizations about grand cycles: *in* Taylor, M. E., (ed.), Short papers for the Second International Symposium on the Cambrian System: United States Geological Survey Open-File Report 81-743, p.8-14.

Aitken, J. D., 1978, Revised models for depositional grand cycles, Cambrian of the southern Rocky Mountains, Canada: Bulletin Canadian Petroleum Geology, v.26, p.515-542.

Algeo, T. J., and Wilkinson, B. H., 1988, Periodicity of mesoscale Phanerozoic sedimentary cycles and the role of Milankovitch orbital modulation: Journal of Geology, v.96, p.313-322.

Anderson, R. Y., 1986, The varve microcosm: propagator of cyclic bedding: Paleoceanography, v.1, p.373-382.

Angevine, C.L., Heller, P.L., and Paola, C., 1988, Quantitative sedimentary basin modeling: Short course notes, Geological Society of America National Meeting, Denver, Colo., 93 pp.

Armin, R. A., and Mayer, L., 1983, Subsidence analysis of the Cordilleran miogeocline: Implications for timing of late Proterozoic rifting and amount of extension: Geology, v.11, p.702-706.

Arthur, M.A., Dean, W.E., Bottjer, D., and Scholle, P.A., 1984, Rhythmic bedding in Mesozoic-Cenozoic pelagic carbonate sequences: the primary and diagenetic origin of Milankovitch-like cycles: *in* Berger, A., Imbrie, J., Hays, J., Kukla, G. and Salzman, B., (eds.), Milankovitch and Climate: Boston, Massachusetts, Reidel, p. 191-222.

Bally, A.W., 1980, Basins and subsidence - A summary: *in* Bally, A.W., Bender, P.L., McGretchin, T.R., and Walcott, R.I. (eds.), Dynamics of Plate Interiors, Geodynamics Series, v. I, p. 5-20.

Barnes, V. E., and Bell, W. C., 1977, The Moore Hollow Group of Central Texas: Bureau Economic Geology, Univ. Texas at Austin, Rept. Invest. #88, p.169

Barron, E. J., Arthur, M. A., and Kauffman, E. G., 1985, Cretaceous rhythmic bedding sequences: a plausible link between orbital variations and climate: Earth & Planetary Science Letters, v.72, p.327-340.

Beach, D. K., and Ginsburg, R. N., 1980, Facies succession of Plio-Pleistocene carbonates, northwestern Great Bahama Bank: American Association of Petroleum Geologists Bulletin., v.64, p.1634-1642.

Berger, A., 1977, Support for the astronomical theory of climatic change: Nature, v. 268, p. 44-45.

Berger, A., Loutre, M.F., Dehant, V., 1989, Influence of the changing lunar orbit on the astronomical frequencies of pre-Quaternary insolation patterns: Paleoceanography, v. 4, p. 555-564.

Berger, A., Imbrie, J., Hays, J., Kukla, G. and Salzman, B., (eds.), 1984, Milankovitch and Climate: Boston, Massachusetts, Reidel, 510 pp.

Boardman, M. R., and Neumann, A. C., 1984, Sources of periplatform carbonates: Northwest Providence Channel, Bahamas: Journal of Sedimentary Petrology, v.54, p.1110-1123.

Bond, G. C., Christie-Blick, N., Kominz, M. A., and Devlin, W. J., 1984, An early Cambrian rift to post-rift transition in the Cordillera of western North America: Nature, v.316, p.742-745.

Bond, G. C., and Kominz, M. A., 1984, Construction of tectonic subsidence curves for the early Paleozoic miogeocline, southern Canadian Rocky Mountains: Implications for subsidence mechanisms, age of breakup and crustal thinning: Geological Society of America Bulletin, v.95, p.155-173.

Bond, G. C., Kominz, M. A., and Devlin, W. J., 1983, Thermal subsidence and eustasy in the lower Paleozoic miogeocline of western North America: Nature, v.306, p.775-779, p.39-62.

Bond, G. C., Kominz, M. A., and Grotzinger, J. P., 1988, Cambro-Ordovician eustasy: evidence from geophysical modeling of subsidence in Cordilleran and Appalachian passivemargins: *in* Paola, C., and Kleinsephn, K., (eds.), New Perspectives in Basin Analysis, 129-161.

Bond, G. C., Kominz, M. A., Grotzinger, J. P., and Steckler, M. S., 1989, Role of thermal subsidence, flexure and eustasy in the evolution of Early Paleozoic passive margin carbonate platforms: *in* Crevello, P., Wilson, J. L., Sarg, J. F., and Read, J. F., (eds.), Controls on Carbonate Platform and Basin Development: Society Economic Paleontologists Mineralogists Special Publication. 44, p. 39-62.

Bond, G. C., Nickeson, P. A., and Kominz, M. A., 1984, Breakup of a supercontinent between 625 Ma and 555 Ma: new evidence and implications for continental histories: Earth and Planetary Science Letters, v.70, p.325-345.

Bosence, D. W. J., 1989, Biogenic carbonate production in Florida Bay: Bulletin of Marine Sciences, v.44, p.419-433.

Bova, J. A., and Read, J. F., 1986, Incipiently drowned facies within a cyclic peritidal ramp sequence, Early Ordovician Chepultepec interval, Virginia Appalachians: Geological Society of America Bulletin, v.98, p.714-727.

Brady, M. J., and Rowell, A. J., 1976, Upper Cambrian subtidal blanket carbonate of the Cordilleran miogeocline, eastern Great Basin: Brigham Young University Geological Studies, v.23, p.153-163.

Bull, W. B., and Cooper, A. F., 1986, Uplifted marine terraces along the Alpine fault, New Zealand: Science, v.234, p.1225-1228.

Burton, R., Kendall, C. G. St.C., and Lerche, I., 1987, Out of our depth: on the impossibility of fathoming eustatic sea level from the stratigraphic record: Earth Science Reviews, v.24, p.237-277.

Calvet, F. and Tucker, M.E., 1988, Outer ramp cycles in the Upper Muschelkalk of the Catalan basin, northeast Spain: Sedimentary Geology, v. 57, p. 185-198.

Chow, N., and James, N. P., 1987, Cambrian Grand Cycles: a northern Appalachian perspective: Geological Society of America Bulletin, v.98, p.418-429.

Christie-Blick, N., and Mountain, G.S., 1989, Sequence stratigraphy and the measurement of sea-level change: *in* Sahagian, D.L., and Watts, A.B., (convenors), American Geophysical Union Chapman conference on causes and consequences of long term sea level changes, Snowbird, Utah, Abstract volume.

Cisne, J. L., 1986, Earthquakes recorded stratigraphically on carbonate platforms: Nature, v.323, p.320-322.

Cisne, J. L., Gildner, R. F., and Rabe, B. D., 1984, Epeiric sedimentation and sea level: synthetic ecostratigraphy: Lethaia, v.17, p.267-288.

Cloetingh, S., 1986, Intraplate stresses: a new tectonic mechanism for relative fluctuations of sea level: Geology, v.14, p.617-620.

Cloyd, K.C., Demicco, R.V. and Spencer, R.J., 1990, Tidal channel, levee, and crevasse-splay deposits from a Cambrian tidal channel system: A new mechanism to produce shallowing-upward sequences: Journal of Sedimentary Petrology, v.60, p. 73-83.

Cook H.E., and Taylor, M. E., 1977, Comparison on continental slope and shelf environments in the Upper Cambrian and lowest Ordovician of Nevada: *in* Cook, H.E., and Enos, P. (eds.), Deep-Water Carbonate Environments, Society of Economic Paleontologists and Mineralogists Special Publication 25, p. 51-81.

Demicco, R. V., 1981, Comparative sedimentology of an ancient carbonate platform: The Conococheague limestone of the central Appalachians: (unpubl. Ph.D. diss.), The Johns Hopkins University, Baltimore, Maryland, 333 pp.

Demicco, R. V., 1983, Wavy and lenticular-bedded carbonate ribbon rocks of the Upper Cambrian Conococheague limestone, central Appalachians: Journal of Sedimentary Petrology, v.53, p.1121-1132.

Demicco, R. V., 1985, Patterns of platform and off-platform carbonates of the Upper Cambrian of western Maryland: Sedimentology, v.32, p.1-22.

Derby, J. R., 1965, Paleontology and stratigraphy of the Nolichucky Formation in southwest Virginia and northeast Tennessee: Ph.D. diss., Blacksburg, Virginia, Virginia Polytechnic Institute and State University, 468 p.

Dill, R. F., 1986, Giant subtidal stromatolites forming in normal salinity waters: Nature, v.324, No.6, p.55-58.

Dix, G.R., 1989, High-energy, inner shelf carbonate facies along a tide-dominated non-rimmed margin, northwestern Australia: Marine Geology, v. 89, p.347-362.

Donovan, D. T., and Jones, E. J. W., 1979, Causes of world-wide changes in sea level: Journal Geological Society of London, v.136, p.187-192.

Dravis, J. J., 1979, Rapid and widespread generation of Recent oolitic hardgrounds on a high energy Bahamian platform, Eleuthra Bank, Bahamas: Journal of Sedimentary Petrology, v.49, p.195-208.

Eby, R.G., 1981, Early Late Cambrian Trilobite Faunas of the Big Horse Limestone and Correlative Units in Central Utah and Nevada: (unpubl. Ph.D. diss.), State University of New York, Stony Brook, 613 pp.

Edwards, L. E., 1984, Insights of why graphic correlation (Shaw's method) works: Journal of Geology, v.92, p.583-597.

Enos, P., 1977, Holocene sediment accumulations of the south Florida shelf margin: *in* Enos, P. and Perkins, R.D., eds., Quaternary sedimentation in south Florida: Geological Society of America Memoir 147, p. 1-130.

Enos, P., and Perkins, R. D., 1977, Quaternary Sedimentation in South Florida: Geological Society of America Memoir 147, 198 pp.

Erdtmann, B.-D., and Miller, J.F., 1981, Eustatic control of lithofacies and biofacies changes near the base of the Tremadocian: *in* Taylor, M. E., (ed.), Short papers for the Second International Symposium on the Cambrian System: United States Geological Survey Open-File Report 81-743, p. 78-81.

Feinstein, S., 1981, Subsidence and thermal history of southern Oklahoma aulacogen: Implications for petroleum exploration: American Association of Petroleum Geologists Bulletin, v. 65, p. 2521-2533.

Fischer, A. G., 1964, The Lofer cyclothems of the Alpine Triassic: *in* Merriam, D. F., (ed.), Symposium of cyclic sedimentation: State Geol. Survey of Kansas, Bulletin 169, p. 107-150.

Fischer, A. G., 1986, Climatic rhythms recorded in strata: Annual Review of Earth & Planetary Sciences, v.14, p.351-376.

Friedman, G.M. and Sanders, J.E., 1978, Principles of Sedimentology, John Wiley and Sons, New York, 792 p.

Ginsburg, R. N., 1971, Landward movement of carbonate mud: New model for regressive cycles in carbonates (abst.): American Association Petroleum Geologists Bulletin, v.55, p.340.

Goldhammer, R. K., Dunn, P. A., and Hardie, L. A., 1987, High frequency glacio-eustatic sea-level oscillations with Milankovitch characteristics recorded in Middle Triassic platform carbonates in northern Italy: American Journal Science, v.287, p.853-892.

Goldhammer, R. K., Dunn, P. A., and Hardie, L. A., 1990, Depositional cycles, composite sea-level changes, cycle stacking patterns, and the hierarchy of stratigraphic forcing: Examples from Alpine Triassic platform carbonates: Geological Society America Bulletin, v.102, p.535-562.

Goodwin, P. W., and Anderson, E. J., 1985, Punctuated aggradational cycles: A general hypothesis of episodic stratigraphic accumulation: Journal of Geology, v.93, p.515-533.

Grotzinger, J. P., 1986, Cyclicity and paleoenvironmental dynamics, Rocknest platform, northwest Canada: Geological Society of America Bulletin, v.97, p.1208-1231.

Grotzinger, J. P., 1986, Upward shallowing platform cycles: a response to 2.2 billion years of low-amplitude, high-frequency (Milankovitch band) sea level oscillations: in Arthur, M. A., and Garrison, R. E., (eds.), Paleoceanography, 403-416.

Hallam, A., 1984, Pre-Quaternary sea-level changes: Annual Review of Earth and Planetary Sciences, v.12, p.205-243.

Hallam, A., 1988, A reevaluation of Jurassic eustasy in the light of new data and the revised Exxon curve: *in* Wilgus, C., Posamentier, H., Ross, C., and Kendall, C. G. St. C., (eds.), Sea-Level Changes: An Integrated Approach, p. 261-274.

Halley, R. B., Harris, P. M., and Hine, A. C., 1983, Bank Margin: *in* Scholle, P. A., Bebout, D. G., and Moore, C. H., (eds.), Carbonate Depositional Environments, American Association Petroleum Geologists Memoir 33, 463-506.

Ham, W.E., Denison, R.E., and Merritt, C.A., 1964, Basement rocks and structural evolution of southern Oklahoma: Oklahoma Geological Survey Bulletin 95, 302 pp.

Hancock, J.M., and Kaufmann, E.G., 1979, The great transgressions of the Late Cretaceous: Journal of the Geological Society of London, v. 136, p. 175-186.

Haq, B. U., Hardenbol, J., and Vail, P. R., 1987, Chronology of fluctuating sea levels since the Triassic: Science, v.235, p.1156-1167.

Hardie, L. A., Bossellini, A., and Goldhammer, R.K., 1986, Repeated subaerial exposure of subtidal carbonate platforms, Triassic, northern Italy: Evidence for high frequency sea level oscillations on a 104 year scale: Paleoceanography, v. 2, p. 447-457.

Hardie, L. A., and Ginsburg, R. N., 1977, Layering: The origin and environmental significance of lamination and thin bedding, *in* Hardie, L. A. (ed.), Sedimentation on the modern carbonate tidal flats of northwest Andros Island, Bahamas: Baltimore, Maryland, Johns Hopkins University Press, p. 50-123.

Hardie, L. A., and Shinn, E. A., 1986, Carbonate depositional environments, modern and ancient: part 3: tidal flats: Colorado School of Mines Quarterly, v.81, p.1-74.

Harris, P. M., 1979, Facies anatomy and diagenesis of a Bahamian ooid shoal: Miami, Fla., Univ. Miami, Sedimenta VII, Comparative Sedimentology Lab, p.163.

Harwood, G.M. and Moore, C.H., 1984, Comparative sedimentology and diagenesis of Upper Jurassic ooid grainstone sequences, East Texas basin: Society of Economic Paleontologists and Mineralogists core workshop no.5 - Carbonate sands, p. 176-232.

Hasson, K. O., and Haase, C. S., 1988, Lithofacies and paleogeography of the Conasauga Group (Middle to Late Cambrian) in the Valley and Ridge province of east Tennessee: Geological Society of America Bulletin, v.100, p.234-246.

Hays, J. D., Imbrie, J., and Shackleton, J. J., 1976, Variations in the Earth's orbit: Pacemaker of the ice ages: Science, v.194, p.1121-1132.

Heckel, P. H., 1986, Sea-level curve for Pennsylvanian eustatic marine transgressive-regressive depositional cycles along midcontinent outcrop belt, North America: Geology, v. 14, p. 330-334.

Heidlauf, D. T., Hsui, A. T., and Klein, G. deV, 1986, Tectonic subsidence analysis of the Illinois Basin: Journal of Geology, v.94, p.779-794.

Herbert, T. D., and Fischer, A. G., 1986, Milankovithc climatic origin of mid-Cretaceous black shale rhythms in central Italy, Nature, v. 321, p. 739-743.

Hine, A. C., 1977, Lily Bank, Bahamas; history of an active oolite sand shoal: Journal Sedimentary Petrology, v.47, No.4, p.1554-1581.

Hine, A.C., and Steinmetz, J.C., 1984, Cay Sal Bank, Bahamas - A partially drowned carbonate platform: Marine Geology, v. 59, p. 135-164.

Hintze, L. F., 1974, Preliminary geologic map of the Notch Peak quadrangle, Millard County, Utah: United States Geological Survey Miscellaneous Field Studies Map MF-636.

Hintze, L. F., and Palmer, A. R., 1976, Upper Cambrian Orr Formation: its subdivisions and correlatives in western Utah: United States Geological Survey Bull. 1405-G, p.1-25.

Hintze, L. F., Miller, J. F., and Taylor, M. E., 1980, Upper Cambrian-Lower Ordovician Notch Peak Formation in western Utah: United States Geological Survey Open-File Report 80-776, p.67.

Jacka, A.D., Thomas, C.M., Beck, R.H., Williams, K.W., and Harrison, S.C., 1969, Guadalupian depositional cycles of the Delaware Basin and Northwest Shelf: *in* Elam, J.G. and Chuber, S., eds., Cyclic Sedimentation in the Permian Basin: West Texas Geological Society Publication 69-56, p. 152-196.

James, N. P., 1984, Facies models 8; Shallowing-upward sequences in carbonates: Geoscience Canada, v.4, No.3, p.126-142.

James, N.P., Stevens, R.K., Barnes, C.R., and Knight, Ian, 1989, Evolution of a Lower Paleozoic continental-margin carbonate platform, northern Canadian Appalachians: *in* Crevello, P., Wilson, J. L., Sarg, J. F., and Read, J. F., (eds.), Controls on Carbonate Platform and Basin Development: Society Economic Paleontologists Mineralogists Special Publication. 44, p. 123-146.

Johnson, J. G., Klapper, G., and Sandberg, C. A., 1985, Devonian eustatic fluctuations in Euramerica: Geological Society of America Bulletin, v.96, p.567-587.

Johnson, M. E., Jia-Yu, R., and Fox, W. T., 1989, Comparison of Late Ordovician epicontinental seas and their relative bathymetry in North America and China: Palaios, v.4, p.43-50.

Kauffman, E. G., 1988, Concepts and methods of high-resolution event stratigraphy: Annual Review Earth and Planetary Sciences, v.16, p.605-654.

Kendall, C. G. St.C., and Lerche, Ian, 1988, The rise and fall of eustasy: *in* Wilgus, C., Posamentier, H., Ross, C., and Kendall, C. G. St. C., (eds.), Sea-Level Changes: An Integrated Approach, p. 3-18.

Kendall, C. St G.C., and Schlager, W., 1981, Carbonates and relative sea level: Marine Geology, v.44, p.181-212.

Kennard, J.M., and James, N.P., 1986, Thrombolites and stromatolites: Two distinct types of microbial structures: Palaios, v.1, p. 492-503.

Kepper, J. C., 1972, Paleoenvironmental pattern in Middle to lower Upper Cambrian interval in eastern Great Basin: American Association of Petroleum Geologists Bulletin, v.56, p.503-527.

King, D.T., and Chafetz, H.S., 1975, Tidal-flat to shallow-shelf deposits in the Cap Mountain Limestone Member of the Riley Formation, Upper Cambrian of central Texas: Journal of Sedimentary Petrology, v. 53, p. 261-273.

Klein, G. deV., 1990, Pennsylvanian time scales and cycle periods: Geology, v. 18, p. 455-457.

Koerschner, W. F. III, 1983, Cyclic peritidal facies of a Cambrian aggraded shelf: Elbrook and Conococheague Formations, Virginia Appalachians (M.S. thesis): Blacksburg, Virginia, Virginia Polytechnic Institute and State University, 184 pp.

Koerschner W.F., and Read, J. F., 1989, Field and modelling studies of Cambrian carbonate cycles, Virginia Appalachians: Journal of Sedimentary Petrology, v. 59, p. 654-687.

Kominz, M.A., 1984, Oceanic ridge volumes and sea-level change - An error analysis: *in* Schlee, J. S., (ed.), Interregional Unconformities and Hydrocarbon Accumulation; American Association Petroleum Geologists Memoir 36, p. 108-128.

Kominz, M. A., and Bond, G. C., 1989, Are cyclic sediments periodic?, *in* Franseen, E.K., and Watney, W.L., (eds.) Sedimentary modeling: computer simulations of depositional systems, Subsurface Geology Series 12, Kansas Geol. Survey, p. 35.

Kreisa, R.D., 1981, Storm-generated sedimentary structures in subtidal marine facies with examples from the Middle and Upper Ordovician of southwestern Virginia: Journal of Sedimentary Petrology, v. 51, p. 399-423.

Levy, M., and Christie-Blick, N., 1989, Pre-Mesozoic palinspastic reconstruction of the eastern Great Basin (western United States): Science, v. 245, p. 1454-1462.

Lochman-Balk, C., 1971, Cambrian of the craton: *in* Holland, E.R. (ed.), Cambrian of the New World, London, Wiley-Interscience, p. 79-167.

Logan, B.W., Harding, J.L., Ahr, W.M., Williams, J.D. and Snead, R.G., 1969, Carbonate sediments and reefs, Yucatan shelf, Mexico, American Association of Petroleum Geologists Memoir 11, p. 1-198.

Logan, B.W., Read, J.F., Hagan, G.M., Hoffman, P., Brown, R.G., Woods, P.J. and Gebelein, C.D., 1974, Evolution and diagenesis of Quaternary carbonate sequences, Shark Bay, Western Australia: American Association of Petroleum Geologists Memoir 22, 358 p.

Lohmann, K. C., 1976, Lower Dresbachian (Upper Cambrian) platform to deep-shelf transition in eastern Nevada and western Utah: An evaluation through lithologic cycle correlation: Brigham Young University Geological Studies, v.23, p.111-122.

Lohmann, K. C., 1977, Causative factors of the outer detrital belt House embayment: A sedimentologic examination of a terrigenous-carbonate depositional system, early Upper Cambrian (Dresbachian), east-central Utah and west-central Nevada: (unpublished Ph.D. Diss.), Stony Brook, New York, State University of New York, 286 pp.

Longacre, S. A., 1970, Trilobites of the Upper Cambrian Ptychaspid Biomere, Wilberns Formation, central Texas: Paleontological Society Memoir 4, 70 pp.

Markello, J. R., 1979, Carbonate ramp to deeper shale-shelf transitions of an Upper Cambrian (Dresbachian) shelf embayment, Nolichucky Formation, southwest Virginia: (M.S. thesis), Blacksburg, Virginia, Virginia Polytechnic Institute and State Univ., 115 pp.

Markello, J. R., and Read, J. F., 1981, Carbonate ramp-to-deeper shale shelf transitions of an Upper Cambrian intrashelf basin, Nolichucky Formation, southwest Virginia Appalachians: Sedimentology, v.28, p.573-597.

Markello, J. R., and Read, J. F., 1982, Upper Cambrian intrashelf basin, Nolichucky Formation, southwest Virginia Appalachians: American Association of Petroleum Geologists Bulletin, v.66, p.860-878.

Matthews, R.K., 1984, Dynamic Stratigraphy, Prentice-Hall, Englewood Cliffs, N.J., 489 pp.

McKenzie, D. P., 1978, Some remarks on the development of sedimentary basins: Earth and Planetary Science Letters, v.40, p.25-32.

Miall, A.D., 1984, Principles of sedimentary basin analysis: New York, Springer-Verlag, 490 pp.

Miller, F. X., 1977, The graphic correlation method in biostratigraphy: *in* Kauffman, E.G., and Hazel, J.E., (eds.), Concepts and Methods of Biostratigraphy, Stroudsburg, Pa., Dowden, Hutchinson & Ross, p. 165-186.

Miller, J.F., 1984, Cambrian and earliest Ordovician conodont evolution, biofacies, and provincialism: Geological Society of America Special Paper 196, p. 43-68.

Miller, J. F., 1987, Upper Cambrian and basal Ordovician conodont faunas of the southwest flank of the Llano uplift, Texas: *in* Grayson, R. C., (ed.), Early and Late Paleozoic conodont faunas of the Llano uplift region, central Texas - Biostratigraphy, systemic boundary relationships, and stratigraphic importance; Guidebook for Field Trip 1, 1987 Meeting of South-Central Section, Geol. Soc. Amer., 1-22.

Miller, J. F., Taylor, M. E., Stitt, J. H., Ethington, R. L., Hintze, L. F., and Taylor, J. F., 1982, Potential Cambrian-Ordovician stratotype sections in the western United States, *in* Bassett, M.G., and Dean, W.T., (eds.), The Cambrian-Ordovician boundary: Sections, fossil distributions, and correlations: National Museum of Wales Geological Series no. 3, p. 155-180.

Milliman, J.D., 1974, Marine Carbonates, New York, Springer-Verlag, 375 pp.

Mitchum, R.M., 1977, Glossary of terms used in seismic stratigraphy: *in* Payton, C. E., (ed.), Seismic stratigraphy - applications to hydrocarbon exploration: Tulsa, Okla: American Association Petroleum Geologists Memoir 26, p. 205-212.

Montanez, I.P., 1989, Regional dolomitization of Early Ordovician Upper Knox Group, Appalachians: (unpublished Ph.D. dissertation), Virginia Polytechnic Institute and State Univ., Blacksburg, VA, 322 p.

Moore, C.H., 1989, Carbonate Diagenesis and Porosity: Developments in Sedimentology 46, Amsterdam, Elsevier, 338 p.

Mullins, H. T., Neumann, A. C., Wilber, R. J., and Boardman, M. R., 1980, Nodular carbonate sediment on Bahamian slopes: possible precursors to nodular limestones: Journal Sedimentary Petrology, v.50, p.117-131.

Nemec, 1988, Coal correlations and intrabasinal subsidence: A new analytical perspective, *in* Paola, C., and Kleinsephn, K., (eds.), New Perspectives in Basin Analysis, 234-248.

Neumann, A. C., and Land, L. S., 1975, Lime mud deposition and calcareous algae, Bight of Abaco, Bahamas: a budget: Journal of Sedimentary Petrology, v.45, p.763-786.

Olsen, P. E., 1986, A 40-million-year lake record of Early Mesozoic orbital climatic forcing: Science, v.234, p.842-848.

Orndorff, R. C., 1988, Latest Cambrian and Earliest Ordovician conodonts from the Conococheague and Stonehenge Limestones of northwestern Virginia: United States Geological Survey Bulletin 1837, A1-18.

Ota, Y., 1986, Marine terraces as reference surfaces in late Quaternary tectonic studies: Examples from the Pacific rim: Royal Society of New Zealand Bulletin, v.24, p.357-375.

Palmer, A. R., 1954, The faunas of the Riley Formation in central Texas: Jour. Paleo, v.28, p.709-786.

Palmer, A. R., 1965, Trilobites of the Late Cambrian Pterocephaliid biomere in the Great Basin, United States: United States Geological Survey Professional Paper 493, p.105 p.

Palmer, A. R., 1971a, The Cambrian of the Great Basin and adjacent areas, western United States: *in* Holland, E.R. (ed.), Cambrian of the New World, London, Wiley-Interscience, p. 1-79.

Palmer, A. R., 1971b, The Cambrian of the Appalachian and eastern New England regions, eastern United States: *in* Holland, E.R. (ed.), Cambrian of the New World, London, Wiley-Interscience, p. 289-332.

Palmer, A.R., 1974, Search for the Cambrian world: American Scientist, v. 62, p. 216-224.

Palmer, A. R., 1981a, On the correlatibility of Grand Cycle tops: *in* Taylor, M. E., (ed.), Short Papers for the Second International Symposium on the Cambrian System: United States Geological Survey Open File Report 81-743, 156-157.

Palmer, A. R., 1981b, Subdivision of the Sauk sequence: *in* Taylor, M. E., (ed.), Short Papers for the Second International Symposium on the Cambrian System: United States Geological Survey Open File Report 81-743, 160-163.

Palmer, A. R., 1983, The Decade of North American Geology 1983 geologic time scale: Geology, v.11, p.503-504.

Palmer, A. R., 1984, The biomere problem: evolution of an idea: Journal Paleontology, v.58, No.3, p.599-611.

Parkinson, N., and Summerhayes, C., 1985, Synchronous global sequence boundaries: American Association of Petroleum Geologists Bulletin, v.69, p.685-687.

Pfiel, R. W., and Read, J. F., 1980, Cambrian carbonate platform margin facies, Shady Dolomite, southwestern Virginia, U.S.A.: Journal Sedimentary Petrology, v.50, p.91-116.

Pitman, W. C. III, 1978, Relationship between eustasy and stratigraphic sequences of passive margins: Geological Society of America Bulletin, v.89, p.1389-1403.

Pitman, W. C., and Golovchenko, X., 1988, Sea-level changes and their effect on the stratigraphy of Atlantic-type margins,: *in* Sheridan, R. E., and Grow, J. A., (eds.), The Atlantic continental margin: U.S., The Geology of North America Volume 1-2, Geological Society of America, p. 429-436.

Purdy, E. G., Pusey, W. C., and Wantland, K. F., 1975, Continental shelf of Belize - regional shelf attributes: *in* Wantland, K. F., and Pusey, W. C., (eds.), Belize Shelf - Carbonate Sediments, Clastic Sediments and Ecology: AAPG Studies in Geology, No. 2, 1-52.

Purser, B.H., and Evans, G., 1973, Regional sedimentation along the Trucial Coast, SE Persian Gulf: *in* Purser, B.H., ed., The Persian Gulf, New York, Springer-Verlag, p. 211-232.

Purser, B.H., and Seibold, E., 1973, The principal environmental factors influencing Holocene sedimentation and diagenesis in the Persian Gulf: *in* Purser, B.H., ed., The Persian Gulf, New York, Springer-Verlag, p. 1-10.

Rassetti, F., 1965, Upper Cambrian trilobite faunas of northeastern Tennessee: Smithsonian Miscellaneous Collections, v.148, p.140.

Read, J.F., 1973, Carbonate cycles, Pillara Formation (Devonian), Canning Basin, Western Australia: Bulletin Canadian Petroleum Geology, v. 21, p. 38-51.

Read, J. F., 1985, Carbonate platform facies models: American Association of Petroleum Geologists Bulletin, v.69, p.1-21.

Read, J. F., 1989, Controls on evolution of Cambrian-Ordovician passive margin, U.S. Appalachians: *in* Crevello, P., Wilson, J. L., Sarg, J. F., and Read, J. F., (eds.), Controls on Carbonate Platform and Basin Development: Society Economic Paleontologists Mineralogists Special Publication. 44, p. 147-166.

Read, J. F., and Goldhammer, R. K., 1988, Use of Fischer plots to define 3rd order sea level curves in peritidal cyclic carbonates, Early Ordovician, Apalachians: Geology, v.16, p.895-899.

Read, J. F., Grotzinger, J. P., Bova, J. A., and Koerschner, W. F., 1986, Models for generation of carbonate cycles: Geology, v.14, p.107-110.

Read, J.F., Osleger, D.A., and Elrick, M., in review, Two-dimensional computer modelling of cyclic carbonate sequences: submitted to the Kansas Geological Survey Anniversary publication on computer modelling of cyclic sequences.

Rees, M. N., 1986, A fault-controlled trough through a carbonate platform: the Middle Cambrian House Range embayment: Geological Society of America Bulletin, v.97, p.1054-1069.

Rees, M. N., Brady, M. J., and Rowell, A. J., 1976, Depositional environments of the Upper Cambrian Johns Wash Limestone (House Range, Utah): Journal Sedimentary Petrology, v.46, No.1, p.38-47.

Reinhardt, J., 1977, Cambrian off-shelf sedimentation, central Appalachians: *in* Cook, H.E., and Enos, P. (eds.), Deep-Water Carbonate Environments, Society of Economic Paleontologists and Mineralogists Special Publication 25, p. 83-112.

Robison, R. A. 1964, Upper Middle Cambrian stratigraphy of western Utah: Geological Society of America Bulletin, v.75, p.995-1010.

Ross, C. A., and Ross, J. R. P., 1985, Late Paleozoic depositional sequences are synchronous and worldwide: Geology, v.13, p.27-30.

Ross, C. A., and Ross, J. R. P., 1988, Late Paleozoic Transgressive-Regressive Deposition: in Wilgus, C. et al., (eds.), Sea-Level Changes: An Integrated Approach: Society Economic Paleontologists Mineralogists Special Publication 42, p. 227-247.

Sadler, P. M., 1981, Sediment accumulation rates and the completeness of stratigraphic sections: Journal of Geology, v.89, p.569-584.

Sahagian, D.L., and Watts, A.B., (convenors), 1989, American Geophysical Union Chapman conference on causes and consequences of long term sea level changes, Snowbird, Utah, Abstract volume.

Sarg, J. F., 1988, Carbonate Sequence Stratigraphy: *in* Wilgus, C. et al., (eds.), Sea-Level Changes: An Integrated Approach: Society Economic Paleontologists Mineralogists Special Publication 42, p. 156-181.

Schlager, W., 1981, The paradox of drowned reefs and carbonate platforms: Geological Society of America Bulletin, v.92, p.197-211.

Schwarzacher, W., 1987, The analysis and interpretation of stratification cycles: Paleoceanography, v.2, p.79-95.

Schwarzacher, W., and Fischer, A.G., 1982, Limestone-shale bedding and perturbations of the Earth's orbit: *in* Einsele, G., and Seilacher, A. (eds.), Cyclic and Event Stratification, Berlin/Heidelberg/New York, Springer-Verlag, p. 72-95.

Scotese, C.R., and McKerrow, W.S., 1990, Revised world maps and introduction: *in* McKerrow, W.S. and Scotese, C.R. (eds.), Palaeozoic Palaeogeography and Biogeography, Geological Society of London Memoir no. 12, p. 1-24.

Seibold, E., Diester, L., Futterer, D., Lange, H., Muller, P., and Werner, F., 1973, Holocene sediments and sedimentary processes in the Iranian part of the Persian Gulf: *in* Purser, B.H., ed., The Persian Gulf, New York, Springer-Verlag, p. 57-80.

Sepkoski, J.J. Jr., 1977, Dresbachian (Upper Cambrian) stratigraphy in Montana, Wyoming and South Dakota: (unpublished Ph.D. diss.), Boston, Mass., Harvard Univ., 563 pp.

Sepkoski, J.J. Jr., 1982, Flat-pebble conglomerates, storm deposits and the Cambrian bottom fauna, *in* Einsele, G. and Seilacher, A., (eds.) Cyclic and Event Stratification, Berlin, Springer-Verlag, p. 371-385.

Shaw, A.B., 1964, Time in Stratigraphy, New York, McGraw-Hill, 365 pp,

Shinn, E. A., Hudson, J.H., Halley, R.B., Lidz, B., Robbin, D.M. and Macintyre, I.G., 1982, Geology and sediment accumulation rates: Carrie Bow Cay, Belize: Smithsonian Contributions to Marine Science, v.12, p.63-76.

Sloan, L.C., and Barron, E.J., 1990, "Equable" climates during Earth history?: Geology, v. 18, p. 489-492.

Sloss, L. L., 1963, Sequences in the cratonic interior of North America: Geological Society of America Bulletin, v.74, p.93-113.

Sloss, L.L., and Speed, R.C., 1974, Relationship of cratonic and continental-margin tectonic episodes, *in* Dickenson, W.R., (ed.), Tectonics and Sedimentation, Society of Economic Paleontologists and Mineralogists Special Publication 22, p. 38-55.

Spencer, R. J., and Demicco, R. V., 1989, Computer models of carbonate platform cycles driven by subsidence and eustacy: Geology, v.17, p.165-168.

Steckler, M.S., and Watts, A.B., 1978, Subsidence of the Atlantic-type continental margin off New York: Earth and Planetary Science Letters, v. 41, p. 1-13.

Stewart, J. H., and Poole, F. G., 1974, Lower Paleozoic and uppermost Precambrian Cordilleran miogeocline, Great Basin, western United States: *in* Dickenson, W. R., (ed.), Tectonics and sedimentation: Society of Economic Paleontologists and Mineralogists Special Publication 22, 28-58.

Stewart, J. H., and Suczek, C. A., 1977, Cambrian and latest Precambrian paleogeography and tectonics in the western United States: *in* Stewart, J. H., Stevens, C. H., and Fritsche, A. E., (eds.), Paleogeography of western United States: Society of Economic Paleontologists and Mineralogists, Pacific Section, Pacific Coast Paleogeography Symposium, 1st, 1-18.

Stitt, J. H., 1971, Late Cambrian and earliest Ordovician trilobites, Timbered Hills and Lower Arbuckle Groups, western Arbuckle Mountains, Murray County, Oklahoma: Oklahoma Geological Survey Bulletin 110, 83 pp.

Stitt, J. H., 1977, Late Cambrian and earliest Ordovician trilobites, Wichita Mountains area, Oklahoma: Okla. Geol. Survey Bull. 124, 79 pp.

Stitt, J. H., Barnes, V. E., Miller, J. F., and Taylor, J. F., 1982, Cambrian and lowest Ordovician stratigraphy and biostratigraphy of southern Oklahoma and central Texas: *in* Taylor, M.E., and Palmer, A.R., (eds.), Guidebook for Field Trip 3, 2nd International Symposium on the Cambrian System, p. 1-56.

Sundberg, F.A., 1990, Morphological Diversification of the Ptychopariid Trilobites in the Marjumiid Biomere (Middle to Upper Cambrian): (unpubl. Ph.D. diss.), Virginia Polytechnic Institute, Blacksburg, Virginia, 425 pp.

Taylor, J.F., 1984, Biostratigraphy and lithostratigraphy of the Cambrian-Ordovician boundary interval, Texas and Oklahoma, U.S.A.: (unpubl. Ph.D. diss.), University of Missouri, Columbia, Mo., 243 pp.

Taylor, M. E., and Miller, J. F., 1981, Upper Cambrian and lower Ordovician stratigraphy and biostratigraphy, southern House Range, Utah, *in* Taylor, M.E., and Palmer, A.R., (eds.), Cambrian stratigraphy and paleontology of the Great Basin and vicinity, western United States: Guidebook for Field Trip 1, 2nd International Symposium on the Cambrian System, p. 73-77.

Vail, P. R., 1987, Seismic stratigraphy interpretation procedure: *in* Bally, A. W., (ed.), Atlas of Seismic Stratigraphy (Vol. 1): American Association Petroleum Geologists Studies in Geology 27, p. 1-10.

Vail, P. R., Hardenbol, J., and Todd, R. G., 1984, Jurassic unconformities, chronostratigraphy, and sea level changes from seismic stratigraphy and biostratigraphy: *in* Schlee, J. S., (ed.), Interregional Unconformities and Hydrocarbon Accumulation; American Association Petroleum Geologists Memoir 36, p. 129-144.

Vail, P. R., Mitchum, R. M., and Thompson, S. III, 1977, Seismic stratigraphy and global changes of sea level, Part 4; Global cycles of relative changes of sea level: *in* Payton, C. E., (ed.), Seismic stratigraphy - applications to hydrocarbon exploration: Tulsa, Okla: American Association Petroleum Geologists Memoir 26, p. 83-97.

van der Voo, R., 1988, Paleozoic paleogeography of North America, Gondwana, and intervening displaced terranes: Comparisons of paleomagnetism with paleoclimatology and biogeographical patterns: Geological Society of America Bulletin, v. 100, p. 311-324.

Van Hinte, J. E., 1978, Geohistory analysis - application of micropaleontology in exploration geology: American Association of Petroleum Geologists Bulletin, v.62, p.201-222.

Van Wagoner, J. C., Mitchum, R. M., Posamentier, H. W. and Vail, P.R., 1987, The key definitions of sequence stratigraphy,*in* Bally, A. W., (ed.), Atlas of Seismic Stratigraphy (Vol. 1): American Association Petroleum Geologists Studies in Geology 27, p. 11-14.

Walker, J.C.G., and Zahnle, K.J., 1986, Lunar nodal tide and distance to the Moon during the Precambrian: Nature, v. 320, p. 600-602.

Walker, K.R., ed., 1985, The geological history of the Thorn Hill Paleozoic section (Cambrian-Mississippian), eastern Tennessee: University of Tennessee Department of Geological Sciences Studies in Geology 10, 128 pp.

Wanless, H.R., and Shepard, F.P., 1936, Sea level and climatic changes related to late Paleozoic cycles: Geological Society of America Bulletin, v.47, p. 1177-1206.

Watso, D. C., and Klein, G. deV, 1989, Origin of the Cambrian-Ordovician sedimentary cycles of Wisconsin using tectonic subsidence analysis: Geology, v.17, p. 879-881.

Wilkinson, B. R., 1982, Cyclic cratonic carbonates and Phanerozoic calcite seas: Journal Geological Education, v.30, p.180-203.

Wilson, J.L., 1952, Upper Cambrian stratigraphy in the central Appalachians: Geological Society of America Bulletin, v. 63, p. 275-322.

Wilson, J.L., 1975, Carbonate Facies in Geologic History, New York, Springer-Verlag, 471 pp.

Wilson, J. E., and Jordan, C., 1983, Middle shelf: *in* Scholle, P. A., Bebout, D. G., and Moore, C., (eds.), Carbonate Depositional Environments: American Association Petroleum Geologists Memoir 33, p. 297-344.

Winland, H.D., and Matthews, R.K., 1974, Origin and significance of grapestone, Bahama Islands: Journal of Sedimentary Petrology, v. 44, p. 921-927.

Yeats, R.S., 1978, Neogene acceleration of subsidence rates in southern California: Geology, v. 6, p. 456-460.

Yose, L., and Heller, P., 1989, Sea-level control of mixed-carbonate-siliciclastic, gravity-flow deposition: Lower part of the Keeler Canyon Formation (Pennsylvanian), southeastern California: Geological Society of America Bulletin, v.101, p.427-439.

Zadnik, V.E., 1960, Petrography of the Upper Cambrian dolomites of Warren County, New Jersey: (unpubl. Ph.D. diss.), University of Illinois, Champaign, Il., 155 pp.

Zeigler, A.M., Parrish, J.T., and Scotese, C.R., 1981, Cambrian world paleogeography, biogeography and climatology: *in* Taylor, M. E., (ed.), Short papers for the Second International Symposium on the Cambrian System: United States Geological Survey Open-File Report 81-743, p. 252.

APPENDIX I:
GRAPHIC CORRELATION PLOTS

GRAPHIC CORRELATION DATA

•

TOP OF TRILOBITE/CONODONT ZONE	STEAMBOAT PASS	ORR RIDGE	THREADGILL-LANGE	KINDBLADE RANCH	CONASAUGA BASIN
Saukia (Corbinia apopsis)	845		284	385	
Saukia serotina	841		280	381	
(Eoconodontus notchpeakensis)	798		267	347	
Saukia junia	795		266	342	
(Proconodontus muelleri)	785		252	321	
Saukia pyrene (Rasettia magna)	772		246	306	
Ellipsocephaloides (Dartonaspis)			209	217	
Idahoia			164	135	
Taenicephalus			152	119	
Elvinia (Biomere Boundary)	441		138	103	
Dunderbergia		360			
Prehousia		285			
Dicanthopyge		262			
Aphelaspis		303	114		137
Crepicephalus (Biomere Boundary)		223	88		50
Cedaria		72	40		

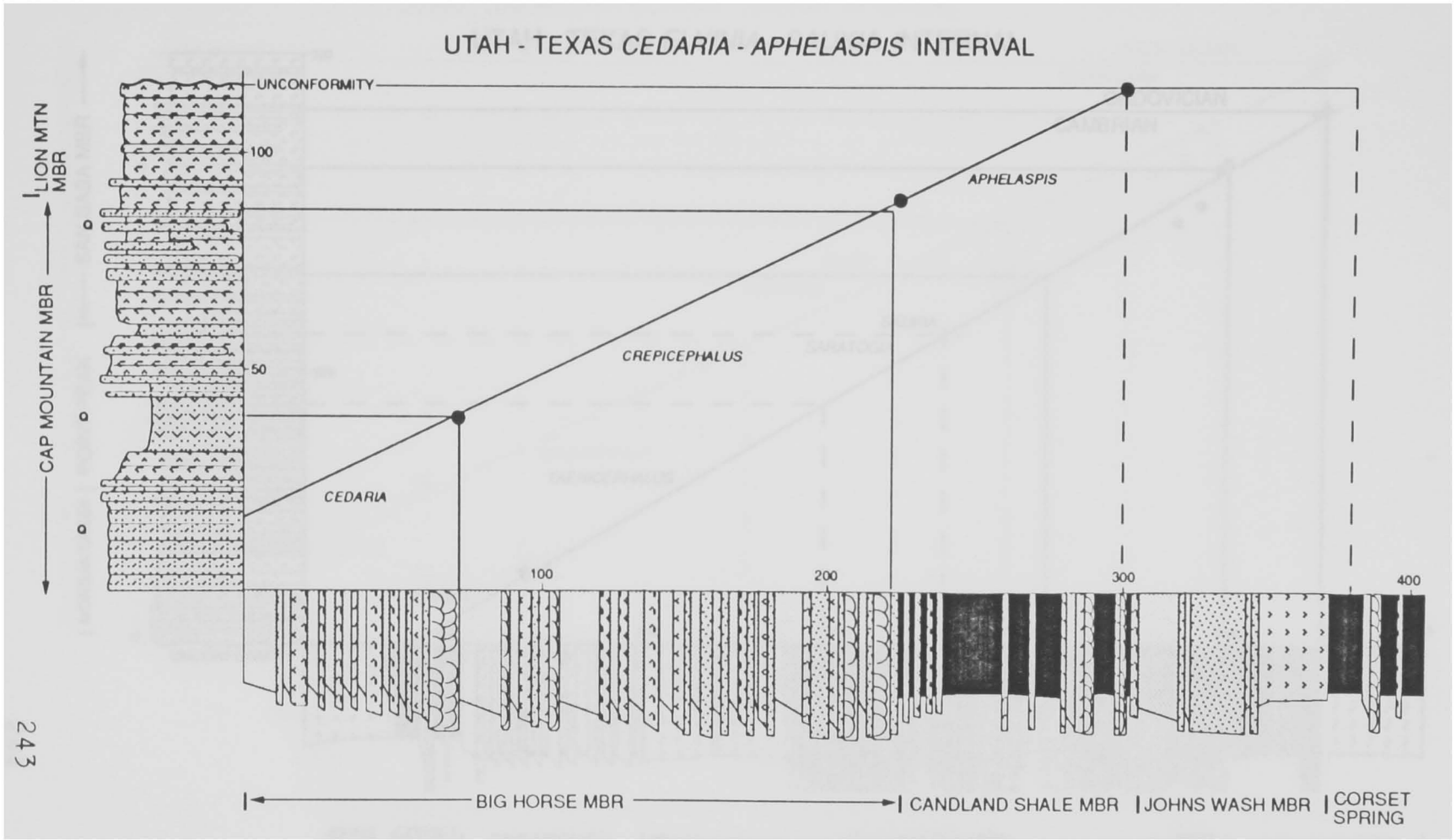
UTAH - TEXAS *CEDARIA* - *APHELASPIS* INTERVAL
UNCONFORMITY
100
50
0
0
0
LION MTN MBR
CAP MOUNTAIN MBR
APHELASPIS
CREPICEPHALUS
CEDARIA
100
200
300
400
BIG HORSE MBR
CANDLAND SHALE MBR
JOHNS WASH MBR
CORSET SPRING

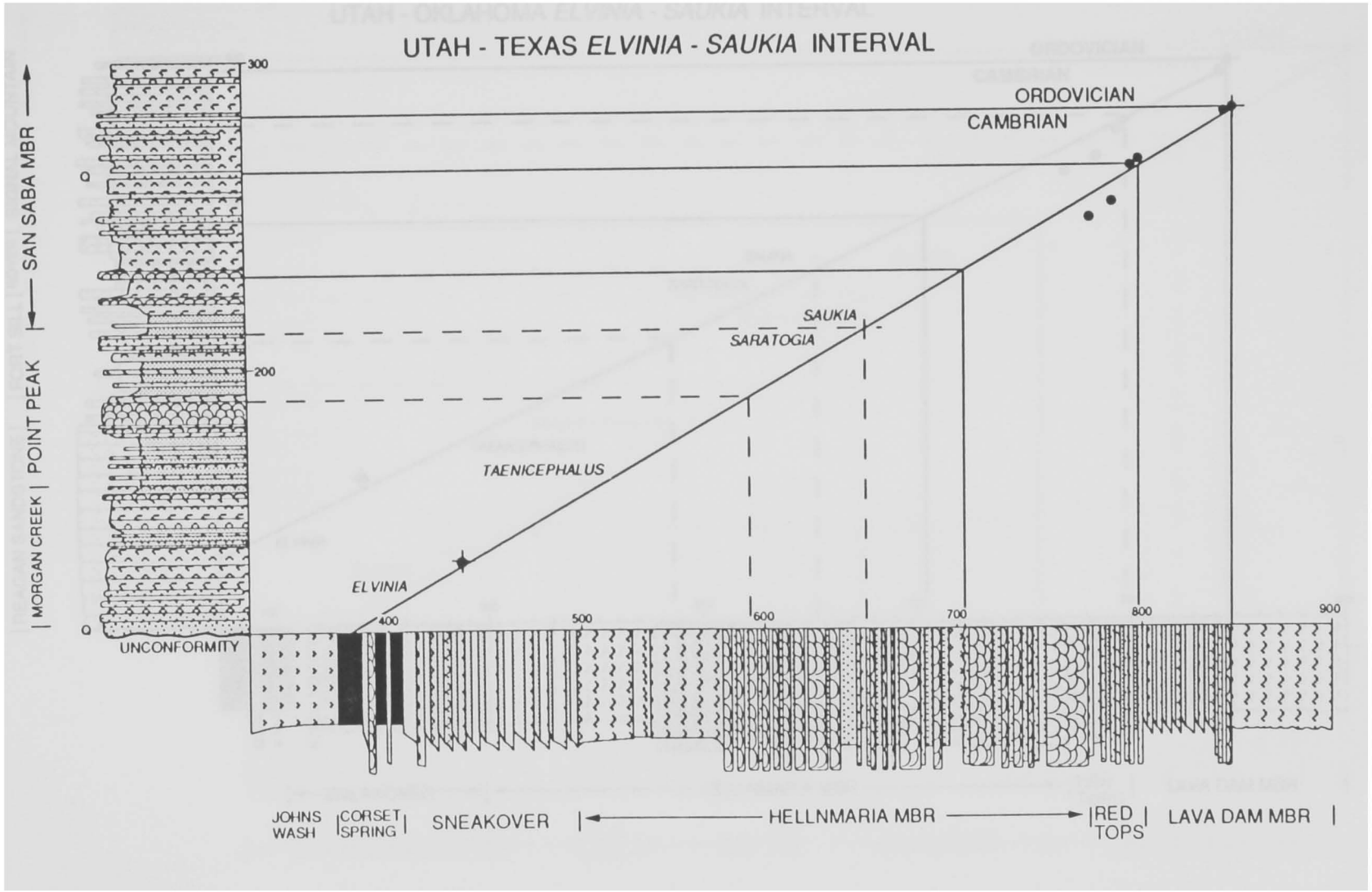
UTAH - TEXAS *ELVINIA - SAUKIA* INTERVAL
ORDOVICIAN
CAMBRIAN
SAUKIA
SARATOGIA
TAENICEPHALUS
ELVINIA
UNCONFORMITY
300
200
0
400
500
600
700
800
900
MORGAN CREEK | POINT PEAK — SAN SABA MBR
JOHNS WASH
CORSET SPRING
SNEAKOVER
HELLNMARIA MBR
RED TOPS
LAVA DAM MBR

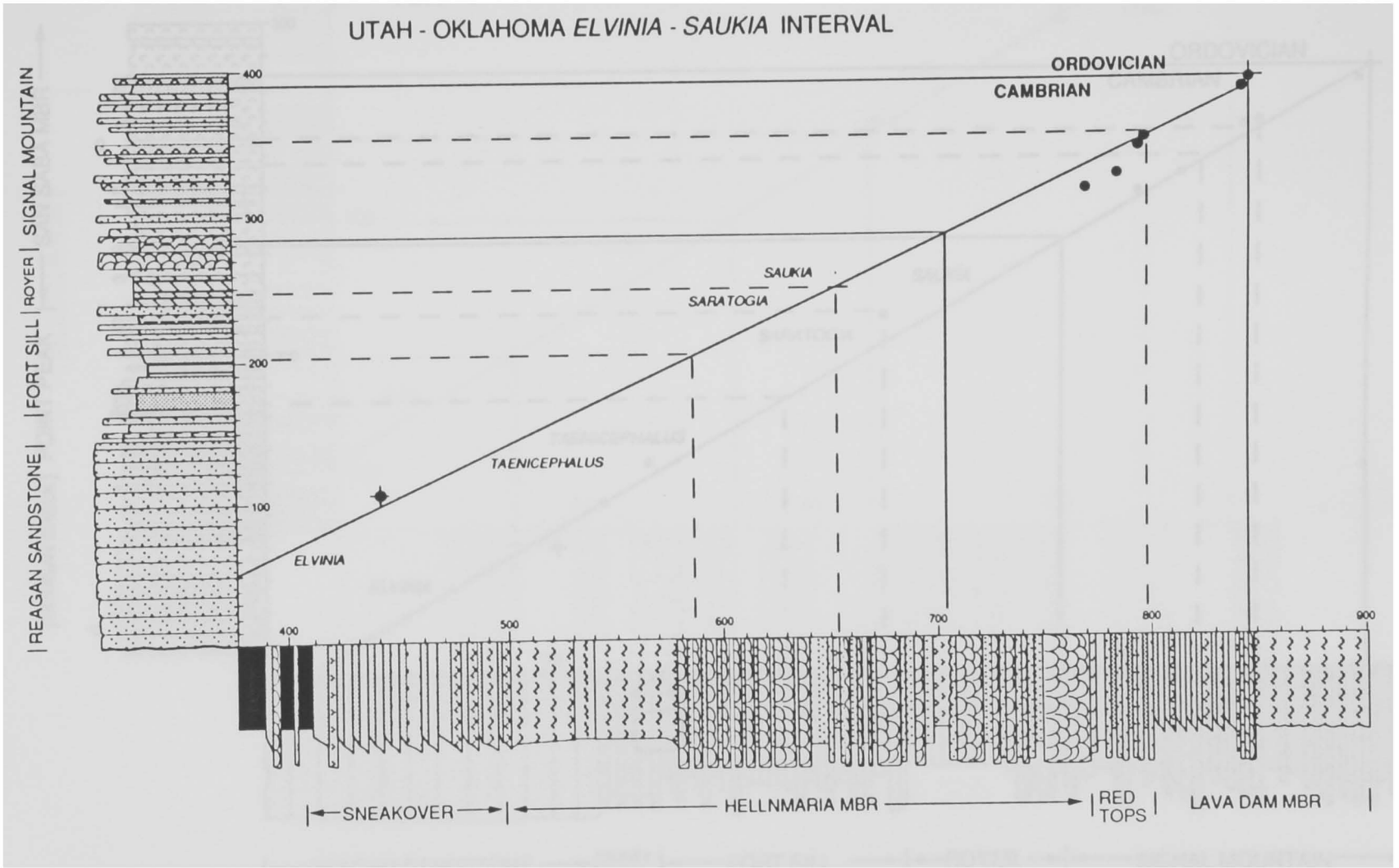
UTAH - OKLAHOMA ELVINIA - SAUKIA INTERVAL
REAGAN SANDSTONE
FORT SILL
ROYER
SIGNAL MOUNTAIN
ORDOVICIAN
CAMBRIAN
400
300
200
100
SAUKIA
SARATOGIA
TAENICEPHALUS
ELVINIA
400
500
600
700
800
900
SNEAKOVER
HELLNMARIA MBR
RED TOPS
LAVA DAM MBR

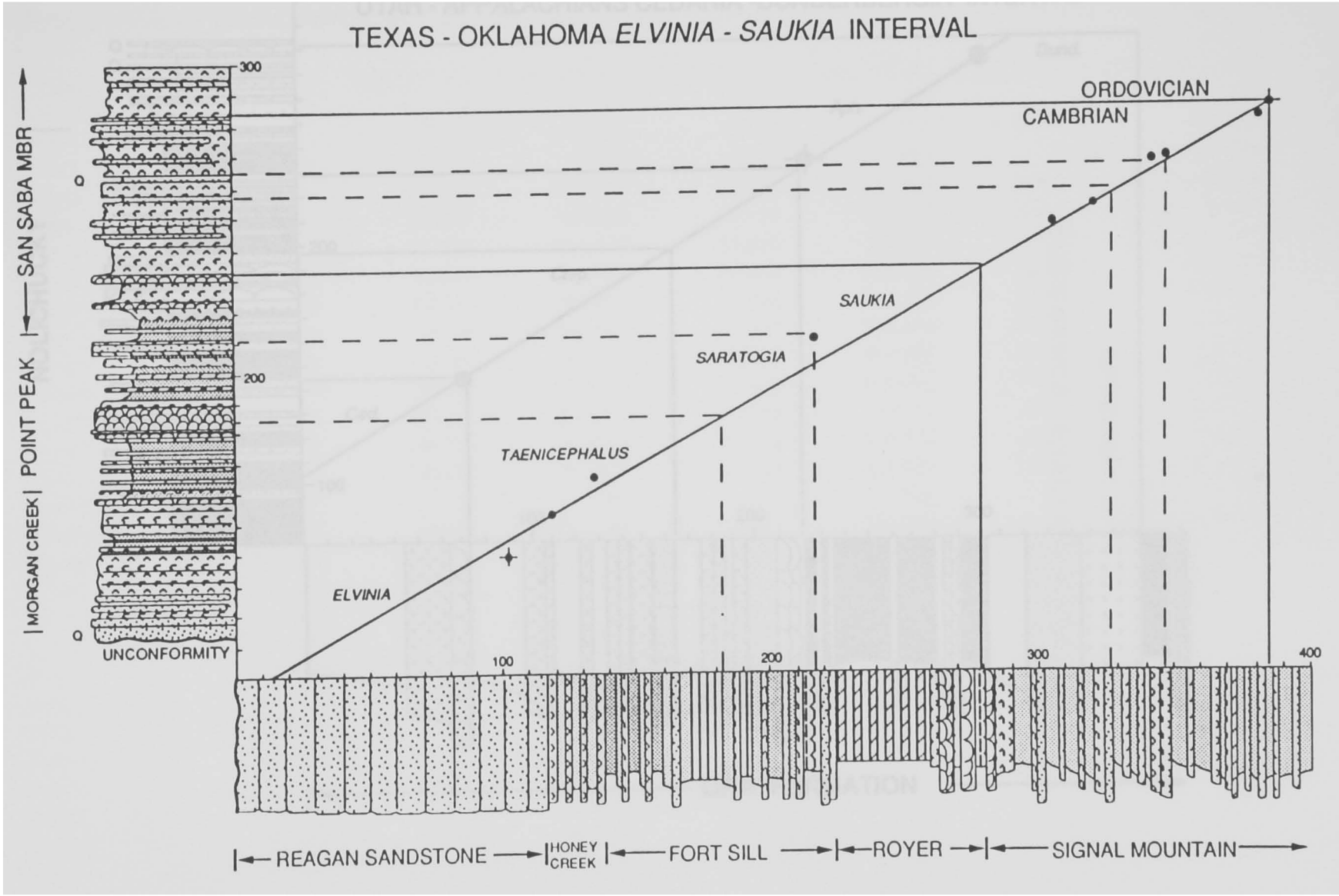
TEXAS - OKLAHOMA *ELVINIA - SAUKIA* INTERVAL
MORGAN CREEK
POINT PEAK
SAN SABA MBR
300
200
0
0
UNCONFORMITY
ORDOVICIAN
CAMBRIAN
SAUKIA
SARATOGIA
TAENICEPHALUS
ELVINIA
100
200
300
400
REAGAN SANDSTONE
HONEY CREEK
FORT SILL
ROYER
SIGNAL MOUNTAIN

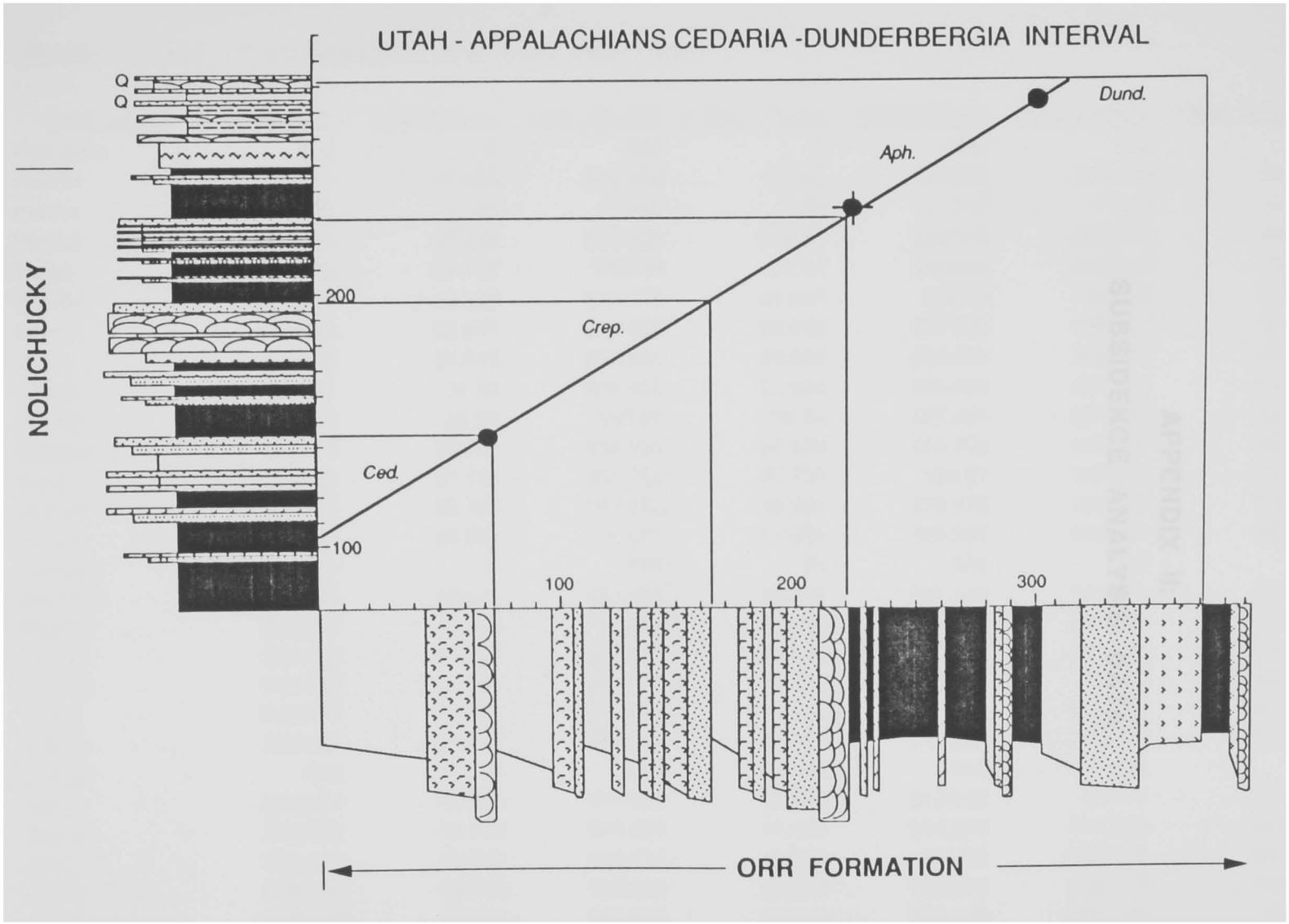
UTAH - APPALACHIANS CEDARIA -DUNDERBERGIA INTERVAL
NOLICHUCKY
Q
Q
200
100
Ced.
Crep.
Aph.
Dund.
100
200
300
ORR FORMATION

APPENDIX II:
SUBSIDENCE ANALYSIS DATA

HOUSE RANGE, UTAH, SUBSIDENCE ANALYSIS DATA

UNIT NAME	TIME OBS.	P-RIFT Tobs	TIME DELITH	P-RIFT Tdelith	TIME WDmin	TIME WDmax	TIME TECTSUB
PreCamb	560	0	560	0	560	560	560
ProMtn	542.301	17.699	544.292	15.708	544.376	544.844	545.293
Pioch1	540	20	540	20	540	540	540
Pioch2	539.551	20.449	539.332	20.668	539.343	539.216	538.986
Tatow	538.883	21.117	538.89	21.11	538.926	538.769	538.71
HowlM	537.731	22.269	538.149	21.851	538.23	538.05	538.266
HowlU	536.323	23.677	537.135	22.865	537.253	537.083	537.518
Chis1	535.655	24.345	536.404	23.596	536.567	536.311	536.538
Chis2	535.51	24.49	536.102	23.898	536.069	535.694	536.031
Dome	534.32	25.68	535.26	24.74	535.251	534.833	535.514
Whwind	533.799	26.201	534.531	25.469	534.429	533.937	534.467
Swas	532.876	27.124	533.762	26.238	533.57	533.072	533.913
Wheel	531.214	28.786	531.093	28.907	530.875	530.562	529.844
Marj	526.068	33.932	525.961	34.039	526.037	526.081	525.315
Weeks1	525	35	525	35	525	525	525
Weeks2	521.086	38.914	521.415	38.585	521.414	521.653	522.151
BigHo1	519.391	40.609	519.864	40.136	519.851	520.139	520.856
BigHot	519.108	40.892	519.674	40.326	519.653	519.905	520.76
BigHo2	518.049	41.951	518.852	41.148	518.862	519.07	520.172
Candl	516.777	43.223	516.615	43.385	516.603	516.757	516.092
JoWa1	516.353	43.647	516.318	43.682	516.302	516.278	516.095
JoWa2	516	44	516	44	516	516	516
CoSpr	515.064	44.936	514.021	45.979	514.042	513.77	511.153
Sneako	513.894	46.106	512.562	47.438	512.398	511.923	509.761
Helln1	511.202	48.798	510.075	49.925	509.82	509.575	508.817
Helln2	506.755	53.245	506.622	53.378	506.665	506.775	506.922
RedTop	505.936	54.064	506.011	53.989	506.078	506.131	506.49
Lava1	505	55	505	55	505	505	505

Lava2	503.623	56.377	503.717	56.283	503.308	503.052	504.151
House	497.641	62.359	497.694	62.306	497.45	497.334	498.574
Film1	491.856	68.144	493.156	66.844	493.204	493.26	495.837
Film2	488	72	488	72	488	488	488
Film3	486.451	73.549	486.2	73.8	486.097	485.947	486.043
Film4	483.853	76.147	483.82	76.18	483.762	483.59	484.074
Film5	481.36	78.64	481.649	78.351	481.77	481.665	482.306
Film6	479.995	80.005	480.362	79.638	480.319	480.207	481.193
WahWah	478	82	478	82	478	478	478
Juab	476.275	83.725	476.65	83.35	476.452	476.378	477.126
Kanosh	470.254	89.746	469.351	90.649	469.308	469.458	468.023
Lehman	468	92	468	92	468	468	468
WaRnch	463.827	96.173	463.761	96.239	463.756	463.789	464.874
CrysPk	462.345	97.655	462.325	97.675	462.284	462.052	464.231
Eureka	454	106	454	106	454	454	454
unconf	448	112	448	112	448	448	448
ElySp	438	122	438	122	438	438	438

P-RIFT Ttectsub	R1(ts+sl)slpor	DELITH at end	OBS.SUM.THK	DELITH at depo	WDmin	WDmax	Y Tobs
0							
14.707	-352.408	-724.739	-700	-724.739	0	20	-532.54012
20	-479.25	-919.728	-791	-922.748	5	40	-602.59669
21.014	-522.753	-991.419	-828	-1008.323	5	40	-615.97023
21.29	-534.604	-1036.073	-883	-1064.861	1	15	-635.69061
21.734	-553.642	-1113.751	-978	-1159.861	1	20	-669.21048
22.482	-585.702	-1224.974	-1094	-1289.622	5	25	-709.3529
23.462	-627.766	-1306.073	-1149	-1383.325	1	30	-728.08524
23.969	-649.51	-1338.208	-1161	-1421.991	30	60	-732.12514
24.486	-671.684	-1427.672	-1259	-1529.776	5	30	-764.93011
25.533	-716.622	-1505.958	-1302	-1623.223	20	50	-779.09813
26.087	-740.382	-1583.762	-1378	-1721.689	20	40	-803.91132
30.156	-914.945	-1859.754	-1515	-2063.499	30	60	-847.68191
34.685	-1109.216	-2355.105	-1939	-2720.759	10	60	-976.08918
35	-1122.722	-2435.388	-2027	-2843.817	20	50	-1001.4456
37.849	-1198.983	-2714.712	-2304	-3222.512	20	50	-1090.7713
39.144	-1233.628	-2841.432	-2424	-3386.36	10	30	-1127.7604
39.24	-1236.204	-2855.615	-2444	-3406.36	2	10	-1133.8395
39.828	-1251.948	-2918.881	-2519	-3493.272	1	20	-1156.3462
43.908	-1361.153	-3098.153	-2609	-3729.479	15	60	-1182.8828
43.905	-1361.072	-3116.457	-2639	-3760.884	2	30	-1191.6096
44	-1363.616	-3136.602	-2664	-3794.484	0	2	-1198.8302
48.847	-1405.863	-3208.186	-2704	-3907.693	10	60	-1217.7808
50.239	-1417.991	-3257.893	-2754	-3991.142	20	60	-1241.0752
51.183	-1426.221	-3345.942	-2869	-4133.429	20	40	-1293.0527
53.078	-1442.742	-3481.808	-3059	-4330.948	1	20	-1374.1824
53.51	-1446.505	-3506.975	-3094	-4365.948	2	15	-1388.5076
55	-1459.492	-3550.311	-3134	-4423.765	10	30	-1404.6521

55.849	-1466.765	-3582.573	-3169	-4467.801	20	40	-1427.97
61.426	-1514.53	-3740.913	-3321	-4674.551	15	40	-1523.538
64.163	-1537.965	-3859.099	-3468	-4830.308	5	20	-1607.6912
72	-1605.091	-3998.251	-3566	-5007.283	20	50	-1659.629
73.957	-1631.231	-4069.676	-3625	-5107.478	20	50	-1679.6116
75.926	-1657.537	-4165.066	-3724	-5239.928	15	40	-1712.0395
77.694	-1681.149	-4254.818	-3819	-5360.78	5	20	-1741.9206
78.807	-1696.018	-4307.165	-3871	-5432.422	20	35	-1757.7859
82	-1738.675	-4405.418	-3947	-5563.884	15	30	-1780.362
82.874	-1752.691	-4454.715	-3996	-5632.383	15	30	-1799.3128
91.977	-1898.722	-4736.856	-4167	-6002.765	15	50	-1861.5251
92	-1899.088	-4776.132	-4231	-6071.318	2	20	-1883.3225
95.126	-1903.358	-4823.604	-4307	-6151.048	1	10	-1921.6697
95.769	-1904.236	-4840.57	-4334	-6178.048	1	10	-1934.6867
106	-1918.208	-4943.606	-4486	-6334.628	1	15	-2002.5161
112	-1918.517	-4944.338	-4487	-6335.907	0	0	-2046.0058
122	-1938.629	-5086.959	-4679	-6527.907	2	15	-2109.8623

Y Tdelith	Y Ttectsub	R2 Tobs	R2 Tdelith	R2 Ttectsub	P-RIFT Tobs(lopor)	P-RIFT Tdel(lopor)
					0	0
-481.905153	-448.841615	-180.13212	-129.49715	-96.433615	17.699	16.283
-613.40546	-612.760092	-123.34669	-134.15546	-133.51009	20	20
-633.07574	-642.616123	-93.217228	-110.32274	-119.86312	20.449	20.632
-645.976554	-650.659498	-101.08661	-111.37255	-116.0555	21.117	21.137
-667.401717	-663.524894	-115.56848	-113.75972	-109.88289	22.269	21.986
-696.313689	-684.994389	-123.6509	-110.61169	-99.292389	23.677	23.146
-716.86886	-712.738648	-100.31924	-89.10286	-84.972648	24.345	23.845
-725.291277	-726.923019	-82.615138	-75.781277	-77.413019	24.49	24.079
-748.560884	-741.269718	-93.246114	-76.876884	-69.585718	25.68	25.042
-768.457149	-769.96457	-62.476129	-51.835149	-53.34257	26.201	25.692
-789.196296	-784.955466	-63.529321	-48.814296	-44.573466	27.124	26.57
-859.23778	-891.099318	67.2630866	55.7072203	23.8456825	28.786	28.809
-985.830166	-1001.43038	133.126824	123.385834	107.785617	33.932	33.906
-1008.40682	-1008.8122	121.276384	114.315178	113.909805	35	35
-1089.64518	-1073.92124	108.2117	109.33782	125.061757	38.914	38.828
-1123.37988	-1102.5538	105.867617	110.248124	131.074198	40.609	40.496
-1127.45544	-1104.65296	102.364535	108.74856	131.551045	40.892	40.701
-1144.94624	-1117.44049	95.6018242	107.00176	134.507512	41.951	41.589
-1191.40273	-1202.94786	178.270216	169.750268	158.205138	43.223	43.333
-1197.44712	-1202.88701	169.462452	163.62488	158.184992	43.647	43.655
-1203.88728	-1204.81265	164.785822	159.728721	158.803351	44	44
-1243.24141	-1299.29359	188.082235	162.621595	106.569412	44.936	45.513
-1271.47095	-1325.10659	176.915762	146.520055	92.8844068	46.106	46.893
-1318.10451	-1342.28921	133.168285	108.116493	83.9317944	48.798	49.586
-1379.86441	-1376.0119	68.5595953	62.8775873	66.7301031	53.245	53.324
-1390.44344	-1383.55821	57.9974059	56.0615553	62.946788	54.064	53.986
-1407.72371	-1409.1913	54.8398949	51.7682915	50.3006972	55	55

-1429.25632	-1423.5273	38.7949714	37.5086835	43.2377029	56.377	56.349
-1524.66312	-1513.03092	-9.007957	-10.133118	1.49908089	62.359	62.625
-1590.7388	-1554.13251	-69.726237	-52.773796	-16.16751	68.144	67.397
-1660.24091	-1662.38023	-54.537987	-55.149911	-57.289225	72	72
-1683.19174	-1687.36815	-48.380547	-51.960738	-56.137152	73.549	73.802
-1712.54528	-1711.73561	-54.502497	-55.008278	-54.198607	76.147	76.222
-1738.36804	-1732.974	-60.771607	-57.219043	-51.824999	78.64	78.429
-1753.25996	-1746.04064	-61.767864	-57.241956	-50.022644	80.005	79.742
-1779.80922	-1782.2666	-41.686967	-41.13422	-43.591596	82	82
-1794.54096	-1791.8656	-46.621775	-41.849955	-39.174604	83.725	83.59
-1868.93076	-1884.28817	37.1969448	29.7912405	14.4338256	89.746	90.403
-1881.77652	-1884.50514	15.7655074	17.3114822	14.5828625	92	92
-1920.33439	-1913.26608	-18.311677	-16.976386	-9.9080842	96.173	96.239
-1932.81708	-1919.00659	-30.450646	-28.581079	-14.770587	97.655	97.675
-1999.82025	-2002.86288	-84.30805	-81.612254	-84.654881	106	106
-2042.89049	-2046.04768	-127.48881	-124.37349	-127.53068	112	112
-2106.131	-2109.45642	-171.23333	-167.502	-170.82742	122	122

P-RIFT Ttec(lopor)	R1(ts+sl)(lopor)	DELITH at end(lopor)	Y Tobs(lopor)	Y Tdel(lopor)	Y Ttec(lopor)	R2 Tobs(lopor)
0						
15.735	-352.41	-724.74	-470.5756	-434.6998	-431.9194	-118.17
20	-447.94	-887.58	-539.9509	-547.2325	-547.2234	-92.01
20.893	-481.09	-948.22	-553.1944	-565.7126	-565.4018	-72.11
21.257	-494.59	-994.53	-572.723	-580.346	-579.0766	-78.13
21.836	-516.07	-1075.36	-605.9169	-604.6839	-601.7074	-89.84
22.789	-551.42	-1190.64	-645.669	-637.4096	-632.9838	-94.25
23.593	-581.24	-1259.21	-664.2192	-656.8398	-651.0932	-82.98
23.943	-594.25	-1281.69	-668.2198	-663.2961	-663.8513	-73.97
24.732	-623.53	-1375.71	-700.7058	-689.6147	-689.1419	-77.18
25.611	-656.13	-1441.36	-714.736	-707.1523	-709.6487	-58.61
26.441	-686.92	-1527.32	-739.3079	-730.5552	-735.4562	-52.39
29.568	-802.94	-1736.28	-782.6529	-788.775	-795.1192	20.29
34.212	-975.29	-2219.14	-909.8115	-913.8185	-911.8264	65.48
35	-1004.51	-2313.19	-934.9214	-939.3598	-939.1189	69.59
38.751	-1112.19	-2627.27	-1023.3784	-1025.3087	-1024.7558	88.81
40.388	-1159.19	-2757.76	-1060.0078	-1061.1518	-1060.733	99.18
40.518	-1162.89	-2773.29	-1066.0278	-1065.4917	-1065.2396	96.87
41.237	-1183.54	-2842.27	-1088.3157	-1084.1279	-1083.0723	95.22
43.683	-1253.76	-2981.18	-1114.5942	-1119.9707	-1119.9673	139.16
43.792	-1256.89	-3003.29	-1123.2361	-1126.4803	-1126.5116	133.66
44	-1262.85	-3027.34	-1130.3865	-1133.4179	-1133.0623	132.46
46.512	-1290.8	-3086.57	-1149.1528	-1163.3968	-1163.4734	141.64
47.818	-1305.33	-3137.99	-1172.2208	-1190.1177	-1194.1226	133.11
49.856	-1328	-3243.81	-1223.6928	-1240.6011	-1245.8159	104.31
53.012	-1363.12	-3398.17	-1304.0336	-1307.1815	-1306.0146	59.09
53.648	-1370.19	-3426.82	-1318.2195	-1318.5653	-1316.8858	51.97
55	-1385.23	-3471.43	-1334.207	-1335.7712	-1335.296	51.02

56.217	-1396.68	-3508.18	-1357.2982	-1358.235	-1364.6547	39.38
62.899	-1459.53	-3682.18	-1451.9368	-1456.6272	-1459.4119	7.59
66.256	-1491.11	-3809.09	-1535.2718	-1525.1288	-1523.1045	-44.16
72	-1545.13	-3934.64	-1586.7045	-1586.451	-1585.8276	-41.58
74.14	-1576.15	-4012.16	-1606.4927	-1609.2598	-1609.9311	-30.34
76.258	-1606.87	-4112.84	-1638.6053	-1638.8792	-1638.8724	-31.74
78.141	-1634.17	-4204.35	-1668.1959	-1664.9143	-1662.7023	-34.03
79.292	-1650.87	-4258.35	-1683.9068	-1679.9747	-1679.6476	-33.04
82	-1690.12	-4353.37	-1706.2634	-1705.1493	-1704.4558	-16.14
83.282	-1705.57	-4404.39	-1725.0299	-1722.341	-1723.9274	-19.46
91.634	-1806.25	-4634.76	-1786.6373	-1791.2707	-1791.1769	19.61
92	-1810.66	-4680.28	-1808.2227	-1806.3747	-1805.6213	2.44
95.435	-1819.67	-4735.71	-1846.197	-1844.652	-1843.9196	-26.53
96.485	-1822.42	-4755.03	-1859.0874	-1857.0439	-1856.61	-36.67
106	-1847.36	-4872.51	-1926.2572	-1923.5595	-1922.7369	-78.9
112	-1847.73	-4873.32	-1969.3241	-1966.3164	-1965.4685	-121.59
122	-1882.88	-5029.54	-2032.5597	-2029.0968	-2028.2117	-149.68

R2 Tdel(lopor)	R2 Ttec(lopor)	P-RIFT Tobs(hipor)	P-RIFT Tdel(hipor)	P-RIFT Ttec(hipor)	R1(ts+sl)(hipor)
		0	0	0	
-82.29	-79.51	17.7	15.88	15.49	-407.29
-99.29	-99.28	20	20	20	-525.86
-84.62	-84.31	20.45	20.5	20.76	-564.74
-85.75	-84.48	21.12	21.04	21.26	-590.46
-88.61	-85.63	22.27	21.96	22.21	-638.84
-85.99	-81.56	23.68	23.36	24.24	-742.82
-75.6	-69.85	24.35	24.12	25.22	-793.07
-69.05	-69.6	24.49	24.35	25.5	-807.28
-66.09	-65.61	25.68	25.5	26.68	-868.02
-51.02	-53.52	26.2	26.29	27.48	-908.98
-43.63	-48.53	27.12	27.36	28.31	-951.32
14.17	7.82	28.79	29.33	30.35	-1055.95
61.47	63.46	33.93	33.75	34.31	-1258.48
65.15	65.39	35	35	35	-1293.99
86.88	87.44	38.91	38.54	39.42	-1434.58
98.03	98.45	40.61	40.26	40.43	-1466.65
97.4	97.65	40.89	40.49	40.39	-1465.24
99.41	100.46	41.95	41.41	40.85	-1480.02
133.78	133.79	43.22	42.96	42.87	-1544.2
130.41	130.38	43.65	43.34	42.95	-1546.83
129.43	129.79	44	44	44	-1580.15
127.4	127.32	44.94	45.19	45.36	-1599.6
115.21	111.21	46.11	46.81	47.6	-1631.72
87.4	82.19	48.8	49.76	51.09	-1681.71
55.94	57.1	53.25	53.14	52.87	-1707.21
51.63	53.31	54.06	53.75	52.85	-1706.96
49.46	49.94	55	55	55	-1737.79

38.45	32.03	56.38	57.08	57.82	-1766.07
2.9	0.12	62.36	63.09	63.03	-1818.24
-34.02	-32	68.14	68.12	66.81	-1856.15
-41.32	-40.7	72	72	72	-1908.16
-33.11	-33.78	73.55	73.74	73.67	-1928.65
-32.01	-32	76.15	76.35	75.33	-1948.98
-30.75	-28.54	78.64	78.49	77.14	-1971.18
-29.11	-28.78	80.01	79.96	79.26	-1997.11
-15.03	-14.33	82	82	82	-2030.76
-16.77	-18.36	83.73	83.97	85.3	-2064.29
14.98	15.07	89.75	90.1	90.9	-2121.29
4.29	5.04	92	92	92	-2132.47
-24.99	-24.25	96.17	96.36	96.03	-2145.12
-34.62	-34.19	97.66	97.85	95.77	-2144.29
-76.2	-75.37	106	106	106	-2176.4
-118.58	-117.74	112	112	112	-2176.75
-146.21	-145.33	122	122	122	-2239.76

DELITH at end(hipor)	Y Tobs(hipor)	Y Tdel(hipor)	Y Ttec(hipor)	R2 Tobs(hipor)	R2 Tdel(hipor)	R2 Ttec(hipor)
-739.13	-649.9192	-592.3646	-589.733	-242.63	-185.08	-182.45
-926.43	-729.201	-735.419	-735.7553	-203.34	-209.56	-209.9
-991.35	-744.3356	-752.0625	-752.4225	-179.59	-187.32	-187.68
-1059.56	-766.6529	-769.9974	-769.5201	-176.19	-179.54	-179.06
-1183.57	-804.5867	-800.3956	-798.4456	-165.74	-161.55	-159.6
-1380.39	-850.0152	-845.3202	-841.7982	-107.2	-102.5	-98.98
-1471.37	-871.2143	-869.4904	-864.8647	-78.15	-76.42	-71.8
-1495.6	-875.7862	-876.5934	-876.8784	-68.51	-69.32	-69.6
-1623.47	-912.911	-912.4053	-911.5602	-44.9	-44.39	-43.55
-1701.1	-928.9447	-936.5868	-937.8387	-19.96	-27.6	-28.86
-1799.37	-957.0254	-968.768	-971.5661	-5.71	-17.45	-20.25
-1978.01	-1006.5598	-1027.0272	-1031.3872	49.39	28.92	24.56
-2457.4	-1151.8761	-1150.5413	-1149.4734	106.6	107.94	109.01
-2563.32	-1180.5716	-1184.0236	-1184.0973	113.42	109.97	109.89
-2885.99	-1281.6599	-1275.1105	-1275.2059	152.92	159.46	159.37
-2998.14	-1323.5198	-1317.67	-1317.7871	143.13	148.98	148.87
-3020.64	-1330.3994	-1323.0903	-1323.325	134.84	142.15	141.91
-3089.14	-1355.8699	-1345.4646	-1345.0375	124.15	134.56	134.99
-3220.91	-1385.9009	-1381.9963	-1382.5367	158.3	162.2	161.66
-3245.12	-1395.7768	-1390.7171	-1391.2258	151.05	156.11	155.6
-3294.06	-1403.9483	-1406.0315	-1405.9752	176.2	174.12	174.17
-3343.25	-1425.3944	-1433.1657	-1433.7907	174.2	166.43	165.81
-3414.62	-1451.7563	-1469.1219	-1472.0509	179.96	162.6	159.67
-3552.11	-1510.5783	-1532.1946	-1535.5953	171.13	149.51	146.11
-3705.58	-1602.3914	-1601.2571	-1600.8287	104.82	105.96	106.38
-3725.95	-1618.603	-1613.2969	-1612.5694	88.35	93.66	94.39
-3780.53	-1636.8735	-1637.5294	-1637.3375	100.92	100.26	100.45

-3833.11	-1663.262	-1676.8325	-1680.8365	102.81	89.24	85.23
-4001.99	-1771.4146	-1783.7099	-1785.3932	46.82	34.53	32.84
-4134.56	-1866.6494	-1865.5223	-1863.4307	-10.5	-9.37	-7.28
-4233.44	-1925.4265	-1924.3141	-1923.9543	-17.27	-16.15	-15.79
-4292.56	-1948.0404	-1949.4941	-1950.2326	-19.39	-20.85	-21.58
-4389.11	-1984.7385	-1985.9948	-1985.9687	-35.76	-37.02	-36.99
-4481.57	-2018.5545	-2014.8736	-2013.1887	-47.37	-43.69	-42.01
-4547.04	-2036.5089	-2034.1726	-2033.7873	-39.4	-37.06	-36.67
-4634.84	-2062.0579	-2060.1083	-2059.669	-31.3	-29.35	-28.91
-4686	-2083.5042	-2084.3669	-2085.5739	-19.21	-20.07	-21.28
-4871.01	-2153.9088	-2155.3163	-2155.5251	-32.62	-34.02	-34.23
-4918.81	-2178.5766	-2175.913	-2175.4059	-46.1	-43.44	-42.93
-4976.35	-2221.9734	-2220.9005	-2220.3968	-76.85	-75.78	-75.28
-4999.41	-2236.7045	-2235.6245	-2235.3255	-92.41	-91.33	-91.04
-5140.05	-2313.4659	-2309.9757	-2309.3901	-137.06	-133.57	-132.99
-5140.76	-2362.6825	-2358.8908	-2358.2765	-185.93	-182.14	-181.53
-5348.43	-2434.9479	-2430.7133	-2430.0569	-195.19	-190.95	-190.3

HOUSE RANGE - LATE CAMBRIAN

UNIT NAME	LITHOFACIES	TIME OBS	Late Cam. Tobs	TIME DELITH	Late Cam. Tdelith	TIME WDmin	TIME WDmax	Late Cam. Tlectsub	R1(ls+sl)(slpor)
0	top Weeks	523	0.2	523	0.2	523	523	0.2	-12.16
0	basal Orr thromb	522.953	0.25	522.968	0.23	522.98	522.975	0.23	-13.33
1	basal deep ramp	522.774	0.43	522.758	0.44	522.863	522.881	0.47	-23.87
2		522.755	0.45	522.744	0.46	522.824	522.849	0.48	-24.42
3		522.726	0.47	522.71	0.49	522.77	522.784	0.52	-26
4		522.698	0.5	522.685	0.52	522.718	522.74	0.54	-27.03
5		522.679	0.52	522.671	0.53	522.692	522.714	0.55	-27.54
6		522.637	0.56	522.621	0.58	522.632	522.646	0.61	-29.86
7		522.59	0.61	522.58	0.62	522.575	522.6	0.65	-31.55
8		522.576	0.62	522.569	0.63	522.537	522.569	0.65	-31.85
9		522.538	0.66	522.524	0.68	522.478	522.502	0.7	-34.05
10		522.472	0.73	522.466	0.73	522.415	522.453	0.76	-36.38
11		522.459	0.74	522.455	0.75	522.407	522.431	0.76	-36.66
12		522.44	0.76	522.432	0.77	522.356	522.368	0.79	-37.73
13		522.407	0.79	522.409	0.79	522.314	522.334	0.81	-38.56
14		522.364	0.84	522.357	0.84	522.253	522.266	0.86	-41
15		522.322	0.88	522.321	0.88	522.198	522.221	0.9	-42.47
16		522.276	0.92	522.288	0.91	522.152	522.186	0.92	-43.55
17		522.234	0.97	522.239	0.96	522.092	522.118	0.98	-45.88
18		522.181	1.02	522.193	1.01	522.033	522.071	1.02	-47.73
19		522.172	1.03	522.185	1.02	521.997	522.04	1.02	-47.94
20		522.141	1.06	522.149	1.05	521.941	521.975	1.06	-49.66
21		522.071	1.13	522.088	1.11	521.877	521.925	1.12	-52.07
22		522.06	1.14	522.078	1.12	521.874	521.904	1.12	-52.3
23		522.024	1.18	522.035	1.17	521.816	521.837	1.17	-54.33
24		521.978	1.22	521.996	1.2	521.759	521.791	1.21	-55.9
25		521.965	1.24	521.985	1.22	521.756	521.769	1.21	-56.17
26		521.889	1.31	521.895	1.31	521.681	521.695	1.31	-60.46
27		521.875	1.33	521.885	1.32	521.677	521.674	1.32	-60.76
28		521.8	1.4	521.795	1.41	521.603	521.599	1.42	-65.01
29		521.79	1.41	521.787	1.41	521.6	521.578	1.42	-65.22
30		521.705	1.5	521.687	1.51	521.522	521.522	1.53	-69.99
31	Big Horse thrombi	521.543	1.66	521.582	1.62	521.485	521.485	1.6	-73.16
32		521.524	1.68	521.559	1.64	521.434	521.422	1.62	-74.1
33	top Cedaria (521.:	521.515	1.69	521.552	1.65	521.432	521.401	1.63	-74.3
34		521.3	1.9	521.3	1.9	521.3	521.3	1.9	-86.12
35		521.27	1.93	521.275	1.93	521.293	521.275	1.92	-86.75
36		521.257	1.94	521.257	1.94	521.24	521.209	1.94	-87.23

37		521.231	1.97	521.235	1.97	521.209	521.18	1.96	-87.79
38		521.216	1.98	521.214	1.99	521.156	521.114	1.99	-88.39
39		521.2	2	521.2	2	521.151	521.091	2	-88.67
40		521.053	2.15	521.053	2.15	521.06	521.028	2.15	-92.75
41		521.032	2.17	521.035	2.17	521.055	521.004	2.17	-93.21
42		520.967	2.23	520.97	2.23	520.988	520.953	2.23	-94.91
43		520.945	2.26	520.952	2.25	520.982	520.929	2.25	-95.36
44		520.88	2.32	520.887	2.31	520.915	520.878	2.31	-97.06
45		520.841	2.36	520.854	2.35	520.868	520.842	2.34	-97.82
46	little thrombs	520.787	2.41	520.812	2.39	520.855	520.815	2.37	-98.74
47		520.765	2.44	520.782	2.42	520.799	520.747	2.41	-99.63
48		520.731	2.47	520.753	2.45	520.752	520.711	2.43	-100.35
49		520.705	2.5	520.717	2.48	520.694	520.642	2.48	-101.49
50		520.56	2.64	520.573	2.63	520.603	520.58	2.63	-105.53
51		520.534	2.67	520.55	2.65	520.559	520.545	2.65	-106.07
52		520.425	2.78	520.442	2.76	520.479	520.488	2.76	-108.99
53		520.386	2.81	520.409	2.79	520.431	520.451	2.78	-109.76
54		520.339	2.86	520.361	2.84	520.369	520.402	2.83	-111.01
55		520.291	2.91	520.322	2.88	520.32	520.365	2.87	-111.93
56		520.257	2.94	520.274	2.93	520.258	520.295	2.92	-113.49
57		520.224	2.98	520.247	2.95	520.212	520.259	2.95	-114.16
58		520.034	3.17	520.058	3.14	520.108	520.191	3.14	-119.34
59		519.969	3.23	520.005	3.2	520.054	520.152	3.19	-120.55
60		519.902	3.3	519.938	3.26	519.987	520.1	3.26	-122.35
61		519.841	3.36	519.889	3.31	519.934	520.062	3.3	-123.48
62		519.824	3.38	519.873	3.33	519.929	520.038	3.31	-123.7
63		519.769	3.43	519.819	3.38	519.865	519.988	3.36	-125.19
64		519.759	3.44	519.809	3.39	519.862	519.966	3.37	-125.37
65		519.679	3.52	519.699	3.5	519.782	519.887	3.51	-129.12
66		519.646	3.55	519.667	3.53	519.725	519.84	3.54	-130.04
67	lowest BH oncolite	519.592	3.61	519.624	3.58	519.712	519.813	3.58	-130.99
68		519.551	3.65	519.583	3.62	519.652	519.765	3.62	-132.01
69		519.525	3.68	519.561	3.64	519.646	519.741	3.64	-132.52
70		519.499	3.7	519.535	3.67	519.591	519.694	3.66	-133.12
71		519.477	3.72	519.516	3.68	519.585	519.671	3.68	-133.57
72		519.438	3.76	519.477	3.72	519.526	519.623	3.71	-134.52
73		519.399	3.8	519.446	3.75	519.517	519.597	3.74	-135.24
74		519.332	3.87	519.353	3.85	519.442	519.521	3.85	-138.25
75		519.289	3.91	519.319	3.88	519.431	519.495	3.88	-139.06
76		519.265	3.94	519.295	3.91	519.377	519.449	3.9	-139.6
77		519.217	3.98	519.257	3.94	519.365	519.423	3.93	-140.44
78		519.187	4.01	519.226	3.97	519.309	519.376	3.96	-141.15

79	519.159	4.04	519.203	4	519.278	519.347	3.98	-141.7
80 short NW drownin	518.969	4.23	518.944	4.26	519.153	519.248	4.31	-150.43
81	518.932	4.27	518.907	4.29	519.094	519.201	4.34	-151.44
82	518.91	4.29	518.888	4.31	519.051	519.166	4.36	-151.88
83	518.884	4.32	518.861	4.34	518.995	519.12	4.38	-152.5
84	518.821	4.38	518.813	4.39	518.981	519.092	4.42	-153.55
85	518.795	4.41	518.786	4.41	518.925	519.046	4.44	-154.13
86	518.767	4.43	518.763	4.44	518.918	519.021	4.46	-154.66
87	518.728	4.47	518.723	4.48	518.859	518.974	4.5	-155.59
88	518.689	4.51	518.691	4.51	518.812	518.937	4.53	-156.32
89	518.674	4.53	518.675	4.53	518.759	518.892	4.54	-156.68
90	518.659	4.54	518.661	4.54	518.755	518.869	4.55	-156.89
91	518.631	4.57	518.632	4.57	518.699	518.823	4.58	-157.64
92	518.598	4.6	518.605	4.6	518.691	518.798	4.6	-158.24
93	518.583	4.62	518.589	4.61	518.639	518.753	4.61	-158.55
94 upper BH thrombs	518.471	4.73	518.503	4.7	518.613	518.72	4.68	-160.31
95	518.44	4.76	518.473	4.73	518.557	518.673	4.7	-161.03
96	518.412	4.79	518.449	4.75	518.55	518.649	4.72	-161.57
97	518.384	4.82	518.421	4.78	518.494	518.603	4.75	-162.21
98 upper BH thrombs	518.297	4.9	518.354	4.85	518.474	518.572	4.8	-163.6
99	518.282	4.92	518.319	4.88	518.392	518.44	4.85	-164.93
100	518.265	4.94	518.301	4.9	518.339	518.395	4.87	-165.46
101	518.248	4.95	518.285	4.92	518.335	518.371	4.88	-165.7
102	518.217	4.98	518.216	4.98	518.243	518.234	4.98	-168.59
103 Crep/Aph BB (51	518.2	5	518.2	5	518.2	518.2	5	-169.01
104	518.133	5.07	518.095	5.11	518.071	518.037	5.15	-175.29
105	518.12	5.08	518.086	5.11	518.025	518	5.15	-175.54
106	518.105	5.1	518.062	5.14	517.935	517.854	5.19	-176.93
107	518.083	5.12	518.049	5.15	517.887	517.816	5.2	-177.4
108	517.981	5.22	517.891	5.31	517.733	517.642	5.42	-186.76
109	517.949	5.25	517.872	5.33	517.682	517.603	5.43	-187.37
110	517.903	5.3	517.841	5.36	517.615	517.549	5.46	-188.41
111	517.877	5.32	517.826	5.37	517.608	517.522	5.47	-188.86
112	517.819	5.38	517.734	5.47	517.485	517.362	5.59	-194.03
113	517.795	5.41	517.72	5.48	517.437	517.324	5.6	-194.51
114	517.767	5.43	517.676	5.52	517.337	517.174	5.66	-196.93
115	517.743	5.46	517.661	5.54	517.288	517.136	5.67	-197.4
116	517.661	5.54	517.533	5.67	517.148	516.968	5.84	-204.62
117	517.643	5.56	517.523	5.68	517.101	516.93	5.85	-204.98
118 major Candland s	517.351	5.85	517.079	6.12	516.81	516.694	6.43	-229.85
119	517.329	5.87	517.066	6.13	516.777	516.663	6.44	-230.22
120	517.147	6.05	516.786	6.41	516.564	516.462	6.78	-244.86

121	517.134	6.07	516.778	6.42	516.534	516.432	6.79	-245.01
122	516.95	6.25	516.495	6.71	516.32	516.231	7.12	-259.41
123	516.939	6.26	516.489	6.71	516.291	516.201	7.13	-259.53
124	516.87	6.33	516.38	6.82	516.16	516.037	7.25	-264.8
125	516.794	6.41	516.327	6.87	516.082	515.979	7.28	-266.15
126 first Candland thrc	516.725	6.48	516.29	6.91	516.065	515.948	7.3	-266.81
127	516.56	6.64	516.037	7.16	515.864	515.753	7.59	-279.11
128	516.517	6.68	516.013	7.19	515.853	515.724	7.6	-279.58
129	516.439	6.76	515.892	7.31	515.716	515.558	7.73	-285.2
130	516.406	6.79	515.869	7.33	515.653	515.506	7.74	-285.76
131	516.393	6.81	515.861	7.34	515.623	515.476	7.75	-285.84
132	516.335	6.87	515.769	7.43	515.501	515.316	7.85	-290.08
133	516.311	6.89	515.752	7.45	515.44	515.265	7.86	-290.51
134	516.3	6.9	515.746	7.45	515.411	515.236	7.86	-290.57
135 lowest Johns Was	516.083	7.12	515.598	7.6	515.288	515.157	7.94	-294.1
136	515.455	7.75	515.284	7.92	515.136	515.066	8.06	-299.21
137 JoWa fenes. mdst	515	8.2	515	8.2	515	515	8.2	-305.19
138 thick Corset Sprin	514.618	8.58	514.458	8.74	514.752	514.82	8.91	-335.04
139	514.581	8.62	514.439	8.76	514.745	514.802	8.92	-335.44
140	514.554	8.65	514.399	8.8	514.678	514.702	8.96	-337.33
141	514.503	8.7	514.373	8.83	514.668	514.682	8.98	-337.83
142	514.375	8.83	514.185	9.02	514.548	514.559	9.2	-347.21
143	514.362	8.84	514.178	9.02	514.517	514.534	9.2	-347.33
144	514.325	8.88	514.123	9.08	514.444	514.432	9.27	-350.03
145	514.294	8.91	514.105	9.1	514.402	514.398	9.27	-350.39
146	514.243	8.96	514.028	9.17	514.322	514.293	9.36	-354.07
147	514.212	8.99	514.011	9.19	514.287	514.266	9.37	-354.41
148	514.187	9.01	513.997	9.2	514.247	514.233	9.37	-354.61
149	514.115	9.09	513.89	9.31	514.156	514.123	9.5	-359.77
150	514.1	9.1	513.881	9.32	514.124	514.098	9.5	-359.88
151 lowest Sneakover	514.086	9.11	513.87	9.33	514.085	514.049	9.51	-360.24
152	514.024	9.18	513.837	9.36	514.045	514.021	9.52	-360.76
153	513.993	9.21	513.819	9.38	514.003	513.987	9.53	-361.01
154	513.948	9.25	513.784	9.42	513.955	513.934	9.55	-362.06
155	513.869	9.33	513.74	9.46	513.904	513.896	9.57	-362.77
156	513.838	9.36	513.716	9.48	513.86	513.846	9.59	-363.5
157	513.818	9.38	513.704	9.5	513.82	513.813	9.59	-363.73
158	513.787	9.41	513.679	9.52	513.776	513.762	9.61	-364.43
159	513.673	9.53	513.616	9.58	513.718	513.721	9.63	-365.45
160	513.657	9.54	513.603	9.6	513.678	513.672	9.64	-365.86
161	513.591	9.61	513.567	9.63	513.63	513.635	9.66	-366.48
162	513.578	9.62	513.556	9.64	513.591	513.587	9.66	-366.77

163	513.554	9.65	513.542	9.66	513.55	513.553	9.67	-367.04
164 Elv/Taen BB (513	513.5	9.7	513.5	9.7	513.5	513.5	9.7	-368.32
165	513.453	9.75	513.454	9.75	513.429	513.441	9.74	-368.77
166	513.438	9.76	513.433	9.77	513.367	513.36	9.76	-369.1
167	513.425	9.78	513.419	9.78	513.306	513.306	9.77	-369.2
168	513.363	9.84	513.333	9.87	513.223	513.215	9.89	-370.69
169	513.284	9.92	513.257	9.94	513.143	513.152	9.96	-371.44
170	513.256	9.94	513.219	9.98	513.075	513.069	10.01	-372.09
171	513.181	10.02	513.147	10.05	512.996	513.006	10.07	-372.8
172	513.16	10.04	513.117	10.08	512.93	512.924	10.11	-373.27
173	513.138	10.06	513.095	10.11	512.867	512.868	10.13	-373.52
174	513.112	10.09	513.059	10.14	512.8	512.785	10.17	-374.09
175	513.097	10.1	513.043	10.16	512.739	512.731	10.18	-374.21
176	513.085	10.12	513.025	10.18	512.677	512.65	10.21	-374.55
177 lowest Notch Peal	513.042	10.16	512.983	10.22	512.608	512.592	10.25	-374.98
178	513.031	10.17	512.967	10.23	512.547	512.512	10.26	-375.18
179	513.008	10.19	512.943	10.26	512.483	512.456	10.29	-375.47
180	512.997	10.2	512.928	10.27	512.422	512.376	10.3	-375.66
181	512.965	10.24	512.896	10.3	512.356	512.319	10.33	-376.03
182	512.943	10.26	512.866	10.33	512.291	512.237	10.37	-376.52
183	512.896	10.3	512.82	10.38	512.22	512.178	10.41	-376.99
184	512.881	10.32	512.799	10.4	512.157	512.097	10.44	-377.33
185	512.832	10.37	512.751	10.45	512.086	512.038	10.48	-377.83
186	512.819	10.38	512.733	10.47	512.024	511.957	10.5	-378.12
187	512.772	10.43	512.687	10.51	511.954	511.898	10.54	-378.6
188	512.757	10.44	512.666	10.53	511.891	511.817	10.57	-378.94
189	512.71	10.49	512.62	10.58	511.82	511.758	10.61	-379.42
190	512.697	10.5	512.602	10.6	511.759	511.678	10.63	-379.72
191	512.654	10.55	512.56	10.64	511.689	511.62	10.67	-380.16
192	512.641	10.56	512.542	10.66	511.628	511.539	10.69	-380.45
193	512.603	10.6	512.504	10.7	511.56	511.481	10.73	-380.86
194	512.592	10.61	512.488	10.71	511.499	511.401	10.74	-381.07
195	512.554	10.65	512.451	10.75	511.431	511.343	10.78	-381.51
196	512.541	10.66	512.432	10.77	511.369	511.263	10.8	-381.8
197	512.509	10.69	512.4	10.8	511.303	511.206	10.83	-382.15
198	512.496	10.7	512.382	10.82	511.241	511.125	10.86	-382.44
199	512.462	10.74	512.348	10.85	511.174	511.068	10.89	-382.81
200	512.449	10.75	512.33	10.87	511.112	510.988	10.91	-383.1
201	512.414	10.79	512.296	10.9	511.045	510.931	10.94	-383.48
202	512.404	10.8	512.28	10.92	510.984	510.85	10.96	-383.68
203 non-cyclic Hellnm.	511.826	11.37	511.701	11.5	510.745	510.713	11.52	-390.49
204 non-cyclic Hellnm.	511.708	11.49	511.578	11.62	510.65	510.643	11.64	-392.01

205 non-cyclic Hellnm.	511.205	12	511.074	12.13	510.434	510.517	12.16	-398.34
206 non-cyclic Hellnm.	511.183	12.02	511.052	12.15	510.383	510.475	12.18	-398.64
207 non-cyclic Hellnm.	510.798	12.4	510.693	12.51	510.213	510.37	12.53	-402.87
208	510.77	12.43	510.664	12.54	510.17	510.327	12.56	-403.25
209 lowest Hellnmaria	510.742	12.46	510.638	12.56	510.162	510.297	12.59	-403.57
210	510.605	12.6	510.503	12.7	510.085	510.238	12.72	-405.19
211	510.59	12.61	510.488	12.71	510.081	510.21	12.73	-405.33
212	510.533	12.67	510.43	12.77	510.029	510.162	12.79	-406.08
213	510.507	12.69	510.406	12.79	510.021	510.133	12.82	-406.41
214	510.426	12.77	510.325	12.88	509.962	510.082	12.9	-407.35
215	510.398	12.8	510.299	12.9	509.954	510.052	12.93	-407.72
216	510.333	12.87	510.237	12.96	509.9	510.004	12.98	-408.41
217	510.271	12.93	510.182	13.02	509.883	509.97	13.04	-409.08
218	510.214	12.99	510.127	13.07	509.832	509.923	13.09	-409.7
219	510.158	13.04	510.078	13.12	509.816	509.89	13.14	-410.32
220	510.117	13.08	510.038	13.16	509.77	509.845	13.18	-410.75
221	510.066	13.13	509.992	13.21	509.756	509.812	13.22	-411.32
222	510.019	13.18	509.946	13.25	509.707	509.766	13.26	-411.82
223	509.948	13.25	509.884	13.32	509.688	509.731	13.32	-412.56
224	509.912	13.29	509.848	13.35	509.643	509.687	13.36	-412.97
225	509.875	13.33	509.815	13.39	509.632	509.656	13.39	-413.4
226	509.862	13.34	509.801	13.4	509.594	509.615	13.4	-413.46
227	509.779	13.42	509.728	13.47	509.571	509.578	13.47	-414.35
228	509.755	13.45	509.704	13.5	509.53	509.536	13.49	-414.62
229	509.71	13.49	509.663	13.54	509.517	509.504	13.53	-415.11
230	509.663	13.54	509.618	13.58	509.469	509.458	13.58	-415.63
231 proj. base Saukia	509.4	13.8	509.4	13.8	509.4	509.4	13.8	-418.38
232	509.36	13.84	509.36	13.84	509.354	509.357	13.84	-419.5
233	509.281	13.92	509.289	13.91	509.331	509.322	13.91	-421.23
234	509.186	14.01	509.195	14.01	509.268	509.271	14	-423.55
235	509.135	14.07	509.149	14.05	509.226	509.235	14.05	-424.72
236 laminar fenestrae	509.078	14.12	509.093	14.11	509.175	509.19	14.1	-426.05
237	508.998	14.2	509.021	14.18	509.151	509.155	14.17	-427.83
238	508.973	14.23	508.996	14.2	509.11	509.114	14.19	-428.39
239	508.892	14.31	508.924	14.28	509.087	509.079	14.26	-430.14
240	508.82	14.38	508.852	14.35	509.031	509.032	14.33	-431.89
241	508.775	14.43	508.812	14.39	508.99	508.996	14.37	-432.92
242	508.729	14.47	508.77	14.43	508.977	508.965	14.41	-433.89
243	508.712	14.49	508.752	14.45	508.938	508.926	14.42	-434.23
244	508.646	14.55	508.692	14.51	508.919	508.892	14.48	-435.68
245	508.581	14.62	508.628	14.57	508.865	508.846	14.54	-437.22
246	508.389	14.81	508.462	14.74	508.812	508.797	14.7	-441.3

247	508.302	14.9	508.385	14.82	508.759	508.756	14.77	-443.11
248	508.235	14.97	508.324	14.88	508.74	508.723	14.83	-444.49
249 scal.eros.surf. ove	508.082	15.12	508.174	15.03	508.658	508.664	14.98	-448.27
250	508.037	15.16	508.133	15.07	508.618	508.629	15.02	-449.3
251	507.734	15.47	507.877	15.32	508.535	508.567	15.27	-455.61
252	507.714	15.49	507.856	15.34	508.495	508.527	15.28	-456
253	507.701	15.5	507.843	15.36	508.491	508.5	15.29	-456.22
254	507.669	15.53	507.81	15.39	508.448	508.458	15.32	-457.05
255	507.532	15.67	507.69	15.51	508.409	508.416	15.44	-459.95
256	507.507	15.69	507.665	15.54	508.368	508.376	15.46	-460.5
257	507.451	15.75	507.615	15.59	508.351	508.343	15.51	-461.74
258	507.428	15.77	507.591	15.61	508.311	508.303	15.53	-462.22
259	507.368	15.83	507.536	15.66	508.293	508.27	15.58	-463.53
260	507.319	15.88	507.492	15.71	508.252	508.234	15.62	-464.54
261	507.246	15.95	507.427	15.77	508.23	508.2	15.68	-466.02
262	507.212	15.99	507.393	15.81	508.176	508.158	15.71	-466.78
263 v.thk. uppermost l	506.747	16.45	507.001	16.2	508.049	508.077	16.08	-476.4
264	506.709	16.49	506.962	16.24	508.004	508.034	16.12	-477.22
265	506.664	16.54	506.917	16.28	507.934	507.978	16.16	-478.35
266	506.64	16.56	506.894	16.31	507.927	507.95	16.19	-478.96
267	506.51	16.69	506.764	16.44	507.83	507.882	16.31	-482.2
268 lowest Red Tops (	506.47	16.73	506.726	16.47	507.79	507.852	16.35	-483.14
269	506.446	16.75	506.685	16.52	507.771	507.821	16.41	-484.57
270	506.426	16.77	506.665	16.54	507.737	507.793	16.43	-485.11
271	506.403	16.8	506.627	16.57	507.698	507.751	16.48	-486.41
272	506.335	16.87	506.565	16.64	507.678	507.717	16.54	-487.9
273	506.296	16.9	506.5	16.7	507.651	507.683	16.63	-490.24
274	506.235	16.97	506.445	16.76	507.606	507.65	16.68	-491.55
275	506.201	17	506.412	16.79	507.551	507.608	16.71	-492.29
276	506.185	17.02	506.395	16.81	507.535	507.586	16.72	-492.54
277	506.155	17.05	506.343	16.86	507.513	507.554	16.8	-494.45
278	506.134	17.07	506.323	16.88	507.495	507.531	16.82	-494.97
279	506.112	17.09	506.285	16.92	507.477	507.501	16.87	-496.25
280	506.082	17.12	506.254	16.95	507.423	507.46	16.9	-497.04
281	506.07	17.13	506.233	16.97	507.405	507.432	16.93	-497.77
282 upper Red Tops g	506.029	17.17	506.196	17	507.383	507.407	16.96	-498.68
283	505.993	17.21	506.159	17.04	507.327	507.364	16.99	-499.49
284 Lava Dam deeper	505.973	17.23	506.124	17.08	507.304	507.335	17.04	-500.73
285	505.89	17.31	506.04	17.16	507.222	507.273	17.12	-502.8
286	505.865	17.34	506.005	17.2	507.156	507.194	17.17	-503.88
287	505.845	17.36	505.984	17.22	507.094	507.141	17.19	-504.42
288	505.805	17.4	505.928	17.27	507.021	507.059	17.26	-506.19

289	505.772	17.43	505.895	17.31	506.955	507.005	17.29	-507.02
290	505.734	17.47	505.841	17.36	506.883	506.923	17.36	-508.7
291	505.712	17.49	505.818	17.38	506.821	506.87	17.38	-509.29
292	505.687	17.51	505.784	17.42	506.755	506.791	17.42	-510.33
293	505.673	17.53	505.768	17.43	506.694	506.739	17.43	-510.66
294	505.649	17.55	505.734	17.47	506.628	506.66	17.48	-511.75
295	505.635	17.57	505.718	17.48	506.568	506.609	17.49	-512.08
296	505.615	17.59	505.689	17.51	506.504	506.53	17.53	-512.99
297	505.601	17.6	505.673	17.53	506.444	506.479	17.54	-513.32
298	505.582	17.62	505.647	17.55	506.38	506.401	17.57	-514.14
299	505.572	17.63	505.636	17.56	506.322	506.35	17.58	-514.38
300	505.556	17.64	505.613	17.59	506.259	506.272	17.61	-515.1
301	505.542	17.66	505.597	17.6	506.199	506.221	17.62	-515.43
302	505.53	17.67	505.579	17.62	506.138	506.144	17.64	-515.98
303	505.508	17.69	505.556	17.64	506.076	506.091	17.67	-516.56
304	505.493	17.71	505.535	17.67	506.014	506 014	17.69	-517.14
305	505.469	17.73	505.51	17.69	505.951	505.961	17.71	-517.77
306	505.453	17.75	505.487	17.71	505.889	505.883	17.74	-518.44
307	505.433	17.77	505.465	17.74	505.827	505.831	17.76	-518.97
308	505.413	17.79	505.437	17.76	505.762	505.753	17.79	-519.81
309	505.4	17.8	505.424	17.78	505.731	505.726	17.8	-520.06
310	505.366	17.83	505.389	17.81	505.664	505.672	17.84	-520.9
311	505.356	17.84	505.374	17.83	505.605	505.595	17.85	-521.28
312	505.328	17.87	505.344	17.86	505.54	505.542	17.88	-522.02
313	505.317	17.88	505.329	17.87	505.48	505.465	17.9	-522.4
314	505.267	17.93	505.278	17.92	505.409	505.408	17.94	-523.65
315	505.257	17.94	505.263	17.94	505.349	505.332	17.96	-524.06
316	505.18	18.02	505.185	18.02	505.269	505.271	18.03	-525.93
317	505.156	18.04	505.151	18.05	505.203	505.192	18.08	-526.98
318 LD oold grsts/stro	505.125	18.08	505.122	18.08	505.188	505.173	18.1	-527.67
319	505.101	18.1	505.097	18.1	505.125	505.12	18.12	-528.16
320	505.091	18.11	505.086	18.11	505.099	505.094	18.13	-528.33
321	505.075	18.13	505.069	18.13	505.05	505.054	18.14	-528.63
322	505.053	18.15	505.047	18.15	505.021	505.027	18.16	-529.18
323	505	18.2	505	18.2	505	505	18.2	-530.15

DELITH at end(slpor)	OBS.SUM.THK	DELITH at depo	WDmin	WDmax	Y Tobs(slpor)	Y Tdel(slpor)	Y Ttec(slpor)	R2 Tobs(slpor)	R2 Tdel(slpor)	R2 Ttec(slpor)
-19.09	-10	19.09	30	60	-39.3544	-36.4078	-29.2151	-27.2	-24.25	-17.06
-21.65	-12.5	21.76	2	10	-40.8682	-37.4471	-29.8854	-27.54	-24.12	-16.56
-38.65	-21.9	39.25	10	30	-46.6231	-44.2545	-33.8026	-22.75	-20.38	-9.93
-39.76	-22.9	40.46	8	15	-47.233	-44.7076	-35.1067	-22.81	-20.29	-10.69
-42.37	-24.4	43.28	10	30	-48.1635	-45.8073	-36.9111	-22.16	-19.81	-10.91
-44.35	-25.9	45.36	10	20	-49.0616	-46.6156	-38.6471	-22.03	-19.59	-11.62
-45.43	-26.9	46.55	5	12	-49.6707	-47.0681	-39.5146	-22.13	-19.53	-11.97
-49.27	-29.1	50.7	10	30	-51.0167	-48.6833	-41.5151	-21.15	-18.82	-11.65
-52.51	-31.6	54.13	10	20	-52.5217	-50.0069	-43.4139	-20.97	-18.46	-11.87
-53.32	-32.3	55.03	8	15	-52.9698	-50.3618	-44.6787	-21.12	-18.51	-12.83
-56.82	-34.3	58.82	10	30	-54.1856	-51.8132	-46.6411	-20.14	-17.76	-12.59
-61.41	-37.8	63.66	10	20	-56.2955	-53.6824	-48.7344	-19.92	-17.31	-12.36
-62.13	-38.5	64.54	1	10	-56.7108	-54.0367	-49.0001	-20.05	-17.38	-12.34
-63.77	-39.5	66.43	10	30	-57.3176	-54.7773	-50.693	-19.59	-17.05	-12.97
-65.62	-41.2	68.39	8	15	-58.3712	-55.5176	-52.0861	-19.81	-16.96	-13.53
-69.67	-43.5	72.73	10	30	-59.7432	-57.1904	-54.1077	-18.74	-16.19	-13.1
-72.5	-45.7	75.75	10	20	-61.0823	-58.3477	-55.9288	-18.62	-15.88	-13.46
-75.02	-48.1	78.45	8	15	-62.548	-59.408	-57.4507	-19	-15.85	-13.9
-78.9	-50.3	82.61	10	30	-63.8853	-60.9813	-59.4341	-18	-15.1	-13.55
-82.49	-53.1	86.44	10	20	-65.5716	-62.4572	-61.3826	-17.85	-14.73	-13.66
-83.08	-53.6	87.09	8	15	-65.8578	-62.7137	-62.5706	-17.92	-14.78	-14.63
-85.81	-55.2	90.09	10	30	-66.8433	-63.8679	-64.4173	-17.18	-14.21	-14.76
-90.64	-58.9	95.2	10	20	-69.0669	-65.822	-66.5258	-17	-13.76	-14.46
-91.25	-59.5	95.96	0	10	-69.4161	-66.1421	-66.6246	-17.11	-13.84	-14.32
-94.51	-61.4	99.55	10	30	-70.5584	-67.5182	-68.5334	-16.23	-13.19	-14.2
-97.57	-63.8	102.85	10	20	-72.0172	-68.7655	-70.4076	-16.12	-12.87	-14.51
-98.35	-64.5	103.73	0	10	-72.4293	-69.1172	-70.5062	-16.26	-12.95	-14.34
-105.3	-68.5	111.22	10	30	-74.8365	-71.9921	-72.9696	-14.38	-11.53	-12.51
-106.06	-69.2	112.11	0	10	-75.2797	-72.3113	-73.1009	-14.52	-11.56	-12.34
-112.98	-73.2	119.6	10	30	-77.6519	-75.1816	-75.5284	-12.64	-10.17	-10.52
-113.52	-73.7	120.23	0	10	-77.9679	-75.4365	-75.6267	-12.74	-10.21	-10.4
-121.31	-78.2	128.65	10	20	-80.6526	-78.6206	-78.1822	-10.67	-8.63	-8.2
-129.42	-86.7	137.38	0	10	-85.7592	-81.9584	-79.3933	-12.6	-8.8	-6.23
-130.98	-87.7	139.28	10	30	-86.3573	-82.6887	-81.0615	-12.26	-8.59	-6.96
-131.55	-88.2	139.91	0	10	-86.6405	-82.911	-81.1269	-12.34	-8.61	-6.82
-151.09	-99.5	160.89	10	30	-93.3944	-90.8951	-85.4382	-7.27	-4.77	0.68
-152.48	-100.9	162.47	0	10	-94.335	-91.6854	-85.6665	-7.58	-4.93	1.09
-153.38	-101.5	163.62	10	30	-94.7425	-92.2543	-87.3948	-7.51	-5.02	-0.16

-154.63	-102.7	165	5	12	-95.5571	-92.9493	-88.4051	-7.76	-5.16	-0.61
-155.69	-103.4	166.34	10	30	-96.0269	-93.6125	-90.131	-7.64	-5.22	-1.74
-156.48	-104.1	167.22	0	10	-96.5279	-94.0545	-90.2938	-7.86	-5.39	-1.63
-164.87	-110.9	176.49	10	20	-101.1251	-98.6898	-93.2537	-8.38	-5.94	-0.5
-165.83	-111.9	177.66	0	10	-101.781	-99.2566	-93.4162	-8.57	-6.04	-0.2
-169.46	-114.9	181.76	10	20	-103.8097	-101.3022	-95.5925	-8.9	-6.4	-0.69
-170.48	-115.9	182.93	0	10	-104.4958	-101.8683	-95.7873	-9.13	-6.5	-0.42
-174.11	-118.9	187.03	10	20	-106.5217	-103.9111	-97.9611	-9.46	-6.85	-0.9
-175.95	-120.7	189.09	8	15	-107.7362	-104.9474	-99.4846	-9.91	-7.12	-1.66
-178.31	-123.2	191.76	0	10	-109.4166	-106.2656	-99.9058	-10.68	-7.53	-1.17
-179.9	-124.2	193.66	10	30	-110.1008	-107.2066	-101.7192	-10.47	-7.58	-2.09
-181.58	-125.8	195.51	8	15	-111.1577	-108.1159	-103.2399	-10.81	-7.77	-2.89
-183.55	-127	197.77	10	30	-111.9655	-109.244	-105.1149	-10.47	-7.75	-3.62
-191.95	-133.7	206.9	10	20	-116.4646	-113.7499	-108.0533	-10.93	-8.22	-2.52
-193.14	-134.9	208.33	8	15	-117.2703	-114.4687	-109.4725	-11.2	-8.4	-3.4
-199.35	-139.9	215.18	10	20	-120.6441	-117.8402	-112.0504	-11.65	-8.85	-3.06
-201.13	-141.7	217.25	8	15	-121.8499	-118.8692	-113.5956	-12.09	-9.11	-3.84
-203.8	-143.9	220.27	10	20	-123.3019	-120.3649	-115.5897	-12.29	-9.35	-4.58
-206.04	-146.1	222.76	8	15	-124.7838	-121.5794	-117.1642	-12.86	-9.65	-5.24
-208.71	-147.7	225.76	10	30	-125.8328	-123.0731	-119.1548	-12.35	-9.59	-5.67
-210.29	-149.2	227.51	8	15	-126.8503	-123.9129	-120.6304	-12.69	-9.75	-6.47
-221.19	-158	239.46	10	20	-132.6986	-129.7807	-123.9625	-13.36	-10.44	-4.62
-224.14	-161	242.8	8	15	-134.6953	-131.4231	-125.6905	-14.15	-10.87	-5.14
-227.95	-164.1	247.03	10	20	-136.7513	-133.4972	-127.8324	-14.4	-11.15	-5.48
-230.77	-166.9	250.16	8	15	-138.6212	-135.0127	-129.5251	-15.14	-11.53	-6.04
-231.58	-167.7	251.14	0	10	-139.142	-135.5074	-129.6848	-15.44	-11.81	-5.98
-234.57	-170.2	254.56	10	20	-140.826	-137.1757	-131.7267	-15.63	-11.98	-6.53
-235.13	-170.7	255.2	0	10	-141.132	-137.4845	-131.8224	-15.76	-12.12	-6.45
-241.37	-174.4	262.13	10	30	-143.5785	-140.8781	-134.3718	-14.46	-11.76	-5.25
-243.22	-175.9	264.22	10	20	-144.5867	-141.8642	-136.1863	-14.55	-11.82	-6.15
-245.61	-178.4	266.89	0	10	-146.2354	-143.1885	-136.5999	-15.24	-12.19	-5.61
-247.86	-180.3	269.51	10	20	-147.4863	-144.4503	-138.5077	-15.48	-12.44	-6.5
-249.06	-181.5	270.88	0	10	-148.2791	-145.1271	-138.6984	-15.76	-12.61	-6.18
-250.44	-182.7	272.56	10	20	-149.0715	-145.9266	-140.4455	-15.95	-12.81	-7.33
-251.46	-183.7	273.73	0	10	-149.7418	-146.5106	-140.636	-16.17	-12.94	-7.07
-253.58	-185.5	276.22	10	20	-150.9295	-147.7089	-142.5082	-16.41	-13.19	-7.99
-255.33	-187.3	278.19	0	10	-152.1165	-148.6608	-142.7937	-16.88	-13.42	-7.56
-260.53	-190.4	284.02	10	30	-154.1538	-151.5137	-145.1708	-15.91	-13.27	-6.92
-262.45	-192.4	286.19	0	10	-155.4603	-152.5557	-145.5192	-16.4	-13.5	-6.46
-263.71	-193.5	287.74	10	20	-156.189	-153.2909	-147.2286	-16.59	-13.7	-7.63
-265.82	-195.7	290.11	0	10	-157.6458	-154.4543	-147.6083	-17.21	-14.01	-7.17
-267.45	-197.1	292.06	10	20	-158.5557	-155.4029	-149.3792	-17.4	-14.25	-8.23

-268.75	-198.4	293.54	5	12	-159.4045	-156.1064	-150.3588	-17.7	-14.41	-8.66
-283.61	-207.2	309.92	10	30	-165.1545	-164.0106	-154.304	-14.73	-13.58	-3.88
-285.68	-208.9	312.27	10	20	-166.2722	-165.1371	-156.1634	-14.83	-13.7	-4.73
-286.72	-209.9	313.48	8	15	-166.9365	-165.7153	-157.5174	-15.06	-13.84	-5.64
-288.12	-211.1	315.16	10	20	-167.7212	-166.5367	-159.2795	-15.23	-14.04	-6.78
-290.85	-214	318.24	0	10	-169.6214	-167.9961	-159.7197	-16.07	-14.45	-6.17
-292.21	-215.2	319.92	10	20	-170.405	-168.8165	-161.4798	-16.27	-14.69	-7.35
-293.49	-216.5	321.39	0	10	-171.2486	-169.515	-161.6997	-16.58	-14.85	-7.04
-295.59	-218.3	323.87	10	20	-172.4229	-170.7294	-163.5522	-16.83	-15.14	-7.96
-297.4	-220.1	325.94	8	15	-173.5965	-171.7003	-165.0266	-17.28	-15.38	-8.71
-298.23	-220.8	326.96	10	20	-174.0477	-172.1855	-166.688	-17.37	-15.51	-10.01
-298.95	-221.5	327.84	0	10	-174.4988	-172.61	-166.8133	-17.61	-15.72	-9.92
-300.43	-222.8	329.66	10	20	-175.3405	-173.4891	-168.5671	-17.7	-15.85	-10.93
-301.89	-224.3	331.33	0	10	-176.332	-174.3071	-168.8175	-18.1	-16.07	-10.58
-302.67	-225	332.35	10	20	-176.7826	-174.7917	-170.4444	-18.24	-16.25	-11.9
-307.53	-230.2	337.78	0	10	-180.1432	-177.3943	-171.2573	-19.83	-17.08	-10.95
-309.09	-231.6	339.73	10	20	-181.0723	-178.3013	-173.0071	-20.04	-17.27	-11.98
-310.37	-232.9	341.2	0	10	-181.9111	-179.0267	-173.2257	-20.35	-17.46	-11.66
-311.86	-234.2	343.02	10	20	-182.7495	-179.8725	-174.9737	-20.54	-17.67	-12.77
-315.66	-238.2	347.25	0	10	-185.3522	-181.895	-175.5977	-21.75	-18.3	-12
-317.45	-238.9	349.45	15	60	-185.8006	-182.9507	-178.1537	-20.87	-18.02	-13.22
-318.49	-239.7	350.6	10	20	-186.3087	-183.4934	-179.8039	-20.85	-18.03	-14.34
-319.31	-240.5	351.58	0	10	-186.8166	-183.9757	-179.9284	-21.11	-18.27	-14.23
-323.13	-241.9	355.97	15	60	-187.7424	-186.054	-182.7896	-19.16	-17.47	-14.2
-324.03	-242.7	356.98	8	15	-188.2499	-186.5356	-184.1254	-19.24	-17.53	-15.12
-332.66	-245.8	366.68	15	60	-190.2487	-189.6931	-188.1274	-14.96	-14.4	-12.84
-333.35	-246.4	367.45	8	15	-190.6363	-189.9635	-189.5525	-15.1	-14.42	-14.01
-335.19	-247.1	369.65	15	60	-191.0834	-190.6844	-192.3377	-14.15	-13.75	-15.41
-336.26	-248.1	370.87	8	15	-191.739	-191.0747	-193.8215	-14.34	-13.67	-16.42
-349.08	-252.8	385.42	15	60	-194.7755	-195.8126	-198.5745	-8.02	-9.05	-11.82
-350.6	-254.3	387.17	8	15	-195.7272	-196.3815	-200.1459	-8.36	-9.01	-12.78
-353.01	-256.4	390.05	10	20	-197.0943	-197.3094	-202.2084	-8.69	-8.9	-13.8
-354.15	-257.6	391.43	0	10	-197.8665	-197.7583	-202.4238	-9.01	-8.9	-13.57
-361.37	-260.3	399.88	15	60	-199.5881	-200.5087	-206.204	-5.55	-6.47	-12.17
-362.5	-261.4	401.2	8	15	-200.3	-200.9269	-207.6773	-5.8	-6.42	-13.17
-365.9	-262.7	405.28	15	60	-201.1303	-202.2406	-210.7428	-4.2	-5.31	-13.81
-367.03	-263.8	406.6	8	15	-201.8416	-202.6882	-212.2432	-4.45	-5.29	-14.85
-377.06	-267.6	418.39	15	60	-204.2699	-206.5038	-216.5235	0.35	-1.88	-11.9
-377.91	-268.4	419.4	8	15	-204.8025	-206.8015	-217.9583	0.18	-1.82	-12.98
-412.81	-281.9	460.29	15	60	-213.4216	-219.9745	-226.8181	16.43	9.87	3.03
-413.75	-282.9	461.46	5	12	-214.0693	-220.3588	-227.8202	16.15	9.86	2.4
-434.56	-291.3	487.22	15	60	-219.4194	-228.6166	-234.2758	25.44	16.24	10.58

-435.15	-291.9	487.98	5	12	-219.8009	-228.852	-235.1833	25.21	16.16	9.83
-455.69	-300.4	514.05	15	60	-225.1929	-237.1599	-241.6442	34.22	22.25	17.77
-456.17	-300.9	514.68	5	12	-225.5147	-237.3356	-242.518	34.02	22.2	17.01
-463.77	-304.1	524.69	15	60	-227.5323	-240.5252	-246.4603	37.26	24.27	18.33
-467.44	-307.6	529.53	10	20	-229.752	-242.0741	-248.8038	36.4	24.08	17.35
-469.96	-310.8	532.96	0	10	-231.7649	-243.1547	-249.3141	35.04	23.65	17.49
-487.77	-318.4	556.32	15	60	-236.5694	-250.5261	-255.338	42.54	28.58	23.77
-489.39	-320.4	558.49	0	10	-237.8194	-251.2239	-255.6671	41.76	28.36	23.91
-497.67	-324	569.67	15	60	-240.0847	-254.7375	-259.7611	45.12	30.47	25.44
-499.26	-325.5	571.76	10	20	-241.0423	-255.4047	-261.6408	44.72	30.36	24.12
-499.79	-326.1	572.51	5	12	-241.4194	-255.6366	-262.5352	44.42	30.21	23.31
-505.96	-328.8	580.96	15	60	-243.1007	-258.3023	-266.1681	46.98	31.77	23.91
-507.09	-329.9	582.51	10	20	-243.796	-258.7945	-267.9819	46.71	31.71	22.53
-507.53	-330.4	583.14	5	12	-244.1146	-258.9682	-268.8436	46.46	31.6	21.73
-517.48	-340.4	596.7	10	20	-250.3881	-263.2467	-272.4939	43.71	30.85	21.6
-539.22	-369.4	625.7	0	10	-268.4219	-272.2908	-276.995	30.79	26.92	22.21
-559.46	-390.4	651.84	0	2	-281.3756	-280.432	-281.013	23.81	24.76	24.18
-603.15	-408.9	707.2	15	60	-292.1787	-295.8673	-288.3177	42.86	39.17	46.72
-604.6	-410.7	709.17	0	10	-293.2216	-296.406	-288.5235	42.22	39.04	46.92
-607.47	-412	713.25	15	60	-293.9823	-297.5395	-290.4917	43.34	39.79	46.83
-609.42	-414.5	715.93	0	10	-295.4182	-298.2759	-290.7853	42.41	39.56	47.05
-623.65	-420.7	735.05	15	60	-299.0168	-303.5916	-294.3048	48.19	43.61	52.9
-624.2	-421.3	735.83	8	15	-299.3819	-303.7892	-295.2129	47.94	43.54	52.11
-628.19	-423.1	741.47	15	60	-300.4205	-305.3411	-297.3496	49.61	44.69	52.68
-629.47	-424.6	743.27	10	20	-301.2903	-305.8487	-298.5777	49.1	44.54	51.81
-635.05	-427.1	751.1	15	60	-302.7202	-308.0185	-300.9149	51.35	46.05	53.16
-636.29	-428.6	752.85	8	15	-303.5888	-308.4972	-301.9364	50.82	45.91	52.47
-637.25	-429.8	754.32	10	20	-304.289	-308.8914	-303.1033	50.32	45.72	51.5
-645	-433.3	765.19	15	60	-306.304	-311.9007	-305.755	53.47	47.87	54.02
-645.69	-434	766.1	8	15	-306.7235	-312.1535	-306.6865	53.16	47.73	53.19
-646.43	-434.7	767.29	10	30	-307.1149	-312.4626	-307.8212	53.12	47.77	52.42
-648.77	-437.7	770.63	8	15	-308.8474	-313.3893	-308.9843	51.91	47.37	51.77
-649.98	-439.2	772.43	10	20	-309.713	-313.8947	-310.2047	51.3	47.12	50.81
-652.52	-441.4	776.08	10	30	-310.9687	-314.8768	-311.5984	51.09	47.19	50.46
-655.64	-445.2	780.49	10	20	-313.1711	-316.1107	-313.0781	49.6	46.66	49.69
-657.38	-446.7	782.99	10	30	-314.0345	-316.7833	-314.3538	49.46	46.72	49.15
-658.23	-447.7	784.24	10	20	-314.5914	-317.1196	-315.5127	49.14	46.61	48.22
-659.95	-449.2	786.74	10	30	-315.4541	-317.8199	-316.7866	48.98	46.61	47.65
-664.54	-454.7	793.17	10	20	-318.6232	-319.5834	-318.4645	46.82	45.86	46.98
-665.41	-455.5	794.53	10	30	-319.0675	-319.947	-319.6208	46.79	45.91	46.24
-668.06	-458.7	798.26	10	20	-320.8991	-320.9538	-321.0074	45.58	45.52	45.47
-668.75	-459.3	799.29	10	30	-321.2597	-321.2612	-322.1332	45.51	45.5	44.63

-669.77	-460.5	800.76	10	20	-321.9251	-321.6525	-323.3159	45.11	45.39	43.72
-672.82	-463.1	805.06	10	30	-323.4214	-322.8258	-324.7573	44.9	45.49	43.56
-674.65	-465.3	807.65	10	20	-324.7227	-324.11	-326.8021	44.05	44.66	41.97
-675.46	-466	808.84	10	30	-325.1378	-324.6959	-328.5858	43.96	44.4	40.51
-676.01	-466.6	809.63	10	20	-325.4974	-325.0864	-330.339	43.7	44.11	38.86
-679.44	-469.5	814.47	10	30	-327.2118	-327.4833	-332.7218	43.48	43.2	37.97
-682.49	-473.2	818.77	10	20	-329.3937	-329.5988	-335.0154	42.04	41.84	36.42
-684.02	-474.5	820.95	10	30	-330.1664	-330.6556	-336.9627	41.93	41.44	35.13
-686.95	-478	825.02	10	20	-332.2344	-332.6562	-339.2224	40.56	40.14	33.57
-688.22	-479	826.7	10	30	-332.813	-333.4891	-341.1081	40.46	39.78	32.16
-689.1	-480	827.95	10	20	-333.4189	-334.0996	-342.9062	40.1	39.42	30.61
-690.49	-481.2	829.96	10	30	-334.1347	-335.0982	-344.8165	39.96	38.99	29.28
-691.13	-481.9	830.89	10	20	-334.5476	-335.5418	-346.5539	39.66	38.67	27.66
-691.79	-482.5	831.92	10	30	-334.8778	-336.0408	-348.3181	39.67	38.51	26.23
-693.48	-484.5	834.28	10	20	-336.0605	-337.2045	-350.2795	38.92	37.77	24.7
-694.06	-485	835.16	10	30	-336.3629	-337.6476	-352.0116	38.82	37.53	23.17
-695.02	-486.1	836.52	10	20	-336.9951	-338.312	-353.8271	38.48	37.16	21.65
-695.58	-486.6	837.39	10	30	-337.2974	-338.7272	-355.5558	38.37	36.94	20.11
-696.86	-488.1	839.2	10	20	-338.1764	-339.6125	-357.4243	37.86	36.42	18.61
-698.03	-489.1	840.88	10	30	-338.7805	-340.442	-359.2626	37.74	36.07	17.25
-699.9	-491.3	843.47	10	20	-340.0702	-341.7133	-361.2684	36.92	35.28	15.72
-700.72	-492	844.67	10	30	-340.4817	-342.2933	-363.0463	36.85	35.04	14.28
-702.67	-494.3	847.37	10	20	-341.825	-343.6184	-365.0478	36	34.21	12.78
-703.37	-494.9	848.4	10	30	-342.1812	-344.115	-366.7937	35.94	34	11.33
-705.24	-497.1	850.99	10	20	-343.4685	-345.3836	-368.7629	35.13	33.21	9.84
-706.06	-497.8	852.19	10	30	-343.8791	-345.9624	-370.5333	35.06	32.98	8.41
-707.94	-500	854.77	10	20	-345.1651	-347.2296	-372.5263	34.26	32.19	6.9
-708.64	-500.6	855.81	10	30	-345.5206	-347.7252	-374.2369	34.19	31.99	5.48
-710.35	-502.6	858.17	10	20	-346.696	-348.8811	-376.1978	33.47	31.28	3.97
-711.05	-503.2	859.2	10	30	-347.0512	-349.3762	-377.9047	33.4	31.07	2.55
-712.6	-505	861.34	10	20	-348.0891	-350.421	-379.8056	32.77	30.44	1.06
-713.19	-505.5	862.22	10	30	-348.3894	-350.8608	-381.5091	32.68	30.21	-0.44
-714.73	-507.3	864.35	10	20	-349.4265	-351.8772	-383.4061	32.08	29.63	-1.9
-715.43	-507.9	865.39	10	30	-349.7811	-352.399	-385.134	32.01	29.4	-3.34
-716.73	-509.4	867.19	10	20	-350.6538	-353.2773	-386.9714	31.5	28.87	-4.82
-717.43	-510	868.22	10	30	-351.0082	-353.7712	-388.6957	31.43	28.66	-6.26
-718.82	-511.6	870.14	10	20	-351.9347	-354.7037	-390.5572	30.88	28.11	-7.75
-719.52	-512.2	871.17	10	30	-352.2888	-355.1972	-392.2779	30.81	27.9	-9.18
-720.91	-513.8	873.09	10	20	-353.2419	-356.1289	-394.1356	30.23	27.35	-10.66
-721.49	-514.3	873.97	10	30	-353.5141	-356.5671	-395.8252	30.17	27.11	-12.14
-746.08	-541.3	906.69	10	20	-369.1739	-372.3525	-402.4291	21.31	18.13	-11.94
-751.29	-546.8	913.64	10	20	-372.3532	-375.6872	-405.0472	19.65	16.32	-13.04

-773.12	-570.3	942.15	10	20	-385.8388	-389.2832	-410.985	12.5	9.06	-12.65
-773.96	-571.3	943.36	8	15	-386.4262	-389.8742	-412.3841	12.21	8.76	-13.75
-789.68	-589.3	963.69	10	20	-396.6719	-399.489	-417.0393	6.2	3.38	-14.17
-790.8	-590.6	965.29	6	15	-397.4146	-400.2633	-418.2148	5.84	2.99	-14.96
-791.88	-591.9	966.77	0	10	-398.1569	-400.9571	-418.4334	5.41	2.61	-14.86
-797.73	-598.3	974.39	6	15	-401.7844	-404.5554	-420.5361	3.41	0.64	-15.34
-798.31	-599	975.28	0	10	-402.1811	-404.9547	-420.6452	3.15	0.38	-15.31
-800.71	-601.7	978.51	6	15	-403.6877	-406.4979	-422.0637	2.4	-0.41	-15.98
-801.73	-602.9	979.88	0	10	-404.3744	-407.136	-422.2818	2.04	-0.72	-15.87
-805.21	-606.7	984.47	6	15	-406.5121	-409.2879	-423.8895	0.83	-1.94	-16.54
-806.26	-608	985.94	0	10	-407.2504	-409.978	-424.1074	0.46	-2.26	-16.39
-808.89	-611	989.44	6	15	-408.9631	-411.6226	-425.5774	-0.56	-3.21	-17.17
-811.26	-613.9	992.51	0	10	-410.595	-413.0802	-426.0399	-1.51	-4	-16.96
-813.63	-616.6	995.67	6	15	-412.094	-414.5364	-427.4267	-2.39	-4.83	-17.72
-815.77	-619.2	998.44	0	10	-413.5653	-415.8327	-427.8616	-3.24	-5.51	-17.54
-817.42	-621.1	1000.69	6	15	-414.6417	-416.8902	-429.1111	-3.89	-6.14	-18.36
-819.4	-623.5	1003.26	0	10	-415.9796	-418.1055	-429.4913	-4.66	-6.79	-18.18
-821.3	-625.7	1005.85	6	15	-417.2116	-419.3199	-430.821	-5.39	-7.5	-19
-824.08	-629	1009.38	0	10	-419.071	-420.9552	-431.3363	-6.51	-8.4	-18.78
-825.52	-630.7	1011.41	6	15	-420.013	-421.9041	-432.5563	-7.04	-8.93	-19.58
-826.94	-632.4	1013.28	0	10	-420.9806	-422.7733	-432.8543	-7.58	-9.38	-19.46
-827.44	-633	1014.07	6	15	-421.3205	-423.142	-433.8836	-7.86	-9.68	-20.42
-830.66	-636.9	1018.21	0	10	-423.4885	-425.0629	-434.5063	-9.14	-10.72	-20.16
-831.57	-638	1019.56	6	15	-424.1149	-425.6939	-435.6157	-9.5	-11.08	-21
-833.31	-640.1	1021.84	0	10	-425.2887	-426.7714	-435.9674	-10.18	-11.66	-20.86
-835.25	-642.3	1024.42	6	15	-426.5137	-427.9532	-437.265	-10.88	-12.32	-21.64
-845.42	-654.6	1036.72	0	10	-433.352	-433.6662	-439.1287	-14.98	-15.29	-20.75
-847.79	-656.6	1039.09	6	15	-434.3895	-434.7124	-440.37	-14.89	-15.21	-20.87
-851.84	-662.5	1043.22	0	10	-436.4367	-436.5676	-440.9903	-15.21	-15.34	-19.76
-857.12	-667.2	1048.73	6	15	-438.8951	-439.0206	-442.6883	-15.34	-15.47	-19.14
-859.63	-669.7	1051.41	5	12	-440.2134	-440.2196	-443.8193	-15.49	-15.5	-19.1
-862.73	-672.5	1054.68	6	15	-441.6854	-441.6782	-445.1916	-15.64	-15.63	-19.14
-866.88	-676.5	1058.91	0	10	-443.7492	-443.5515	-445.8371	-15.92	-15.72	-18.01
-868.12	-677.7	1060.38	6	15	-444.3936	-444.2015	-446.9391	-16.01	-15.81	-18.55
-872.25	-681.7	1064.61	0	10	-446.4797	-446.072	-447.557	-16.34	-15.94	-17.42
-876.19	-685.3	1068.79	6	15	-448.3318	-447.9403	-449.0606	-16.44	-16.05	-17.17
-878.48	-687.5	1071.17	5	12	-449.4882	-448.9773	-450.1605	-16.57	-16.05	-17.24
-880.78	-689.8	1073.64	0	10	-450.6695	-450.0655	-450.5091	-16.78	-16.17	-16.62
-881.64	-690.6	1074.67	6	15	-451.1058	-450.5317	-451.5545	-16.87	-16.3	-17.32
-885.05	-693.9	1078.2	0	10	-452.7988	-452.0845	-452.0636	-17.12	-16.41	-16.39
-888.54	-697.1	1081.92	6	15	-454.4643	-453.7392	-453.5095	-17.25	-16.52	-16.29
-898.19	-706.6	1091.66	0	10	-459.374	-458.0233	-454.9275	-18.07	-16.72	-13.62

-902.48	-710.9	1096.19	5	12	-461.5938	-460.0066	-456.3443	-18.49	-16.9	-13.24
-905.78	-714.2	1099.72	0	10	-463.3012	-461.5761	-456.8519	-18.81	-17.08	-12.36
-914.36	-721.8	1108.54	6	15	-467.1933	-465.429	-459.0409	-18.93	-17.16	-10.77
-916.57	-724	1110.92	5	12	-468.3362	-466.4806	-460.1077	-19.04	-17.18	-10.81
-931.37	-739	1125.92	0	10	-476.0107	-473.0308	-462.3191	-20.4	-17.42	-6.71
-932.62	-740	1127.16	6	15	-476.516	-473.5669	-463.3838	-20.52	-17.57	-7.38
-933.29	-740.6	1127.92	0	10	-476.8443	-473.8987	-463.4902	-20.63	-17.68	-7.27
-935.02	-742.2	1129.83	6	15	-477.6523	-474.7407	-464.6339	-20.6	-17.69	-7.59
-941.95	-749	1136.87	0	10	-481.1065	-477.7986	-465.6705	-21.16	-17.85	-5.72
-943.19	-750.2	1138.33	6	15	-481.7361	-478.4349	-466.7596	-21.24	-17.94	-6.26
-946.05	-753	1141.31	0	10	-483.1453	-479.7069	-467.211	-21.41	-17.97	-5.47
-947.24	-754.1	1142.66	6	15	-483.7237	-480.317	-468.2726	-21.5	-18.1	-6.05
-950.36	-757.1	1145.9	0	10	-485.2317	-481.7144	-468.7501	-21.71	-18.19	-5.23
-952.7	-759.5	1148.47	5	12	-486.4621	-482.8315	-469.8371	-21.92	-18.29	-5.3
-956.35	-763.1	1152.3	0	10	-488.2934	-484.4802	-470.4202	-22.28	-18.46	-4.4
-958.07	-764.8	1154.26	8	15	-489.1456	-485.342	-471.8504	-22.37	-18.57	-5.07
-980.91	-787.8	1177.26	0	10	-500.7546	-495.2437	-475.2091	-24.35	-18.84	1.19
-983.16	-789.7	1179.51	6	15	-501.6995	-496.2255	-476.3976	-24.48	-19	0.82
-985.71	-791.9	1182.15	10	20	-502.8178	-497.3575	-478.2447	-24.46	-19	0.11
-987.01	-793.1	1183.53	0	10	-503.4138	-497.9358	-478.4293	-24.45	-18.98	0.53
-994.45	-799.5	1191.15	10	20	-506.6385	-501.2003	-480.9851	-24.44	-19	1.22
-996.46	-801.5	1193.33	5	10	-507.6294	-502.1533	-482.0379	-24.49	-19.01	1.1
-998.71	-802.7	1195.75	1	10	-508.2236	-503.1809	-482.5377	-23.65	-18.61	2.04
-999.82	-803.7	1196.92	5	10	-508.7186	-503.6819	-483.4318	-23.61	-18.57	1.68
-1001.86	-804.8	1199.15	5	15	-509.2877	-504.6334	-484.4568	-22.88	-18.23	1.95
-1005.41	-808.2	1202.78	0	10	-510.9689	-506.1845	-484.9821	-23.07	-18.29	2.92
-1008.95	-810.1	1206.58	1	10	-511.9323	-507.8091	-485.6911	-21.7	-17.57	4.54
-1012.09	-813.1	1209.81	5	10	-513.438	-509.1825	-486.8721	-21.89	-17.63	4.68
-1013.79	-814.8	1211.77	8	15	-514.2766	-510.0059	-488.3144	-21.99	-17.72	3.97
-1014.64	-815.6	1212.75	2	8	-514.6711	-510.4299	-488.7337	-22.13	-17.89	3.81
-1017.44	-817.1	1215.76	1	10	-515.4105	-511.7262	-489.3101	-20.96	-17.28	5.14
-1018.54	-818.1	1216.94	2	8	-515.9278	-512.2245	-489.7816	-20.95	-17.25	5.19
-1020.56	-819.2	1219.16	1	10	-516.4696	-513.1708	-490.2529	-20.22	-16.92	6
-1022.31	-820.7	1221	8	15	-517.2081	-513.9424	-491.666	-20.17	-16.9	5.38
-1023.45	-821.3	1222.24	2	10	-517.5035	-514.4648	-492.1368	-19.73	-16.7	5.63
-1025.52	-823.3	1224.41	2	8	-518.512	-515.3849	-492.712	-19.83	-16.7	5.97
-1027.49	-825.1	1226.59	8	15	-519.397	-516.3045	-494.1753	-19.91	-16.81	5.32
-1029.41	-826.1	1228.62	2	10	-519.8885	-517.1738	-494.7759	-19.16	-16.44	5.96
-1034.19	-830.2	1233.56	10	20	-521.9263	-519.2583	-496.9154	-19.13	-16.46	5.88
-1035.99	-831.4	1235.56	10	30	-522.5396	-520.126	-498.6355	-18.66	-16.25	5.24
-1037.17	-832.4	1236.82	10	20	-523.03	-520.6464	-500.2496	-18.61	-16.23	4.17
-1040.29	-834.4	1240.11	10	30	-524.0105	-522.0332	-502.148	-17.82	-15.84	4.04

-1042.14	-836	1242.06	10	20	-524.8189	-522.8499	-503.8626	-17.8	-15.83	3.16
-1045.1	-837.9	1245.18	10	30	-525.7492	-524.1854	-505.7309	-17.05	-15.48	2.97
-1046.39	-839	1246.56	10	20	-526.2876	-524.7538	-507.338	-17	-15.46	1.95
-1048.24	-840.2	1248.55	10	30	-526.8991	-525.5938	-509.0471	-16.57	-15.27	1.28
-1049.1	-840.9	1249.49	10	20	-527.2415	-525.9889	-510.6251	-16.58	-15.33	0.03
-1050.92	-842.1	1251.49	10	30	-527.8282	-526.8282	-512.3307	-16.08	-15.08	-0.58
-1051.77	-842.8	1252.42	10	20	-528.1704	-527.223	-513.8797	-16.09	-15.14	-1.8
-1053.28	-843.8	1254.09	10	30	-528.659	-527.9383	-515.5304	-15.67	-14.94	-2.54
-1054.14	-844.5	1255.03	10	20	-529.001	-528.3328	-517.0763	-15.68	-15.01	-3.76
-1055.49	-845.4	1256.54	10	30	-529.465	-528.9736	-518.7237	-15.32	-14.83	-4.58
-1056.11	-845.9	1257.21	10	20	-529.7091	-529.2447	-520.2152	-15.33	-14.86	-5.83
-1057.3	-846.7	1258.56	10	30	-530.0996	-529.8113	-521.8337	-15	-14.71	-6.73
-1058.16	-847.4	1259.5	10	20	-530.4413	-530.2053	-523.3737	-15.01	-14.78	-7.94
-1059.03	-848	1260.52	10	30	-530.7341	-530.6485	-524.9377	-14.75	-14.66	-8.95
-1060.31	-849.1	1261.9	10	20	-531.2707	-531.2146	-526.5259	-14.71	-14.65	-9.96
-1061.37	-849.8	1263.09	10	30	-531.6365	-531.7313	-528.1125	-14.49	-14.59	-10.97
-1062.76	-851	1264.58	10	20	-532.2215	-532.3462	-529.7231	-14.45	-14.58	-11.96
-1063.98	-851.8	1265.93	10	30	-532.6114	-532.9116	-531.3066	-14.17	-14.47	-12.87
-1065.14	-852.8	1267.2	10	20	-533.0987	-533.4523	-532.8885	-14.13	-14.48	-13.92
-1066.66	-853.8	1268.87	10	30	-533.5857	-534.1402	-534.5452	-13.77	-14.33	-14.73
-1067.36	-854.4	1269.63	5	10	-533.9023	-534.4595	-535.3348	-13.85	-14.4	-15.28
-1069.18	-856.1	1271.69	10	20	-534.7298	-535.3187	-537.0399	-13.83	-14.42	-16.14
-1069.95	-856.6	1272.56	10	30	-534.9731	-535.6868	-538.5399	-13.69	-14.4	-17.26
-1071.55	-858	1274.29	10	20	-535.6541	-536.4227	-540.1908	-13.63	-14.4	-18.17
-1072.31	-858.5	1275.16	10	30	-535.9216	-536.7905	-541.7132	-13.52	-14.39	-19.31
-1075.13	-861	1278.16	10	20	-537.1368	-538.0405	-543.5128	-13.48	-14.39	-19.86
-1075.9	-861.5	1279.03	10	30	-537.3797	-538.408	-545.032	-13.32	-14.35	-20.98
-1080.27	-865.3	1283.62	10	20	-539.2489	-540.3173	-547.0554	-13.32	-14.39	-21.13
-1082.05	-866.5	1285.61	10	30	-539.831	-541.1488	-548.7228	-12.85	-14.17	-21.74
-1083.6	-868	1287.29	1	6	-540.5826	-541.8577	-549.1015	-12.92	-14.19	-21.44
-1084.88	-869.2	1288.78	10	20	-541.1643	-542.4685	-550.691	-13	-14.31	-22.53
-1085.44	-869.7	1289.41	4	10	-541.4066	-542.7372	-551.3466	-13.08	-14.41	-23.02
-1086.23	-870.5	1290.41	8	15	-541.7941	-543.1524	-552.5813	-13.17	-14.52	-23.95
-1087.31	-871.6	1291.68	4	10	-542.3269	-543.6895	-553.3116	-13.15	-14.51	-24.14
-1089.82	-874.2	1294.45	1	8	-543.6095	-544.8363	-553.8402	-13.46	-14.68	-23.69

SOUTHWEST VIRGINIA SUBSIDENCE ANALYSIS DATA

UNIT NAME	TIME OBS.	P-RIFT Tobs(slpor)	TIME DELITH	P-RIFT Tdel(slpor)	TIME TECTSUB	P-RIFT Ttec(slpor)
Chilhowie/Shady	540	20	540	20	540	20
RomeShale	533.44	26.56	531.8	28.21	527.77	32.23
Honaker/Elbrook	525	35	525	35	525	35
Elbrook	523.52	36.48	523.5	36.5	523.8	36.2
Conococheaugue	505	55	505	55	505	55
Conococheague	502	58	502.17	57.83	502.44	57.56
UpperKnox	484	76	484	76	484	76
KnoxUnconformity	478	82	478	82	478	82
MidOrdovician	458	102	458	102	458	102

R1(ts+sl)slpor	DELITH at end(slpor)	SUM.OBS.THK	Y Tobs(slpor)	Y Tdel(slpor)	Y Ttec(slpor)	R2 Tobs(slpor)
-904.25	-1815.42	-1450	-929.0152	-920.9624	-920.9624	-24.76
-1098.82	-2294.92	-1800	-1023.0648	-1038.913	-1038.913	75.75
-1142.9	-2625.22	-2250	-1130.3908	-1125.5788	-1125.5788	12.51
-1153.04	-2674.19	-2310	-1147.7989	-1143.4557	-1143.4557	5.24
-1311.42	-3334.39	-3060	-1333.9665	-1332.4306	-1332.4306	-22.54
-1323.61	-3380.3	-3110	-1359.2884	-1356.7598	-1356.7598	-35.68
-1411.54	-3681.48	-3410	-1488.2555	-1489.2026	-1489.2026	-76.72
-1412.02	-3682.45	-3411	-1523.6594	-1525.1763	-1525.1763	-111.64
-1798.11	-4649.84	-4211	-1619.975	-1623.0419	-1623.0419	178.13

R2 Tdel(slpor)	R2 Ttec(slpor)	R1(ts+sl)(hipor)	DELITH at end(hipor)	R1(ts+sl)(lopor)	DELITH at end(lopor)
-16.71	-16.71	-971.68	-1819.89	-777.59	-1693.39
59.9	59.9	-1177.04	-2304.65	-973.81	-2152.53
17.32	17.32	-1355.63	-2801.23	-1060.41	-2538.29
9.58	9.58	-1376.82	-2870.31	-1076.89	-2593.93
-21.01	-21.01	-1706.75	-3627.31	-1285.96	-3305.97
-33.15	-33.15	-1718.49	-3675.29	-1300.15	-3354.17
-77.67	-77.67	-1834.3	-3981.89	-1398.65	-3667.21
-113.16	-113.16	-1834.27	-3982.35	-1399.16	-3668.21
175.07	175.07	-2121.45	-4831.96	-1730.07	-4575.79

CONASAUGA BASIN SUBSIDENCE ANALYSIS DATA

UNIT NAME	P-RIFT Tobs(slpor)	P-RIFT Tdel(slpor)	P-RIFT Ttec(slpor)	R1(ts+sl)(slpor)	DELITH at end(slpor)
PreCamb	0	0	0		
ECamb	20	20	20	-572.91	-975.09
PumpVa	24.1	25.32	27.44	-701.51	-1189.22
Rutldg	26.13	26.75	27.93	-709.98	-1234.25
Rogers	27.14	28.01	29.23	-732.52	-1276.02
Maryvi	33.5	32.9	32.34	-786.32	-1446.26
Nolsh1	35	35	35	-832.35	-1522.4
Nollm1	35.88	35.82	35.67	-838.58	-1544.42
Nolsh2	38.16	38.73	39.91	-878.32	-1615.19
Nolmid	38.78	39.08	39.8	-877.26	-1635.33
Nolsh3	40.08	40.79	42.01	-897.99	-1673.44
Nolfpc	40.96	41.67	42.8	-905.38	-1692.05
Nolsh4	42.2	43.32	44.85	-924.55	-1727.84
Maynar	43.34	44.11	45.07	-926.58	-1744.28
Maynar	45	45	45	-925.96	-1763.06
CopRid	55	55	55	-947.51	-1979.2
Chep1	59.79	59.9	60.09	-980.59	-2085.66
Chep2	64.41	64.63	64.97	-1012.31	-2188.66
Kingsp	68.02	67.74	66.96	-1025.2	-2255.99
Mascot	76	76	76	-1083.96	-2446.01
KnoxUn	82	82	82	-1084.33	-2446.81
LowChi	88.85	88.08	86.08	-1134.05	-2652.56
MidChi	94.35	92.89	89.79	-1179.24	-2823.5

OBS.SUM.THK	Y Tobs(slpor)	Y Tdel(slpor)	Y Ttec(slpor)	R2 Tobs(slpor)	R2 Tdel(slpor)	R2 Ttec(slpor)
-642	-651.8424	-644.5229	-644.3138	-78.93	-71.61	-71.4
-751	-700.5384	-708.2329	-708.318	0.97	-6.73	-6.81
-805	-723.5089	-724.4733	-724.9899	-13.52	-14.49	-15.01
-832	-734.7187	-738.5348	-743.3132	-2.2	-6.01	-10.79
-1001	-800.912	-790.2529	-790.3726	-14.59	-3.93	-4.05
-1041	-815.6263	-811.3281	-811.2271	16.72	21.02	21.12
-1058	-824.0833	-819.3874	-818.5718	14.5	19.19	20.01
-1102	-845.4267	-847.0088	-845.1273	32.9	31.31	33.19
-1114	-851.107	-850.1729	-848.1273	26.15	27.09	29.13
-1139	-862.782	-865.7823	-863.9892	35.21	32.21	34
-1156	-870.5821	-873.6013	-872.8848	34.8	31.78	32.5
-1180	-881.4027	-888.0193	-887.571	43.15	36.53	36.98
-1202	-891.1402	-894.8321	-895.4836	35.44	31.75	31.1
-1234	-904.9904	-902.3406	-902.2987	20.97	23.62	23.66
-1541	-981.1996	-979.9556	-979.964	-33.69	-32.45	-32.46
-1655	-1013.6093	-1013.6923	-1013.7358	-33.02	-33.1	-33.14
-1765	-1042.6245	-1043.8672	-1043.9478	-30.31	-31.56	-31.64
-1851	-1063.8681	-1062.5276	-1062.7007	-38.67	-37.33	-37.5
-2041	-1106.6868	-1107.7575	-1107.8488	-22.73	-23.8	-23.89
-2042	-1135.4817	-1137.0836	-1137.1939	-51.16	-52.76	-52.87
-2275	-1165.1746	-1164.0717	-1164.1953	-31.13	-30.02	-30.15
-2462	-1186.7692	-1183.6381	-1183.7982	-7.53	-4.39	-4.55

P-RIFT Tobs(lopor)	P-RIFT Tdel(lopor)	P-RIFT Ttec(lopor)	R1(ts+sl)(lopor)	DELITH at end(lopor)	Y Tobs(lopor)	Y Tdel(lopor)
0						
20	20	20	-463.33	-863.79	-480.9186	-476.4255
24.1	24.71	25.75	-551.31	-1037.04	-539.2308	-543.7031
26.13	26.31	26.64	-564.87	-1088.15	-566.7374	-565.4964
27.14	27.42	27.73	-581.57	-1124.37	-580.1608	-580.2552
33.5	33.19	33.03	-662.66	-1329.22	-659.4255	-652.9336
35	35	35	-692.79	-1390.17	-677.0455	-674.3357
35.88	35.93	36.04	-701.34	-1410.16	-687.1725	-685.0959
38.16	38.59	39.44	-729.2	-1472.22	-712.7307	-715.0501
38.78	39.02	39.63	-730.69	-1481.2	-719.5326	-719.8217
40.08	40.56	41.51	-746.1	-1513.92	-733.5132	-736.5326
40.96	41.46	42.35	-753.02	-1533	-742.8536	-745.9906
42.2	42.94	44.06	-766.99	-1564.23	-755.811	-761.4485
43.34	43.87	44.56	-771.13	-1583.82	-767.4713	-770.9918
45	45	45	-774.71	-1607.32	-784.0566	-782.3197
55	55	55	-839.23	-1863.6	-875.3151	-874.408
59.79	59.83	60.12	-881.06	-1979.63	-914.1249	-913.8854
64.41	64.49	64.95	-920.47	-2091.03	-948.8698	-949.2162
68.02	67.81	67.74	-943.22	-2169.22	-974.3084	-972.8214
76	76	76	-1010.67	-2367.61	-1025.5827	-1026.0419
82	82	82	-1011.13	-2368.53	-1060.0638	-1060.8365
88.85	88.34	87.33	-1081.8	-2597.5	-1095.6202	-1094.1839
94.35	93.36	91.7	-1139.87	-2782.18	-1121.4791	-1118.2712

Y Ttec(lopor)	R2 Tobs(lopor)	R2 Tdel(lopor)	R2 Ttec(lopor)	P-RIFT Tobs(hipor)	P-RIFT Tdel(hipor)	P-RIFT Ttec(hipor)
				0	0	0
-475.6528	-17.59	-13.09	-12.32	20	20	20
-544.3048	12.07	7.6	7	24.1	24.11	25.55
-566.4678	-1.87	-0.63	-1.6	26.13	26.45	27.95
-587.5136	1.41	1.31	-5.95	27.14	27.6	28.8
-652.4176	3.24	9.73	10.25	33.5	33.18	33.95
-673.9184	15.75	18.46	18.88	35	35	35
-683.4631	14.17	16.25	17.88	35.88	35.94	35.97
-712.2923	16.46	14.14	16.9	38.16	38.28	38.89
-716.6925	11.15	10.86	13.99	38.78	38.83	39.11
-734.0386	12.58	9.56	12.06	40.08	40.21	40.56
-745.0681	10.17	7.03	7.95	40.96	41.05	41.25
-761.167	11.18	5.54	5.82	42.2	42.38	42.76
-772.1182	3.66	0.14	-0.99	43.34	43.67	44.26
-782.0963	-9.35	-7.61	-7.39	45	45	45
-874.35	-36.09	-35.18	-35.12	55	55	55
-913.9141	-33.06	-32.82	-32.85	59.79	59.81	59.71
-949.3437	-28.4	-28.74	-28.87	64.41	64.48	64.09
-973.0719	-31.09	-29.6	-29.85	68.02	68.18	67.31
-1026.2562	-14.92	-15.38	-15.59	76	76	76
-1061.1133	-48.93	-49.71	-49.98	82	82	82
-1094.5155	-13.82	-12.38	-12.72	88.85	88.86	89.21
-1118.665	18.39	21.6	21.2	94.35	94.51	94.96

R1(ts+sl)(hipor)	DELITH at end(hipor)	Y Tobs(hipor)	Y Tdel(hipor)	Y Ttec(hipor)	R2 Tobs(hipor)	R2 Tdel(hipor)
-532.74	-922.3	-569.7504	-567.4407	-566.4316	-37.01	-34.7
-655	-1130.44	-650.3032	-648.3361	-649.5593	4.69	6.66
-707.8	-1223.28	-688.3009	-692.2736	-692.7942	19.49	15.52
-726.44	-1259.11	-706.8441	-713.1651	-719.6882	19.6	13.27
-839.75	-1503.27	-816.3407	-809.4782	-808.8189	23.4	30.27
-862.93	-1559.33	-840.6811	-839.0109	-838.4499	22.25	23.92
-872.58	-1578.79	-854.6706	-854.0286	-852.3689	17.91	18.55
-901.68	-1631.02	-889.9768	-890.2806	-888.0809	11.7	11.4
-903.87	-1643.13	-899.3731	-898.4901	-895.8192	4.49	5.38
-918.35	-1676.26	-918.6859	-919.2082	-917.3156	-0.33	-0.86
-925.19	-1695.86	-931.5887	-931.4004	-930.9774	-6.4	-6.21
-940.29	-1728.26	-949.4882	-950.6578	-951.0088	-9.2	-10.37
-955.2	-1758.95	-965.5958	-968.742	-969.8903	-10.4	-13.55
-962.62	-1790.15	-988.5068	-987.1855	-986.869	-25.89	-24.57
-1098.43	-2133.5	-1114.5718	-1113.5481	-1113.4401	-16.14	-15.12
-1149.62	-2258.34	-1168.1838	-1167.5674	-1167.5702	-18.57	-17.95
-1197.28	-2381.98	-1216.1806	-1216.1488	-1216.2504	-18.91	-18.87
-1232.39	-2474.95	-1251.3217	-1252.0874	-1252.3027	-18.94	-19.7
-1326.9	-2672.97	-1322.1522	-1321.6184	-1321.8538	4.75	5.28
-1326.9	-2673.47	-1369.7846	-1369.3632	-1369.6774	-42.88	-42.46
-1413.08	-2919.08	-1418.9025	-1418.6174	-1418.9993	-5.82	-5.54
-1481.82	-3100.41	-1454.6241	-1455.3798	-1455.8296	27.19	26.44

CONASAUGA - LATE CAMBRIAN DATA

Unit Name	TIME OBS	P-RIFT Tobs(sl)	TIME DELITH	P-RIFT Tdel(sl)
pre-LC	525	35	525	35
Nol1	521.94	38.07	521.87	38.13
Nol2	521.3	38.7	521.3	38.7
Nol3	520.57	39.43	520.45	39.55
Nol4	520.46	39.54	520.31	39.69
Nol5	520.37	39.63	520.22	39.78
Nol6	520.19	39.81	519.99	40.01
Nol7	520.14	39.86	519.96	40.04
Nol8	519.97	40.03	519.71	40.29
Nol9	519.8	40.2	519.59	40.41
Nolmid	519.46	40.55	519.42	40.58
Nol11	519.37	40.63	519.33	40.67
Nol12	519.23	40.77	519.17	40.83
Nol13	519.03	40.97	518.88	41.12
Nol14	518.94	41.06	518.8	41.2
Nol15	518.83	41.17	518.66	41.34
Nol16	518.64	41.36	518.51	41.49
Nol17	518.2	41.8	518.2	41.8
Nol18	518.09	41.91	518.13	41.87
Nol19	517.96	42.04	517.92	42.08
Nol20	517.39	42.61	516.94	43.06
Nol21	517.21	42.8	516.65	43.35
Mayn1	516.46	43.54	516.01	43.99
Mayn2	516.15	43.85	515.82	44.19
Mayn3	515.95	44.05	515.67	44.33
Mayn4	515.89	44.11	515.63	44.37
Mayn5	515.75	44.26	515.52	44.48
Mayn6	515.55	44.45	515.4	44.6
Mayn7	515.24	44.76	515.17	44.83
Mayn8	515	45	515	45
CopR1	514.22	45.78	514.26	45.74
CopR2	511.94	48.06	511.75	48.25
CopR3	508.88	51.12	508.76	51.24
CopR4	505.81	54.19	505.77	54.23
CopR5	505	55	505	55

TIME WDmin	P-RIFT Twdmin(sl)	TIME WDmax	P-RIFT Twdmax(sl)	TIME TECT
525	35	525	35	525
522.03	37.97	522.04	37.96	521.75
521.3	38.7	521.3	38.7	521.3
520.75	39.25	520.85	39.15	520.32
520.56	39.44	520.59	39.41	520.15
520.41	39.59	520.46	39.54	520.07
520.18	39.82	520.17	39.83	519.81
520.06	39.95	520.06	39.95	519.8
519.81	40.19	519.77	40.23	519.5
519.64	40.36	519.62	40.38	519.42
519.54	40.46	519.52	40.48	519.34
519.44	40.56	519.39	40.61	519.26
519.25	40.75	519.18	40.82	519.09
518.99	41.01	518.88	41.12	518.75
518.84	41.16	518.75	41.25	518.69
518.66	41.34	518.55	41.46	518.55
518.47	41.53	518.39	41.61	518.43
518.2	41.8	518.2	41.8	518.2
518.13	41.87	518.08	41.93	518.16
517.81	42.19	517.61	42.39	517.87
516.92	43.09	516.83	43.18	516.44
516.53	43.47	516.33	43.68	516.05
515.89	44.11	515.87	44.13	515.56
515.74	44.26	515.77	44.23	515.46
515.6	44.4	515.61	44.39	515.38
515.57	44.43	515.57	44.43	515.36
515.46	44.54	515.43	44.57	515.3
515.37	44.63	515.36	44.64	515.24
515.16	44.84	515.16	44.84	515.1
515	45	515	45	515
514.26	45.74	514.21	45.8	514.43
511.75	48.25	511.7	48.3	511.99
508.76	51.24	508.76	51.24	509.08
505.77	54.23	505.82	54.18	505.9
505	55	505	55	505

R1(ts+sl)(sl)	DELITH at end(sl)	OBS.SUM.THK.	Y Tobs(sl)	Y Tdel(sl)
-2.61	-3.33	-1	-53.3005	-50.406
-81.23	-109.47	-41	-103.7067	-102.1641
-92.43	-126.78	-50	-113.8456	-111.3341
-116.01	-162.22	-67	-125.3911	-124.7682
-120.15	-168.17	-69	-127.0698	-127.0998
-122.26	-171.68	-71	-128.5579	-128.4993
-128.39	-180.82	-75	-131.3868	-132.1068
-128.76	-181.81	-76	-132.0576	-132.5294
-135.83	-191.75	-80	-134.7365	-136.4807
-137.88	-196.44	-84	-137.4081	-138.3492
-139.72	-202.91	-92	-142.7293	-140.9593
-141.79	-206.29	-94	-144.0396	-142.3546
-145.75	-212.39	-98	-146.1632	-144.7685
-153.93	-223.96	-102	-149.2633	-149.3476
-155.59	-226.95	-104	-150.5801	-150.5466
-158.96	-232.16	-107	-152.2923	-152.6489
-161.81	-237.87	-111	-155.2357	-154.9608
-167.31	-249.64	-122	-161.8971	-159.6896
-167.98	-252.01	-125	-163.5741	-160.7846
-172.66	-259.13	-128	-165.5192	-163.9408
-195.8	-293.54	-144	-174.0814	-178.612
-202.18	-303.31	-149	-176.824	-182.972
-210.09	-324.63	-169	-187.8466	-192.4252
-211.63	-331.07	-177	-192.4387	-195.301
-213	-335.88	-183	-195.361	-197.4666
-213.37	-337.02	-184	-196.163	-198.0218
-214.29	-340.43	-188	-198.3031	-199.5542
-215.28	-344.48	-193	-201.0908	-201.3315
-217.6	-352.37	-202	-205.617	-204.7597
-219.16	-357.94	-208	-209.0724	-207.1634
-224.35	-377.33	-232	-220.2399	-217.8301
-246.51	-445.32	-302	-252.0175	-252.9243
-272.85	-530.51	-396	-292.9188	-293.0604
-301.75	-617.05	-490	-331.8738	-331.3161
-309.89	-639.77	-515	-341.9139	-340.8453

Y Twdmin(sl)	Y Twdmax(sl)	Y Ttect(sl)	R2 Tobs(sl)	R2 Tdel(sl)	R2 Twdmin(sl)
-52.0708	-51.4098	-46.5066	-50.69	-47.8	-49.46
-100.7866	-100.0578	-101.1642	-22.48	-20.94	-19.56
-112.4516	-111.8857	-108.4931	-21.41	-18.9	-20.02
-121.1901	-118.9851	-124.2445	-9.38	-8.76	-5.18
-124.1067	-123.0886	-126.9791	-6.92	-6.95	-3.96
-126.515	-125.1888	-128.3835	-6.3	-6.24	-4.25
-130.1009	-129.6095	-132.4101	-3	-3.72	-1.71
-131.9821	-131.4469	-132.6642	-3.3	-3.77	-3.22
-135.7181	-135.9324	-137.3061	1.09	-0.65	0.11
-138.3758	-138.1443	-138.6329	0.47	-0.47	-0.5
-139.9022	-139.688	-139.8475	-3.01	-1.24	-0.18
-141.457	-141.7682	-141.1867	-2.25	-0.57	0.33
-144.375	-144.9645	-143.7653	-0.41	0.98	1.38
-148.4301	-149.5712	-149.0742	4.67	4.58	5.5
-150.7027	-151.5692	-150.1513	5.01	5.04	4.88
-153.4257	-154.6572	-152.3174	6.67	6.31	5.54
-156.2773	-156.9477	-154.1526	6.57	6.85	5.53
-160.3728	-159.8823	-157.6887	5.41	7.62	6.94
-161.4429	-161.7684	-158.3232	4.4	7.19	6.54
-166.2658	-168.7369	-162.784	7.14	8.72	6.39
-179.5538	-180.4243	-184.527	21.72	17.19	16.24
-185.2393	-187.7833	-190.4396	25.36	19.21	16.94
-194.633	-194.473	-197.7264	22.25	17.67	15.46
-196.7526	-195.9416	-199.1355	19.19	16.33	14.88
-198.8238	-198.2054	-200.3796	17.64	15.54	14.18
-199.2288	-198.8429	-200.72	17.21	15.35	14.15
-200.847	-200.8539	-201.5629	15.99	14.74	13.45
-202.1597	-201.8649	-202.4642	14.19	13.95	13.12
-205.1674	-204.6467	-204.5737	11.98	12.84	12.43
-207.4201	-207.0037	-205.9871	10.09	11.99	11.74
-217.9911	-218.3428	-214.3642	4.11	6.52	6.36
-252.7701	-253.1471	-249.2818	-5.51	-6.42	-6.26
-292.5457	-292.2762	-289.0762	-20.07	-20.21	-19.69
-330.4578	-329.6027	-330.6566	-30.12	-29.56	-28.7
-339.9014	-339.6934	-341.9914	-32.03	-30.96	-30.01

R2_Twdmax(sl)	R2_Ttect(sl)	P-RIFT_Tobs(hi)	P-RIFT_Tdel(hi)	P-RIFT_wdmin(hi)
-48.8	-43.9	35	35	35
-18.83	-19.94	38.07	38.04	37.9
-19.45	-16.06	38.7	38.7	38.7
-2.97	-8.23	39.43	39.58	39.31
-2.94	-6.83	39.54	39.71	39.48
-2.93	-6.12	39.63	39.79	39.63
-1.22	-4.02	39.81	40.01	39.85
-2.69	-3.91	39.86	40.06	39.97
-0.11	-1.48	40.03	40.27	40.19
-0.27	-0.76	40.2	40.42	40.37
0.03	-0.12	40.55	40.63	40.5
0.02	0.6	40.63	40.71	40.6
0.79	1.99	40.77	40.85	40.77
4.36	4.86	40.97	41.1	41.01
4.02	5.43	41.06	41.18	41.16
4.3	6.64	41.17	41.3	41.32
4.86	7.66	41.36	41.46	41.51
7.43	9.62	41.8	41.8	41.8
6.21	9.66	41.91	41.87	41.87
3.92	9.87	42.04	42.01	42.1
15.37	11.27	42.61	42.67	42.76
14.4	11.74	42.8	42.86	43.03
15.62	12.37	43.54	43.63	43.78
15.69	12.5	43.85	43.83	43.94
14.8	12.62	44.05	44.08	44.17
14.53	12.65	44.11	44.11	44.2
13.44	12.73	44.26	44.28	44.36
13.42	12.82	44.45	44.4	44.46
12.95	13.02	44.76	44.77	44.79
12.15	13.17	45	45	45
6.01	9.99	45.78	45.75	45.75
-6.64	-2.78	48.06	48.63	48.63
-19.43	-16.23	51.12	51.5	51.5
-27.85	-28.9	54.19	54.37	54.37
-29.81	-32.1	55	55	55

P-RIFT wdmax(hi)	R1(ts+sl)(hi)	DELITH at end(hi)	Y Tobs(hi)	Y Tdel(hi)
35	-2.6	-3.33	-16.0508	-14.53
37.91	-88.32	-117.91	-97.4499	-94.9588
38.7	-102.44	-137.98	-113.8229	-112.0058
39.19	-133.06	-179.86	-132.4673	-134.3812
39.44	-136.7	-185.38	-135.1782	-137.5809
39.57	-138.74	-189.06	-137.5813	-139.744
39.84	-144.94	-198.41	-142.1496	-145.1387
39.96	-146.12	-200.33	-143.2329	-146.2905
40.23	-152.49	-209.64	-147.559	-151.7377
40.38	-155.69	-215.77	-151.8732	-155.3752
40.5	-158.83	-224.7	-160.4662	-160.6421
40.63	-160.75	-228.09	-162.5822	-162.6002
40.83	-164.18	-233.88	-166.0116	-165.9654
41.11	-171.74	-244.83	-171.0178	-172.2555
41.24	-173.63	-248.17	-173.1442	-174.2236
41.44	-176.77	-253.48	-175.9092	-177.2201
41.59	-179.99	-259.93	-180.6624	-181.0188
41.8	-186.93	-274.31	-191.4196	-189.3673
41.91	-188.09	-277.7	-194.1277	-191.0705
42.29	-192.47	-284.56	-197.2689	-194.4954
42.94	-213.96	-317.02	-211.0957	-210.377
43.35	-219.32	-326.05	-215.5246	-215.0277
43.91	-241.23	-362.33	-233.3246	-233.2512
44.03	-243.84	-371.06	-240.7402	-237.8786
44.24	-251.51	-382.58	-245.4593	-243.8537
44.28	-251.94	-384.08	-246.7544	-244.6752
44.45	-256.36	-391.37	-250.2104	-248.5885
44.53	-257.83	-396.56	-254.7121	-251.3939
44.8	-268.27	-413.4	-262.0214	-260.057
45	-273.32	-423.08	-267.6013	-265.3182
45.78	-284.79	-451.85	-285.6354	-282.5891
48.64	-357.4	-576.3	-336.9518	-346.8955
51.48	-402.32	-683.97	-403.002	-408.1129
54.33	-454.28	-799.09	-465.909	-466.5973
55	-463.09	-823.33	-482.1225	-479.1891

Y Twdmin(hi)	Y Twdmax(hi)	Y Ttect(hi)	R2 Tobs(hi)	R2 Tdel(hi)
-16.8686	-16.0295	-11.7965	-13.45	-11.93
-93.0694	-92.309	-95.9738	-9.13	-6.64
-113.3809	-112.4468	-109.0396	-11.38	-9.57
-128.8287	-124.7698	-137.4386	0.59	-1.32
-133.0361	-130.9329	-140.7934	1.53	-0.88
-136.6335	-134.1801	-142.668	1.16	-1
-142.1385	-141.0022	-148.3282	2.79	-0.2
-145.1195	-143.9062	-149.423	2.89	-0.17
-150.6194	-150.7354	-155.2075	4.93	0.75
-155.0646	-154.4097	-158.1288	3.82	0.32
-158.3901	-157.3625	-160.9706	-1.64	-1.81
-160.6768	-160.506	-162.7224	-1.83	-1.85
-164.9461	-165.3315	-165.8019	-1.84	-1.79
-170.9131	-172.3588	-172.6288	0.72	-0.52
-174.3507	-175.4717	-174.3186	0.48	-0.6
-178.3637	-180.1535	-177.1307	0.86	-0.45
-182.8505	-183.8305	-180.0109	-0.68	-1.03
-189.9778	-188.9683	-186.2165	-4.49	-2.44
-191.6401	-191.6629	-187.2604	-6.03	-2.98
-197.1917	-200.6978	-191.1871	-4.79	-2.02
-212.8703	-216.2193	-210.3583	2.87	3.59
-219.3844	-225.7417	-215.0834	3.79	4.29
-236.9122	-238.91	-234.2826	7.9	7.97
-240.6911	-241.7248	-236.5624	3.1	5.96
-246.0859	-246.6434	-243.217	6.05	7.66
-246.7588	-247.5927	-243.591	5.18	7.26
-250.4661	-251.4069	-247.4191	6.15	7.78
-252.7552	-253.2295	-248.6774	3.11	6.43
-260.3596	-259.5792	-257.6636	6.25	8.21
-265.178	-264.0944	-261.986	5.71	8
-282.2782	-281.856	-275.8594	-0.85	2.2
-345.9491	-344.9372	-360.7283	20.45	10.51
-406.5613	-405.029	-410.6891	-0.68	-5.79
-464.4678	-462.4584	-466.18	-11.63	-12.32
-476.9351	-475.643	-475.3465	-19.03	-16.1

R2 Twdmin(hi)	R2 Twdmax(hi)	R2 Ttect(hi)	P-RIFT Tobs(lo)	P-RIFT Tdel(lo)
-14.27	-13.43	-9.19	35	35
-4.75	-3.99	-7.65	38.07	38.07
-10.94	-10.01	-6.6	38.7	38.7
4.23	8.29	-4.38	39.43	39.52
3.67	5.77	-4.09	39.54	39.65
2.11	4.56	-3.92	39.63	39.74
2.8	3.94	-3.39	39.81	39.95
1	2.21	-3.3	39.86	39.98
1.87	1.75	-2.72	40.03	40.21
0.63	1.28	-2.44	40.2	40.36
0.44	1.47	-2.14	40.55	40.58
0.08	0.25	-1.97	40.63	40.66
-0.77	-1.16	-1.63	40.77	40.81
0.82	-0.62	-0.89	40.97	41.07
-0.72	-1.84	-0.69	41.06	41.16
-1.59	-3.38	-0.36	41.17	41.29
-2.86	-3.84	-0.02	41.36	41.46
-3.05	-2.04	0.71	41.8	41.8
-3.55	-3.57	0.83	41.91	41.89
-4.72	-8.22	1.29	42.04	42.06
1.09	-2.26	3.61	42.61	42.87
-0.07	-6.42	4.24	42.8	43.12
4.31	2.32	6.94	43.54	43.81
3.15	2.12	7.28	43.85	44.04
5.42	4.87	8.29	44.05	44.22
5.18	4.34	8.35	44.11	44.26
5.9	4.96	8.94	44.26	44.38
5.07	4.6	9.15	44.45	44.53
7.91	8.69	10.61	44.76	44.81
8.14	9.22	11.33	45	45
2.51	2.93	8.93	45.78	45.74
11.45	12.47	-3.33	48.06	48.25
-4.24	-2.71	-8.37	51.12	51.24
-10.19	-8.18	-11.9	54.19	54.23
-13.84	-12.55	-12.25	55	55

P-RIFT Twdmin(lo)	P-RIFT Twdmax(lo)	R1(ts+sl)(lo)	DELITH at end(lo)	Y Tobs(lo)
35	35	-1.5	-2.22	-13.0135
37.87	37.89	-50.09	-78.68	-59.1824
38.7	38.7	-59.02	-93.58	-68.4691
39.2	39.12	-75.05	-121.66	-79.0441
39.39	39.38	-77.71	-126.08	-80.5817
39.55	39.52	-79.26	-129.01	-81.9446
39.77	39.8	-83.31	-136.01	-84.5358
39.91	39.93	-83.77	-137.08	-85.1502
40.13	40.21	-88.24	-144.43	-87.6039
40.33	40.36	-90.7	-149.52	-90.0509
40.44	40.47	-93.11	-156.53	-94.9248
40.54	40.61	-94.51	-159.17	-96.125
40.73	40.82	-97.16	-163.99	-98.0701
40.97	41.11	-102.37	-172.55	-100.9096
41.14	41.25	-103.93	-175.43	-102.1157
41.32	41.45	-106.32	-179.64	-103.684
41.52	41.61	-108.86	-185.03	-106.3799
41.8	41.8	-113.55	-195.95	-112.4814
41.88	41.93	-114.44	-198.54	-114.0174
42.19	42.4	-117.5	-203.97	-115.799
42.96	43.11	-132.68	-230.79	-123.6415
43.32	43.61	-136.9	-238.72	-126.1535
44	44.07	-145.38	-260.38	-136.2495
44.17	44.18	-147.62	-267.49	-140.4556
44.33	44.35	-149.5	-272.79	-143.1323
44.36	44.4	-149.99	-274.05	-143.8669
44.49	44.54	-151.27	-277.81	-145.827
44.59	44.62	-152.67	-282.27	-148.3804
44.82	44.83	-155.78	-290.92	-152.5262
45	45	-157.9	-297.04	-155.6911
45.74	45.8	-164.93	-318.22	-165.9199
48.25	48.3	-192.76	-391.77	-195.0261
51.24	51.24	-224.93	-481.71	-232.4893
54.23	54.18	-258.83	-573.55	-268.1697
55	55	-268.33	-597.67	-277.3658

Y_Tdel(lo)	Y Twdmin(lo)	Y Twdmax(lo)	Y Ttect(lo)	R2 Tobs(lo)	R2 Tdel(lo)
-11.5144	-12.95	-11.7545	-9.2551	-11.51	-10.01
-57.769	-55.855	-55.0872	-57.0705	-9.09	-7.68
-67.0552	-67.9206	-66.9348	-65.3497	-9.45	-8.04
-78.8556	-75.1181	-72.9524	-78.6614	-4	-3.81
-80.7668	-77.7471	-76.7558	-80.8637	-2.87	-3.06
-82.0434	-80.0696	-78.7158	-82.1363	-2.69	-2.79
-85.0629	-83.1947	-82.7368	-85.454	-1.23	-1.75
-85.5486	-85.1495	-84.5134	-85.8283	-1.38	-1.78
-88.7271	-88.3415	-88.5509	-89.4766	0.63	-0.49
-90.9297	-91.0723	-90.6967	-91.4812	0.65	-0.23
-93.9901	-92.6451	-92.2041	-93.4384	-1.82	-0.88
-95.2057	-94.0609	-94.1164	-94.5794	-1.61	-0.69
-97.2937	-96.7323	-97.0611	-96.7148	-0.91	-0.13
-100.9921	-100.1331	-101.1532	-100.9279	1.46	1.38
-102.2261	-102.3976	-103.0601	-102.1724	1.81	1.7
-104.0599	-104.9329	-105.9195	-104.0923	2.64	2.26
-106.3921	-107.6954	-108.051	-106.1206	2.48	2.46
-111.1351	-111.548	-110.7287	-109.8691	1.07	2.41
-112.3133	-112.6456	-112.5596	-110.7653	0.42	2.13
-114.7341	-116.913	-118.9853	-113.8528	1.7	2.76
-125.8379	-127.2734	-128.6221	-129.0051	9.04	6.84
-129.1861	-132.152	-135.2899	-133.1613	10.75	7.72
-138.5748	-141.2551	-141.5066	-141.4677	9.13	6.81
-141.6725	-143.4262	-142.9408	-143.6394	7.16	5.94
-143.9982	-145.5653	-145.1536	-145.4696	6.37	5.5
-144.5853	-145.9872	-145.7754	-145.9534	6.12	5.4
-146.2377	-147.6331	-147.7301	-147.1885	5.44	5.03
-148.1392	-148.9869	-148.7057	-148.5424	4.29	4.53
-151.8366	-152.0804	-151.4288	-151.5506	3.26	3.95
-154.4111	-154.3798	-153.7239	-153.5767	2.2	3.48
-164.1347	-164.0036	-164.07	-162.0146	-0.99	0.8
-196.1259	-195.6663	-195.8267	-194.5687	-2.26	-3.36
-232.7132	-231.878	-231.5296	-230.6075	-7.56	-7.78
-267.5863	-266.3931	-265.5876	-266.8221	-9.34	-8.75
-276.2729	-274.9905	-274.7947	-276.6535	-9.03	-7.94

R2 Twdmin(lo)	R2 Twdmax(lo)	R2 Ttect(lo)
-11.45	-10.25	-7.75
-5.76	-4.99	-6.98
-8.9	-7.92	-6.33
-0.07	2.09	-3.62
-0.04	0.95	-3.15
-0.81	0.54	-2.88
0.11	0.57	-2.15
-1.38	-0.75	-2.06
-0.1	-0.31	-1.24
-0.37	0.01	-0.78
0.46	0.9	-0.33
0.45	0.39	-0.07
0.43	0.1	0.45
2.24	1.22	1.45
1.53	0.87	1.76
1.39	0.4	2.23
1.16	0.81	2.74
2	2.82	3.68
1.79	1.88	3.67
0.58	-1.49	3.64
5.41	4.06	3.68
4.75	1.61	3.74
4.12	3.87	3.91
4.19	4.68	3.98
3.93	4.35	4.03
4	4.21	4.04
3.63	3.53	4.08
3.69	3.97	4.13
3.7	4.35	4.23
3.52	4.17	4.32
0.93	0.86	2.92
-2.9	-3.06	-1.81
-6.95	-6.6	-5.68
-7.56	-6.76	-7.99
-6.66	-6.46	-8.32

THREADGILL CREEK, TEXAS, SUBSIDENCE ANALYSIS DATA

UNIT NAME	TIME OBS	P-RIFT Tobs(slpor)	TIME DELITH	P-RIFT Tdel(slpor)	P-RIFT Ttec(slpor)
Hickory	525	3	525	3	3
CapMtn	522.71	5.29	522.88	5.12	5.06
CapMtn	521.88	6.12	522.09	5.92	5.78
CapMtn	520.61	7.39	520.9	7.1	6.92
CapMtn	519.15	8.86	519.5	8.5	8.19
CapMtn	518.38	9.62	518.79	9.21	8.86
LionMt	516.6	11.4	516.6	11.4	11.4
Unconformity	515	13	515	13	13
Welge	514.64	13.36	514.71	13.29	13.24
MorCrk	513.44	14.56	513.76	14.24	14
MorCrk	512.78	15.22	512.95	15.05	14.95
MorCrk	512.31	15.7	512.4	15.6	15.57
PntPk1	511.41	16.59	511.15	16.85	17.12
PntPk2	510.69	17.31	510.59	17.41	17.54
PntPk3	509.61	18.39	509.27	18.73	19.03
SanSaba	509.01	18.99	508.48	19.52	19.95
SanSaba	507.87	20.13	507.58	20.42	20.65
SanSaba	507.4	20.61	506.9	21.1	21.45
SanSaba	506.2	21.8	505.95	22.05	22.18
SanSaba	505	23	505	23	23
San Saba	504.38	23.63	504.36	23.64	23.59
Tanyard	495	33	495	33	33
Gorman	489.87	38.13	489.83	38.17	38.27
Gorman	488	40	488	40	40
Honeycutt	478	50	478	50	50

R1(ts+sl)(slpor)	DELITH at end(slpor)	SUM.OBS.THK	Y Tobs(slpor)	Y Tdel(slpor)	Y Ttec(slpor)	R2 Tobs(slpor)
-65.71	-133.78	-111	-66.1618	-67.4633	-68.43	-0.45
-101.74	-190.23	-147	-90.4407	-89.7476	-89.9913	11.3
-107.29	-203.78	-160	-98.9896	-97.9263	-97.2865	8.3
-116.18	-224.08	-180	-111.9308	-109.8814	-108.8137	4.25
-125.98	-248.12	-203	-126.4929	-123.7631	-121.2874	-0.51
-131.21	-260.24	-215	-133.9488	-130.6808	-127.8324	-2.74
-150.95	-298.03	-243	-151.0134	-151.551	-151.921	-0.07
-151.58	-299.15	-244	-165.928	-166.3313	-166.5964	-14.35
-154.07	-305.17	-250	-169.2226	-168.9792	-168.7746	-15.16
-161.91	-325.24	-270	-180.0815	-177.503	-175.5804	-18.17
-171.73	-342.42	-281	-185.9671	-184.7	-183.9838	-14.24
-178.14	-354.15	-289	-190.2064	-189.5692	-189.4	-12.07
-194.14	-380.51	-304	-198.0676	-200.3563	-202.6917	-3.93
-198.51	-392.24	-316	-204.2726	-205.1645	-206.2756	-5.76
-213.9	-419.76	-334	-213.4566	-216.2619	-218.6713	0.45
-223.34	-436.05	-344	-218.492	-222.7814	-226.136	4.85
-230.62	-454.6	-363	-227.9272	-230.1443	-231.8119	2.69
-238.9	-468.41	-371	-231.8477	-235.6095	-238.193	7.05
-246.39	-488.07	-391	-241.5153	-243.2319	-243.8989	4.88
-254.92	-507.37	-411	-251.0082	-250.6455	-250.3122	3.91
-258.92	-519.53	-423	-255.8892	-255.6212	-254.8167	3.03
-323.13	-697.05	-603	-323.5641	-322.5483	-321.7046	-0.43
-367.5	-813.25	-713	-356.554	-355.4611	-354.9839	10.95
-382.09	-852.89	-753	-367.9	-366.485	-365.3296	14.19
-415.33	-943.09	-843	-423.249	-421.3357	-419.7909	-7.92

R2 Tdel(slpor)	R2 Ttec(slpor)	R1(ts+sl)(lopor)	DELITH at end(lopor)	R1(ts+sl)(hipor)	DELITH at end(hipor)
-1.75	-2.72	-83.69	-132.2	-116.74	-172.84
11.99	11.75	-98.96	-187.77	-146.13	-247.25
9.36	10	-104.26	-201.03	-161.47	-271.92
6.3	7.36	-112.81	-220.93	-176.77	-301.25
2.22	4.7	-122.24	-244.56	-202.24	-343.13
0.53	3.38	-127.3	-256.48	-209.46	-357.84
-0.6	-0.97	-146.41	-293.64	-237.11	-407.45
-14.76	-15.02	-147.02	-294.73	-237.78	-408.57
-14.91	-14.71	-149.4	-300.63	-241.46	-416.8
-15.59	-13.67	-156.9	-320.33	-257.73	-447.42
-12.97	-12.25	-166.4	-337.18	-269	-466.44
-11.43	-11.26	-172.56	-348.65	-277.32	-480.91
-6.22	-8.55	-187.88	-374.36	-293.41	-505.76
-6.66	-7.77	-191.92	-385.74	-300.69	-519.82
-2.36	-4.77	-206.5	-412.45	-316.85	-548.39
0.56	-2.79	-215.4	-428.19	-326.14	-564.91
0.47	-1.19	-222.06	-446.09	-336.64	-588.01
3.29	0.7	-229.87	-459.44	-345.11	-604.07
3.16	2.49	-236.72	-478.41	-357.85	-629.63
4.27	4.6	-243.12	-497.1	-370.99	-656.55
3.29	4.1	-248.6	-508.91	-382.04	-675.98
0.58	1.43	-311.02	-685.06	-509.23	-924.15
12.04	12.52	-355.75	-801.79	-597.75	-1070.93
15.61	16.76	-370.64	-841.79	-612.18	-1114.61
-6.01	-4.46	-405.24	-933.54	-648.14	-1205.69

TEXAS - LATE CAMBRIAN

Unit Name	Tobs	P-RIFT Tobs	Tdelith	P-RIFT Tdel	R1(sl)	Delith at end(sl)	OBS.SUM.THK.	R2 Tobs(sl)	R2 Tdel(sl)
Hickor	525	2.14	525	0	-153.66	-229.41	-111	-22.12	-23.59
CapMtn	524.2	2.91	524.2	0.8	-170.89	-274.07	-151	-11.87	-11.2
CapMtn	523.49	3.22	523.45	1.55	-177.37	-291.28	-167	-8.15	-6.57
CapMtn	521.3	3.7	521.3	3.7	-208.48	-339.66	-192	15.67	15.39
CapMtn	519.54	5.46	519.51	5.5	-216.78	-363.67	-215	11.57	11.77
CapMtn	518.7	6.3	518.7	6.3	-220.73	-374.17	-226	8.31	8.74
LionM1	517.73	7.28	517.62	7.38	-228.58	-390.58	-239	7.92	7.34
LionM2	516.98	8.03	516.93	8.07	-232.39	-401.09	-249	5.48	5.31
LionM3	516.6	8.4	516.6	8.4	-234.08	-406.02	-254	4.07	4.26
Unc	515	10	515	10	-234.62	-407.04	-255	-8.4	-8.38
Welge	514.69	10.31	514.51	10.49	-241.77	-418.37	-261	-3.74	-5.21
MorCrk	513.6	11.4	513.6	11.4	-249.14	-439.55	-282	-4.99	-5.11
MorCrk	512.91	12.09	512.84	12.16	-257.8	-455.71	-293	-1.73	-2.48
MorCrk	512.41	12.59	512.47	12.53	-260.53	-463.47	-301	-2.87	-2.62
PntPk1	511.41	13.59	511.24	13.76	-275.7	-489.68	-317	4.63	2.99
PntPk2	510.53	14.47	510.6	14.4	-286.08	-501.84	-331	8.4	8.52
PntPk3	509.9	15.1	509.83	15.17	-293.19	-515.59	-341	10.85	9.8
PntPk4	509.4	15.6	509.4	15.6	-295.64	-523.87	-349	9.6	9.07
SanSab	507.89	17.11	508.04	16.96	-298.4	-534.89	-361	1.41	1.8
SanSab	507.01	17.99	507.29	17.71	-300.1	-540.89	-368	-3.16	-1.89
SanSab	506.13	18.87	506.43	18.57	-302.61	-547.88	-375	-6.83	-5.57
SanSab	505.88	19.12	506.22	18.79	-303.14	-549.52	-377	-8.04	-6.54
SanSab	505	20	505	20	-308.27	-559.43	-384	-8.98	-9.93

KINDEBLADE RANCH, OKLAHOMA, SUBSIDENCE ANALYSIS DATA

UNIT NAME	TIME OBS	P-RIFT Tobs(slpor)	TIME DELITH	P-RIFT Tdel(slpor)	R1(ts+sl)slpor
Reagn1	513.6	3.1	513.6	3.1	-56.44
Reagn2	513.16	3.54	513.205	3.5	-64.55
HonCrk	512.662	4.04	512.777	3.92	-73.12
FtSil1	512.31	4.39	512.281	4.42	-87.35
FtSil2	512.164	4.54	512.156	4.54	-89.74
FtSil3	511.519	5.18	511.289	5.41	-113.46
FtSil4	511.138	5.56	510.985	5.72	-118.64
FtSil5	510.903	5.8	510.778	5.92	-122.31
FtSil6	510.786	5.91	510.685	6.02	-123.92
FtSil7	510.493	6.21	510.428	6.27	-128.47
FtSil8	510.2	6.5	510.2	6.5	-132.25
Royer1	508.733	7.97	508.8	7.9	-150.57
Royer2	508.19	8.51	508.296	8.4	-157
SigMt1	507.967	8.73	508.065	8.64	-160.07
SigMt2	507.775	8.93	507.861	8.84	-162.86
SigMt3	507.52	9.18	507.601	9.1	-166.32
SigMt4	507.137	9.56	507.197	9.5	-171.89
SigMt5	506.755	9.95	506.816	9.88	-176.96
SigMt6	506.212	10.49	506.246	10.45	-184.85
SigMt7	506.021	10.68	506.055	10.65	-187.33
SigMt8	505.319	11.38	505.318	11.38	-197.53
SigMt9	505	11.7	505	11.7	-201.76
SMOrd1	504.835	11.87	504.823	11.88	-206.39
SMOrd2	503.792	12.91	503.773	12.93	-233.53
Butrly	502.303	14.4	502.275	14.43	-272.07
MckHls	497.77	18.93	497.737	18.96	-387.08
CoCrk	491.235	25.47	491.213	25.49	-547.05
Kindb	484.618	32.08	484.606	32.09	-701.43
WSprCk	478	38.7	478	38.7	-849.36

DELITH at end(slpor)	OBS.SUM.THK	Y Tobs(slpor)	Y Tdel(slpor)	Y Ttec(slpro)	R2 Tobs(slpor)	R2 Tdel(slpor)
-123.3	-103	-22.5059	-22.3167	-22.2557	33.94	34.13
-141.14	-118	-34.704	-33.2849	-32.2786	29.84	31.26
-160.47	-135	-48.4072	-45.0917	-42.7895	24.71	28.03
-182.83	-147	-58.0276	-58.6741	-60.1113	29.33	28.68
-188.38	-152	-62.0021	-62.0802	-62.9992	27.74	27.66
-227.1	-174	-79.4506	-85.5192	-91.45	34.01	27.94
-240.16	-187	-89.6735	-93.6614	-97.6162	28.97	24.98
-248.91	-195	-95.9481	-99.1831	-101.9426	26.36	23.12
-252.82	-199	-99.0633	-101.6579	-103.8385	24.85	22.26
-263.86	-209	-106.8392	-108.4779	-109.1983	21.63	19.99
-273.62	-219	-114.5789	-114.5051	-113.6515	17.67	17.75
-319.88	-265	-152.7919	-151.038	-149.1026	-2.22	-0.47
-336.48	-282	-166.7114	-163.9917	-161.367	-9.72	-7
-343.97	-289	-172.3931	-169.8942	-167.1984	-12.32	-9.82
-350.62	-295	-177.2688	-175.0887	-172.4788	-14.41	-12.23
-359.13	-303	-183.7214	-181.6848	-178.9982	-17.4	-15.36
-372.45	-315	-193.3638	-191.8801	-189.4383	-21.47	-19.99
-385.02	-327	-202.9226	-201.4351	-198.8671	-25.96	-24.47
-403.91	-344	-216.4105	-215.6221	-213.4324	-31.56	-30.77
-410.13	-350	-221.1272	-220.3472	-217.9959	-33.8	-33.02
-434.59	-372	-238.3402	-238.4458	-236.5751	-40.81	-40.91
-445.09	-382	-246.0987	-246.1896	-244.2039	-44.34	-44.43
-456.2	-392	-250.0962	-250.4829	-248.8445	-43.71	-44.1
-523.32	-455	-275.1242	-275.7042	-275.7772	-41.6	-42.18
-619.06	-545	-310.1417	-310.9643	-313.164	-38.07	-38.9
-910.23	-819	-411.7755	-412.7882	-419.2656	-24.7	-25.71
-1329.86	-1214	-545.9682	-546.8641	-554.0112	1.08	0.19
-1751.36	-1614	-668.3377	-669.1684	-671.1426	33.09	32.26
-2169.93	-2014	-778.4854	-779.2435	-772.675	70.88	70.12

R2 Ttec(slpor)	R1(ts+sl)lopor	DELITH at end(lopor)	R1(ts+sl)hipor	DELITH at end(hipor)
34.19	-56.44	-123.3	-162.07	-236.93
32.27	-64.55	-141.14	-180.08	-265.18
30.33	-73.12	-160.47	-195.72	-292.76
27.24	-87.26	-182.78	-205.56	-308.55
26.74	-89.61	-188.29	-209.3	-316.12
22.01	-106.35	-219.78	-233.76	-357.07
21.02	-111.64	-232.97	-239.9	-372.86
20.36	-115.38	-241.79	-247.34	-386.15
20.08	-117.02	-245.74	-248.87	-390.94
19.27	-121.65	-256.87	-258.04	-407.63
18.6	-125.51	-266.71	-261.32	-418.12
1.47	-144.14	-313.32	-284.87	-474.91
-4.37	-150.67	-330.03	-291.49	-493.74
-7.12	-153.79	-337.57	-306.56	-504.75
-9.62	-156.62	-344.27	-310.69	-513.32
-12.68	-160.13	-352.83	-314.22	-523.78
-17.55	-165.78	-366.23	-322.44	-540.55
-21.91	-170.92	-378.88	-327.85	-553.35
-28.58	-178.9	-397.87	-341.21	-579.09
-30.66	-181.42	-404.12	-343.94	-586.11
-39.04	-191.74	-428.71	-361.33	-619.19
-42.45	-196.02	-439.27	-366.34	-632.23
-42.46	-200.7	-450.44	-374.85	-645.81
-42.25	-228.14	-517.86	-415.75	-728.41
-41.1	-267.05	-613.99	-476.56	-850.55
-32.19	-383.84	-907.03	-639	-1200.11
-6.96	-545.24	-1328.09	-866.17	-1625.23
30.29	-700.4	-1750.36	-1051.68	-2053.71
76.69	-848.79	-2169.38	-1228.67	-2484

VITA

David Allen Osleger was born in Pittsburgh, Pennsylvania on November 16, 1956. He was graduated from Ringgold High School in Monongahela, Pennsylvania in 1974. David received his A.B. in Geology from Lafayette College in Easton, Pennsylvania in May, 1978. He attended the University of Texas at El Paso from September 1979 to May 1981, and did his Masters thesis on Pennsylvanian rocks of west Texas and southern New Mexico. David worked as an exploration geophysicist for Gulf Oil Company in New Orleans from June 1981 to June 1985 when he entered the Ph.D. program at Virginia Polytechnic Institute. He was graduated in August 1990 and will be doing post-doctoral research at the University of Southern California.